



1506  
UNIVERSITÀ  
DEGLI STUDI  
DI URBINO  
CARLO BO

**DIPARTIMENTO SCIENZE BIOMOLECOLARI (DISB)**

**Corso di Dottorato di Ricerca in: Scienze della Vita, Salute e Biotecnologie**

**Curriculum: Biologia della Cellula e degli Organismi**

**CICLO XXX**

# **Investigation of the effects of *Campylobacter jejuni* virulence factors in human cells: different pathways involved**

---

**Settore Scientifico Disciplinare (SSD): BIO-16**

**Relatore:**  
**Prof. Stefano Papa**

**Dottorando:**  
**Dott.ssa Gianna Di Sario**

**Co-relatore:**  
**Dott.ssa Barbara Canonico**

**Anno Accademico 2016/2017**



## Table of contents

Abbreviations	5
Abstract	8
Introduction	9
1. Biology of <i>Campylobacter jejuni</i>	9
1.1 Epidemiology of <i>C. jejuni</i>	10
1.2 Transmission of <i>C. jejuni</i>	11
1.3 Pathogenesis of <i>C. jejuni</i>	12
1.4 Post-infectious sequelae of <i>C. jejuni</i>	13
1.4.1 The Guillain-Barré syndrome	13
1.5 Molecular basis of <i>C. jejuni</i> pathogenesis	17
1.5.1 Lipooligosaccharides	17
1.5.2 Capsule	18
1.5.3 Flagella	18
1.5.4 The cytolethal distending toxin	19
1.5.5 Glycosylation system	20
1.6 The outer membrane vesicles (OMVs)	21
1.7 <i>C. jejuni</i> -host cell interactions	23
2. Mechanisms of cell death	31
2.1 Apoptosis	31
2.1.1 Bcl-2 family proteins	33
2.1.2 Extrinsic and intrinsic pathway	34
2.1.3 pRb, p53 and CD59	35
2.2 Necrosis	37
2.3 Autophagy	37
Aims and objectives	39
Materials and Methods	40
3. Human tumour myeloid cells (U937) and normal monocytes	40
3.1 Ethic statement	40
3.2 Bacterial strains	40

3.3 Growth conditions	41
3.4 Cell lines and monocytes isolation	41
3.5 <i>C. jejuni</i> cell lysate preparation	42
3.6 Detection of cytotoxin activity in <i>C. jejuni</i> lysates	42
3.7 Pre-treatment of U937 cells and monocytes with <i>C. jejuni</i> lysates	42
3.8 Pre-treatment of U937 cells with <i>C. jejuni</i> OMVs	43
3.9 Pre-treatment of U937 cells with Rapamycin	43
3.10 Nanoparticle Tracking Analysis (NTA)	43
3.11 Morphological feature evaluation	43
3.12 Flow cytometry and confocal microscopy stainings	44
3.13 Trypan blue viability test	48
3.14 Confocal microscopy analyses	48
3.15 Statistical analyses	48
4. Human intestinal cell model and molecular work	49
4.1 Bacterial strains, plasmids and primers	49
4.2 Growth conditions and storage	51
4.3 Preparation of a specific OD <sub>600</sub> <i>C. jejuni</i> suspension	52
4.4 DNA Purification	53
4.5 Purified DNA Quantitation	54
4.6 Polymerase Chain Reaction Technique	54
4.7 Tris-Acetate-EDTA agarose ethidium bromide gel electrophoresis	55
4.8 Purification of PCR products	55
4.9 Ligation and transformation stages	56
4.10 PCR from boiled/lysed bacteria colonies	57
4.11 Overnight culture preparation	58
4.12 Isolation of plasmid DNA: QIAprep Miniprep production	58
4.13 Restriction endonuclease digestion	58
4.14 Inverse PCR mutagenesis	59
4.15 DNA sequencing	60
4.16 Transformation of <i>C. jejuni</i> by Electroporation	61
4.17 Construction of a <i>C. jejuni</i> 11168H <i>cdtA</i> GFP mutant strain	62

4.18 Isolation of <i>C. jejuni</i> OMVs	64
4.19 Quantitation of total proteins by bicinchoninic acid assay (BCA)	65
4.20 Pre-treatment of T84 intestinal Eukaryotic cells with <i>C. jejuni</i> whole cells and OMVs	66
4.21 CHOP and BIP proteins detection by SDS-PAGE and Western blotting	67
4.22 Total RNA isolation	67
4.23 cDNA synthesis	69
4.24 Reverse Transcription PCR (RT-PCR)	70
Results	72
5. Monocytes from donor's human blood	72
Discussion	85
6. U937 cell model: U937 cells preincubated with <i>C. jejuni</i> lysates	88
Discussion	109
7. U937 cell model: U937 cells preincubated with <i>C. jejuni</i> OMVs	112
Discussion	126
8. Human intestinal cell model	127
Discussion	131
9. Construction of <i>C. jejuni</i> 11168H GFP mutant strain	132
Discussion	136
Conclusions	137
Appendices	143
Appendix 1-Primer design	143
Appendix 2- Different orientations of the Km <sup>R</sup> cassette	145
References	146



## **Abbreviations**

AAG, autoagglutination

AIDP, acute inflammatory demyelinating polyneuropathy

AMAN, acute motor axonal neuropathy

AMSAN, acute motor sensory axonal neuropathy

AnxV, Annexin V

ATF6, activating transcription factor-6

BCA, bicinchoninic acid assay

Bcl-2, B-cell lymphoma-2 protein

BSA, albumin standards

CCV, Campylobacter-containing vacuole

CDT , cytolethal distending toxin

CHOP, C/EBP homologous protein

CL, Cardiolipin

CPSs, Capsular polysaccharides

CTRL, untreated control cells

D-MEM, Dulbecco's modified eagle medium

DR, death receptor

eIF2 $\alpha$ , eukaryotic transcriptional initiation factor

ER, endoplasmic reticulum

ERAD , endoplasmic reticulum-associated degradation

FADD, Fas-associated death domain protein

FasL, Fas ligand

FBS, fetal bovine serum

FCS, foetal calf serum

FlaA, flagellin A

FlaB, flagellin B,

FSC, forward light scatter

FSC, forward scatter

GBS, Guillain-Barré syndrome

IBD, inflammatory bowel diseases

IECs, intestinal epithelial cells

IPCRM, Inverse PCR mutagenesis

IRE-1, inositol-requiring protein-1

ISPCR, insert specific primers PCR

Km, Kanamycin

LAMP-1, lysosomal-associated membrane protein-1

LB, Luria-Bertani

LBP, LPS binding protein

LE, late endosome

LOS, lipooligosaccharides

LPS, lipopolysaccharide

LTDR, LysoTracker Deep Red

LTG, LysoTracker Green

m TORC1, mTOR complex 1

m TORC2, mTOR complex 2

MAC, membrane attack complex

MDC, Monodansylcadaverine

MFI, mean fluorescence intensity

MOMP, mitochondrial outer membrane permeabilization

mTOR, mammalian target of rapamycin

MUT, mutant

MVB, multivesicular bodies

NAO, Nonyl Acridine Orange

NR, Nile Red



NTA, nanoparticle tracking analysis

OMVs, outer membrane vesicles

PBMCs, peripheral blood mononuclear cells

PERK, protein kinase RNA-like ER kinase

PI construct, Plasmid + Insert

PI, Propidium Iodide

PI3K, phosphoinositide 3-kinase

PIK construct, Plasmid Insert Kanamycin cassette

pRb, retinoblastoma protein

RM, Rapamycin

ROS, reactive oxygen species

RPMI, Roswell Park Memorial Institute

RT, at room temperature

SSC, side light scatter

TLR4, Toll-like receptor 4

TMRE, Tetramethylrhodamine ethyl ester perchlorate

TNFR1, TNF receptor 1

TNF- $\alpha$ , tumour necrosis factor alpha

TRAIL, TNF-related apoptosis inducing ligand

UPR, unfolded protein response

VAIN, variable anaerobe chamber

VPPCR, vector primer PCR

WR, working reagent

WT, wild type

XBP1, X-box binding protein

## Abstract

The gram-negative bacterium *Campylobacter jejuni* represents a major agent causing food-borne gastroenteritis in humans worldwide. *C. jejuni* infection is also an important precondition for Guillain-Barré syndrome. The cytotoxic effects of *Campylobacter* have been ascribed to the actions of several different toxins. The best characterized *C. jejuni* toxin is the cytolethal distending toxin (CDT), released by bacteria via outer membrane vesicles (OMVs). Many bacterial pathogens, including *C. jejuni*, utilize OMVs to transport virulence factors, such as the CDT (cytolethal distending toxin), into host cells. To date, different authors described the peculiar relationship among *C. jejuni* virulence factors and human intestinal and myeloid cells. It is known that resident macrophages contribute to the maintenance of tissue by acting as the first line of defense against pathogens and by initiating wound repair. These monocyte-derived cells establish (together with dendritic cells) the role of “guardian of the gut”. The aim of this work was to investigate the effects of *C. jejuni* virulence factors in human cells focusing the attention on cellular pathways that this bacterium activates or deactivates during host cell infection. Among the several virulence factors, the CDT was the most investigated. To do that, effects induced by three different *C. jejuni* wild type strains were compared with the effects induced by the *C. jejuni cdtA* mutant strain, in three different cell lines: monocytes isolated from donor’s human blood, tumour myeloid cells (U937) and human intestinal epithelial cells (T84). *C. jejuni* lysates, OMVs and whole cells were separately used for the infections. Carried out cytometric, microscopy and molecular analyses revealed that *C. jejuni* induce DNA damage, apoptosis, mitochondrial and lysosomal destabilization as well as intracellular lipid content alterations, ICAM-1 upregulation and activation of autophagic, secretory and endocytic pathways in a CDT dependent manner. Nevertheless, although they are important for *C. jejuni* infection, CDT seems not to have a role in ER stress and UPR activation, CD14 and CD59 upregulation. Involvement of all these pathways enhances *C. jejuni* invasion, persistence and survival, allowing the possible onset of post infectious sequelae such as the Guillain-Barré syndrome.

# Introduction

## 1. Biology of *Campylobacter jejuni*

The *Campylobacter* genus belongs to the family Campylobacteraceae, the order Campylobacterales, the class Epsilonproteobacteria, and the phylum Proteobacteria. Since its first description, the genus has grown to include several important human and animal pathogens that are primarily classified through phylogenetic means. The genus *Campylobacter* consists of 26 species, 2 provisional species, and 9 subspecies (as of December 2014).

Although the infections were attributed to *Vibrio fetus* (now known to be *Campylobacter fetus*), the first recognized case of *Campylobacter* infection (termed campylobacteriosis) were reported in the early 20<sup>th</sup> century in farm animals, and during the next three decades, it was believed to be a rare, opportunistic, invasive pathogen that occurred principally in debilitated hosts. Only in the early 1980s the importance of these infections was recognized as a cause of human gastrointestinal illness. By the mid-to-late 1980s, *Campylobacter* species have been identified as one of the most common bacterial causes of diarrhoea worldwide.

*C. jejuni* like all *Campylobacter* species, is a microaerophilic, non-fermentative Gram-negative organism. Being structurally similar to other Gram-negative bacilli, *C. jejuni* cells are slender, spirally 'curved rods', approximately 0.2-0.8 wide and 0.5-5µm long. It is motile with a characteristic corkscrew like motion via a single polar unsheathed flagellum at one or both ends of the cell (Vandamme et al, 2015).

For an efficient cultivation *in vitro*, the microaerophilic nature of *C. jejuni* requires an atmosphere with reduced oxygen and elevated carbon dioxide concentrations: gas mixtures of 5% oxygen, 10% carbon dioxide and 85% nitrogen provide optimal cultivation conditions for most *C. jejuni* isolates (Bolton et al, 1983).

The *C. jejuni* genome is small (1.6-2.0 megabases) and can establish long-term associations with their hosts, sometimes with pathogenic consequences (Young et al, 2007).

The complete genome sequence of *C. jejuni* was characterized and hypervariable regions that might be important in the survival of this organism were found (Parkhill et al, 2000). Most of the hypervariable sequences that have been found are in regions that encode proteins that are involved in the biosynthesis or modification of surface-accessible carbohydrate structures, such as the capsule, lipooligosaccharide (LOS) and flagellum; these structures have a key role

in *C. jejuni* biology, in particular for host-bacterium interactions (Young et al, 2007). *C. jejuni* is naturally competent, meaning that it can take up DNA from the environment. This leads to recombination between strains, which allows the generation of even more genetic diversity. The horizontal transfer of both plasmid and chromosomal DNA occurs both *in vitro* and *in vivo* during chick colonization; this indicates that natural transformation may have a significant role in genome plasticity (Wilson et al, 2003) (Avrain et al, 2004).

### **1.1 Epidemiology of *C. jejuni***

To date, campylobacteriosis is one of the most widespread infectious diseases of the last century. Recent reports suggested that in the past decade the incidence and prevalence of campylobacteriosis increased globally in both developed and developing countries. In North America, Europe, and Australia was recorded a remarkable increase, and data from parts of Africa, Asia, and the Middle East indicated that campylobacteriosis was endemic in these areas, especially in children (**Fig. 1.1**) (Kaakoush et al, 2015). In developed countries, where waterborne infection is less likely, animals are the primary source of human infection and disease. By contrast, *Campylobacter* is hyperendemic in the developing world, because of poor sanitation and close human contact with animals. In these countries *Campylobacter* species are usually limited to children, with illness/infection ratios decreasing with age, suggesting that exposure in early life might lead to the development of protective immunity (Rao et al, 2001).

Several factors have been hypothesized to influence the prevalence of *Campylobacter* infections; for example, in the last years it has been hypothesized that it might be influenced by population-level immunity (Havelaar et al, 2009).

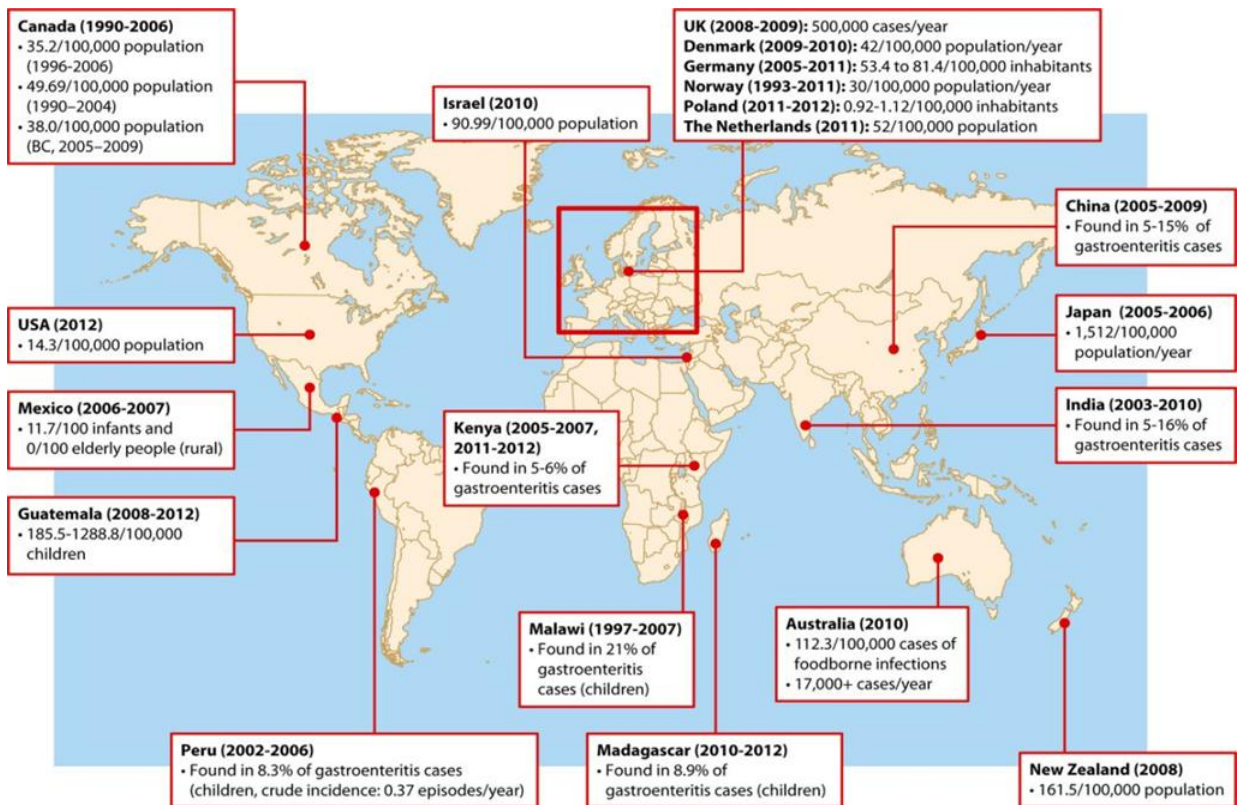


**Fig. 1.1** Incidence and prevalence of Campylobacteriosis worldwide (American Society of Microbiology, 2015).

## 1.2 Transmission of *C. jejuni*

*C. jejuni* is commonly considered to be a commensal organism of chickens and other avian species. Several environmental reservoirs can lead to human infection by *C. jejuni*. It colonizes the chicken gastrointestinal tract in high numbers, primarily in the mucosal layer, and it is passed between chicks within a flock through the faecal-oral route. *C. jejuni* can infect humans directly through consumption of contaminated food, particularly poultry products, unpasteurized milk, and water (**Fig. 1.2**) (Friedman et al, 2004) (Kapperud et al, 1992) (Neimann et al, 2003). In humans, *C. jejuni* can invade the intestinal epithelial layer, resulting in inflammation and diarrhoea.

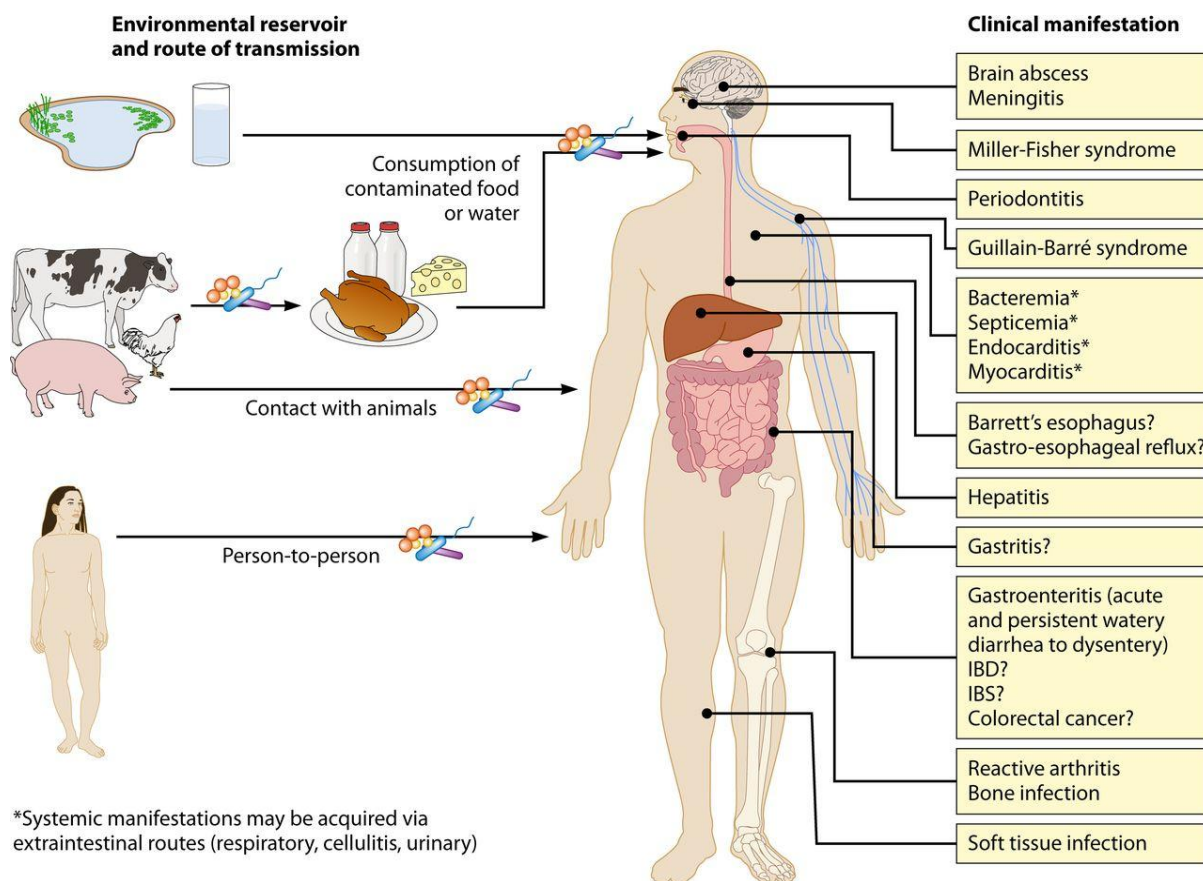


**Fig. 1.2** Consumption of undercooked or contaminated food and contact with animals can lead to transmission of *Campylobacter* to humans. Depending on species, strains involved and the ingestion dose, gastrointestinal and/or extra-gastrointestinal manifestations can occur (Kaakoush et al, 2015).

### 1.3 Pathogenesis of *C. jejuni*

*C. jejuni* is successful in competing with the human intestinal microbiota; an infectious dose of few hundred bacteria is sufficient to overcome the colonization resistance of humans leading to campylobacteriosis (Hofreuter, 2014). More than 80% of the registered campylobacteriosis are caused by *C. jejuni*, for this reason the term ‘campylobacteriosis’ is frequently associated to *C. jejuni* infection. Campylobacteriosis typically causes gastroenteritis/enterocolitis, and clinical picture varies significantly in duration, severity and associated symptoms (Ketley, 1997). Following an incubation of ~24-72 hours, symptoms like cramping abdominal pain, fever, vomiting and headaches can develop (Blaser, 1997). Upon onset of abdominal pain, diarrhoea develops quickly. Depending on virulence of the infecting strain and host immune status, it varies from a mild, non-inflammatory, watery presentation to severe and bloody.

Although gastroenteritis is the major clinical condition resulting from *C. jejuni* infection, other serious conditions within the gastrointestinal tract have been associated with *C. jejuni*, including inflammatory bowel diseases (IBD), post infectious functional gastrointestinal disorders, such as irritable bowel syndrome and functional dyspepsia, and celiac disease (Kaakoush et al, 2015).

#### **1.4 Post-infectious sequelae of *C. jejuni***

In addition to gastrointestinal infections, *C. jejuni* can trigger extra-intestinal manifestations, as either a local isolated infection (which is a systemic manifestation after an episode of enteritis) or a postinfectious immune disorder. Overall, the incidence of extra-intestinal manifestations associated with *C. jejuni* infection is low compared with gastroenteritis. Post-infectious complications can be severe, and potentially life-threatening. These manifestations include Guillain-Barré syndrome (GBS), Miller Fisher Syndrome, Bell's palsy (unilateral facial paralysis) and reactive arthritis. To date, the post-infectious disease most extensively studied is GBS.

##### **1.4.1 The Guillain-Barré syndrome**

The Guillain-Barre' syndrome (GBS) is an acute post-infectious ascending paralysis that can affect peripheral and cranial nerves (particularly VII, facial nerve) and manifests as rapidly evolving weakness and sensory disturbance in arms, legs and, in some cases, facial, bulbar and respiratory muscles (Goodfellow & Willison, 2016). This disorder affects children and adults of all ages and both sexes, although men are more frequently affected than women.

In most cases (60-70%), the neuropathy is preceded by a bacterial or viral illness. Usually, an initial respiratory tract infection or gastroenteritis is followed by an acute phase in which paralysis of muscles develops and reaches a plateau. After this phase, a gradual resolution of the paralysis follows, that lasts from weeks to months.

Current strategies for GBS therapy include plasma exchange and intravenous immunoglobulin (IVIg), that have been shown to improve outcomes for patients with GBS (Hughes et al, 2014) (van Doorn et al, 2010).

*C. jejuni*, cytomegalovirus, Epstein-Barr virus, and *Mycoplasma pneumonia* infections are recognized as triggering agents of about two-third of GBS cases (Sinha et al, 2004). In 1982 Rhodes and Tattersfield reported for the first time the link between *C. jejuni* infection and GBS development (Rhodes & Tattersfield, 1982). Several subsequent studies documented the

prevalence of *C. jejuni* infection or seropositivity in patients with GBS, confirming the finding to be widespread and reproducible (Rees et al, 1995). At present, *C. jejuni* is recognized as the most identifiable pathogen associated with development of GBS because 25-40% of GBS patients suffer from *C. jejuni* infection 1-3 weeks prior to the illness (Mishu & Blaser, 1993); nevertheless, the risk of developing GBS after *C. jejuni* infection exposition is quite low, only 1 in 1000 patients develops GBS (Magira et al, 2003). The annual incidence of GBS is approximately between 1.2 and 2.3 cases per 100,000 persons (van Doorn et al, 2008).

Depending on the electrophysiological properties, GBS is classified in different subtypes: acute inflammatory demyelinating polyneuropathy (AIDP), acute motor axonal neuropathy (AMAN), and a severe form of AMAN that is termed acute motor sensory axonal neuropathy (AMSAN), which is much less common (Griffin et al, 1996). AMAN is an axonal subtype (30 to 65% of patients) particularly widespread in Asia and Central and South America (Kuwabara & Yuki, 2013) (Bae et al, 2014), while AIDP is more prevalent in Europe and North America. Especially for the AMAN type, the pathogenesis of the disease is believed to involve molecular mimicry between sialylated lipooligosaccharide structures, that are contained on the cell envelope, and ganglioside epitopes of *C. jejuni* and neural gangliosides. This mechanism generates a cross-reactive immune response, resulting in a cascade of immune-mediated inflammatory responses, degeneration of the peripheral nerve and interruption of neurotransmission (**Fig. 1.3**). In serum samples from numerous patients affected by AMAN, subsequently to *C. jejuni* infection, high titres of antibodies against the following gangliosides were contained: GM1, GM1b, GD1a or GalNAc-GD1a (Ogawara et al, 2000). Basically, the LPS (lipopolysaccharide) from *C. jejuni* contains a terminal tetrasaccharide identical to that of GM1 (Yuki et al, 1993). The concept of ‘molecular mimicry’ is gathered from these observations, which imply the sharing of homologues epitopes between bacterial LPS and ganglioside surface components of peripheral nerves, particularly on the axolemma. It was supposed that, because of these molecular analogies, antibodies that are produced to attack bacteria could also attack neuronal axons, leading to GBS.

The immune response is generated by a specific immune recognition which involves T-lymphocytes, monocytes, and various cytokines responsible for causing the demyelination (**Fig. 1.4**). Recent studies also established the relevant role of macrophages in immune-mediated nerve damage, which are essential in both the effector phase of the disease and initiating the repair phase (Hartung & Toyka, 1990) (Baichwal et al, 1988). Previous studies



also demonstrated that human monocytes can phagocytose *Campylobacter* species *in vitro* and that *C. jejuni*, ingested by human macrophages, convert to a coccal form (Kiehlbauch et al, 1985).

Moreover, in the last 10 years, cell sorting investigations (Van Rhijn et al, 2002) revealed that *Campylobacter* DNA was present in CD14<sup>+</sup> and CD33<sup>+</sup> populations, indicating that myelomonocytic cells are *Campylobacter* DNA-carrying cells. A possible explanation was that although ingested bacteria could be killed by monocytes, bacterial DNA is resistant to degradation and persists within the cells, without causing clinical symptoms, in a viable but non culturable form (Hickey et al, 2005).

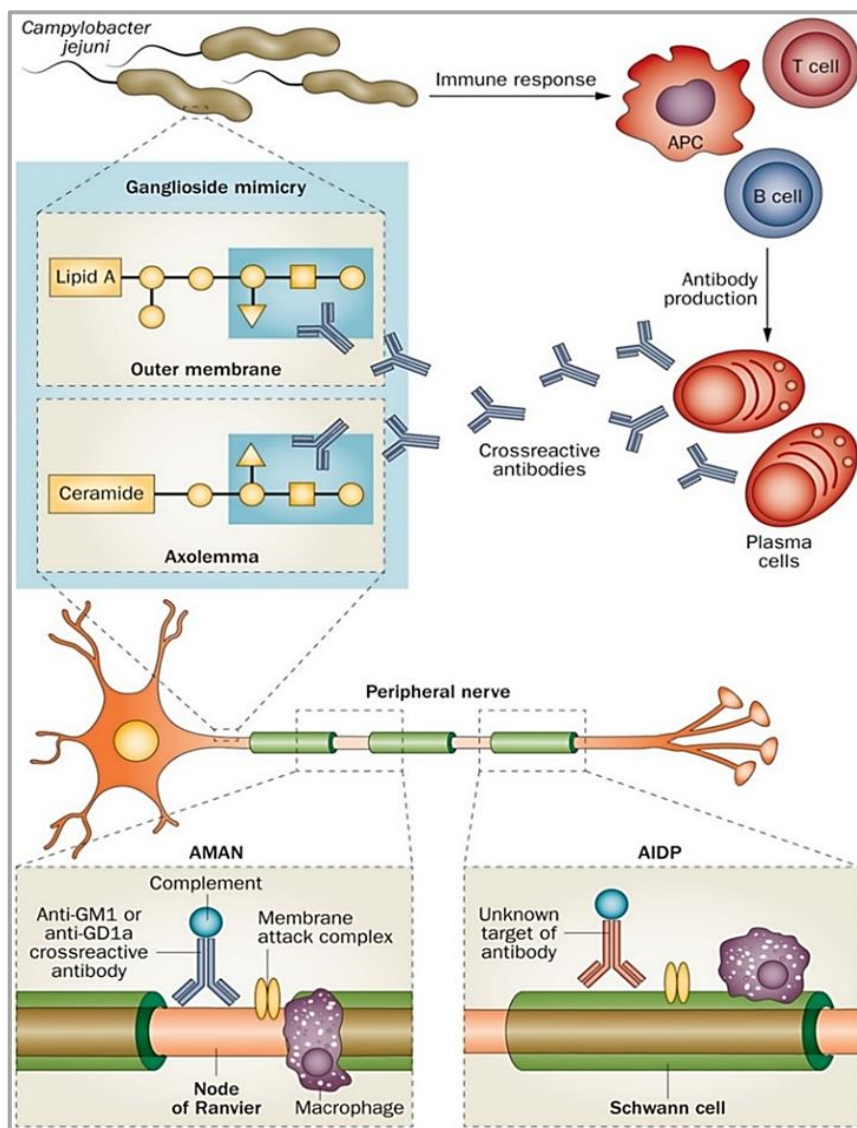


**Fig. 1.3:** Molecular mimicry and antiganglioside antibodies are at the base of the immunopathogenesis of GBS. (van den Berg et al, 2014).

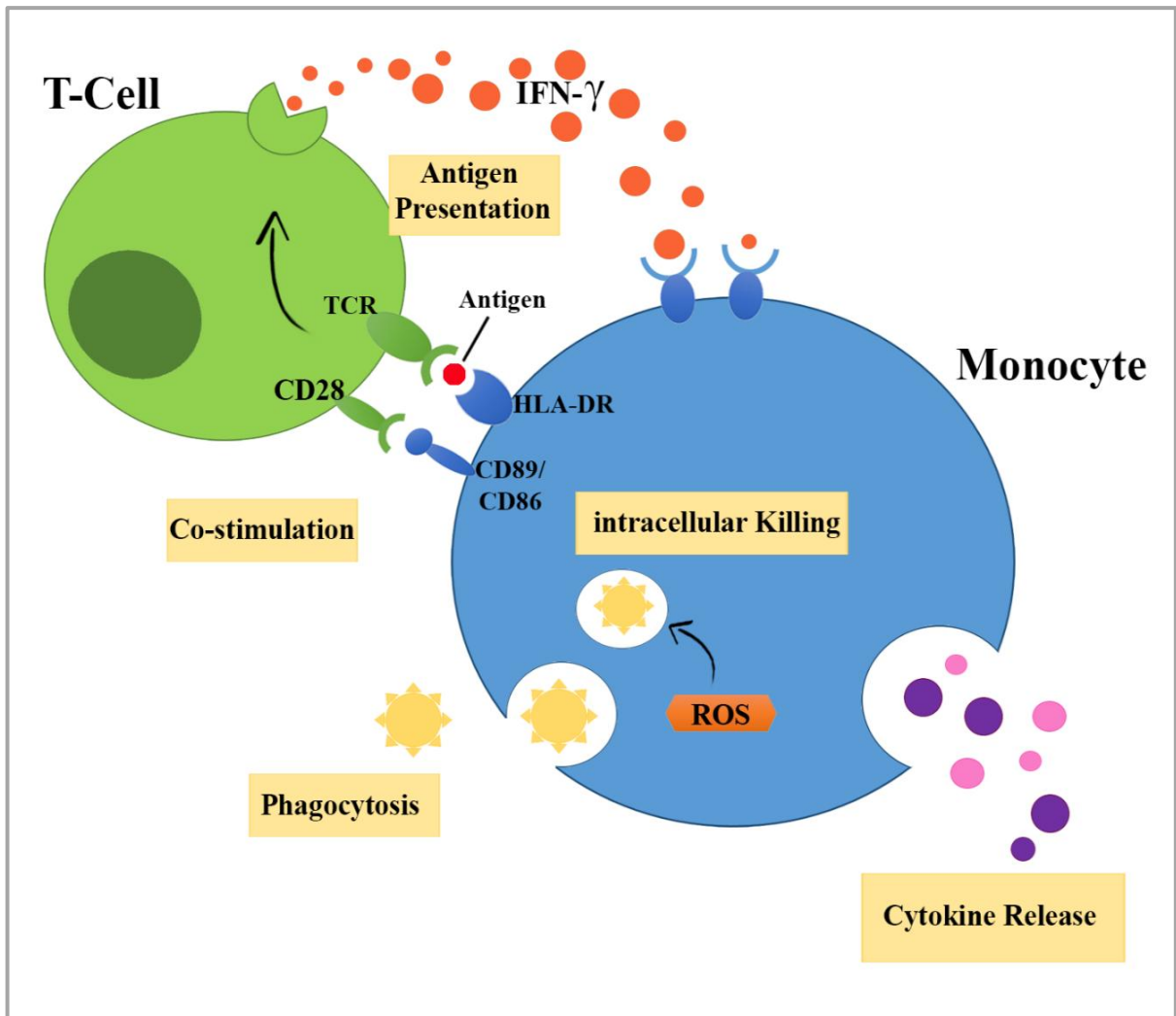


**Fig. 1.4** Monocyte functions. Monocytes and T-cells are critical to the host response to acute bacterial infection but monocytes are primarily viewed as amplifying the inflammatory signal. Although monocytes are specialized in defense against pathogens, *C. jejuni* elaborated CDT dependent and independent mechanisms to survive in human monocytic cells. (Image created by Gianna Di Sario)

## 1.5 Molecular basis of *C. jejuni* pathogenesis

To date bacterial factors implicated in host cell invasion and disease pathogenesis are: lipooligosaccharides, capsule, flagellar apparatus, cytolethal distending toxin (CDT) and post-translational glycosylation system (O-linked and N-linked glycosylation).

### 1.5.1 Lipooligosaccharides

In Gram-negative bacteria a main component of most outer membranes is the lipopolysaccharide (LPS). It has crucial roles in protection of bacteria from harsh environments and toxic compounds (Dong et al, 2014). LOS is analogous to the lipopolysaccharide (LPS) found in other Gram-negative families; LPS is made up of an O-polysaccharide chain, core oligosaccharide and a lipid A component in the outer membrane. LOS, lacking an O-polysaccharide repeating structure, is a low molecular weight form of bacterial LPS (Gilbert et al, 2008). They have a role in adhesion, invasion and colonisation of host and intestinal niches, protection from complement-mediated killing and surviving in different non-intestinal environments (Guerry et al, 2002) (Karlyshev et al, 2005). LOS are highly variable structures and *C. jejuni* uses this variability as an expedient for avoiding host defences and adapting to different microenvironments. LOS are also capable of mimicking human antigens (Guerry & Szymanski, 2008). In particular, molecular mimicry of *C. jejuni* LOS with gangliosides in nervous tissue induces the generation of cross-reactive anti-ganglioside antibodies resulting in GBS and Miller Fisher syndrome (see 1.4.1) (Ang et al, 2004). Indeed, it was demonstrated that specific types of the *C. jejuni* LOS biosynthesis gene locus are clearly associated with immune-mediated neuropathy and with the presence of ganglioside-mimicking structures in LOS (Godschalk et al, 2004).

It is well known that membrane CD14 molecule is involved in LPS-induced cytokine production in human blood cells (Alexander & Rietschel, 2001) (Landmann et al, 1996). CD14 is a 55-kDa glycoprotein, which is mainly expressed on mature monocytes, macrophages and activated granulocytes. It is a myeloid membrane glycoprotein which serves as a receptor for complexes of lipopolysaccharide (LPS) and LPS binding protein (LBP) (Heinzelmann & Bosshart, 2005). The specific cellular recognition of agonistic LPS/lipid A is initialized by the combined extracellular actions of LBP, the membrane-bound or soluble forms of CD14 and the newly identified Toll-like receptor 4 (TLR4) \*MD-2 complex, leading to the rapid activation of an intracellular signaling network. Moreover, it is well known that

CD14 molecule is involved in a CD14-dependent phagocytosis that monocytes use to phagocytose Gram-negative bacteria (Neu et al, 2013).

### 1.5.2 Capsule

Capsular polysaccharides (CPSs) are commonly present on bacterial surface and play an important role in bacterial pathogenesis, survival and persistence (Llobet et al, 2008). Although capsule might be crucial for successful adhesion to epithelial cells, it does not provide protection against host innate defence and the potent antimicrobial action of human  $\beta$ -defensins 2 or 3 (Zilbauer et al, 2005). As elucidated during sequencing of the shotgun library of NCTC11168 (Karlyshev et al, 1999) and in subsequent studies (Gundogdu et al, 2007) (Guerry et al, 2012), capsule components are codified by genes that are split in three different regions: the first and the last regions comprise *kps* genes, that encode the KpS proteins involved in capsular assembly and transport; whereas the central region is highly variable and is involved in polysaccharide synthesis. Therefore, CPSs are involved in structural variation, mimicry to host antigens, and resistance to phagocytosis and complement-mediated killing.

### 1.5.3 Flagella

*Campylobacter* motility is mediated by a single unsheathed flagellum that can be contained at one or both poles. Flagella represent the primary adherence factor that creates contact between eukaryotic cell membrane and specific bacterial-invasion factors (Hu et al, 2008).

Flagellar motility is vital to many aspects of *C. jejuni* biology, including motility, host colonization, virulence in ferret models, secretion and host-cell invasion. This apparatus allows *C. jejuni* to colonize both human and animal host cells (Wassenaar et al, 1993). A correlation between the presence of intact flagellum and the ability of *C. jejuni* to adhere and invade host cells was demonstrated in the last 20 years (Grant et al, 1993) (Konkel et al, 2004). Flagella are also involved in: secretion of virulence proteins, autoagglutination (AAG), microcolony formation and avoidance of the innate immune response (Guerry, 2007). Structurally, flagella are composed of a major flagellin, FlaA, and a minor flagellin, FlaB, that are both approximately 59 kDa in size and are highly homologous. *flaA* and *flaB* genes are respectively regulated by  $\sigma_{28}$  (encoded by *fliA*) and a  $\sigma_{54}$ -dependent promoter (encoded by *rpoN*). Mutation of *flaA* results in the production of a truncated flagellar filament composed

of FlaB and having a severe reduction in motility. On the contrary, mutants in *flaB* have no significant changes in motility and produce a flagellar filament that appears structurally normal (Nuijten et al, 1990).

#### **1.5.4 The cytolethal distending toxin**

CDT is a heterotrimeric holotoxin produced by a diverse group of Gram-negative pathogenic bacteria, belonging to the subclass of AB<sub>2</sub> toxin superfamily. As in the case of other AB toxins, CDT comprise three subunits, CdtA, CdtB, and CdtC (Ge et al, 2008).

The A subunit of the toxin, CdtB, is an enzyme, with an average molecular size of 29 kDa, that exhibits cation-dependent metalloenzyme activities, *in vitro*, characteristic of endonucleases (Elwell & Dreyfus, 2000; Lara-Tejero & Galan, 2000), inositol polyphosphate 5-phosphatases (Dlakic, 2001) and sphingomyelinases (Hofmann et al, 2000). The B component consist in two heterogeneous subunits, CdtA (23 kDa) and CdtC (21 kDa). CdtA and CdtC act as carriers to deliver the catalytic subunit, CdtB, into host cells (Smith & Bayles, 2006). CdtB reaches the nucleus by an endoplasmic reticulum-associated degradation (ERAD) or non-ERAD pathway (followed by translocation across the nuclear membrane) where exhibits DNase I-like activity and induces limited DNA damage such as double-strand damage, leading to the activation of DNA repair responses and cell cycle arrest at the G<sub>2</sub>/M phase (Canonico et al, 2014; Lara-Tejero & Galan, 2001)

The importance of the CdtB is clearly demonstrated in the case of *Salmonella typhi* that, lacking the genes for CdtA and CdtC, can translate only the CdtB protein. It was proposed that *S. typhi* synthesizes and secretes CdtB once it has reached an intracellular compartment of the host cell (Haghjoo & Galan, 2004). To interact with the target cells, the A subunit, that imparts biological activity to the holotoxin, is likely translocated across the plasma membrane of the target cells through a receptor-mediated process. In addition, a second important element is thought to be important for the binding of CDT to a specific area of the host membrane: it is known as lipid raft (see Lipid rafts section).

In the last 15 years different authors (Guerra et al, 2005) (DiRienzo, 2014) (Gargi et al, 2013) suggested a novel model system through which all CDTs are trafficked in a retrograde manner from the cell membrane to Golgi and endoplasmic reticulum to translocate to cytosolic targets and nucleus. More studies will be required to better define the nature of this process for *C. jejuni* CDT.

### 1.5.5 Glycosylation system

*C. jejuni* possesses two protein-glycosylation systems: The N-linked glycosylation system, which modifies serine or threonine residues, and the O-linked glycosylation system, which modifies asparagine residues (Young et al, 2007).

N-linked glycosylation machinery of *C. jejuni* is encoded by a single gene cluster of 16 kb named *pgl* cluster (protein glycosylation) (Szymanski et al, 1999). The first N-linked oligosaccharyltransferase identified in bacteria was PglB, a key enzyme in the *pgl* locus.

Although N-linked glycosylation system is conserved in all *C. jejuni* strains studied to date, its role in *C. jejuni* biology is not clear and has to be better investigated.

It was demonstrated a correlation between N-linked glycosylation system and bacterial virulence. Different *C. jejuni* glycosylation mutants, that were deficient in their ability to glycosylate certain proteins, showed reduction in adhesion and invasion of human intestinal epithelial cells *in vitro* and colonization of the chick gastrointestinal tract (Karlyshev et al, 2004) (Kakuda & DiRita, 2006). In according to recent studies (Larsen et al, 2004) this system might be also involved in the evasion of the immune system.

Structure of N-linked glycan was clarified by mass spectrometry and NMR spectrometry analyses that revealed that this glycan is a heptasaccharide with the following structure: GalNAc-a1,4-Gal- NAc-a1,4-(Glc1,3)GalNAc-a1,4-GalNAc-a1,4-Gal- NAc-a1,3-Bac-b1,N-Asn, where Bac is bacillosamine, 2,4-diacetamido-2,4,6-trideoxyglucose (Knauer & Lehle, 1999)

In contrast to the N-linked system, the genetic locus of the O-linked system is more heterogeneous and genetically diverse (Champion et al, 2005); the putative flagellar glycosylation locus of *C. jejuni* NCTC 11168 contains ~50 genes, among which are the genes encoding the flagellin structural proteins FlaA and FlaB. O-linked glycosylation is crucial for successful flagellin assembly and motility, therefore influencing adhesion, invasion and virulence *in vivo* (Thibault et al, 2001). Defects in O-linked glycosylation result in: loss of motility, decrease in the adherence to and invasion of host cells, and decreased virulence in ferrets (Guerry et al, 2006). O-linked glycosylation of flagellin is necessary for the proper assembly of the flagellar filament, which has led to the hypothesis that the O-glycan might have a role in the interactions of flagellin subunits with one or many elements of the flagellar apparatus.

## 1.6 The outer membrane vesicles (OMVs)

OMVs have emerged as pathogenic nanoparticles that can travel beyond the mucosa to distant locations within the host, with the ultimate goals of causing cellular destruction, promoting bacterial survival and facilitating the development of pathogenesis in the host (Pathirana & Kaparakis-Liaskos, 2016) (**Fig. 1.5**).

OMVs are blebs generated from the outer membrane of the cell envelope of all Gram-negative species of bacteria studied to date (Amano et al, 2010). They are typically 20-200 nm in diameter, and are released only by viable cells during the course of normal metabolism and in all cell growth phases in all environmental conditions studied (Bonnington & Kuehn, 2014). These nanostructures contain outer membrane proteins, phospholipids, lipooligosaccharides (LOS), and numerous periplasmic proteins of wide molecular mass range (Mashburn-Warren et al, 2008).

Once the OMVs are free from the bacterium, they appear as small membrane vessels including periplasmic constituents and outer membrane components. In the last decade, OMVs are increasingly recognized as key determinants for bacterial virulence (Kulp & Kuehn, 2010) and play a major role in host-pathogen interactions, including the trafficking and eventual release of diverse virulence factors from many pathogenic bacteria (Ellis & Kuehn, 2010). Recently, it was reported that the *C. jejuni* wild type strain 81-176 produces OMVs that contain biologically active CDT: during pathogenesis, release of OMVs by *C. jejuni* is a route of this bacterium to deliver all CDT subunits to the surrounding environment, infecting host cells and causing the typical cytolethal distending effects *in vivo* and *in vitro* (Lindmark et al, 2009). Several roles were attributed to OMVs: they may act as delivery vehicles for bacterial toxins lacking typical signal sequences (Balsalobre et al, 2006; Kouokam et al, 2006), promote cell-cell communication via transit of signaling molecules (Mashburn & Whiteley, 2005), and can inhibit phagosome-lysosome fusion during macrophage infection (Fernandez-Moreira et al, 2006). OMVs are also potentially rich in antigens that serve as initial targets for innate and adaptive immune recognition (Bergman et al, 2005). OMVs may also have defensive roles during infection, by sequestering antibiotics and antibodies, as well as acting as decoy antigens to divert the attention of the immune system away from the invading bacteria (Ellis & Kuehn, 2010) (Chattopadhyay & Jaganandham, 2015). Moreover, Elmi et al. demonstrated that apart from CDT, OMVs secreted by *C. jejuni* delivered also other virulence-associated *C. jejuni* proteins (Elmi et al, 2012).

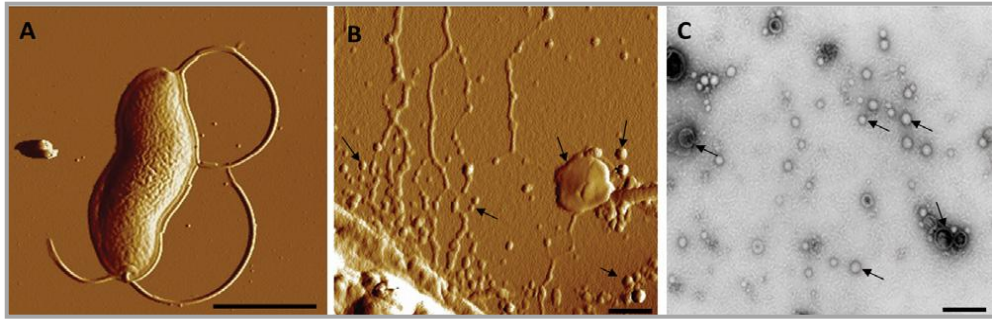


**Fig. 1.5** Atomic force micrographs of (A) a *C. jejuni* strain 81-176 cell (Bar: 1  $\mu\text{m}$ ) and of (B) OMVs on the surface of a *C. jejuni* cell (Bar: 100 nm). (C) Electron micrograph of OMVs isolated from *C. jejuni* strain 81-176 (arrows indicate OMVs) (Bar: 100 nm) (Lindmark et al, 2009).

It was hypothesized that OMVs produced by Gram-negative bacteria can invade host cells through four different routes. These routes can require clathrin coated pits, formation of caveolae, and using of lipid rafts or direct membrane fusion (**Fig.1.6**).

Recent research within the field have identified mechanisms whereby OMVs interact with host cells to mediate inflammation and immunity have been studied by several authors (Pathirana & Kaparakis-Liaskos, 2016). OMVs from different pathogens including *H. pylori* (Ismail et al, 2003) *C. jejuni* (Elmi et al, 2012) and *E. coli* (Kaparakis-Liaskos & Ferrero, 2015) have shown to trigger the production of a range of proinflammatory molecules, such as interleukin-8, in human epithelial cells resulting in modulation and control of proliferation (Li et al, 2015b), apoptosis, (Mondal et al, 2016) and immune response.



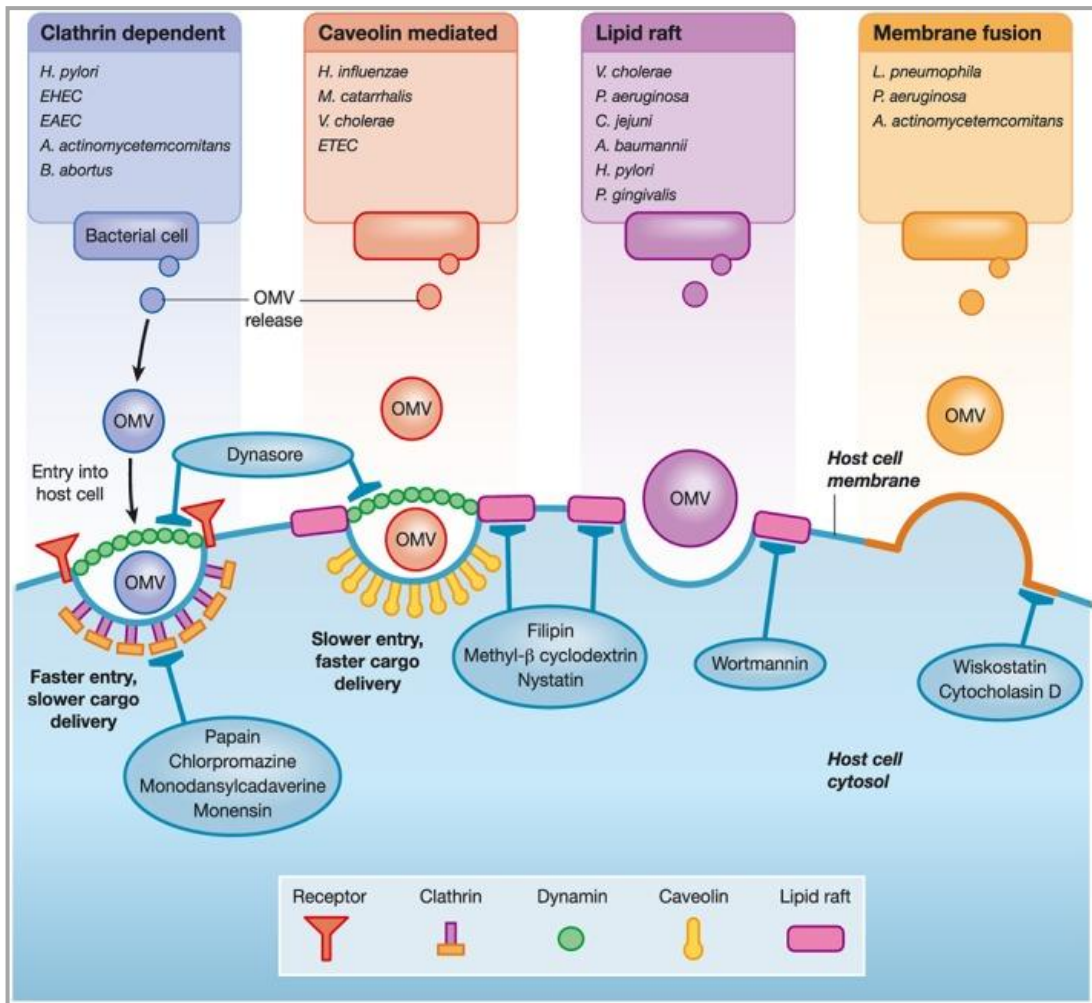


**Fig. 1.6** O' Donoghue et al. demonstrated that OMVs produced by Gram-negative species enter host cells by several different pathways. OMVs entry can be impaired by the use of inhibitors against components of these pathways such as chlorpromazine, papain, monensin-ionophore, monodansylcadaverine, dynasore, methyl-β cyclodextrin, filipin and nystatin; wortmannin, wiskostatin, cytocholasin D (O'Donoghue & Krachler, 2016).

### 1.7 *C. jejuni*-host cell interactions

Bacterial pathogens, especially those with an intracellular life cycle, have shown to be able to manipulate the human host cell to ensure their own survival. Cytoskeletal rearrangements, induction of anti-apoptotic pathways and control of the host cell cycle are all used to benefit bacterial infection and growth (Siegl & Rudel, 2015)

*C. jejuni* infection is a multistep process that includes colonization of the intestinal mucosa and interactions with and invasion of the human intestinal epithelial cells (IECs) (Young et al., 2007). Bacterial factors such as motility, glycosylation and capsule are involved in *C. jejuni* internalization (Szymanski et al, 2002) (Bacon et al, 2001); mutations in these

pathways lead to deficiencies in ability to adhere to and invade host human and animal cells (Hendrixson & DiRita, 2004; Morooka et al, 1985; Watson & Galan, 2008).

*C. jejuni* entry process appears to utilize the host-cell cytoskeleton as observed in many other bacterial pathogens such as *Listeria monocytogenes*, *Shigella flexneri* and *Salmonella typhimurium* (Cossart & Sansonetti, 2004). Unlike these reported bacteria, a recent study suggested that *C. jejuni* is internalized into human intestinal epithelial cells through a microtubule-dependent, actin-independent fashion.

Different strategies are adopted by bacteria in order to survive and replicate within host cells. As a matter of fact, different behaviours can be adopted by *C. jejuni* when invade either phagocytic or non-phagocytic eukaryotic cells. Therefore, *C. jejuni* internalization proceed to specific routes depending on the intracellular environment.

Robert O. Watson et al. reported that *C. jejuni* survives within intestinal epithelial cells by deviating from the canonical endocytic pathway; the bacterium showed the ability to avoid its delivery to lysosomes, where invading bacteria are commonly killed, shortly after internalization (Watson & Galan, 2008). In epithelial cells, *C. jejuni* is able to construct an intracellular niche known as *Campylobacter*-containing vacuole (CCV). *C. jejuni* can modify the CCV to suit its metabolic needs and survive. CCVs are distinct from lysosomes and are functionally separated from the canonical endocytic pathway; indeed, they are not accessible to endocytic tracers (Watson & Galan, 2008). It was also hypothesized that *C. jejuni* internalization is caveolin-1 dependent. A caveolin-1-stabilized lipid membrane may be required for a proper signaling through tyrosine kinases, which are also required for *C. jejuni* internalization rather than for endocytosis. As a matter of fact, efficient signaling through receptor tyrosine kinases requires lipid rafts or caveolae (Helms & Zurzolo, 2004) (Simons & Toomre, 2000). In addition, CCVs showed to contain LAMP-1 (lysosomal-associated membrane protein-1), an endocytic marker, that marks the end stage, when late endosomes are fused with lysosomes (Eskelinen, 2006). At the final stages of endocytosis, to degrade bacteria endolysosomal vesicles are formed in eukaryotic cells (Hamasaki & Yoshimori, 2010; Huang & Brumell, 2009)

On the contrary, *C. jejuni* seems not to be able to deviate this system in professional phagocytes like macrophages, which are specialized to engulf and rapidly kill bacteria (Kiehlbauch et al, 1985; Wassenaar et al, 1997), but contradictory papers are present in literature about this issue. Despite of the phagocytic activity of macrophages, it was supposed that *C. jejuni* was able to infect and utilizes monocytes for its spreading in humans and animals (Hickey et al, 2005). Hickey TE et al. showed that *C. jejuni* 81-176 was capable of

extensive replication within human monocytic cell vacuoles and induced apoptotic death by means cytolethal distending toxin. Michael A. Jones et al. also confirmed that monocytes and macrophages are important cell types with which *C. jejuni* interacts in mammals (Jones et al, 2003). These might be relevant in perpetuating the inflammatory disease because it has been shown that *C. jejuni* can persist within peripheral blood monocytes for up 7 days (Kiehlbauch et al, 1985). Moreover, monocytic cells could be important contributors to the induction and maintenance of gut inflammation because express a range of cell receptors such as CD14 and CD11a, which are involved in cell signaling in response to different bacterial pathogen-associated molecular patterns (Galdiero et al, 2001).

In addition, previous studies reported that monocytes play an important role in the control of immune-related diseases like GBS. Once in circulation, they can migrate into the tissues and have the potential to differentiate into macrophages or particular types of dendritic cells. Taken together, these data confirm that *C. jejuni* can survive intracellularly in both intestinal cells and monocytes, even though more studies are needed to investigate the relationship between *C. jejuni* and monocytes. Understanding *C. jejuni* ability to modulate the cellular environment is key in understanding its ability to cause disease.

### **Lipid rafts**

Lipid rafts are self-organized parts of the lipid bilayer of eukaryotic cells, enriched in sphingolipids, cholesterol and proteins, that represent sub compartments that serve as stabilized platforms for specific biological functions in eukaryotic cells. Hence, the integrity of lipid rafts is important for the correct functionality of trafficking, signaling cascades and other cellular processes (Michel & Bakovic, 2007).

Bacteria can cross epithelial barriers via a transcellular route by exploiting lipid rafts. Bacteria endocytosed via this route appear to avoid lysosomal fusion (Zaas et al, 2005), hence deviating the classical endocytic pathway generally used by cells to kill invading microorganisms.

OMVs have been shown to deliver bacterial virulence factors into host cells by fusion with the host cell plasma membrane or via receptor-mediated endocytic pathways (Ellis & Kuehn, 2010) (Kulp & Kuehn, 2010). Different bacterial pathogens, including *E. coli* (Kesty et al, 2004), *H. pylori* (Kaparakis et al, 2010) and *P. aeruginosa* (Bomberger et al, 2009), produce OMVs that are able to bind lipid rafts. Binding of OMVs to lipid rafts has been reported also

for *C. jejuni*, which seems to be able to deliver its virulence factors by OMVs into human IECs (see 1.6).

In blood cells as well, in particular T cells, lipid rafts can be involved in bacterial invasion; depending on the differentiation status of T cells, lipid rafts seclude various protein receptors involved in cell signaling, cytoskeleton reorganization, membrane trafficking, and the entry of infectious organisms into the cells (Thomas et al, 2004).

### **The Endoplasmic reticulum**

The ER is a large membrane-bound organelle that ensures intra- and inter- molecular disulphide bond formation, protein N-linked glycosylation,  $\text{Ca}^{2+}$  storage, and lipid biosynthesis. These components are subsequently delivered to their destination compartments, which include the ER itself, the Golgi apparatus, the plasma membrane, the extracellular milieu, or the endocytic and autophagic pathways. ER functions are highly interconnected and perturbation in one directly affects the others (Bettigole & Glimcher, 2015). The ER is composed of a series of continuous membranes organized into subdomains that include the rough-, smooth- and transitional-ER, and the nuclear envelope. The rough ER, which is mainly laminar, is associated with polyribosomes for protein synthesis and  $\text{Ca}^{2+}$  signaling. The smooth ER is primarily composed of tubular structures providing the site of lipid biosynthesis, has a main role in  $\text{Ca}^{2+}$  signaling, and is referred as the chief point of contact with other organelles (Park & Blackstone, 2010). For its role in secretory pathways and its biosynthetic functions, the ER stands as a nutrient-rich intracellular location that is presumably devoid of bactericidal functions, such as antimicrobial peptides or hydrolytic enzymes, representing a suitable niche for the intracellular survival, persistence and proliferation of intracellular bacterial pathogens.

ER plays also a crucial role in cellular homeostasis by modulating processing and folding of secretory membrane proteins. When protein folding in the ER is compromised or protein folding requirements exceeds, unfolded or misfolded proteins accumulate and induce ER stress. ER stress leads to the activation of the unfolded protein response (UPR), an evolutionary conserved cytoprotective signalling pathway, to restore normal ER functioning (Schroder & Kaufman, 2005) (van Schadewijk et al, 2012).

The UPR can be directly activated by certain secreted bacterial virulence factors, such as pore forming toxins (Bischof et al, 2008), subtilase cytotoxin (Wolfson et al, 2008) and cholera toxin (Cho et al, 2013) (**Table 1.1**). These toxins induce UPR by activating UPR mediators

directly. Microorganism-mediated UPR modifications therefore tune the quality and the magnitude of the immune response. On the contrary, bacteria like *Legionella pneumophila* modulate the cellular environment by suppressing the UPR via multiple mechanisms (Treacy-Abarca & Mukherjee, 2015). *L. pneumophila* is a Gram negative intracellular bacteria that can survive and replicate within eukaryotic cells; this ability is essential for its virulence.

Bacteria	Toxin or effector	Effect	Mode of action	Refs
<i>Brucella abortus</i>	VceC	Induces the UPR	BiP binding	62
	BspC, BspG, BspH, Bspl and BspK	Induces the UPR	N.D.	60
<i>Brucella melitensis</i>	TcpB	Induces the UPR	N.D.	69
<i>Escherichia coli</i> (Shiga toxin-producing)	Subtilase (SubAB)	Activates IRE1, ATF6 and PERK	BiP degradation	75–77
	Shiga toxin 1 (Stx1A)	Activates IRE1	IRE1 binding?	103
<i>Helicobacter pylori</i>	VacA	Induces the UPR	PERK activation	67,68
<i>Listeria monocytogenes</i>	Listeriolysin O	Induces the UPR	Intracellular calcium imbalance?	70
<i>Mycobacterium tuberculosis</i>	N.D.	Induces ER stress	N.D.	66
<i>Simkania negevensis</i>	N.D.	Inhibits the UPR	N.D.	40
<i>Vibrio cholerae</i>	Cholera toxin (CTA)	Activates IRE1	IRE1 binding	2
Various	Pore-forming toxins	Activates IRE1 and ATF6	p38 MAPK pathway activation	74

ATF6, activating transcription factor 6; BiP, binding immunoglobulin protein; ER, endoplasmic reticulum; IRE1, inositol-requiring enzyme 1; MAPK, mitogen-activated protein kinase; N.D., not determined; PERK, protein kinase R (PKR)-like ER kinase; UPR, unfolded protein response.

**Table 1.1** At present, it has been found that UPR can be directly activated by many secreted bacterial virulence factors (Celli & Tsois, 2015).

Bacterial interactions with the UPR are intricate. Recent findings support that UPR is a key component of the crosstalk among ER, intracellular bacteria and their pathogenic activities.

Bacteria may adapt to live in the ER resulting in UPR subversion that promotes the proliferation of intracellular bacterial pathogens; meanwhile, UPR may contribute to inflammatory and immune responses against invading bacteria. Modulation of ER functions during infection can promote bacterial infection by providing a replicative niche, but at the same time the resulting disruption of the secretory pathway can provide a pattern of pathogenesis that aids the innate immune system in recognizing intracellular infection and in mounting an appropriate defence. However, considering the more rapid evolution of bacterial pathogens compared to their hosts, it is likely that bacteria have evolved to modulate the UPR to their advantage during infection (Celli & Tsois, 2015)

UPR modulates genes required for protein folding, protein degradation, glycosylation, lipogenesis, Ca<sup>2+</sup> signalling and autophagy in order to correct the offending agent that trigger the ER stress. Biochemically, UPR is mediated by three ER stress receptors: protein kinase RNA-like ER kinase (PERK), inositol-requiring protein-1 (IRE-1) and activating transcription factor-6 (ATF6).

During steady state, all these ER stress receptors are maintained in an inactive state through their association with the ER-chaperone protein GRP78 (BiP). Having BiP higher affinity for misfolded proteins than for UPR mediators, under stress conditions, BiP dissociates from IRE-1, PERK and ATF6, leading to their activation and initiation of the UPR (**Fig.1.7**).

Activation of IRE-1, PERK and ATF6 initiates signalling pathways of the UPR to restore homeostasis in the ER, via increasing the production of chaperones to assist in protein folding, arresting translation of proteins not involved in resolving ER stress, and degradation of misfolded proteins via the ER-associated degradation (ERAD) pathway.

ERAD is the process by which misfolded or unassembled proteins are destroyed in eukaryotic cells. This complex system involves recognition of degradation signals, dislocation of proteins across the ER membrane and degradation by the ubiquitin-proteasome system in the cytoplasm.

Dissociation of BiP from PERK leads to autophosphorylation and thereby PERK activation. Activated PERK phosphorylates the  $\alpha$  subunit of eukaryotic transcriptional initiation factor (eIF2 $\alpha$ ), resulting in the inactivation of eIF2 $\alpha$  and translational attenuation by interfering with 5'-cap assembly (Harding et al, 1999) (Harding et al, 2000), which prevents further accumulation of unfolded proteins in the ER (Luchetti et al, 2017). General translational inhibition results in an increase in cap-independent translation, facilitating the accumulation of the transcription factor ATF4 (Vattem & Wek, 2004). Afterward, ATF4 transcriptionally upregulates the transcription factor C/EBP homologous protein (CHOP) (Ma et al, 2002), which has been shown to modulate apoptosis in different cellular stress conditions.

The second arm of the UPR is initiated by ATF6. Dissociation of BiP from ATF6 leads to translocation of ATF6 to the Golgi complex where it is cleaved by site-1 and site-2 proteases into an active transcription factor. The resulting cytoplasmic fragment liberated from the membrane enters the nucleus resulting in transcriptional activation of its target genes (Yoshida et al, 2000) (Yoshida et al, 2001), such as BiP, CHOP and X-box binding protein (XBP1). In this manner ATF6 indirectly regulates autophagy and apoptosis via XBP1 and CHOP (Song et al, 2017).

IRE1 $\alpha$  is a multifunctional protein that possesses kinase and endonuclease activities. Dissociation of BiP from the luminal domain of IRE1 $\alpha$  leads to its homodimerization and autophosphorylation which triggers the excision of 26 base pairs from the XBP1 mRNA, and subsequent mRNA relegation causes a translational reading frame shift yielding the highly active transcription factor known as XBP1s (Calton et al, 2002). XBP1s forms a heterodimer with pATF6(N) and binds to the enhancer element called the UPR element, resulting in the

transcriptional activation of ERAD genes such as HRD1, EDEM and Derlins (Lee et al, 2003), leading to transcription of ER-chaperone proteins. The splicing of XBP1 mRNA is considered to be an ER stress marker. The IRE1 $\alpha$ -signalling axis is the most highly conserved branch of the UPR, it is present across species from yeast to humans.

All these three branches work cohesively to correct ER stress but can also lead to apoptosis under unresolvable stress conditions. ATF4, XBP1 and ATF6 direct a transcriptional program that upregulates chaperones, components of the ERAD pathway, and factors involved in autophagy and apoptosis that act to restore cellular homeostasis or, if the ER dysfunction cannot be resolved, initiate programmed cell death (Celli & Tsolis, 2015).

XBP1 and ATF6 support the ER folding capacity by upregulating chaperones, glycosylases, ERAD components, intracellular support machinery and protein disulphide isomerases. Moreover, *Xbp1*/IRE1 $\alpha$  may limit the influx of proteins into the ER by degrading ER-localized mRNA. In a parallel branch, PERK stops protein synthesis to allow time for the ER to correct existing misfolded proteins, while downstream its target genes induce an antioxidant response to oppose ROS production generated by iterative protein folding cycles. Temporal and branch-specific UPR control is crucial for determining adaptation versus survival (Lin et al, 2007): indeed, depending on the stress conditions either prosurvival IRE1 or PERK remain activated. Successful neutralization of the instigating stress results in cell survival, whereas the outcome for failure is cell death.

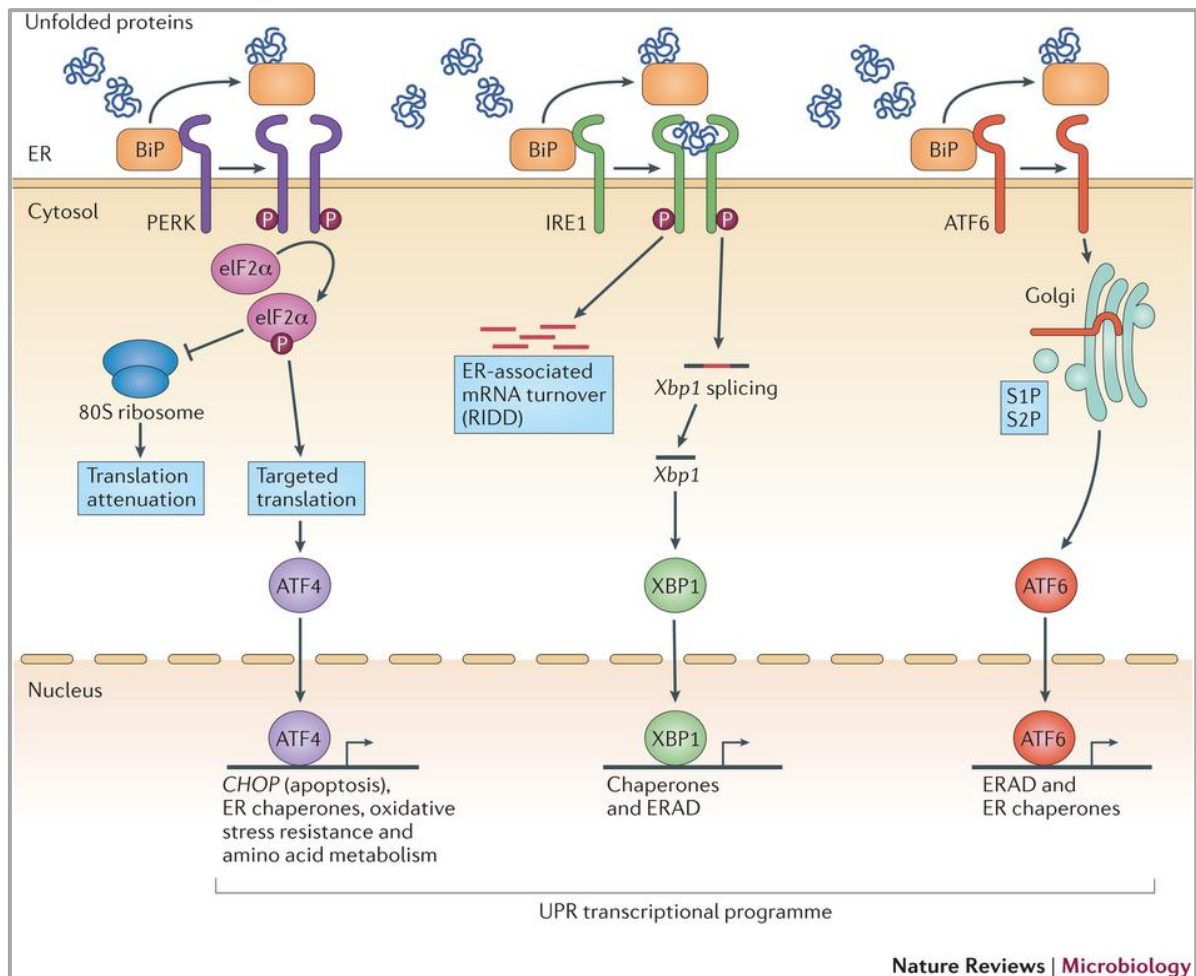


**Fig. 1.7** UPR mediators are held inactive by BiP protein, but under stress conditions, BiP dissociates from these three mediators, leading to their activation (Bettigole & Glimcher, 2015).

The UPR can be induced *in vitro* by chemicals such as Thapsigargin and Tunicamycin. Thapsigargin blocks the ER  $\text{Ca}^{2+}$  ATPase pump causing ER  $\text{Ca}^{2+}$  store depletion, and Tunicamycin blocks N-linked glycosylation of proteins. These two chemicals, leading to high levels of stressors, rapidly activate all three components of UPR (Rutkowski & Kaufman, 2004)

The effective immunity depends on ER homeostatic processes such as  $\text{Ca}^{2+}$  signalling, metabolism of lipids, glycosylation and oxidative protein folding. These same pathways, which are required to support the immune system functioning, are modulated by UPR. For instance, lipid metabolism has a central role in immune cell function. Membrane fluidity regulates lipid rafts formation, which are also crucial in *C. jejuni* infection, receptor clustering and signalling dynamics. IRE1 and PERK can directly induce biosynthesis of fatty acids, phospholipids and cholesterol, likely to safeguard intracellular membrane homeostasis.



Protein glycosylation has also an important role in the immune system by regulating cell-trafficking, surface receptors dynamics and apoptosis.

Autophagy is a key immunological process charged with degrading proteins aggregates, damaged organelles and intracellular pathogens (see 2.2). It facilitates antigen processing and presentation on both MHC-I and MHC-II, capturing and killing of intracellular microbes, efferocytosis, production of type I interferon and cell survival and differentiation. Chemical ER stress can induce autophagy via IRE1 and PERK pathways (Ogata et al, 2006); *in vivo* other UPR components may be involved.

## **2. Mechanisms of cell death**

While philosophers seek the meaning of life, cell biologists are becoming ever more interested in the meaning of death (Savill & Fadok, 2000). Early and last papers about cell death distinguish three distinct mechanisms of programmed cell death that are named apoptosis, autophagy and necrosis (Fuchs & Steller, 2015).

Apoptotic and autophagic events are going to be described below (see 2.1 and 2.2). Necrosis is characterized by organelle and cellular swelling, rupture of the plasma membrane and release of the intracellular content (Vanden Berghe et al, 2014). The necroptosis is a non-apoptotic mode of cell death that is elicited by TNF receptor 1 (TNFR1) when caspases are inhibited (Degterev et al, 2005); necroptosis has often been regarded as synonymous with regulated necrosis (Galluzzi et al, 2014).

The functional relationship between apoptosis ('self-killing') and autophagy ('self-eating') is intricate in the sense that, under certain circumstances, autophagy constitutes a stress adaptation that avoids cell death (and suppresses apoptosis), whereas in other cellular settings, it constitutes an alternative cell death pathway. Depending on the upstream signals and the different instances, cells activate one or both of these responses; they can combine them or switch between the two responses in a mutually exclusive manner (Maiuri et al, 2007).

### **2.1 Apoptosis**

Previous papers reported that CDT causes cell cycle arrest and cell death in a range of target cells (Canonica et al, 2014; Shenker et al, 2001; Svensson et al, 2001), upon cell cycle arrest DNA repair occurs and cell apoptosis results. Apoptosis has since been recognized and accepted as a distinctive and important mode of “programmed” cell death, which involves the

genetically determined elimination of cells. It occurs normally during development and aging and as a homeostatic mechanism to maintain cell populations in tissues. It is also thought that apoptosis is a defense mechanism such as in immune reactions or when cells are damaged by disease or noxious agents (Norbury & Hickson, 2001). Apoptosis marks unwanted cells with 'eat me' signals that are going to be recognized by phagocytes which mediate their engulfment and degradation (Savill & Fadok, 2000).

In the last decade, many apoptotic cascades have been described with the attempt to categorize all signal transduction pathways that lead to cell death, such as intrinsic and extrinsic, mitochondrial and death receptor (DR), p53-dependent and -independent, and caspase-dependent and -independent pathways in association with initiation, commitment, and execution phases (Ashe & Berry, 2003).

Apoptotic event is a highly conserved process, firstly studied on *Caenorhabditis elegans* (Horvitz, 1999). In biochemical terms, two distinct phases in apoptosis can be recognized, the initiation and execution phase. In accord with the source of the triggers, that can be extracellular or intracellular, intrinsic and extrinsic mechanisms of initiation can be defined. For these reasons, apoptosis can be classified in intrinsic and extrinsic pathways. Intrinsic pathway can be triggered by intracellular signals, for example by DNA damage, and involves specifically mitochondria; whilst the extrinsic pathway can be triggered by extracellular signals, for example, by growth factor withdrawal, steroid hormones, ligation of death receptors. Both these apoptotic cell death systems are mediated by molecular pathways that culminate in the activation of a family of cysteine proteases, known as the caspases, which orchestrate the dismantling and clearance of the dying cell. Activated caspases generate a cascade of proteolytic and nucleolytic events that amplify the initial signal (the execution phase). However, different studies indicate that a cell that has been treated with an apoptotic inducer can also initiate a suicide programme that does not rely on caspase activation (Chipuk & Green, 2005); therefore apoptotic cell death can be distinguished in caspase-dependent and caspase-independent apoptosis.

Light and electron microscopy have identified the various morphological changes that develops during apoptosis. During the early process it is possible to observe cell shrinkage and pyknosis by light microscopy; in this stage, cells are smaller in size, the cytoplasm is dense, the organelles are more tightly packed, and the chromatin is condensate. Then, extensive plasma membrane blebbing occurs followed by karyorrhexis and separation of cell fragments into apoptotic bodies during a process called "budding." During this process the organelle integrity is still maintained and an intact plasma membrane encloses all the

intracellular content. After execution phase, these bodies are subsequently phagocytosed by macrophages, parenchymal cells, or neoplastic cells and degraded within phagolysosomes.

Unlike necrosis, this programmed cell death does not cause inflammatory reactions because apoptotic cells are rapidly phagocytosed avoiding the release of the intracellular content and anti-inflammatory cytokines are not produced by engulfing cells (Kurosaka et al, 2003).

Phagocytosis is due to the expression of cell surface markers that result in the early phagocytic recognition of apoptotic cells by adjacent cells. This is achieved by the movement of the normal inward-facing phosphatidylserine of the cell's lipid bilayer to expression on the outer layers of the plasma membrane (Bratton et al, 1997).

Although externalization of phosphatidylserine is a well-known recognition ligand for phagocytes on the surface of the apoptotic cell, recent studies have shown that also other proteins, such as Annexin I and calreticulin, could be as important as phosphatidylserine.

Annexin V is a recombinant phosphatidylserine-binding protein that interacts strongly and specifically with phosphatidylserine residues and is largely used in cytometry, for the detection of apoptosis (Arur et al, 2003).

### **2.1.1 Bcl-2 family proteins**

Bcl-2 family proteins are considered to be key regulators of apoptosis. All family members share homology with the archetypal member of the family, B-cell lymphoma-2 protein (Bcl-2), which contains four Bcl-2 homology domains: BH 1-4. Bcl-2 family proteins can be functionally subdivided into anti-apoptotic (Bcl-2, Bcl-XL, Bclw, Mcl-1) and pro-apoptotic members. Two subfamilies of pro-apoptotic Bcl-2 family members have been identified: 'BH3-only' family, containing only a catalytic domain BH3 (Bid, Bim, Bik, Bad, Bmf, Hrk, Noxa, and PUMA), and 'multidomain' family, also named Bax family, containing BH1, BH2, and BH3 domains (Bax, Bak e Bok). One of the 'BH3-only' protein function is activating the multidomain family members Bax and Bak.

Depending on the prevalence of either pro-apoptotic or anti-apoptotic members, the destiny of the cell is decided. It was demonstrated that Bcl-2 proteins are necessary for the completion of apoptotic programs (Wei et al, 2001) (Yin et al, 2002).

Core members of the Bcl-2 family share structural similarity with the pore-forming domains of bacterial toxins, emphasizing the relevance of these proteins to membrane biology (reviewed by (Schendel et al, 1998). Several Bcl-2 family proteins insert into intracellular

membranes, particularly membranes of mitochondria and endoplasmic reticulum (ER), operating as guardians of these organelles.

Many Bcl-2-family proteins, both anti-apoptotic and pro-apoptotic, have C-terminal transmembrane domains that insert in the outer membrane of mitochondria. Pro-apoptotic proteins such as Bax and Bak induce mitochondrial outer membrane permeabilization (MOMP), causing the release of caspase-activating proteins and other cell death mediators; Bax or Bak are necessary for MOMP and for controlling the permeability of mitochondrial membranes. Mitochondria induce apoptosis by releasing proteins that participate in caspase activation (for example, cytochrome c) and by neutralizing inhibitors of caspases (Reed, 2002).

About ER, it was found that overexpression of anti-apoptotic Bcl-2 proteins seem to protect cells against cell death induced by ER stress (see The endoplasmic reticulum section), whereas pro-apoptotic Bcl-2-family proteins (such as Bax or Bak) are required (Scorrano et al, 2003). But how Bcl-2-family proteins regulate ER-initiated cell death mechanisms is unclear.

Bcl-2 family proteins are also present in lysosomes where have a critical role of cell life and death mediators. Lysosomes participate to apoptosis and necrosis, and are also critically involved in autophagy. Therefore, upon overexpression of either anti-apoptotic or pro-apoptotic proteins, lysosomes can mediate cell survival or death (Pattingre et al, 2005)

### **2.1.2 Extrinsic and intrinsic pathway**

Extrinsic pathway is activated by the transduction of the apoptotic signal after the binding of death receptors, for example Fas, TNF receptor 1 (TNFR1) and TNF-related apoptosis inducing ligand (TRAIL) receptor R1 and R2, to their ligands FasL, TNF and TRAIL. On the contrary, the intrinsic pathway of apoptosis is mediated by mitochondria and is regulated by the Bcl-2 protein family. In a possible scenario of extrinsic pathway, the binding of Fas ligand (FasL) to its receptor Fas leads to the cleavage and activation of pro-caspase 8 to initiator caspase 8. This step can be mediated by the adaptor protein Fas-associated death domain protein (FADD) and can be inhibited by FADD-like apoptosis regulator (also known as FLIP), a catalytically inactive homologue of caspase 8. Subsequently, initiator caspase 8 cleaves and activates caspase 3 and caspase 7 leading to the degradative phase of apoptosis.

The intrinsic pathway of apoptosis is regulated by Bcl-2 family proteins (see 2.1.1) ‘BH3-only’ proteins can either sequester anti-apoptotic proteins, or directly activate the

‘multidomain’ proteins, such as BAK and BAX. Once the apoptotic signalling is initiated, Bak and Bax induce the release of cytochrome C from the mitochondrion leading to its binding to APAF1 and the formation of a complex with pro-caspase 9, known as apoptosome that is thought to initiate apoptosis (Rodriguez & Lazebnik, 1999). Activation of caspase 9 in the apoptosome in turn induces apoptosis through the activation of caspase 3 and caspase 7. An alternative pathway of Fas-induced cell death involves crosstalk between the extrinsic and the intrinsic apoptotic pathways. This crosstalk is mediated by the cleavage of Bid that leads to the formation of truncated Bid, which interacting with Bak or Bax, is able to modify mitochondrial permeability leading to cytochrome C release from mitochondria. Bak or Bax expression can also be regulated by p53 (Vousden & Lane, 2007) (Marino et al, 2014) (**Fig. 1.8**).

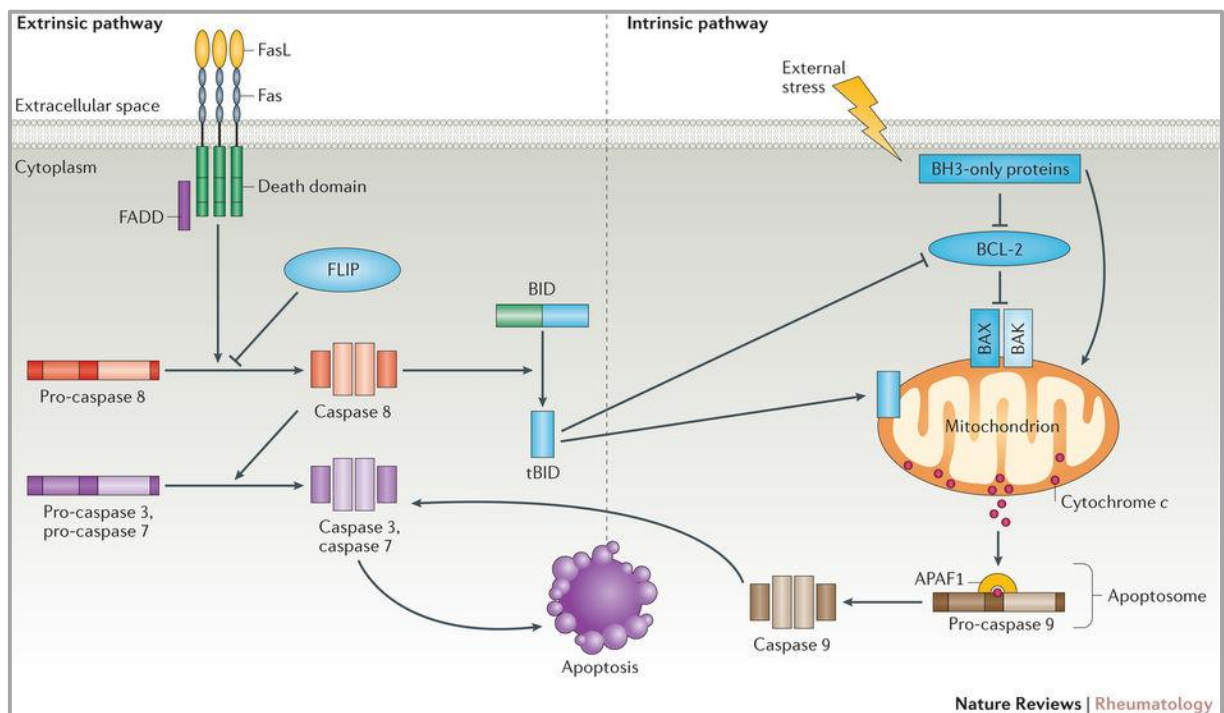


**Fig. 1.8** Extrinsic and intrinsic apoptotic pathways (Cuda et al, 2016).

### 2.1.3 pRb, p53 and CD59

The tumour suppressors *pRb* (retinoblastoma protein) and *p53* are genes which encode for products that negatively affect the cell cycle progression thus protecting the cell from the accumulation of potentially tumorous mutations. Respectively, to control the cell cycle progression, pRb negatively regulates the transcription factor E2F, whereas p53 inhibits the

cell growth by up-/down- regulating genes involved in apoptosis, cell cycle, senescence and differentiation, DNA repair, transcription and translation as well as cytoskeleton, cell adhesion, angiogenesis and migration (Menendez et al, 2009). For these reasons *p53* has many functions in genomic stability control, apoptosis, metabolism and antioxidant defence (Siegl & Rudel, 2015). Apoptosis induction is one of the main tumour suppressor activities of *p53* (Schmitt et al, 2002). In recent years, numerous bacterial pathogens, such as *H. pylori*, *C. trachomatis*, *S. flexneri* and *N. gonorrhoeae* have been shown to inactivate *p53*, through ubiquitin-proteasome degradation system, to block the protective response of the host cell. The degradation of *p53* seems to prolong survival of the pathogen's niche, nevertheless, also other ways to modulate *p53* were observed in pathogens. Anyway, these evidences support the hypothesis that *p53* mediates host defence and cell fate during bacterial infection. It was also found an association among inflammation, upregulation of *p53* levels and CD59 (MIRL) (Nalca & Rangnekar, 1998; Sampaziotis et al, 2002) and It was supposed that *p53* was a direct regulator of the immune response by modulating CD59 levels.

The GPI-protein CD59 is expressed on the surface of neutrophils, monocytes and erythrocytes in order to protect them from the Complement-mediated cell lysis.

Complement is an important component of innate immunity and modulator of adaptive immunity, particularly important for defence against bacterial infections and the efficient removal of debris. The membrane attack complex (MAC) is the pore-forming toxin of the complement system, a relatively early evolutionary acquisition that confers upon complement the capacity to directly kill pathogen, some authors define MAC as a 'bactericidal missile' (Morgan et al, 2017). The role of CD59 is to inhibit the formation of the MAC. CD59 is also involved in the classical endocytic pathway, by facilitating the endocytosis process (Conner & Schmid, 2003). For these reasons many pathogens use CD59 as entrance to infect host cells. CD59 upregulation might lead to complement inhibition and protection of the bacteria from the complement, this could be an optimal expedient for bacteria to prevent the complement attack. Recent studies also associated defects in CD59 on blood cells with recurrent GBS (Mevorach et al, 2016), suggesting that this molecule might have an important role in interaction between bacteria and blood cells and therefore in the onset of GBS. To date, only in one paper the relationship between CD59 and *C. jejuni* is described (Canonica et al, 2014).

## **2.2 Necrosis**

The ability to control/manipulate timing and mode of death in infected host cells plays a pivotal role in many microbial infections. Control of cell death by the host can be used to manage microbial spread and enhance the induction of immunity; conversely, the manipulation of host cell death pathways is exploited by many viral and microbial pathogens as part of their life cycle. In contrast to apoptosis, necrosis is marked by rapid loss of plasma membrane integrity. Plasma membrane leakage in necrosis is widely thought to occur prior to or concomitant with exposure of phosphatidylserines and other 'eat-me signals'. This early rupture of the plasma membrane releases endogenous danger signals or damage-associated molecular patterns, which are potent stimulants of inflammation (Butler et al, 2012). A necrosis-like form of death has been observed and it demonstrated to allow the release of viable bacteria for subsequent re-infection. The necrotic cell death may be an important factor in granuloma formation, inflammatory tissue damage and ultimately bacterial transmission. It was shown that it can occur through defined biochemical programs and it is negatively regulated by caspase activity (Sun & Wang, 2014).

## **2.3 Autophagy**

Autophagy is a catabolic process involving the degradation of cytoplasmic components, protein aggregates and organelles by forming autophagosomes, which are degraded by fusion to lysosomes (Mizushima & Komatsu, 2011). Therefore, the vesicles that fuse with lysosomes and the sequestered material contained into them is degraded. Monodansylcadaverine (MDC) is a specific autophagolysosomes marker typically used to investigate at the molecular level the autophagic machinery (Munafo & Colombo, 2001).

Although in many scenarios autophagy contributes to cell death, it has a protective, pro-survival function. Some evidences showed that in mice autophagy is an alternative killing mechanism which is activated where apoptosis cannot be executed (Lum et al, 2005) (Shimizu et al, 2004), other ones indicate that it enable the classic hallmarks of apoptosis, such as phosphatidylserine exposure and membrane blebbing, which represent the 'find-me' and 'eat me' signals of the apoptotic process (Qu et al, 2007).

Autophagy can be induced by several conditions, including starvation, hormone treatment (van Sluijters et al, 2000) and stress (Schwartz et al, 1992), and it occurs in several subsequent stages. It is involved in cell death and tumour suppression, neurodegeneration, ageing,

inflammation, immunity and genome stability. We also know that apart from starvation, autophagy is induced by many other perturbations, including hypoxia and metabolic, osmotic and oxidative stresses (Farre & Subramani, 2016)

At first, cytoplasm and various organelles such as endoplasmic reticulum, mitochondria and peroxisomes are sequestered by a membrane in order to generate an autophagosome. Nascent autophagosomes engender by a structure named phagophore or isolation membrane. In mammalian cells, phagophore membranes appear to initiate primarily from the ER in dynamic equilibrium with other cytosolic membrane structures, such as the trans-Golgi. Secondly, autophagosome fuses with lysosomes and acquires lysosomal membrane proteins and enzymes. The sequestered material is finally degraded in vesicles called autophagolysosomes or autolysosomes. Material digested during the degradation process is then recycled and reabsorbed by the cell.

Lysosomes are also involved in another degradation process: the lysosomal exocytosis. This is defined as a process that a lysosome responds to extracellular stimuli, docks at the interior of the cell surface and fuses with the plasma membrane to their contents (Blott & Griffiths, 2002). Through this process, lysosomes secrete their content within the extracellular space. This phenomenon can be detected via translocation of lysosomal membrane proteins, such as LAMP-1, on the plasma membrane. In this way, lysosomes fuse with plasma membrane through a  $\text{Ca}^{2+}$  regulated mechanism resulting in the release of the lysosomal content within the extracellular space. This process is also important in mechanisms of defence against bacterial infections (Roy et al, 2004).



## Aims and objectives

The aim of this work was to investigate the effects of *C. jejuni* virulence factors in human cells focusing the attention on cellular pathways that this bacterium might activate or deactivate during host cell infection to enhance its invasion and persistence. Among the several virulence factors, the CDT was the most investigated. For this purpose, the effects induced by three different *C. jejuni* wild type strains was compared with the effects induced by the *C. jejuni cdtA* mutant strain in three different cell lines: monocytes isolated from donor's blood, tumour myeloid cells (U937) and human intestinal epithelial cells (T84). To infect abovementioned cell lines, *C. jejuni* strains were used in three different forms: as bacterial lysates, as OMVs and as whole bacteria. This allowed us to investigate the importance of OMVs and whole bacteria during *C. jejuni* infection. Although it is well known that intestinal epithelial cells are typical *C. jejuni* target cells, much less is known about the relationship between *C. jejuni* and monocytes. This topic was particularly investigated in this work since in the last two decades it was assumed a possible critical role of monocytes and macrophages in GBS onset.

The objectives of this work were:

- Investigating the effects of two wild type strains, *C. jejuni* ATCC 33291 and *C. jejuni* ISS 1, and a *C. jejuni* 11168H *cdtA* mutant strain in human monocytes previously isolated from donor's blood focusing the attention on pro-survival and pro-apoptotic pathways.
- Investigating the effects of two wild type strains, *C. jejuni* ATCC 33291 and *C. jejuni* ISS 1, and a *C. jejuni* 11168H *cdtA* mutant strain in human tumour myeloid cells (U937), focusing the attention on apoptotic and autophagic pathways.
- Investigating the effects of OMVs previously isolated from *C. jejuni* 11168H wild type and *C. jejuni* 11168H *cdtA* mutant strains in U937 cells in order to compare the effects of the lysates with the effects of the OMVs in this specific cell line.
- Investigating the effects of whole cells and OMVs from *C. jejuni* 11168H wild type and *C. jejuni* 11168H *cdtA* mutant strain in human intestinal epithelial cells (T84) to study the ER stress and UPR activation.
- The construction of a *C. jejuni* 11168H *cdtA* mutant in the GFP strain by using a methodology based on the electroporation of a recipient *C. jejuni* strain with a linear PCR fragment carrying an antibiotic resistance cassette and the kanamycin cassette.

## Materials and Methods

### 3. Human tumour myeloid cells (U937) and normal monocytes

#### 3.1 Ethic statement

PBMCs (peripheral blood mononuclear cells) were isolated from buffy coats of anonymized donors obtained from the Transfusion Centre of Urbino Hospital. No specific approval from an institutional review board was required for the use of buffy coats for the following reasons: (1) no personal patient information was made available; (2) buffy coats could not be used for treatment of patients and were waste products for the blood transfusion centre and (3) blood donors were verbally informed that parts of the donation that cannot be used for patient treatment may be used for scientific research.

#### 3.2 Bacterial strains

<i>C. jejuni</i> strains	Description	References
11168H <i>cdtA</i> mutant	Isogenic mutant of <i>Cj0079</i> obtained from <i>Campylobacter</i> mutant bank <a href="http://crf.lshtm.ac.uk/wren_mutants.html">http://crf.lshtm.ac.uk/wren_mutants.html</a>	LSHTM mutant bank
ATCC 33291	<i>Campylobacter jejuni</i> subsp. <i>jejuni</i> (ATCC® 33291™)	ATCC®, U.S.A
ISS 1	<i>Campylobacter jejuni</i> subsp. <i>jejuni</i> obtained from ‘Istituto Superiore di Sanità’ <i>Campylobacter</i> bank. Clinical strain isolated from stool specimen of patients with gastroenteritis; PCR characterized for the presence of the CDT virulence genes <i>cdtA</i> , <i>cdtB</i> , <i>cdtC</i> .	Istituto Superiore di Sanità, Italy

### 3.3 Growth conditions

*C. jejuni* strains were revived from -80 glycerol stocks (see 4.2) by pipetting onto blood agar plates containing autoclaved Columbia agar base (Oxoid, U.K) supplemented with 7% (vol/vol) horse blood (Oxoid) and *Campylobacter* Selective Supplement (Oxoid). Strains were routinely sub-cultured every 3-4 days up to a maximum of 10 passages. *C. jejuni* cultures were grown in pre-equilibrated Brucella broth (Oxoid) in 50 ml bottles (Duran, Germany) with shaking at 120 rpm on a 3005 analogue orbital shaker (GFL, Germany) in microaerophilic conditions.

### 3.4 Cell lines and monocytes isolation

U937 (human myelomonocytic cell line) cells (Sigma-Aldrich, U.S.A) were grown in RPMI (Roswell Park Memorial Institute) 1640 supplemented with 10% heat-inactivated fetal bovine serum (FBS), 2 mM glutamine, 25 mM HEPES pH 7.5, and 1% antibiotics and was maintained at 37°C in humidified air with 5% CO<sub>2</sub>. PBMCs were isolated from freshly collected buffy-coat preparations of whole human blood from healthy donors. To harvest monocytes from the peripheral blood, buffy coats were subjected to a double density gradient centrifugation as described below (Menck et al, 2014). 30-35 ml of buffy coat was layered on top of the Ficoll-Paque<sup>TM</sup> Plus solution (GE Healthcare, U.K) into a 50 ml centrifuge tube for the first density gradient. The sample was centrifuged at 400 x g without brake for 30 min at room temperature (RT) and the white ring of PBMCs which is located between the two phases was collected with a serological pipette and was transferred to a 50 ml centrifuge tube. The tube was filled with PBS-EDTA (1 mM), up to 40 ml in total, and centrifuged at 300 x g for 10 min without brake at RT. The resultant supernatant was aspirated and the pellets were washed with 40 ml PBS-EDTA (1 mM). For each donor the resultant pellets, containing PBMCs, were pooled in 20 ml RPMI-1640 without phenol red + 10% FBS. For the second density gradient the iso-osmotic Percoll solution (density: 1.131 g/ml) was prepared as described in the protocol (Menck et al, 2014). For each donor 25 ml of the prepared Percoll solution was transferred to a 50 ml tube and the PBMC solution previously prepared was layered on the top of the Percoll solution. The tubes were centrifuged at 550 x g without brake for 30 min at RT. For each gradient the white ring containing monocytes, which is located between the two phases, was collected with a serological pipette and transferred to a 50 ml centrifuge tube. Monocytes were washed with PBS-EDTA (1 mM) by centrifugation at 400 x

g for 10 min without brake at RT. The supernatant was aspirated and pellets were resuspended in RPMI 1640 medium supplemented with 10% FBS, 2 mM l-glutamine, 100 U/ml penicillin and 100 mg/ml streptomycin and incubated in 5% CO<sub>2</sub> at 37°C in polylysine-coated 6-well tissue-culture plates. After 24 hours, non-adherent cells were removed by gentle washing and adherent cells remained in culture were used for subsequent assays.

### **3.5 *C. jejuni* cell lysate preparation**

*C. jejuni* ATCC 33291, *C. jejuni* ISS 1 and *C. jejuni* 11168H *cdtA* mutant strains were grown in 50 ml Brucella broth (Oxoid) at 37°C in a shaking incubator under microaerophilic condition for 48 hours. The bacterial suspensions were adjusted spectrophotometrically to approximately 10<sup>8</sup> bacteria/ml and centrifuged at 4,000 rpm for 10 min. The pellets were resuspended in 20 ml of Dulbecco's modified eagle medium (D-MEM) (Sigma-Aldrich) and lysed by sonication (2 x 30 s bursts with 30 s intervals between each burst) by using a sonicator (Sonifier 450, Branson, U.S.A). Cell debris and un-lysed bacterial cells were then removed by centrifugation at 4,000 rpm for 10 min. Aliquots of each lysate were sterilized by a 0.22 µm membrane filter (Millipore, Italy) and stored at -20°C before use.

### **3.6 Detection of cytotoxin activity in *C. jejuni* lysates**

U937 cells were seeded into 24-well tissue culture plates at a density of 2.6 x 10<sup>5</sup> cells per well for 2 hours prior to the addition of the lysates diluted 1:5, 1:10, 1:50, 1:100 and 1:500 respectively. The cultures were incubated at 37°C in 5% CO<sub>2</sub> atmosphere and examined microscopically at 24 hours' intervals for 4 days to evaluate morphological changes.

The best acting dilution was the 1:100 which was chosen for all subsequent evaluations. All strains were tested in at least three independent experiments.

### **3.7 Pre-treatment of U937 cells and monocytes with *C. jejuni* lysates**

U937 cells and monocytes were incubated for 6, 12, 24, 48 and 72 hours with 2 ml media enriched with *C. jejuni* cell lysates (1:100 dilution) from ATCC 33291, ISS 1 and 11168H *cdtA* mutant strains previously prepared (see 3.5). Treated cells were analysed by means of flow cytometry and confocal microscopy to evaluate different cellular parameters. For the negative control, cells were incubated with media only.

### **3.8 Pre-treatment of U937 cells with *C. jejuni* OMVs**

U937 cells were incubated for 24, 48 and 72 hours with 2 ml media enriched with OMVs isolated from *C. jejuni* 11168H wild type and 11168H *cdtA* mutant strains. Approximately  $10 \times 10^9$  particles were added to 2 ml media. Treated cells were analysed by means of flow cytometry and confocal microscopy to evaluate different cellular parameters. For the negative control, cells were incubated with media only.

### **3.9 Pre-treatment of U937 cells with Rapamycin**

Rapamycin (RM) is an efficient pharmacological inhibitor of mTOR (mammalian target of rapamycin) which is able to induce autophagy in mammal cells (Sehgal, 2003). mTOR is a complex composed of two entities, mTORC1 (mTOR complex 1) and mTORC2 (mTOR complex 2). mTORC1 is a downstream target of PI3K (phosphoinositide 3-kinase) and is sensitive to the RM (Inoki et al, 2002). mTOR plays an important role in cell growth and proliferation (Wullschleger et al, 2006) and its activation was recently associated to intestinal inflammation induced by *C. jejuni* (Sun et al, 2012). U937 cells were pre-treated with RM 100 nM for 2 hours before the treatment with lysates.

### **3.10 Nanoparticle Tracking Analysis (NTA)**

Isolated OMVs were diluted at 1:100 in PBS and stored at -20°C for further analysis. NTA measurements were performed with a NanoSight LM20 (NanoSight, U.K), equipped with a sample chamber with a 640-nm laser and a Viton fluoroelastomer O-ring. The samples were injected in the sample chamber with sterile syringes until the liquid reached the tip of the nozzle. All measurements were performed at RT.

### **3.11 Morphological feature evaluation**

To evaluate changes in cell morphology and size both cytometry and confocal microscopy were used. In flow cytometry, populations that differ in size and morphology were distinguished by using their physical characteristics: forward scatter (FSC, cell size) and side scatter (SSC, cell granularity). Although a quantitative analysis was carried out in flow cytometry, a qualitative analysis was performed in confocal microscopy.

### 3.12 Flow cytometry and confocal microscopy stainings

#### *Flow cytometric detection of cell death and flow cytometric absolute count*

Cell death features were evaluated using supravital Propidium Iodide (PI) (Sigma-Aldrich) that is capable of binding and labeling DNA. No permeabilized cells were incubated 30 min in the dark with 50 $\mu$ g/ml PI. Cells were washed with PBS and then analysed by flow cytometry. Apoptotic and necrotic cells were detected as PI<sup>dim</sup> and PI<sup>bright</sup> clusters, respectively.

To investigate programmed cell death features (early and late apoptotic, as well as necrotic cells) it was also used a double staining FITC-conjugated Annexin V-PI (AnxV-PI). AnxV allows to detect phosphatidylserines exposed on the outer cell membrane following caspase-activation. AnxV-PI staining was carried out in according to manufacturer's instructions (Immunostep, Spain)

Absolute cell counting was performed by using Dako CytoCount<sup>TM</sup> beads (Thermo Fisher Scientific, U.S.A). 200  $\mu$ l of sample was carefully dispensed at the bottom of the tube and 50  $\mu$ l beads were added. Samples were acquired by using a FACSCanto cytometer (Becton Dickinson, BD, U.S.A) within 60 min. Approximately 20,000 cell events were collected. Set-up and calibration procedures were optimised for the absolute counting protocols (Brando et al, 2000).

#### *Nucleic acid staining*

SYBR GREEN I (Thermo Fisher Scientific) is able to stain nucleic acids. The staining with this fluorochrome was performed with a final dilution of 1:10,000 (Salucci et al, 2013). Samples were analysed by flow cytometry using the appropriate fluorescence channel.

#### *Determination of mitochondrial potential ( $\Delta\Psi_m$ ), mitochondrial mass and mitochondrial reactive oxygen species (ROS)*

Mitochondrial features were investigated by TMRE, NAO and MitoSOX stainings. Tetramethylrhodamine ethyl ester perchlorate (TMRE) (Sigma-Aldrich) is a  $\Delta\Psi_m$ -specific stain able to selectively enter into mitochondria depending on  $\Delta\Psi_m$  producing red fluorescence. TMRE 40 nM was added to the sample 15 min before the acquisition time. Samples were analysed by confocal microscopy and flow cytometry using the appropriate fluorescence channel (Canonico et al, 2014).

The cardiolipin-sensitive probe Nonyl Acridine Orange (NAO) (Sigma-Aldrich) is able to monitor changes in mitochondrial lipids (Luchetti et al, 2012) (Canonico et al, 2016).

In the present study, this probe was used to measure the mitochondrial mass/number independently of mitochondrial membrane potential ( $\Delta\Psi$ ). After a 15 min incubation at 37°C in the dark with 100nM NAO, samples were acquired by flow cytometry using the appropriate fluorescence channels.

MitoSOX Red (Thermo Fisher Scientific) is a fluorogenic dye specifically targeted to mitochondria in live cells. Oxidation of this probe by superoxide that is contained in mitochondria produces a red fluorescence. MitoSOX 5 $\mu$ M was added to the sample 10 min before the time of acquisition. Samples were analysed by flow cytometry using the appropriate fluorescence channel (Canonico et al, 2016).

#### *Assessment of lysosomal involvement*

To label and trace lysosomes in monocytes and U937 cells the acidotropic dye LysoTracker Green (LTG) and LysoTracker Deep Red (LTDR) (Thermo Fisher Scientific) were used. LysoTracker probes are fluorescent acidotropic probes for labeling and tracking acidic organelles in live cell: it means that the amount of fluorescence obtained from staining with LysoTracker is directly related to the volume of lysosome-related organelles in a cell (Chazotte, 2011). Cells were cultured at 37°C and resuspended in pre-warmed (37°C) medium containing 100 nM LysoTracker (diluted in RPMI). After 45 min incubation green lysosomal fluorescence was detected by flow cytometry and confocal microscopy.

#### *ER stress evaluation*

ER-Tracker Green (Thermo Fisher Scientific) is a live-cell stain highly selective for the ER. This stain consists of the green-fluorescent BODIPY® FL dye and glibenclamide that binds to the sulphonylurea receptors of ATP-sensitive K<sup>+</sup> channels which are prominent on the ER and have a critical role in ER luminal homeostasis. Indeed, ER K<sup>+</sup> channels are involved in functions such as protein folding, apoptosis, and Ca<sup>2+</sup> homeostasis (Hogg & Adams, 2001) (Ghasemi et al, 2014).

PBMC were incubated with 100 nM ER-Tracker Green for 30 min at 37°C and subjected to flow cytometry and confocal analyses.

#### *Intracellular Ca<sup>2+</sup> levels detection*

To measure intracellular Ca<sup>2+</sup> levels FURA-2 AM (Thermo Fisher Scientific) was used which is known as an intracellular Ca<sup>2+</sup> indicator, ratiometric and UV light-excitable. After treatment with lysates, cells were stained with FURA-2 AM 2µM for 15 minutes at 37°C. After incubation time, samples were acquired by flow cytometry using the appropriate fluorescence channel.

#### *Surface receptor expression evaluation*

To evaluate CD54 (ICAM-1), CD317, CD59 and CD14 expression fluorochrome-conjugated monoclonal antibodies were added to 50 µl of cell pellet. Mouse monoclonal anti-human antibodies anti-CD54-PE conjugated (clone D3.6) (Exalpha Biologicals, U.S.A), Alexa Fluor® 647 anti-CD317 (BioLegend, U.S.A), anti-CD59-Pe-Cy5 conjugated (BD) and anti-CD14-PE conjugated (clone M5E2) (BD) were added at dilutions according to manufacturer's instructions. After 15 min incubation at RT, samples were acquired by flow cytometry and/or confocal microscopy.

#### *Intracellular detection of Bcl-2, p53 and pRb antigens*

Monocytes were washed in PBS for 10 min at RT, resuspended in 300 µl formaldehyde 3.7% and incubated at 4°C for 15 min. 2 ml perm/washing buffer was added and cells were centrifuged at 1200 rpm for 10 min. Pellets were resuspended in 300 µl Cytoperm reagent (Li et al, 2015a). Monoclonal anti-human antibodies Anti-Bcl-2 PE conjugated (clone N46-467) (BD), Anti-p53 FITC conjugated (clone D0-8) (BioLegend) and Anti-pRb PE conjugated (clone MOPC-21) (BD) were added to samples at concentrations according to manufacturer's instructions. Cells were incubated at 4°C for 30 min before being processed by flow cytometry and/or confocal microscopy.

#### *Evaluation of intracellular lipids*

To evaluate lipid content and oxidation, three different dyes were used: Bodipy® 665/676 (Thermo Fisher Scientific), LipidTOX™ (Thermo Fisher Scientific) and Nile Red (NR) (Sigma-Aldrich)

Bodipy® 665/676 staining: Bodipy is a fluorescent probe suitable for oxidation studies in neutral lipids (Raudsepp et al, 2014). Cells were incubated with the dye at the final concentration of 1µg/ml for 30 minutes at 37°C and acquired by flow cytometry.



LipidTOX™ staining: LipidTOX stains neutral lipids and it is commonly used to characterize the potentially toxic effects of compounds on lipid metabolism in mammalian cells. Cells were incubated with the dye at the final dilution of 1X.

NR staining: NR is a phenoxazine dye that can be used on viable cells to localize and quantify neutral and polar lipids. Polar lipids (i.e., phospholipids) which are mostly present in membranes, are stained in red (emission > 590 nm), whereas neutral lipids (esterified cholesterol and triglycerides), which are present in lipid droplets, are stained in yellow (570–590 nm) (Diaz et al, 2008). In this work, NR was prepared at 100µg/ml in dimethylsulfoxide. NR was added to the culture medium for 15 min at a final concentration of 1µg/ml in a cellular suspension adjusted to 10<sup>6</sup> cells/ml. After incubation, samples were acquired by flow cytometry, collecting at least 10,000 events for each tube.

#### *Autophagic vacuole detection*

Autophagic vacuoles were detected in flow cytometry by monodansylcadaverine (MDC) staining, a specific autophagolysosomes marker typically used to investigate the autophagic machinery (Vazquez & Colombo, 2009). Cells were incubated with 50µM MDC at 37°C for 10 minutes.

#### *LAMP-1 surface expression (lysosomal exocytosis assay)*

Cell surface CD107a (LAMP-1), which is found on lysosomes and intracellular lytic granules, was measured. LAMP-1 surface expression was used as a marker of lysosomal exocytosis (Andrews, 2017). CD107a-PeCy5 antibody (clone H4A3, BioLegend) was added to 50µl of cellular suspension at the concentration indicated in the manufacturer's instructions. Cells were incubated for 1 hour at RT and acquired by flow cytometry. To evaluate the lysosomal exocytosis, in many cell types LAMP-1 values are associated to cytosolic Ca<sup>2+</sup> content (Ivanov et al, 2004).

#### *Cytometric investigations*

Cytometric experiments were carried out with a FACSCanto II flow cytometer (BD) equipped with an argon laser (Blue, Ex 488 nm), a helium-neon laser (Red, Ex 633 nm) and a solid state diode laser (Violet, Ex 405 nm). Analyses were performed with FACSDiva™ software (BD); approximately 10,000 cell events were acquired for each sample.

### 3.13 Trypan blue viability test

This test was used to determine the number of viable cells present in the cell suspension. Monocytes or U937 cells in suspension were 1:1 diluted in 0.4% Trypan Blue solution (Sigma-Aldrich). 10  $\mu$ l of the cell solution prepared was used to fill the haemocytometer chamber (Naubauer chamber). After 1-2 min incubation cells were counted under Nikon Eclipse TS100 fluorescence microscope (Nikon corporation, Italy) applying the following formula. Cells were visually examined to determine whether cells took up or excluded dye: viable cells typically show a clear cytoplasm (unstained) whereas nonviable cells show a blue cytoplasm (stained) (Strober, 2001).

$$\text{Concentration (cells/ml)} = \frac{\text{number of cells}}{\text{number of squares}} \times 10,000 \times \text{dilution}$$

### 3.14 Confocal microscopy analyses

Confocal microscopy analyses were applied by a Leica TCS SP5 II confocal microscope (Leica Microsystem, Germany) with 488, 543 and 633 nm illuminations and oil-immersed objectives. For confocal live imaging, cells were grown on MatTek glass bottom chambers (MatTek Corporation, Slovak Republic). The images were further processed and analysed in ImageJ software (NIH, U.K).

### 3.15 Statistical analyses

Data are shown as mean  $\pm$  standard deviation (SD) of at least three independent experiments. Analyses of variance (ANOVA) approaches were used to compare values among more than two different experimental groups for data that met the normality assumption. One-way ANOVA or two-way ANOVA were followed by a Bonferroni *post-hoc* test. The means of two groups were compared by using *t* test. P values less than 0.05 were considered statistically significant. All statistical analyses were done using GraphPad Prism 5.0 (GraphPad software, U.S.A).

#### 4. Human intestinal cell model and molecular work

##### 4.1 Bacterial strains, plasmids and primers

Table 1. Bacterial strains used in this study:

<i>C. jejuni</i> strains	Description	References
11168H	A hypermotile derivative of the original sequence strain NCTC 11168 that shows higher levels of caecal colonisation in a chick colonisation model	(Jones et al, 2004; Karlyshev et al, 2002)
11168H <i>cdtA</i> mutant	Isogenic mutant of <i>Cj0079</i> obtained from <i>Campylobacter</i> mutant bank <a href="http://crf.lshtm.ac.uk/wren_mutants.html">http://crf.lshtm.ac.uk/wren_mutants.html</a>	LSHTM mutant bank
11168H <i>cdtB</i> mutant	Isogenic mutant of <i>Cj0078</i> obtained from <i>Campylobacter</i> mutant bank <a href="http://crf.lshtm.ac.uk/wren_mutants.html">http://crf.lshtm.ac.uk/wren_mutants.html</a>	LSHTM mutant bank
11168H GFP	Hypermotile derivative of the original sequence strain NCTC 11168 containing GFP with a <i>porA</i> promoter	(Jervis et al, 2015)

Table 2. *E. coli* strains used in this study:

<i>E. coli</i> strains	Description	Reference
<i>E. coli</i> XL-2	Blue MRF competent cells	Agilent, U.S.A

Table 3. Plasmids used in this study:

Plasmids	Description	Reference
pGEM-T Easy	PCR cloning vector, ampicillin resistant	Promega, U.K
pGEM- <i>cdtA</i>	pGEM-T Easy vector containing <i>Cj0079</i> CDS fragment (0.7 kb)	This study
pGEM- <i>cdtA</i> -Km <sup>R</sup>	pGEM-T Easy containing <i>Cj0079</i> with a 1.4 kb Km <sup>R</sup> inserted at position 411 of the <i>Cj0079</i> nucleotide sequence	This study

Table 4. Primers used in this study:

Primer Name	Sequence
<i>cdtA</i> -F	TGGAGAATTTGAAGATACTG
<i>cdtA</i> -R	TCTCCTTGGCGATATAAAG
<i>cdtA</i> -IPCR-F	GGGAGATCTATCGATAGCAAAGGATTTG
<i>cdtA</i> -IPCR-R	GGGAGATCTAATCCAATTCCTTGTGC
Km <sup>R</sup> forward-out	TGGGTTTCAAGCATTAGTCCATGCAAG
Km <sup>R</sup> reverse-out	GTGGTATGACATTGCCTTCTGCG
SP6 universal primer	ATTTAGGTGACACTATAG
T7 universal primer	TAATACGACTCACTATAGGG

XBP1-F	ACACGCTTGGGGATGAATGC
XBP1-R	CCATGGGAAGATGTTCTGGG
Spliced XBP1-F	TGCTGAGTCCGCAGCAGGTG
Spliced XBP1-R	GCTGGCAGGCTCTGGGGAAG
GAPDH-F	GGATGATGTTCTGGAGAGCC
GAPDH-R	CATCACCATCTTCCAGGAGC

#### 4.2 Growth conditions and storage

*C. jejuni* strains were revived from -80°C glycerol stocks by pipetting onto blood agar plates containing autoclaved Columbia agar base (Oxoid) supplemented with 7% (vol/vol) horse blood (TCS Microbiology, U.K) and *Campylobacter* Selective Supplement (Oxoid).

Depending on the different applications, appropriate concentrations of antibiotics were added to the medium as follows: ampicillin (100 µg/ml), kanamycin (50 µg/ml), and chloramphenicol for *E. coli* (50 µg/ml) or *C. jejuni* growth (10 µg/ml). In detail, plates for *C. jejuni cdtA* and *cdtB* mutant strains were supplemented with kanamycin, plates for *C. jejuni* 11168H GFP strain growth were supplemented with chloramphenicol and plates for *C. jejuni* 11168H *cdtA* mutant GFP strain growth were supplemented with kanamycin and chloramphenicol.

Bacteria were restreaked every 2-3 days with passages being no more than 10 to preserve bacteria viability.

*C. jejuni* strains were grown for 24 hours prior to use in all subsequent experiments (unless otherwise stated). *C. jejuni* were grown in a variable anaerobe chamber (VAIN) (Don Whitley Scientific, U.K) under microaerobic conditions at 37°C containing 85% N<sub>2</sub>, 10% CO<sub>2</sub>, and 5% O<sub>2</sub>.

To prepare 15 blood agar plates, 400 ml of Columbia agar base (400 ml of distilled water was added to 15.6 g of Columbia agar base in powder), one vial of *Campylobacter* selective

supplement (Skirrow, Oxoid) and 28 ml of horse blood (7%). Kanamycin blood agar plates contained 50 µg/ml kanamycin.

*C. jejuni* overnight cultures were prepared by adding an adequate bacterial suspension to 10 ml of Brucella broth in a 30 ml flask (Thermo Fisher Scientific, U.S.A) (preincubated under the same growth conditions for 24 hours). Subsequently flasks were incubated for 24 hours (or for the desired experimental time) at 37°C under microaerobic conditions on a shaker (75 rpm).

*E. coli* cells were revived from -80°C glycerol stocks and plated onto Luria-Bertani (LB) agar plates and were incubated at 37°C under aerobic conditions (Sonyo, Canada). LB plates with *E. coli* grown overnight were sealed with Parafilm M (Sigma-Aldrich) and stored at 4°C for a maximum of 2-3 weeks. Overnight cultures of *E. coli* were prepared by selecting a single colony, picked up with a small inoculation loop (1 µl) and added to 10 ml LB broth in a 30 ml universal. Cultures were grown at 37°C for 16-18 hours under aerobic conditions into a shaking incubator at 200 rpm (Weiss Gallenkamp, U.K).

To prepare 10 LB agar plates, 250 ml of distilled water was added to 9.25 g LB agar (Oxoid) in powder. LB/ampicillin/IPTG/X-Gal plates (8-10 plates) were prepared by adding 250 µl ampicillin (100 mg/ml), 40 µl IPTG (Isopropyl β-D-1-thiogalactopyranoside) (1 pmol/µl) and 500 µl 2% (wt/vol) X-Gal (5-bromo-4-chloro-3-indolyl-β-D-galactopyranoside) to 250 ml of LB agar.

Bacteria glycerol stocks were created for long-term storage of *C. jejuni* and *E. coli* strains of interest. Glycerol stocks were prepared for *C. jejuni* (from an overnight plate) and *E. coli* (from an overnight liquid culture) cells using 10% (vol/vol) glycerol, 10% (vol/vol) foetal calf serum (FCS) (Sigma-Aldrich) and 80% (vol/vol) Mueller-Hinton broth mixture (*C. jejuni*) or 15% (vol/vol) glycerol in LB broth (*E. coli*). Next, 500 µl aliquots were snap-frozen using dry ice in 100% (vol/vol) ethanol and stored in a -80°C freezer (New Brunswick Scientific, U.K).

#### **4.3 Preparation of a specific OD<sub>600</sub> *C. jejuni* suspension**

50 ml of Brucella broth were preincubated in a 300 ml flask at 37°C and placed into a microaerobic chamber for 24 hours. *C. jejuni*, grown on blood agar plates for 24 hours, were collected using a sterile inoculation loop and resuspended in 1 ml PBS into a 1.5 ml microcentrifuge tube. 100 µl of this suspension was resuspended in 900 µl Brucella broth in a sterile 1.5 ml microcentrifuge tube. This diluted suspension was vortexed and transferred to a 1 ml spectrophotometer cuvette (Thermo Fisher Scientific) and the OD<sub>600</sub> recorded using a

spectrophotometer (cell density meter CO8000, WPA, U.K). 1 ml of an appropriate blank was used before recording.

In summary, the defined volume of the original *C. jejuni* suspension was added to 50 ml of equilibrated Brucella broth to produce an initial inoculum with an OD<sub>600</sub> of 0.1 was calculated as follows:

$$\frac{\text{Required } OD_{600} \text{ in final solution}}{\text{Initial } OD_{600} \text{ reading} \times \text{Dilution factor}} \times \text{Final volume (ml)} \times \text{Conversion (from ml to } \mu\text{l)}$$

$$= \frac{0.1}{OD_{600} \text{ reading} \times 10} \times 50 \times 1000$$

**= Volume of cells ( $\mu\text{l}$ ) to add from original bacterial suspension**

#### 4.4 DNA Purification

*C. jejuni* genomes were purified using the Pure Link Genomic DNA kit (Invitrogen, U.S.A). This method consisted of four steps:

**Gram negative bacteria lysate preparation:** Cells were harvested using an inoculation loop (approximately  $2 \times 10^9$  cells), resuspended in 1 ml PBS and centrifuged for 2 minutes at 13,000 rpm. The pellet was resuspended in 180  $\mu\text{l}$  of digestion buffer and 20  $\mu\text{l}$  of proteinase K to lyse the cells. After 90 minutes of incubation at 55°C, 20  $\mu\text{l}$  of RNase A were added and the lysate was incubated at room temperature for 2 minutes. 200  $\mu\text{l}$  of Lysis/Binding buffer was added and vortexed to obtain a homogenous solution. Finally, 200  $\mu\text{l}$  of 97-100% ethanol was added to the lysate and mixed well by vortexing for 5 seconds.

**DNA binding:** The prepared lysate (~640  $\mu\text{l}$ ) was added to a spin column, placed into a collection tube and centrifuged at 10,000 x g for 1 minute at room temperature. Subsequently the collection tube was discarded and the spin column was then placed into a clean one.

**DNA washing:** The DNA was washed with 500  $\mu\text{l}$  of Wash buffer 1 and centrifuged at 10,000 x g for 1 minute. The DNA was then washed with 500  $\mu\text{l}$  Wash buffer 2 and centrifuged at maximum speed.

**DNA eluting:** The spin column was placed into a 1.5 ml microcentrifuge tube and 50  $\mu\text{l}$  Milli-Q water were added. After 1-minute incubation, the column was subjected to centrifugation at maximum speed. This procedure was repeated for a second time. After this

step the purified DNA was obtained and stored at  $-20^{\circ}\text{C}$ . The concentration and the purity of the resultant sample was checked using a NanoDrop 1000 Spectrophotometer (Thermo Fischer Scientific, U.S.A).

#### 4.5 Purified DNA Quantitation

Genomic DNA was quantitated using a NanoDrop 1000 Spectrophotometer (Thermo Fischer Scientific).  $1.5\ \mu\text{l}$  sample was pipetted onto the end of a fiber optic cable (the receiving fiber). A second fiber optic cable (the source fiber) was then brought into contact with the liquid sample causing the liquid to bridge the gap between the fiber optic ends. A pulsed xenon flash lamp provided the light source and a spectrometer utilizing a linear CCD array was used to analyse the light after passing through the sample and the  $\text{ng}/\mu\text{l}$  was recorded.

#### 4.6 Polymerase Chain Reaction Technique

A typical PCR consists of a series of 25-30 repeated temperature changes, called ‘cycles’, with each cycle consisting of three discrete temperature steps:

- Denaturation step: The reaction starts with a 2-minute initial denaturation step at  $95^{\circ}\text{C}$ . This step causes the DNA melting of the DNA template by disrupting the hydrogen bonds between complementary bases, yielding single-stranded DNA molecules.
- Annealing step: Typically, 30 seconds to 1 minute. To optimize the annealing conditions, the annealing temperature ( $T_a$ ) is usually set to  $5^{\circ}\text{C}$  below the calculated melting temperature of the primers (Appendix 1).
- Extension/elongation step: This reaction is typically performed at the optimal temperature for Taq DNA polymerase ( $72-74^{\circ}\text{C}$ ) for 5 minutes. In this step the DNA polymerase synthesizes a new DNA strand complementary to the DNA template strand by adding dNTPs.

Each reaction tube contained the following volumes/concentrations:

Component	Volumes	Final concentration
PCR Master Mix	$25\ \mu\text{l}$	1X
DNA	$1\ \mu\text{l}$	$< 250\ \text{ng}$
Forward primer	$0.075\ \mu\text{l}$	$0.1-1.0\ \mu\text{M}$
Reverse primer	$0.075\ \mu\text{l}$	$0.1-1.0\ \mu\text{M}$



For typical PCR reactions, the template should be present at 10 to 1000 copies per reaction. Before initiating the PCR reaction, DNA must be isolated (see 4.4). To prevent pipetting errors, the PCR MyTaq mix format was used. The PCR MyTaq mix is a premixed ready-to-use solution, containing Taq DNA polymerase, dNTPs, and MgCl<sub>2</sub> and reaction buffers at optimal concentrations for efficient amplification of DNA templates by PCR.

PCR mix was set up as follows:

MyTaq mix (Bioline, U.K)	25 µl
Forward primers	0.075 µl
Reverse primers	0.075 µl
DNA	1 µl

PCR products were analysed on a 0.7% TAE-agarose-ethidium bromide gel electrophoresis as described in 4.7.

#### **4.7 Tris-Acetate-EDTA agarose ethidium bromide gel electrophoresis**

In order to prepare the 0.7% agarose gel (Bioline, U.K), 1.05 g of agarose powder was mixed with 150 ml of electrophoresis buffer (Tris-acetate-EDTA, TAE 1X). The contents were mixed, heated and poured into a casting tray containing a sample comb. Once the gel had solidified, the comb was removed and the electrophoresis buffer was poured into the electrophoresis chamber followed by addition of 10-12 µl of sample loaded into appropriate wells. Once the ethidium bromide was added into the buffer (final concentration 0.5 µg/ml). An adequate migration (120V, 500mA) was performed and the gel was viewed on (Consort EV, Sigma-Aldrich) an ultraviolet Trans-illuminator was used to identify and scan DNA bands (Bio Imaging System, Syngene, U.K).

#### **4.8 Purification of PCR products**

QIAquick PCR Purification Kit (Qiagen, Germany) was used to purify and remove impurities (such as primers, nucleotides, enzymes etc.) from DNA samples of size 100 bp to 10 kb. Initially, 5 volume buffer PB was added to 1 volume of PCR reaction and the mixture was placed in a column. To wash, 750 µl buffer PE were added to the column and twice centrifuged. The column was placed into a clean 1.5 ml microcentrifuge tube and to elute

DNA, 30 µl of Milli-Q water were added. After centrifugation, the resultant sample contained the purified DNA.

#### 4.9 Ligation and transformation stages

The plasmid was introduced into bacterial cells, specifically *E. coli* cells, using a standard heat-shock transformation. This method, called ‘transformation’, allows the introduction of foreign DNA into competent cells. To clone PCR products (which have been previously cleaned) the pGEM-T-Easy Vector was used (Promega) which is a "TA" cloning vector that has "A" & "T" overhangs. Taq polymerase leaves an extra "T" or "A" at the end of the amplified DNA in the PCR reaction, so the PCR product ligates readily into the vector.

The ligation reaction was set up as described with the reactions described below and incubated for 1 hour at room temperature after mixing. Alternatively, if the maximum number of transformants is required, the ligation should be incubated overnight at 4°C.

Reagent	Standard Reaction	Positive control	Background Control
2X Rapid Ligation buffer	5 µl	5 µl	5 µl
pGEM-T Easy Vector (50 ng)	1 µl	1 µl	1 µl
PCR product	X µl	-	-
Control Insert DNA	-	2 µl	-
T4 DNA Ligase	1 µl	1 µl	1 µl
Deionized water to a final volume of	10 µl	10 µl	10 µl

Following this procedure, 50 µl of thawed competent cells were added to 2 µl of the ligation mix and incubated on ice for 20 minutes. The reaction was heat-shocked for 45-50 seconds at exactly 42°C and incubated on ice for 2 minutes. After adding 950 µl room temperature SOC medium (Sigma-Aldrich), the reaction was incubated for 1.5 hours at 37°C with shaking (~150/200 rpm). Approximately 200 µl of each transformation culture were plated onto LB/ampicillin/IPTG/X-Gal plates previously prepared (see 4.2), using an L-shaped cell spreader.

The pGEM-T-Easy vector used was able to encode the  $\beta$ -galactosidase gene across the multiple cloning site allowing of making a “blue/white screening”, a rapid technique used to detect successful ligation and transformation. Colonies with the insert should appear white, whereas colonies without the insert should appear blue. Only cells that contained the plasmid were able to grow and form colonies. This screening allowed us to identify *E. coli* cells that have the desired form of plasmid DNA within them. After an overnight incubation in 5% CO<sub>2</sub> at 37°C, blue and white colonies were grown in the LB/ampicillin/IPTG/X-Gal plates. White single colonies transformants were selected and picked up using a 1  $\mu$ l loop, plated in LB/amp plates and overnight incubated in 5% CO<sub>2</sub> at 37°C. Plates with resultant colonies were stored at 4°C.

#### 4.10 PCR from boiled/lysed bacteria colonies

To check the success of the transformation step, single colonies of *E. coli* were picked up and resuspended in 100  $\mu$ l sterilized Milli-Q water, lysed through boiling (95°C on the PCR block) and cleaned by centrifugation (13,000 rpm/5 minutes). Then, 1  $\mu$ l of each sample was subjected to vector primer PCR (VPPCR), and insert specific primers PCR (ISPCR), using primers previously used for the amplification of the CDS of interest (*cdtA* gene) to test for positive transformants.

The VPPCR reaction was set up as follows:

Forward T7 primer (100 pmol/ $\mu$ l)	0.075 $\mu$ l
Reverse SP6 primer (100 pmol/ $\mu$ l)	0.075 $\mu$ l
Boiled supernatant	1 $\mu$ l
VPPCR pre mix	to 25 $\mu$ l

Standard PCR programs were performed (see 4.6) and the resultant electrophoretic gel was analyzed to confirm the presence of the interested insert into the correct gene. After checking, exclusively *E. coli* colonies which contained the right insert into the required location could be streaked for the next step. Therefore, selected colonies were plated in fresh LB/amp agar plates allowing glycerol stock preparation and the Miniprep production.

#### **4.11 Overnight culture preparation**

The overnight incubated liquid bacteria cultures were essential for the preparation of the bacterial glycerol stock (see 4.2) and the Miniprep production. These were prepared as follows: single colonies, grown into LB/amp agar plates, were selected using a 1 µl loop and resuspended in 10 ml of LB Broth enriched with ampicillin (0.1%) using 30 ml tubes. After inoculation, the cultures were pre-incubated overnight into a shaking incubator.

#### **4.12 Isolation of plasmid DNA: QIAprep Miniprep production**

To purify the plasmid DNA, QIAprep Miniprep Kit (Qiagen) was used. This procedure is based on three basic steps: the preparation and cleaning of bacteria lysate under alkaline conditions, the adsorption of the DNA onto the QIAprep silica membrane and the washing and the elution of the plasmid DNA. The following procedure was applied: overnight *E. coli* cultures in 10 ml LB medium were lysed, cleared by centrifugation and applied to the QIAprep module where plasmid DNA adsorbed to the silica membrane and eluted in a microcentrifuge tube. After centrifugation, the pellet was resuspended with 250 µl of buffer P1 and transferred to a 1.5 ml microcentrifuge tube. To perform the wash step, 250 µl P2 buffer and 350 µl N3 buffer were added to the tube, then the reaction was immediately mixed by inverting the tube 4-5 times. The mixture was centrifuged for 10 minutes at 13,000 *g* in a table top centrifuge and pipetted in a clean spin column. Then, the tube was centrifuged for 30-60 seconds, discarded and twice washed, firstly adding 500 µl buffer PB, secondly adding 750 µl of buffer PE. Finally, the tube was discarded, centrifuged at maximum speed and the column was placed into a clean 1.5 ml microcentrifuge tube. To elute the DNA, a small volume of Milli-Q water (30 µl) was added to the centre of the column and centrifuged.

Purified DNA was quantitated using a NanoDrop 1000 Spectrophotometer and the sample purity was checked (see 4.5). Purified samples were stored at -20°C.

#### **4.13 Restriction endonuclease digestion**

Standard restriction digests were prepared using a final volume of 20 µl. 0.5-1.0 µg plasmid DNA was digested with 10 U of the appropriate restriction endonuclease and buffer. Reactions were prepared into 1.5 ml microcentrifuge tubes and incubated at the appropriate temperature and time duration recommended by the manufacturer. Lastly digests were purified using the QIAquick PCR Purification kit (Qiagen) (see 4.8).

#### 4.14 Inverse PCR mutagenesis

Inverse PCR mutagenesis (IPCRM) was performed when the CDS to be mutated did not contain a BamHI, BclI or BglII restriction site. As illustrated in the following figure, IPCRM primers were designed by selecting 15-20 nucleotides in the centre of the CDS to be mutated with an interspacing region of 10-15 nucleotides.



**Fig. 4.1** IPCRM primers designed for *cdtA* sequence. To allow the functionality of the BglII restriction site the IPCRM primers have to contain three guanine residues at the 5' -end followed by the BglII complementary sequence –AGATCT.

The IPCRM reaction was prepared by mixing the following reagents:

buffer 1 (10X)	10 $\mu$ l
AccuPrime Taq DNA high fidelity polymerase* (5 U/ $\mu$ l) (Invitrogen)	0.4 $\mu$ l
DNTPs in buffer 1 concentration	400 $\mu$ M
Milli-Q water	89.6 $\mu$ l

IPCRM reaction was set up as follows:

IPCRM Pre-mix	98.4 $\mu$ l
DNA (0.1-10 ng)	1.0 $\mu$ l
IPCRM primers	0.6 $\mu$ l

IPCRM reaction steps:

- Step 1: 94°C for 2 minutes
- Step 2: Denature at 94°C for 1 minute
- Step 3: Anneal at 45°C for 1 minute
- Step 4: Extension at 72°C for X minutes (X = size of plasmid in kb  $\times$  1.5 minutes)
- Step 5: 72°C for 7 minutes

Steps 2-4 were repeated 40 times

The amplified IPCRM product was analysed on an electrophoretic gel (see 4.7) and purified using the QIAquick PCR Purification kit (Qiagen) (see 4.8).

#### **4.15 DNA sequencing**

Sequencing of plasmid DNA was performed using ABI Prism Terminator Ready Reaction Mix (Applied Biosystems, U.K). Sequencing reactions were also performed on genomic DNA using similar concentrations as for plasmid DNA.

ABI Reaction Mix	8 $\mu$ l
Plasmid or genomic DNA (200-500 ng)	1 $\mu$ l
Forward or reverse CDS specific primer (1 pmol/ $\mu$ l)	4 $\mu$ l
Sterilised Milli-Q water	to 20 $\mu$ l

PCR cycle:

- Step 1: Denature at 96°C for 10 seconds
- Step 2: Anneal at 50°C for 5 seconds
- Step 3: Extension at 60°C for 4 minutes

Steps 1-3 were repeated 25 times

Sequencing reactions were performed on a GeneAmp 9600 thermal cycler (Perkin-Elmer, U.K). The entire sequencing reaction was then transferred to a 1.5 ml microcentrifuge tube containing 80  $\mu$ l 75% (vol/vol) isopropanol. The sample was briefly vortexed and incubated at -20°C for 1 hour. The sample was then centrifuged at 13,000 rpm for 30 minutes and the supernatant discarded. 400  $\mu$ l of 75% (vol/vol) isopropanol was added to the pellet and briefly vortexed before centrifuging at 13,000 rpm for 5 minutes. The supernatant was removed and the pellet was dried at room temperature for approximately 20 minutes. 10  $\mu$ l HiDi solution (Applied Biosystems) was applied to the pellet and the reaction mixture sequenced using the LSHTM ITD Faculty facilities. Analysis of sequence data was performed using Chromas v1.61 software (Technelysium Pty. Ltd).

#### **4.16 Transformation of *C. jejuni* by Electroporation**

For electroporation, cells were grown to mid-log phase, washed extensively to eliminate all salts and mixed with the DNA to be transformed. In detail, bacteria cells were collected from 24 hour grown plates and resuspended in 10 ml cold EBF buffer into a 30 ml universal.

EBF buffer was prepared as follows:

100% (vol/vol) Glycerol	15 ml
10% (wt/vol) Sucrose	10 ml
Sterilised Milli-Q water	to 100 ml

The tube was centrifuged and the pellet was resuspended in 1 ml cold EBF. The content was transferred into a 1.5 ml microcentrifuge tube and centrifuged at 4°C in a cold room for 2 minutes at 13,000 x g. Subsequently, the pellet was resuspended in 250 µl cold EBF. 5 µl of DNA of interest were mixed to 50 µl cell suspension; the resulting reaction was incubated for 5-10 minutes on ice and occasionally resuspended by flicking. All following reactions were conducted at 4°C on ice. 60 µl sample were transferred into a Gene Pulser Electroporation cuvette (Bio-Rad, U.K). The cuvette was put in a micro-electroporation chamber of a Gene Pulser Xcell™ Electroporation System (Bio-Rad) and pulsed to 200 Ω. The Gene Pulser was set at 25 µFD and 2.5 kV. After pulsing, 100 µl rich medium (SOC medium) were added to electroporated cells and the whole volume was plated into a blood agar plate.

Electroporated cells grew up in blood agar plates for 48 hours in microaerobic conditions. After 48 hours, bacterial cells were harvested using a sterile inoculation loop and resuspended in 800 µl Brucella broth. 200-400 µl aliquots were pipetted in blood agar plates enriched with chloramphenicol (10 µl/ml) and kanamycin (50 µg/ml) antibiotics. The bacterial solution was spread using a sterile spreader and plates were incubated for up 5-7 days at 37°C under microaerobic conditions. Resultant colonies were restreaked in fresh blood agar plates enriched with chloramphenicol and kanamycin. Colonies were subsequently used to prepare the glycerol stock (see 4.2).

#### **4.17 Construction of a *C. jejuni* 11168H *cdtA* GFP mutant strain**

##### **Mutagenesis strategy**

The methodology used in this study is based on electroporation of a recipient *C. jejuni* strain with a linear PCR fragment carrying an antibiotic resistance cassette and the kanamycin cassette. The process consists of three main stages: construction of a PI construct (Plasmid + Insert), construction of a PIK (Plasmid Insert Kanamycin cassette) construct and transformation by electroporation (see 4.16).



### Stage 1 - PI production

After designing primers for the CDS of interest (Appendix 1) the CDS/CDS fragment was amplified using PCR (see 4.6) and purified using a QIAquick PCR Purification Kit (4.8). The next step was to insert the DNA, the PCR product, into a plasmid or cloning vector, pGEM-T Easy vector, so that the DNA fragment could be propagated. The ligation was followed by transformation into *E. coli* XL-2 cells (see 4.9). The plasmid DNA was isolated and positive transformants, checked by PCR (see 4.10).

### Stage 2 - PIK production

The aim of the second stage was to incorporate a Km<sup>R</sup> cassette into the CDS of interest. The Km<sup>R</sup> cassette (aphA-3 (Trieu-Cuot et al, 1985)) was obtained from pJMK30 (van Vliet et al, 1998) following a BglII restriction digest. The *C. jejuni* CDS to be mutated was analysed for the presence of a single BamHI, BclI or BglII site within the sequence using NEBcutter v2.0 (<http://tools.neb.com/NEBcutter2/index.php>). The unique restriction site should ideally be located near the centre of the amplified CDS/CDS fragment to improve efficiency of recombination.

To allow insertion of the Km<sup>R</sup> cassette, 2 µg plasmid DNA containing the cloned CDS of interest was digested with approximately 20 units' restriction enzyme (BamHI, BclI or BglII) (see 4.13). The digest was purified using the QIAquick PCR Purification kit (see 4.8) and sample concentration was recorded using a NanoDrop ND-1000 spectrophotometer. The following ligation reaction was then set up:

Plasmid DNA digested with unique restriction enzyme ( $\approx 250$ ng/ $\mu$ l)	2 $\mu$ l
Km <sup>R</sup> cassette digested with BglII ( $\approx 20$ ng/ $\mu$ l)	5 $\mu$ l
10X Ligase buffer	1 $\mu$ l
T4 DNA Ligase (3 Weiss units/ $\mu$ l)	2 $\mu$ l

The reaction was incubated overnight at 4°C. Transformation of the reaction mixture into XL-2 cells was performed as previously described (see 4.10). Transformants were selected and plated on LB/ampicillin/kanamycin plates and incubated overnight at 37°C. Resultant colonies were restreaked onto LB/ampicillin/kanamycin plates and checked for the insertion

of a Km<sup>R</sup> cassette by carrying out an orientation specific primer PCR and an ISPCR, using the original primers used for amplification of the CDS of interest to test positive transformants. To check the orientation of the Km<sup>R</sup> cassette and the success of the transformation step, a PCR from boiled/lysed bacteria single colonies was carried out. To transform this *E. coli*, single colonies were selected from the respective plates, resuspended in Milli-Q water, lysed through boiling and purified. Next, 1 µl of each sample was subjected to VPPCR using vector specific primers and orientation specific primer PCR (kanamycin forward out and *cdtA* gene specific forward primers) (Appendix 2). After an adequate migration, DNA bands were scanned and analyzed. Exclusively *E. coli* colonies which showed to have the kanamycin cassette into the PI were plated in fresh LB/ampicillin plates and overnight incubated. Only positive transformants colonies grown on LB/amp plates were used for PIK glycerol stock preparation and Miniprep production (see 4.12).

#### **4.18 Isolation of *C. jejuni* OMVs**

The OMV isolation process consisted of three stages:

**Stage 1:** 50 ml of Brucella Broth were preincubated, for 24 hours before inoculation, with shaking at 75 rpm in the VAIN.

**Stage 2:** *C. jejuni* from a 24 hour grown blood agar plate was resuspended in 1ml Brucella broth and used to inoculate 50 ml pre-equilibrated Brucella broth to an OD<sub>600</sub> of 0.1; PBS was used as blank for spectrophotometer determination.

**Stage 3:** *C. jejuni* cultures were grown for 18 hours to mid-log phase (overnight) and the OD<sub>600</sub> was re-checked using Brucella broth as blank. Samples were centrifuged at 4000 x g for 30 minutes at 4°C and the resulting supernatant was filtered through a 0.22 µm membrane (Millipore, U.K). Subsequently, filtrate was centrifuged at 4000 x g for 30 minutes at 4°C using an Ultra-4 centrifugal filter unit (Millipore) with a nominal 10 kDa cut-off to concentrate the filtrate to 2 ml volume.

The concentrated filtrate was transferred into a new glass centrifuge tube. The weight was checked (7.0 g per tube) and ultra-centrifuged at 45,000 x g for 3 hours at 4°C using a Beckman Optima™ TL 100 ultracentrifuge (Beckman Coulter, U.K). The centrifuged tube was discarded and the resulting OMVs pellet was carefully resuspended with 200 µl of PBS and stored at -20°C. All isolation steps were carried out at 4°C (on ice) to preserve OMVs stability. Approximately 100 µg of OMVs by protein content was isolated from 50 ml of

culture supernatant (Elmi et al, 2016). At the end, the resulting sample can be processed for the quantitation of total proteins.

#### 4.19 Quantitation of total proteins by bicinchoninic acid assay (BCA)

Quantitation of total proteins isolated from 50 ml of culture supernatant, was determined by BCA assay (Thermo Fisher Scientific). This method combines the well-known reduction of  $\text{Cu}^{+2}$  to  $\text{Cu}^{+1}$  by protein in an alkaline medium (the Biuret reaction) with the highly sensitive and selective colorimetric detection of the cuprous cation ( $\text{Cu}^{+1}$ ) using a unique reagent containing bicinchoninic acid (Smith et al, 1985). The chelation of two molecules of BCA with one cuprous ion causes the peculiar purple-coloured reaction of this assay. We can obtain the resultant BCA/complex, readable at 562 nm to the spectrophotometer, following the following Pierce BCA Protein Assay Kit protocol.

Before starting the Standard protocol, the preparation of diluted albumin standards (BSA) and working reagent was required. BSA standards were prepared as described in the following table:

Vials	Volume of diluent ( $\mu\text{l}$ )	Volume and Source BSA ( $\mu\text{l}$ )	Final BSA concentration ( $\mu\text{g/ml}$ )
A	0	300 of stock solution	2000
B	125	375 of stock solution	1500
C	325	325 of stock solution	1000
D	175	175 of vial B dilution	750
E	325	325 of vial C dilution	500
F	325	325 of vial E dilution	250
G	325	325 of vial F dilution	125
H	400	100 of vial G dilution	25
I	400	0	0

The BCA working reagent (WR) was prepared as described in the following formula:

$$(\# \text{ standards} + \# \text{ unknowns}) \times (\# \text{ replicates}) \times (\text{volume of WR per sample}) =$$

Total volume of WR required

Having 6 unknown/samples and 2 replicates, the resulting formula was:

$$(9 \text{ standards} + 6 \text{ unknowns}) \times (2 \text{ replicates}) \times (200 \mu\text{l}) = 6000 \mu\text{l WR required}$$

Having calculated the WR volume required, WR was prepared by mixing 50 parts of BCA Reagent A with 1 part of BCA Reagent B (50: 1, Reagent A: B); in this specific case 120  $\mu\text{l}$  Reagent B was combined with 6000  $\mu\text{l}$  Reagent A.

The microplate procedure was performed using a sample to WR ratio equal to 1: 20 (as a consequence, the working range of the assay was limited to 125-2000  $\mu\text{g/ml}$ ). For this reason, 10  $\mu\text{l}$  of each sample were pipetted into the microplate wells and 200  $\mu\text{l}$  WR were added to each. Then the plate was put on a plate shaker for 30 seconds to mix the solutions and was incubated on the dark at 37°C for 30 minutes. After this incubation period, the plate was cooled to room temperature and the absorbance at 562 nm was measured on a plate reader (Spectra Max M3, Molecular Devices, U.K) by using the SoftMax Pro 5 software (Molecular Devices).

To determine the protein concentration of each sample it was used a standard curve prepared by plotting the average blank-corrected 562 nm measurement for each BSA standard vs. its concentration in  $\mu\text{g/ml}$ . The blank correction was done subtracting the average 562 nm absorbance measurement of the blank standard replicates from the 562 nm measurements of all other individual standard and sample replicates. The resulting standard curve is necessary to calculate the concentration value ( $\mu\text{g/ml}$ ) for each sample.

#### **4.20 Pre-treatment of T84 intestinal Eukaryotic cells with *C. jejuni* whole cells and OMVs**

T84 cells ( $1 \times 10^5$  per well) were two times washed with DMEM/F-12 (Gibco™, Thermo Fisher Scientific) at 37°C and then incubated for 4, 6, 16, 20 hours with 1 ml media enriched with OMVs previously isolated or *C. jejuni* whole cells ( $\text{OD}_{600}$ : 0.1) from bacteria strains. For the positive control, cells were incubated with Thapsigargin (25  $\mu\text{M}$ ) (Cell Signaling

Technology, U.S.A). Thapsigargin is well known as an endoplasmic reticulum  $\text{Ca}^{2+}$  pump inhibitor because of the rapid interaction with SERCA enzymes ( $\text{Ca}^{2+}$ -ATPase family) (Rutkowski & Kaufman, 2004).

#### **4.21 CHOP and BIP proteins detection by SDS-PAGE and Western blotting**

Proteins contained into lysates were separated by SDS-PAGE (NuPage Novex Bis-Tris 4 – 12%; Invitrogen). For Western blots, separated proteins contained into the pre-run polyacrylamide gel were blotted and transferred onto nitrocellulose membranes (iBlot2, Thermo Fisher Scientific) using the iBlot 2 Dry Blotting System (Thermo Fisher Scientific). The membrane was blocked with PBS 1X supplemented with 2% (wt/vol) non-fat dried milk and incubated overnight at 4°C. The membrane was incubated with primary mouse anti-CHOP (Sigma-Aldrich) or primary mouse anti-BiP (Sigma-Aldrich) antibodies respectively (1: 2500 dilution in PBS 1X supplemented with 0.1% (vol/vol) Tween-20 and 2% (wt/vol) non-fat dried milk) for 1 hour at room temperature with shaking (35 rpm/min speed, Platform Shaker STR6, Stuart Scientific, U.K). After incubation, the membranes were rinsed four times with PBS 1X supplemented with 0.1% (vol/vol) Tween-20 and were incubated for 1 hour at room temperature with infrared fluorescence – conjugated secondary antibodies (goat anti-rabbit IR800) (Sigma-Aldrich) a 1: 10,000 dilution of blocking buffer. Before visualization, membranes were washed 4 times with PBS supplemented with 0.1% (vol/vol) Tween -20 and once with PBS 1X. The blots were visualized and scanned with an Infrared Imager (Odyssey CLx Imaging System, LI-COR Biosciences, U.K) and analysed using the Image Studio Software (LI-COR Biosciences).

#### **4.22 Total RNA isolation**

After preincubation with OMVs and *C. jejuni* whole cells (see 4.20), total mRNA was isolated from T84 cell lysates using the PureLink RNA Mini Kit (Thermo Fisher Scientific). T84 cell lysis and RNA extraction were performed in three passages: lysis, homogenization and RNA Purification.

The growth medium was removed from the cells and 0.6 ml Lysis Buffer were added to the wells. Lysis buffer used in this passage contained 1% 2-mercaptoethanol (10 µl 2-mercaptoethanol for every 1 ml Lysis buffer). By pipetting cells were disrupted and the reaction was transferred into 1.5 µl microcentrifuge tubes. Tubes were vortexed until the cell pellet was dispersed and the cells appeared completely lysed. During the second passage,

lysates were transferred into clean tubes and homogenized using a Precellys<sup>R</sup> tissue homogenizer (Precellys, U.K) for three times. After each homogenization cycle, tubes were chilled 5 minutes in ice. Subsequently binding, washing and elution of RNA were performed as follows: one volume of 70% ethanol was added to each volume of cell homogenate and the reaction was vortexed to disperse any visible precipitate. 700  $\mu$ l of the sample were transferred to the spin cartridge (with the collection tube) and centrifuged at 12,000 x g for 15 seconds, then the flow-through was discarded. This step was repeated until the entire sample had been processed. To wash the sample, 700  $\mu$ l wash buffer 1 were added to the spin cartridge and centrifuged at 12,000 x g for 15 seconds at room temperature; the flow-through was discarded and the spin cartridge was placed into a new collection tube. For the second washing 500  $\mu$ l wash buffer 2 (previously enriched with ethanol 100%) was added to the tube that was centrifuged at 12,000 g for 15 second, for 2 minutes. This passage was repeated two times.

In order to dry the membrane with attached the RNA, the spin cartridge was centrifuged at 12,000 x g for 2 minutes. The collection tube was discarded and the spin cartridge was inserted into a recovery tube; 40  $\mu$ l RNase free water was added to the centre of the spin cartridge and incubated for 1 minute. A final centrifugation of the spin cartridge (2 minutes) allowed the RNA to elute from the membrane into the recovery tube. The quality and the quantity of our RNA was determined by using a NanoDrop spectrophotometer with UV absorbance at 260 nm (see 4.5). RNA samples that were not immediately used were stored at -80°C.

To assure highly pure RNA without genomic DNA contamination, after RNA purification a DNase treatment was performed (Turbo DNA-Free Kit).

In detail, 4  $\mu$ l TURBO DNase buffer 10X were added to the tube containing purified RNA and an incubation for 45 minutes at 37°C followed. 4  $\mu$ l inactivation reagent were added to the reaction and the tube was incubated for 5 minutes at room temperature, mixing occasionally by flicking. Followed a centrifugation at 10,000 x g for 15 minutes. 30  $\mu$ l supernatant were transferred into a new clean tube. Samples were immediately used or stored at -80°C for a long term storage.

### 4.23 cDNA synthesis

The first-strand cDNA synthesis from purified total RNA was performed with SuperScript III First-Strand Synthesis System for RT-PCR (Thermo Fisher Scientific). The following protocol was used for positive and negative RT control reaction preparation:

Total RNA was diluted to 100 pg/ $\mu$ l with DEPC-treated water and RNA/primer mixtures was prepared in sterile 0.5 ml tubes as described below (total volume, 10  $\mu$ l):

Component	+RT control	-RT control
Diluted total RNA (100 pg/ $\mu$ l)	1 $\mu$ l	1 $\mu$ l
Oligo (dT) <sub>20</sub>	1 $\mu$ l	1 $\mu$ l
10 mM dNTPs mix	1 $\mu$ l	1 $\mu$ l
DEPC-treated water	7 $\mu$ l	7 $\mu$ l

Samples were incubated at 65°C for 5 minutes, then placed on ice for at least 1 minute. The contents were collected by a brief centrifugation and the following components were added:

Component	+RT control	-RT control
10X RT buffer	2 $\mu$ l	2 $\mu$ l
25 mM MgCl <sub>2</sub>	4 $\mu$ l	4 $\mu$ l
0,1 M DTT	2 $\mu$ l	2 $\mu$ l
RNaseOUT (40 U/ $\mu$ l)	1 $\mu$ l	1 $\mu$ l
SuperScript III RT (200 U/ $\mu$ l)	1 $\mu$ l	-
DEPC-treated water	-	1 $\mu$ l

Tubes were gently mixed, collected by brief centrifugation and put into the PCR block and the following programme was performed:

- Step 1: 25°C, for 10 minutes
- Step 2: 50°C, for 50 minutes
- Step 3: 85°C, for 5 minutes

Tubes were briefly centrifuged to collect the reactions. 1  $\mu$ l of RNase H was added to each tube and incubated for 20 minutes at 37°C in order to remove the RNA template from the cDNA: RNA hybrid molecules by digestion with RNase after first-strain synthesis.

#### 4.24 Reverse Transcription PCR (RT-PCR)

Once synthesised the cDNA from mRNA, the RT-PCR reaction was set up as follows:

XBP1 forward + reverse primers (FR)	1 $\mu$ l
cDNA	2 $\mu$ l
PCR master mix	50 $\mu$ l

Reagents were added in succession and gently mixed by pipetting. Tubes were put into the PCR block and the following programme was performed:

- Step 1: 95°C, for 3 minutes
- Step 2: Denaturation at 95°C, for 15 seconds
- Step 3: Annealing at 50°C, for 20 seconds
- Step 4: Extension at 72°C, for 30 seconds

Steps 2-3 were repeated 35 times

To view the samples, an agarose gel was run as described in section 4.7, but with the following modifications. The gel was prepared by mixing TAE 1X (150 ml) with 3.3% (wt/vol) agarose (2.2 g) and 3.3% (wt/vol) Sea Plaque agarose (2.2 g). 20  $\mu$ l of the PCR reaction was analysed on the agarose gel previously prepared and after an adequate migration, an ultraviolet trans-illuminator was used to identify and scan DNA bands (Syngene).

Hs\_GAPDH\_1\_SG QuantiTect<sup>R</sup> Primer Assay (Qiagen) was used as loading control for RT-PCR samples. For each tube, the RT-PCR of GAPDH was set up as follows:

Hs GAPDH 1 SG	1 $\mu$ l
cDNA	1 $\mu$ l
PCR master mix	20 $\mu$ l



Samples amplified with GAPDH primers were loaded into a 0.7% agarose gel. After an adequate migration the resulting gel was analysed (see 4.7).

## Results

### 5. Monocytes from donor's human blood

#### PCR analyses of *C. jejuni* strains.

Before lysate preparation and OMV isolation, it was verified the *cdtA* gene presence or absence in *C. jejuni* wild type and *cdtA* mutant strains respectively. The resulting electrophoresis confirmed the wild type nature of *C. jejuni* ATCC 33291, *C. jejuni* ISS 1 (**Fig. 5.1**), and *C. jejuni* 11168H (**Fig.5.2**), and the presence of the *cdtA* gene mutation in the *C. jejuni* 11168H *cdtA* mutant strain (**Fig. 5.2**).

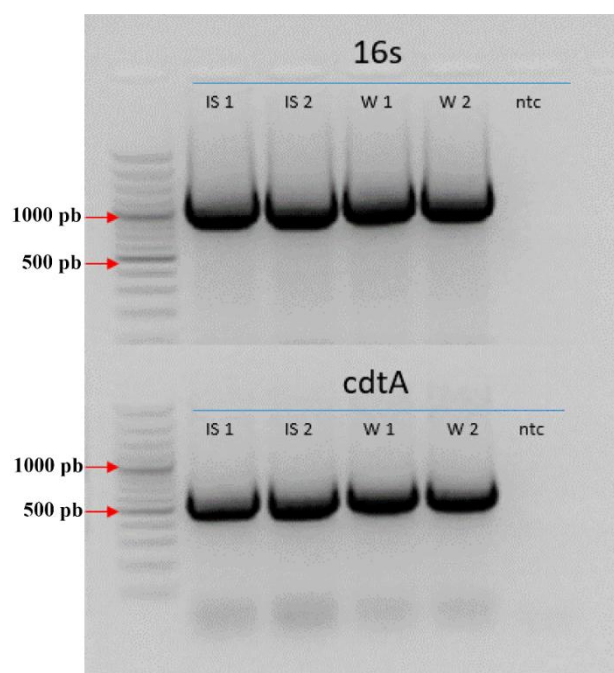


**Fig. 5.1** Electrophoresis from genomic DNA purified by two clones of the *C. jejuni* ATCC 33291 wild type strain (**W1** and **W2**) and two clones of the *C. jejuni* ISS 1 wild type strain (**IS1** and **IS2**). *C. jejuni* genomes were purified using the PureLink Genomic DNA kit, amplified by PCR and analysed on TAE-agarose-ethidium bromide gel electrophoresis. The **ntc** shows the negative control. Quality of isolated genomic DNA was controlled by standard 16S rDNA. These results confirmed the presence of the *cdtA* gene in all investigated clones.

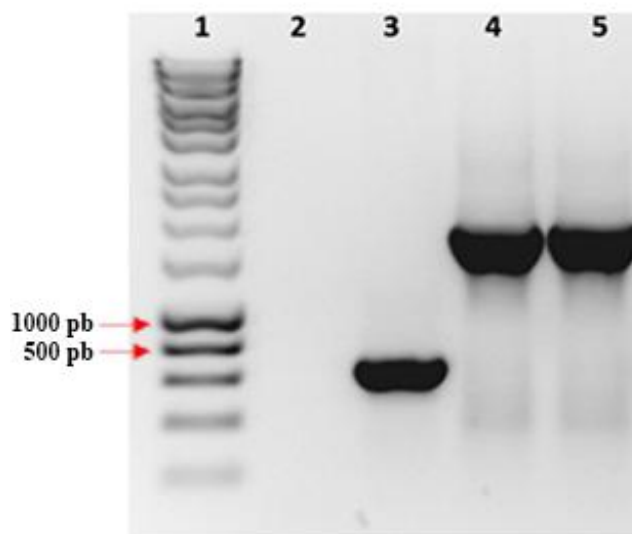


**Fig.5.2** Electrophoresis from genomic DNA purified by *C. jejuni* 11168H wild type strain (lane 3) and two clones of the *C. jejuni* 11168H *cdtA* mutant strain (lanes 4 and 5). *C. jejuni* genomes of wild type and *cdtA* mutant strains were purified using the PureLink Genomic DNA kit, amplified by PCR and analysed on TAE-agarose-ethidium bromide gel electrophoresis. The lane 2 shows the negative control. These results confirmed the presence of the *cdtA* gene mutation in the *C. jejuni* 11168H *cdtA* mutant strain.

### **Morphological features, cell death and absolute count**

It has been widely shown how CDT intoxication induces cellular distension/enlargement in target cells (Dixon et al, 2015). Forward light scatter parameter (FSC) was used as an indicator of cell size in cytometry; these data were taken together with microscopy analyses of morphologic appearance.

We compared FSC values of untreated control cells with FSC values of cells that were treated with lysates previously prepared. All treatments induced a moderate increase in FSC values and cell enlargement after 24 hours (**Fig. 5.3A**). At 48 hours, as predicted, cells preincubated with lysates from the wild type strains showed the typical distension induced by the CDT, whereas cells preincubated with the *C. jejuni* 11168H *cdtA* mutant lysate revealed a significant reduction in FSC values, also due to the apoptotic shrinkage that occurred in these last (see data on Propidium iodide positivity)

The PI (Propidium iodide) supravital labelling allowed us to detect and discriminate necrotic and apoptotic cells (**Fig. 5.3C**). PI results demonstrated that lysates caused a significant increase in PI positive cells (apoptotic cells) overall. Of note, from 24 hours onwards, both lysates from the wild type strains acted as death-inducers, but in two different ways. To

deeply monitor the phenomenon of cell death, we performed cell count by using Trypan blue viability test and absolute counting beads in cytometry (see 3.13 and 3.12). Microscopy visualization of this cellular rarefaction and total cell count are shown in **Fig. 5.3B** and **5.3D** respectively. Reduction in cell number was particularly evident in monocytes preincubated with the *C. jejuni* ATCC 33291 lysate.

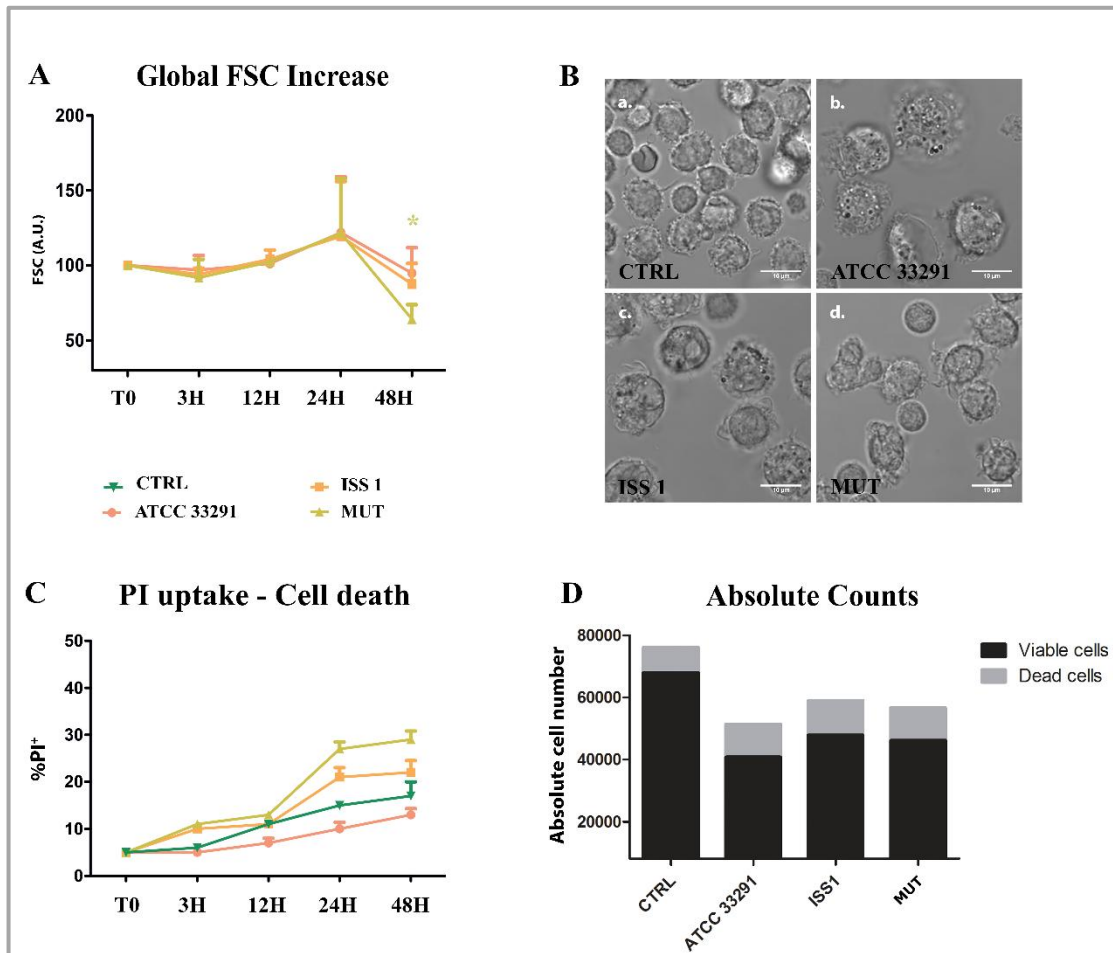


**Fig. 5.3** Morphological features and cell death rate. **(A)** Trends of FSC values for each treatment during the time course from T0 to 48 hours. FSC values were converted to arbitrary units (A.U.) setting control (T0) as 100. Each value is expressed as a mean  $\pm$  SD (Results from  $n \geq 3$  independent experiments). Two-way ANOVA with Bonferroni's multiple comparison test revealed  $*P < 0.05$  MUT vs control (T0) at 48 hours,  $*P < 0.05$  ISS 1 vs respective 24 hours, at 48 hours. The trend during the time course was determined to be significant ( $***P < 0.001$ ). **(B)** Bright field images of monocytes after 24 hours preincubation with *C. jejuni* ATCC 33291 lysate (b), *C. jejuni* ISS 1 lysate (c) and *C. jejuni* 11168H *cdtA* mutant lysate (d), compared to the untreated control cells (a). **(C)** Trends of percentage of PI positive cells for each experimental condition during the time course from T0 to 48 hours. Each value was expressed as a mean  $\pm$  SD (Results from  $n \geq 3$  independent experiments). **(D)** Absolute counts of viable and dead cells after 48 hours preincubation with lysates, compared to untreated control cells. Results from a representative experiment.

## Mitochondrial and lysosomal alterations

Perturbations of mitochondrial transmembrane potential resulted after preincubation with lysates (**Fig. 5.6A** and **Fig.5.7A**). TMRE MFI (mean fluorescence intensity) gradually decreased in monocytes infected with the *C. jejuni* ATCC 33291 lysate during the time course (from 3 to 48 hours). At 48 hours, these last showed the lowest TMRE value, compared with other experimental conditions, in which a decrease in TMRE MFI was followed by a return to the original/control values (T0).

Cardiolipin (CL) is an easily oxidizable phospholipid present in mitochondria. To investigate mitochondrial status, we also evaluated cardiolipin content by Nonyl Acridine Orange (NAO) staining. As shown in **Fig. 5.7B**, non-significant variations in cardiolipin content occurred in monocytes preincubated with the lysates. At the same time, by using the MitoSOX staining, we detected a dramatic increase in mitochondrial ROS from 24 hours onwards in all experimental conditions, compared to the control (T0) (**Fig. 5.7C**).

In order to investigate whether *C. jejuni* lysates altered host lysosome integrity during infection, cells were stained with Lyso Tracker Green: a lysosomotropic dye that emits fluorescence when accumulate in acidic compartments, such as lysosomes. As shown in **Fig. 5.6B** and **5.7D**, in terms of amount of LTG-accumulating lysosomes, *C. jejuni* lysates induced in monocytes a reduction at 12 hours followed by a significant increase at 24-48 hours, specifically in cells preincubated with the *C. jejuni* ISS 1 lysate.

These findings are consistent with PI results that showed that the mortality rate was low at 12 hours and pronounced at 24-48 hours. These data also demonstrated that, if monocytes initially reduced their lysosomal compartments in size, number and functionality, subsequently they increased them in late phases of the infection.

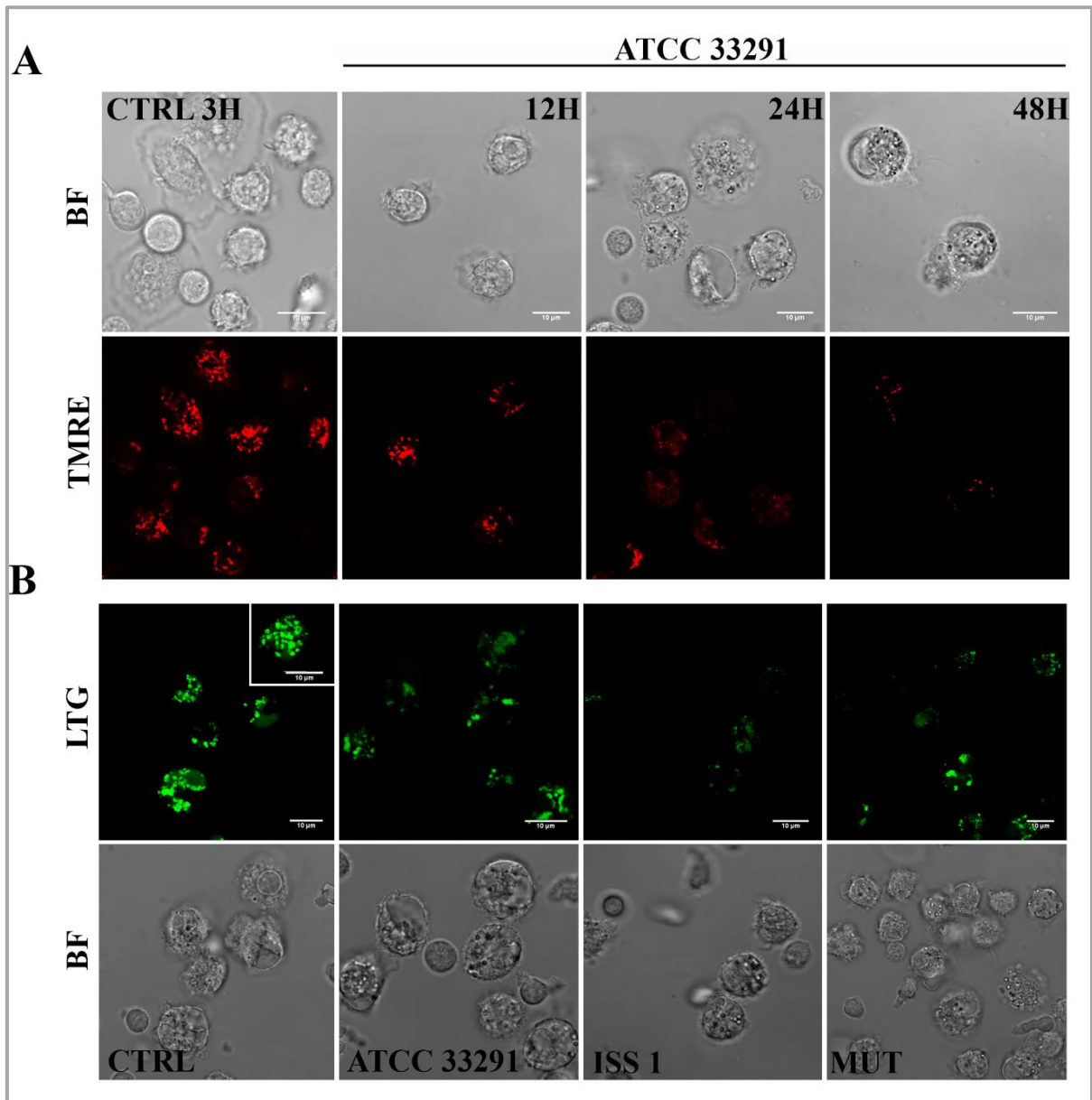


**Fig. 5.6 (A)** Single confocal optical sections of TMRE (mitochondria), with the relative bright field (BF) images, of CTRL cells and monocytes infected with *C. jejuni* ATCC 33291 lysate for 12, 24 and 48 hours. **(B)** Single confocal optical sections of LTG (lysosomes) with the relative BF images for CTRL cells, and cells infected with ATCC 33291, ISS 1 and 11168H *cdtA* mutant lysates for 12 hours.

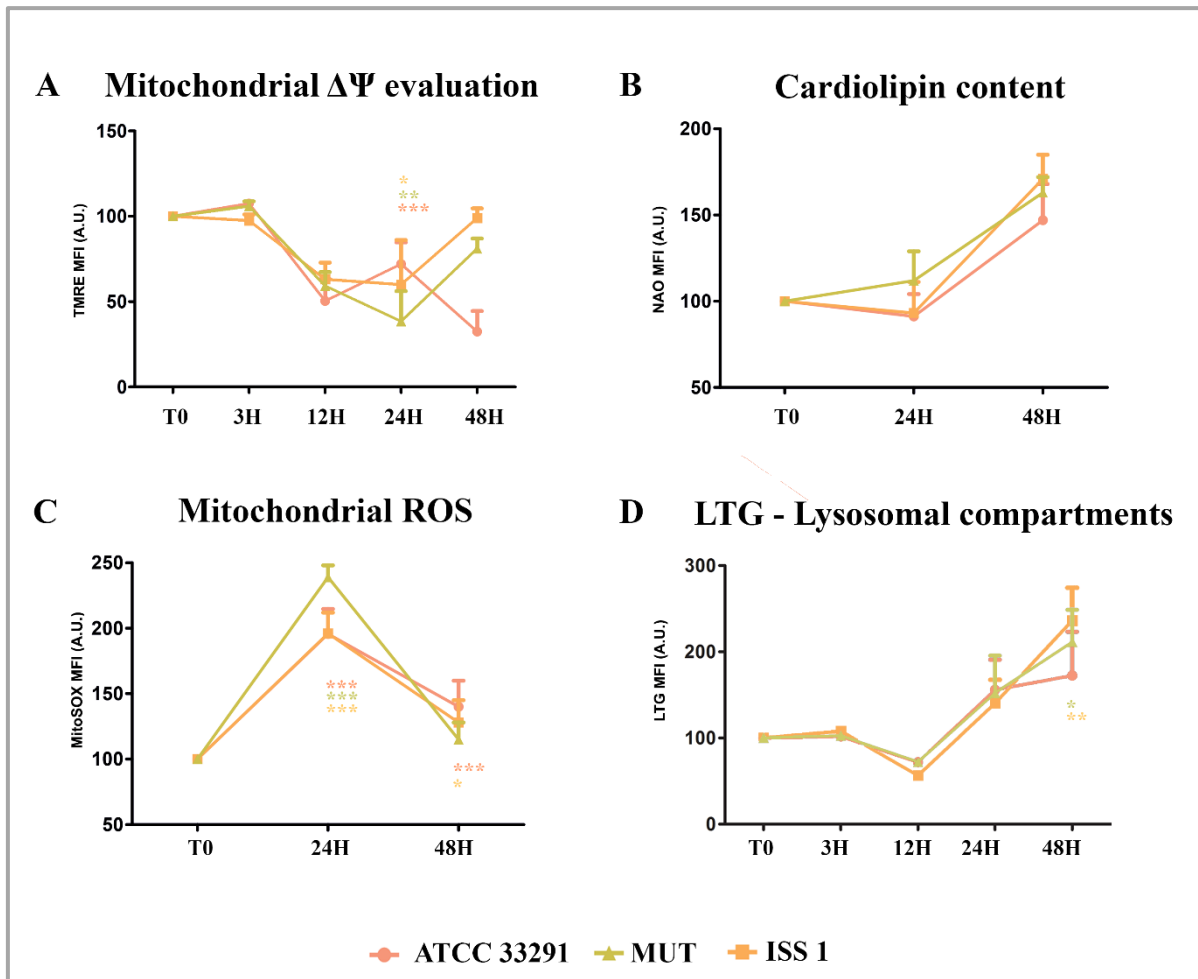


**Fig. 5.7 (A)** Trends of TMRE MFI for each treatment during the time course from T0 to 48 hours. Mean values were converted to A.U. setting control (T0) as 100. Each value is expressed as a mean  $\pm$  SD (Results from  $n \geq 3$  independent experiments). Two-way ANOVA with Bonferroni's multiple comparison test revealed: \* $P < 0.05$  ISS1 vs control (T0) at 24 hours, \*\* $P < 0.001$  MUT vs control (T0) at 24 hours, \*\*\* $P < 0.001$  ATCC 33291 vs control (T0) at 48 hours. The trend during the time course was determined to be significant (\*\*\* $P < 0.001$ ).

**(B)** Trends of NAO MFI for each experimental condition during the time course from T0 to 48 hours. Mean values were converted to A.U. setting control (T0) as 100. Each value is expressed as a mean  $\pm$  SD (Results from  $n \geq 3$  independent experiments).

**(C)** Trends of MitoSOX MFI for each treatment during the time course from T0 to 48 hours. Mean values were converted to A.U. setting control (T0) as 100. Each value is expressed as a mean  $\pm$  SD (Results from  $n \geq 3$  independent experiments) Two-way ANOVA with Bonferroni's multiple comparison test revealed: \*\*\* $P < 0.001$  ATCC 33291 vs control (T0) at 24 and 48 hours, \*\*\* $P < 0.001$  MUT vs control (T0) at 24 hours, \*\*\* $P < 0.001$  ISS 1 vs control (T0) at 24 hours, \* $P < 0.05$  ISS 1 vs control (T0) at 48 hours, \*\*\* $P < 0.001$  ATCC 33291 and ISS 1 vs MUT at 24 hours.

**(D)** Trends of LTG MFI for each treatment during the time course from T0 to 48 hours. Mean values were converted to A.U. setting control (T0) as 100. Each value is expressed as a mean  $\pm$  SD (Results from  $n \geq 3$  independent experiments). Two-way ANOVA with Bonferroni's multiple comparison test revealed: \* $P < 0.05$  MUT vs control (T0) at 48 hours, \*\* $P < 0.01$  ISS 1 vs control (T0) at 48 hours. The trend during the time course was determined to be significant (\*\*\* $P < 0.001$ ).

### **p53 and Bcl-2 detection**

Our results revealed a decrease in p53 content in monocytes preincubated with the wild type lysates for 12 hours. This status remained stable until 24 hours, then p53 intracellular content increased, reaching initial physiological levels (**Fig. 5.8A**). These fluctuations reflected the balance between growth arrest and apoptosis mechanisms (Siegl & Rudel, 2015). Apoptosis was accompanied by morphological changes, including nucleus condensation, apoptotic blebs formation and appearance of cytoplasmic vacuoles and granulation (**Fig 5.8C**).

The apoptotic threshold of a cell was determined by a ratio of pro-apoptotic and anti-apoptotic signals, and apoptosis occurred when pro-apoptotic signals outweighed the counteracting anti-apoptotic factors (Verbeke et al, 2006).

Anti-apoptotic Bcl-2 family proteins are known to influence the apoptotic threshold. Our findings revealed the following scenario for Bcl-2 (**Fig. 5.8B**): from T0 to 12 hours a drop in Bcl-2 intracellular levels was observed, in particular in monocytes preincubated with the *C. jejuni* ATCC 33291 lysate; at 24 hours Bcl-2 values of all experimental conditions were very similar.



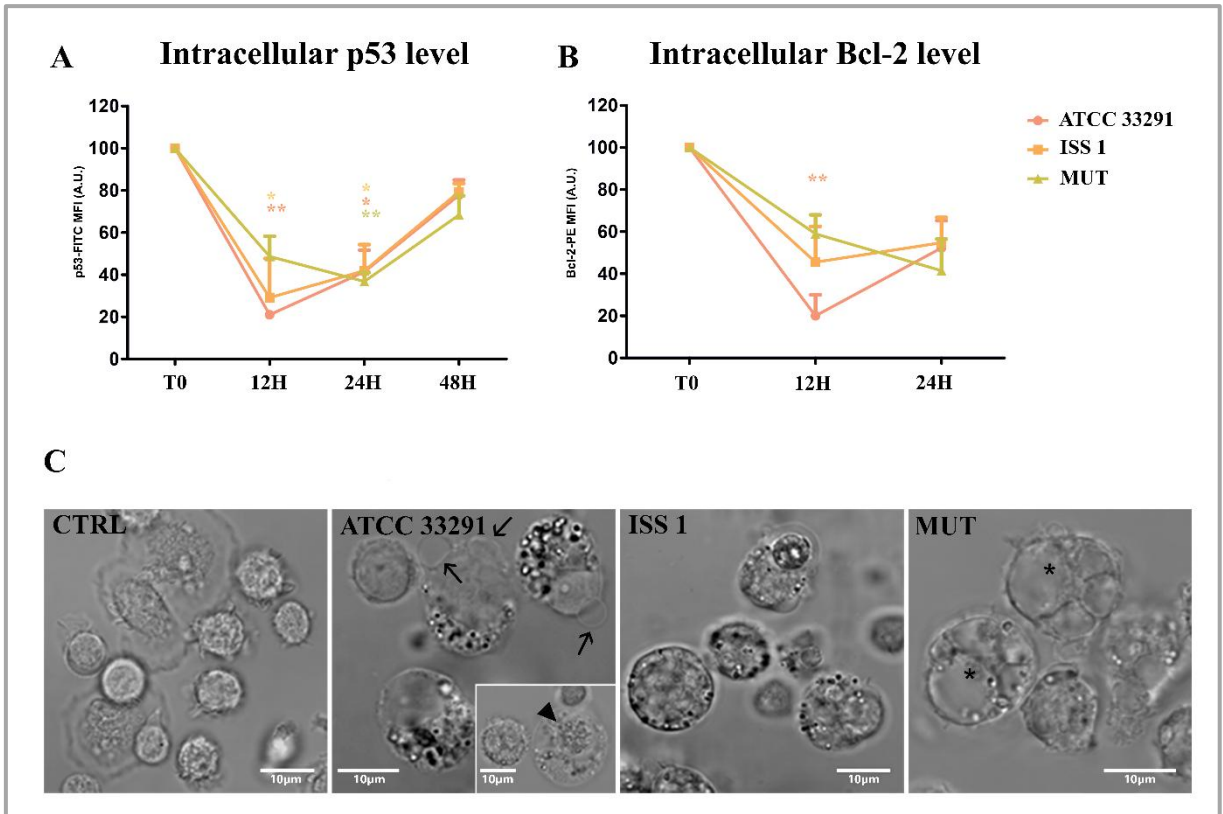


**Fig. 5.8** p53 and Bcl-2 protein levels and morphologic features of cell death. **(A)** Graphs showing p53 intracellular content for each experimental condition during the time course from T0 to 48 hours. Mean values were converted to A.U. setting control (T0) as 100. Each value is expressed as a mean  $\pm$  SD (Results from  $n \geq 3$  independent experiments). Two-way ANOVA with Bonferroni's multiple comparison test revealed: \* $P < 0.05$  ISS1 vs control (T0) and \*\* $P < 0.01$  ATCC vs control (T0) at 12 hours, \* $P < 0.05$  ATCC and ISS1 vs control (T0) at 24 hours, \*\* $P < 0.01$  MUT vs control (T0) at 24 hours.

**(B)** Graphs showing Bcl-2 intracellular content for each experimental condition during the time course from T0 to 48 hours. Mean values were converted to A.U. setting control (T0) as 100. Each value is expressed as a mean  $\pm$  SD (Results from  $n \geq 3$  independent experiments). Two-way ANOVA with Bonferroni's multiple comparison test revealed: \*\* $P < 0.01$  ATCC vs control (T0) at 12 hours.

**(C)** Bright field images of monocytes after 24 hours preincubation with *C. jejuni* ATCC 33291, ISS1 and 11168H *cdtA* mutant lysates, compared to untreated control cells (CTRL). In infected cells it is possible to appreciate apoptotic blebs (black arrows), condensed nuclei (arrowhead), cytoplasmic vacuoles (asterisks) and a diffuse granulation (in particular in ATCC 33291 and ISS 1).

## ER stress and modulation of intracellular Ca<sup>2+</sup> levels

ER stress might be both a trigger and consequence of chronic inflammation. Monocytes were stained with ER-Tracker Green and Fura-2 AM in order to investigate ER stress and intracellular Ca<sup>2+</sup> level perturbations. ER-Tracker Green dye is a cell-permeant, live-cell stain that is highly selective for the ER. It stains ER membranes and it is known to be a ER stress marker in both cytometry and microscopy (Conn, 2011). Our data showed that ER stress occurred after 12-24 hours of treatment (**Fig. 5.9A**), especially in monocytes infected with the *C. jejuni* ATCC 33291 lysate. Moreover, the lysate from the *cdtA* mutant strain caused more ER modifications than the ISS 1 wild type strain; we supposed that ER stress is not an effect associated to the CDT, but it is due to other *C. jejuni* virulence factors.

In addition, FURA-2 AM results showed an increase in intracellular Ca<sup>2+</sup> content in monocytes preincubated for 48 hours with the *C. jejuni* ATCC 33291 lysate compared with other experimental conditions (data not statistically significant) (**Fig. 5.9B**).

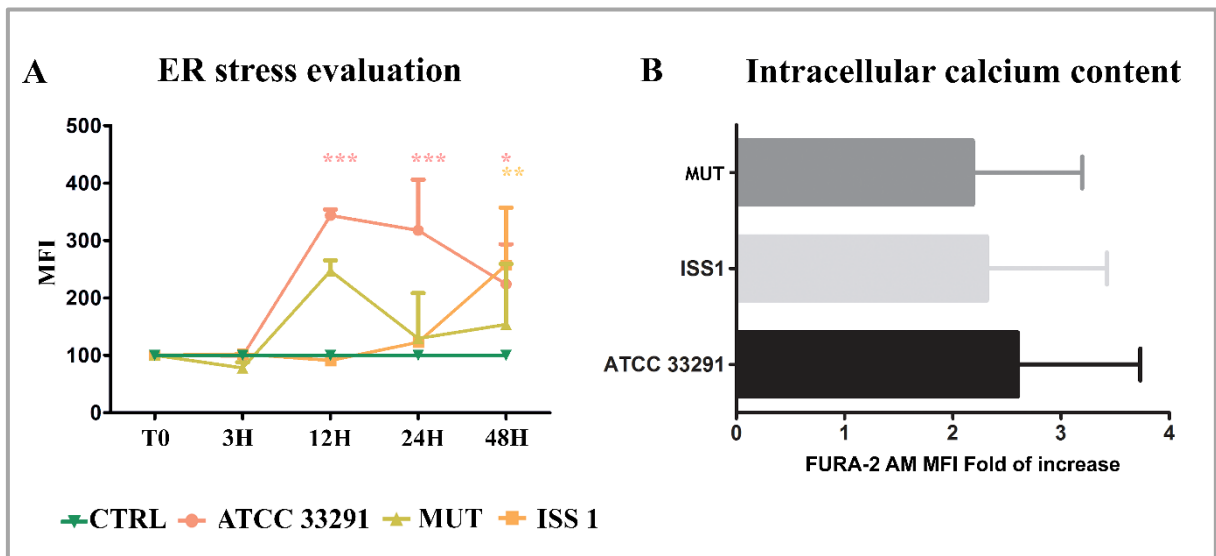


**Fig. 5.9 (A)** Graph showing ER-Tracker Green MFI for each experimental condition during the time course from T0 to 48 hours. Mean values were converted to A.U. setting control (T0) as 100. Each value is expressed as a mean  $\pm$  SD (Results from  $n \geq 3$  independent experiments). Two-way ANOVA with Bonferroni's multiple comparison test revealed: \*\*\* $P < 0.001$  ATCC 33291 vs control (T0) at 12 and 24 hours, \* $P < 0.05$  ATCC 33291 vs control (T0) at 48h, \*\* $P < 0.01$  ISS 1 vs control (T0) at 48 hours, \*\*\* $P < 0.001$  ATCC 33291 vs ISS 1 at 12 hours and \*\* $P < 0.01$  at 24 hours, \*\*\* $P < 0.001$  ATCC 33291 vs MUT at 24 hours. **(B)** Fold of increase in intracellular Ca<sup>2+</sup> content, measured by means of FURA-2 AM, referred to control samples after 48 hours preincubation. Each value is expressed as a fold of increase  $\pm$  SD (Results from  $n \geq 3$  independent experiments).

### Surface CD59 expression

CD59 expression was studied in monocytes in order to investigate if MAC complex was involved in cell response triggered by *C. jejuni* lysates. It was found that from 24 to 48 hours in infected monocytes an upregulation of CD59 surface expression occurred: it was particularly evident in cells preincubated with the *C. jejuni* ISS 1 lysate, followed by monocytes preincubated with the mutant strain lysate (**Fig.5.10**). This condition, being CD59 a critical complement regulator in protecting human cells from MAC formation and MAC-induced phenomena, seems to predispose monocytes to survive. In fact, it is known that CD59 over-expression may assist malignant cells to escape immunologic surveillance and complement-mediated cytotoxicity (Verbeke et al, 2006).

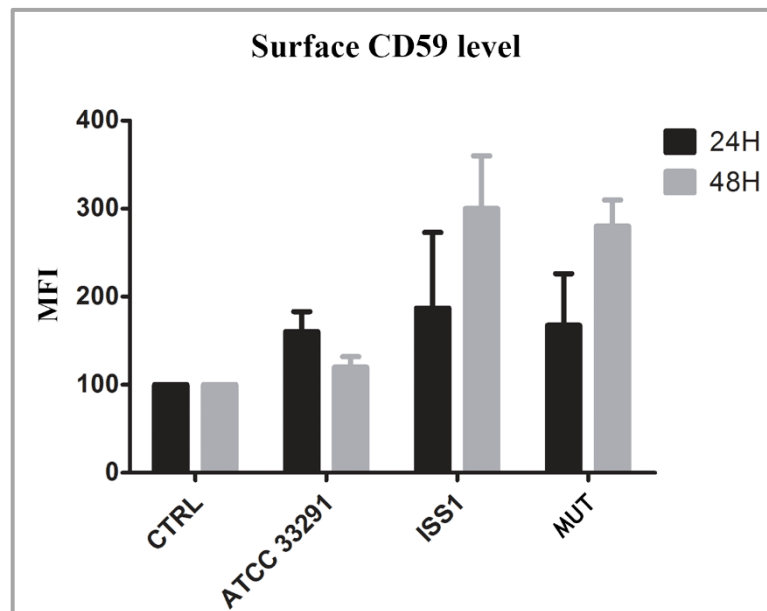


**Fig.5.10** Bar graph of CD59 expression for each experimental condition after 24 and 48 hours of treatment. Mean values were converted to A.U. setting control (T0) as 100. Each value is expressed as a mean  $\pm$  SD (Results from  $n \geq 3$  independent experiments).

### Surface LAMP-1 expression: lysosomal exocytosis

Infected and uninfected cells were also analysed for the presence of lysosomal protein LAMP-1 at cell surface. Being cells specialized to phagocytose, monocytes typically express low levels of surface LAMP-1 (CD107a). It was observed an increase in LAMP-1 expression principally in monocytes preincubated with the wild type lysates from T0 to 24 hours (**Fig. 5.11A**). Increasing the exposition time (48 hours), it was worth to note that a downregulation of LAMP-1 to hypo-physiologic levels occurred. Our data on lysosomal exocytosis, suggested that lysosomes, in the first infection stages, may “dump” indigested materials, reducing their accumulation within lysosomes, whereas at 48 hours a drop in exocytotic activity it was registered. These findings have to be coupled with LTG results: in fact, the decrease in lysosomes size and number was not due to the exocytosis activation. On the contrary at 48 hours, when LTG fluorescence peaked, LAMP-1 strongly decreased. This process might have an important role in secretion and plasma membrane repair since lysosomes play a key role in resealing the membrane to prevent cell death (McNeil, 2002).

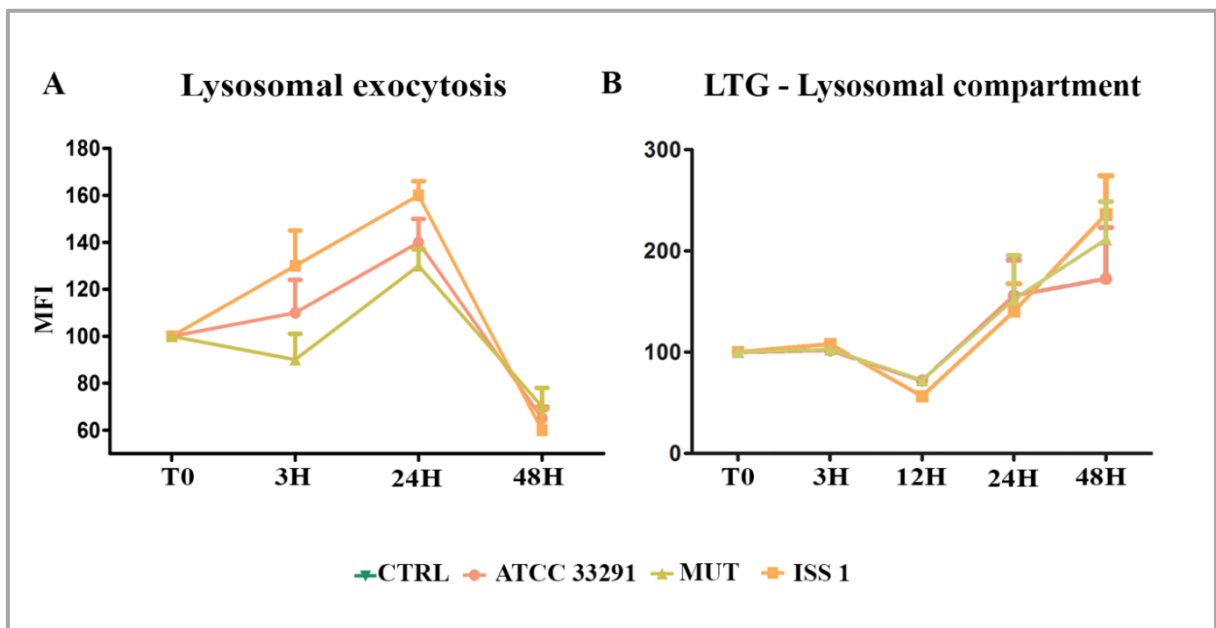


**Fig.5.11** (A) Graph showing lysosomal exocytosis for each experimental condition during the time course from T0 to 48 hours. Mean values were converted to A.U. setting control (T0) as 100. Each value is expressed as a mean  $\pm$  SD (Results from  $n \geq 3$  independent experiments). (B) Trends of LTG MFI for each treatment during the time course from T0 to 48 hours (described in **Fig. 5.7**).

### CD14 and ICAM-1 (CD54) variations

In infected monocytes, an early decrease in CD14 expression (T0-12 hours) was followed by an important increase in CD14 expression after 24 hours of treatment (**Fig. 5.12**).

Increased ICAM-1 expression induced by various pathogens was shown to mediate cell-to-cell adhesion in inflamed tissues (Tamai et al, 2005). As showed in **Fig. 5.13A**, an increase in ICAM-1 expression was detectable in monocytes particularly at 3 and 48 hours. Furthermore, confocal pictures revealed a variation in surface ICAM-1 distribution: a ‘punctuate’ organization with a loss of ‘cap’ distribution occurred confirming that a reshaping of the plasma membrane arose because of the infection (**Fig. 5.13B**).

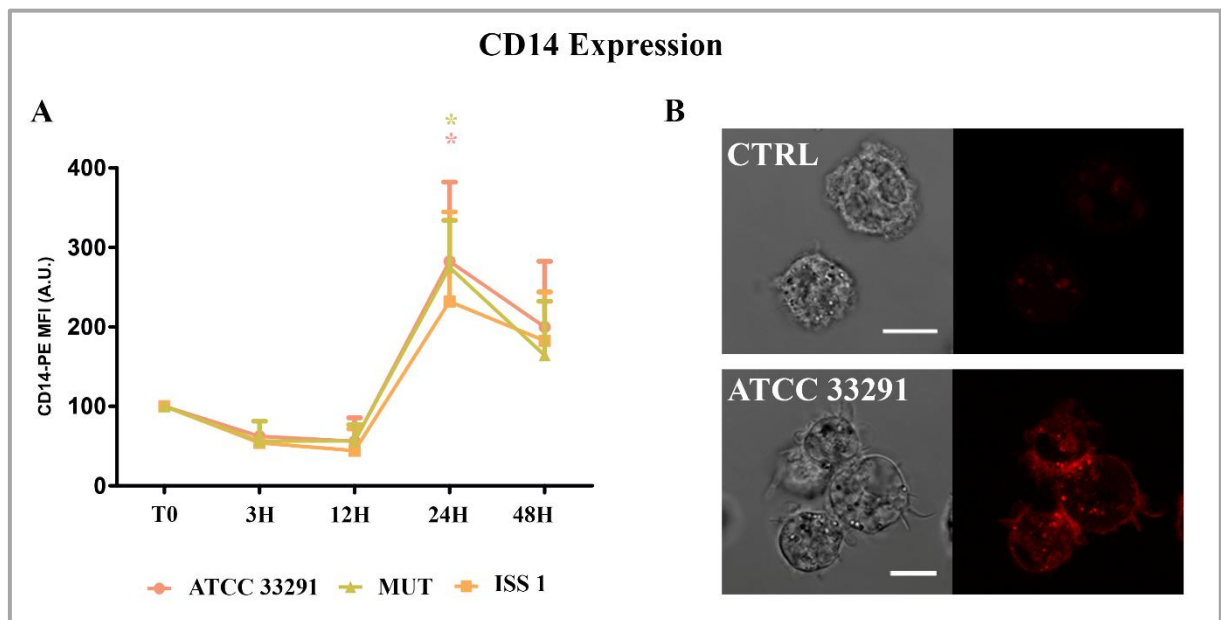


**Fig. 5.12** CD14 expression. **(A)** Graph showing CD14 expression in monocytes preincubated with lysates. Mean values were converted to A.U. setting control (T0) as 100. Each value is expressed as a mean  $\pm$  SD (Results from  $n \geq 3$  independent experiments). Two-way ANOVA with Bonferroni’s multiple comparison test revealed: \* $P < 0.05$  MUT and ATCC 33291 vs control (T0) at 24 hours, \* $P < 0.05$  MUT and ATCC 33291 vs respective 24 hours, at 3 hours; \* $P < 0.05$  MUT, ATCC 33291 and ISS 1 vs respective 24 hours, at 12 hours. The trend during the time course was determined to be significant (\*\* $P < 0.001$ ). **(B)** Confocal images of CD14-PE with the relative bright field images from monocyte control cells and monocytes preincubated with the *C. jejuni* ATCC 33291 lysate for 24 hours. Bars: 10 $\mu$ m.

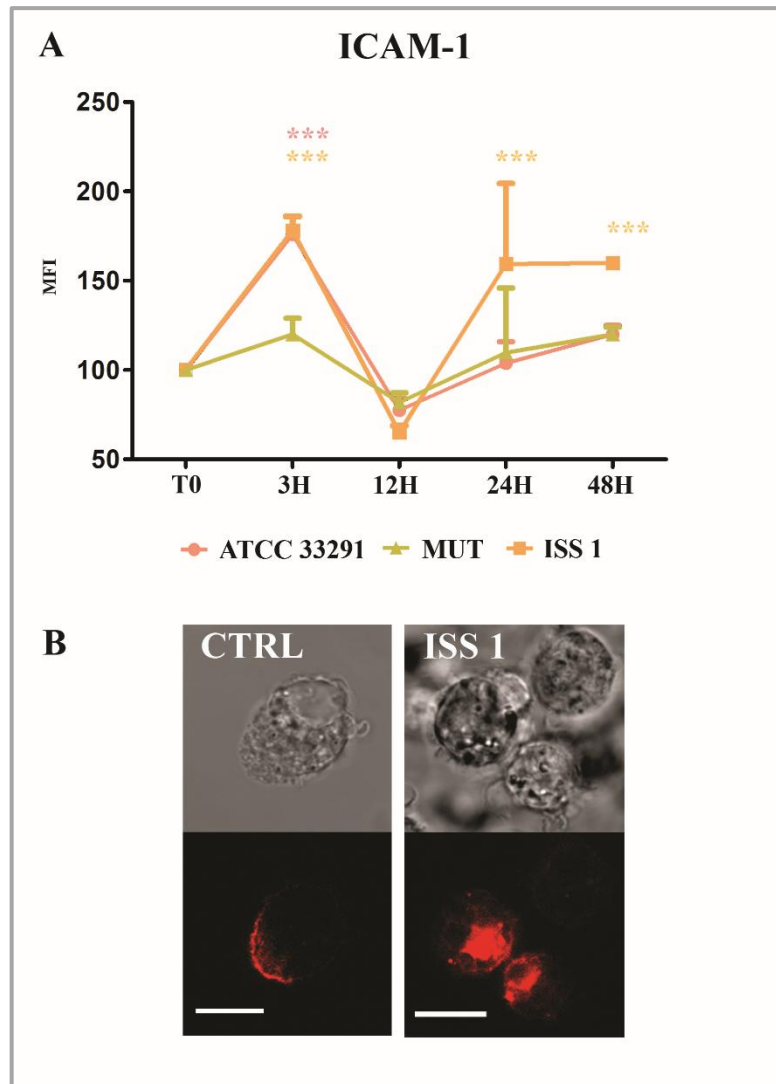


**Fig. 5.13** ICAM-1 expression. **(A)** Graph showing ICAM-1 expression Mean values were converted to A.U. setting control (T0) as 100. Each value was expressed as a mean  $\pm$  SD (Results from  $n \geq 3$  independent experiments). Two-way ANOVA with Bonferroni's multiple comparison test revealed: \*\*\* $P < 0.001$  ISS 1 vs control (T0) at 3, 24 and 48 hours, \*\*\* $P < 0.001$  ATCC 33291 vs control (T0) at 3 hours, \* $P < 0.05$  ISS 1 and ATCC 33291 vs respective 12 hours, at 3 hours. The trend during the time course was determined to be significant (\* $P < 0.05$ ). **(B)** Confocal images of CD54-PE with the relative bright field images from monocyte control cells and monocytes preincubated with ISS 1 lysate after 48 hours of treatment. Bars: 10 $\mu$ m.

## Discussion

Our results highlight that the **cellular distension**, typically induced by CDT, is mainly appreciable in monocytes preincubated with lysates from the wild type strains, particularly after 48 hours. During the time course, cell death increased, qualifying *C. jejuni* ATCC 33291 lysate as the best cell death-inducer, followed by *C. jejuni* ISS 1 lysate. Taking PI results together with other **cell death parameters**, we can say that it is very likely that a reduction in PI positive cells at 48 hours in monocytes treated with the *C. jejuni* ATCC 33291 strain is not due to a greater cell viability of these cells but to a greater **DNA damage**, that does not allow the binding between PI dye and DNA. This finding was also confirmed by absolute cell count at 48 hours.

In order to evaluate mitochondrial mass and morphology, as well as the involvement of **mitochondria** in the apoptotic pathway, cells were stained with TMRE and NAO, two mitochondria-specific fluorochromes. The collapse of the mitochondrial transmembrane potential leads to the opening of the mitochondrial permeability transition pores, the release of cytochrome c into the cytosol and the activation of the apoptotic cascade. Depending on the specific apoptotic stage in which cells are, mitochondrial transmembrane potential can increase or decrease: more polarized mitochondria (i.e. hyperpolarized, where the interior is more negative) will accumulate more cationic dye, whereas depolarized mitochondria (where the interior is less negative) accumulate less dye because of an extremely collapsed mitochondrial status (Hüttemann et al, 2012). The *C. jejuni* strain that induced the most relevant mitochondrial alterations was the ATCC 33291, confirming that this strain favours an intrinsic apoptotic pathway

In addition, an increase in the content of **reactive oxygen species** occurred in monocytes preincubated with lysates, probably in a CDT independent manner, as demonstrated by MitoSOX result, which are consistent with TMRE results.

We found mitochondria and lysosomes differently targeted by the different strains in monocytes. Indeed, whereas *C. jejuni* ATCC 33291 wild type strain showed to induce an intrinsic apoptotic pathway, characterized by the induction of mitochondria alterations, the *C. jejuni* ISS 1 wild type strain mostly induced lysosomal alterations, therefore an extrinsic apoptotic pathway. Furthermore, although at 48 hours host **acidic compartments/lysosomes** started to respond differently to the different lysates, from 3 to 12 hours the trend is the same for all experimental conditions: a significant decrease in LTG fluorescence indicates that a

neutralization of host acidic compartments occurred in infected cells in response to *C. jejuni* virulence factors contained within the lysates.

Changes in lysosomal acidic compartments, ER and p53 expression occurred together from T0 to 24 hours.

The **p53** tumour suppressor responds to certain cellular stresses by inducing transcriptional programs that can lead to growth arrest or apoptosis. P53-dependent growth arrest and apoptosis are usually caused by stimuli that trigger DNA damage (Amaral et al, 2010).

In this investigation, lysates from the wild type strains induced an important decrease in p53 intracellular content from T0 to 12 hours; this effect is not shown in cells preincubated with the mutant strain. This finding underlines that this specific effect is mainly due to the CDT. Different authors have demonstrated that the degradation of p53 prolongs pathogen survival (Zaika et al, 2015). However, p53 levels increase after 48 hours. This increase might be also associated to data about lysosomal compartments and lysosomal exocytosis at the same time point. Our findings also revealed a strong decrease in **Bcl-2** content specifically after 12 hours in monocytes treated with the ATCC 33291 lysate: this pro-apoptotic response is consistent with the deep mitochondria alterations induced by this strain that has been already described.

Overall, lysates induced **ER stress** in monocytes compared to the untreated control cells. Of note, an important stress was induced by the *C. jejuni* ATCC 33291 strain. Surprisingly, the lysate from the *cdtA* mutant strain caused more ER alterations than the ISS 1 wild type strain; inducing us to suppose that ER stress is not associated to the CDT, but it is due to other *C. jejuni* virulence factors. ER data are consistent with the increase in cytosolic Ca<sup>2+</sup> content induced by lysates.

**CD59** is an 18-kDa cell surface protein that inhibits the formation of the MAC, the pore-forming toxin of the complement system that cells activate in order to kill pathogens. The marked increase of CD59 expression observed in monocytes treated with lysates could promote the pro-inflammatory/non-lytic role of MAC, resulting in protection of the bacterium/virulence factors from the complement attack. CD59 revealed to be as a general infection marker in monocytes. The maximum increase of CD59 is registered at 48 hours for ISS 1 and 11168H *cdtA* mutant lysates, whereas cells treated with the *C. jejuni* ATCC 33291 lysate showed a reduction at this time point: this is consistent with the presence of an apoptotic rate. Upregulation of CD59 in monocytes preincubated with the mutant strain suggested that CDT is not implicated in processes described above.

Although monocytes express basal lysosomal exocytosis processes because of their phagocytic nature, **LAMP-1** upregulation was caused by lysates used in our investigations.



However, our findings suggested that virulence factors contained in lysates are able to activate lysosomal exocytosis in monocytes in a CDT-dependent manner.

The **CD14** involvement in host defence against viral and bacterial infections has been investigated in several experimental models. It was reported that CD14 is upregulated by bacterial LPS and contribute to CD14-mediated phagocytosis of Gram-negative bacteria (Grunwald et al, 1996). In this work there were not found particular differences in CD14 expression between cells preincubated with the wild type and mutant strains, on the contrary variations between uninfected and infected cells and variations in CD14 expression during the time course were statistically significant.

**ICAM-1** mobility is of general importance for immune responses that require firm adhesion (Comrie et al, 2015). Adhesion molecules, such as ICAM-1, direct immune cells to the inflammation site by the process of rolling, activation, adhesion, and transmigration (Ley et al, 2007). Altered ICAM-1 mobility perturbs inter-cellular adhesion. In this work, ICAM-1 expression showed marked fluctuations from T0 to 48 hours, peaking after 3 hours of treatment and dropping at 12 hours, with a subsequent increase at 48 hours. Being this behaviour mainly evident in cells preincubated with the lysates from the wild type strains, it is possible to affirm that CDT is involved in these modifications.

Even though some statistically significant results were achieved by this part of the project, a better method has to be optimized to study the effects of *C. jejuni* virulence factors in monocytes isolated from donors, and to better investigate the behaviour that different *C. jejuni* strains can explicate and the CDT role. This model has some limitations: the great biologic variability of primary myeloid cells from different donors, the moderate recovery obtainable from each separation procedure (monocytes represent 3-7% of total white blood cells, monocytes absolute count is  $1.5 \times 10^8$  to  $7.0 \times 10^8/l$  blood in healthy human adults) and the differentiation to macrophages that begins when monocytes stably adhere. In addition, because of the high mortality rate that occurred in monocyte cultures after 48 hours, no investigations were carried out after this time point.

## 6. U937 cell model: U937 cells preincubated with *C. jejuni* lysates

### Subdivision of U937 cells sub-populations

To better investigate the effects of the CDT contained within lysates and OMVs isolated from the *C. jejuni* wild type and mutant strains (see 7. Chapter 3) in U937 cells, cytometric analyses were conducted not only on total U937 cells, but also focusing the attention on different U937 sub-populations. Sub-populations were established depending on the morphological parameters and considering that the presence of enlarged cells after the treatment was due to the effects caused by the CDT. Therefore, in U937 cells, all investigated parameters were studied in: -total U937 cells, -distended cells, -viable/non-apoptotic cells and -dead cells (**Fig 6.1**). Particular attention was given to ‘distended cells’ because they were certainly affected by the CDT. In chapter 5 it was not possible to classify monocytes in these sub-populations because of the reduced number of available cells in the samples.

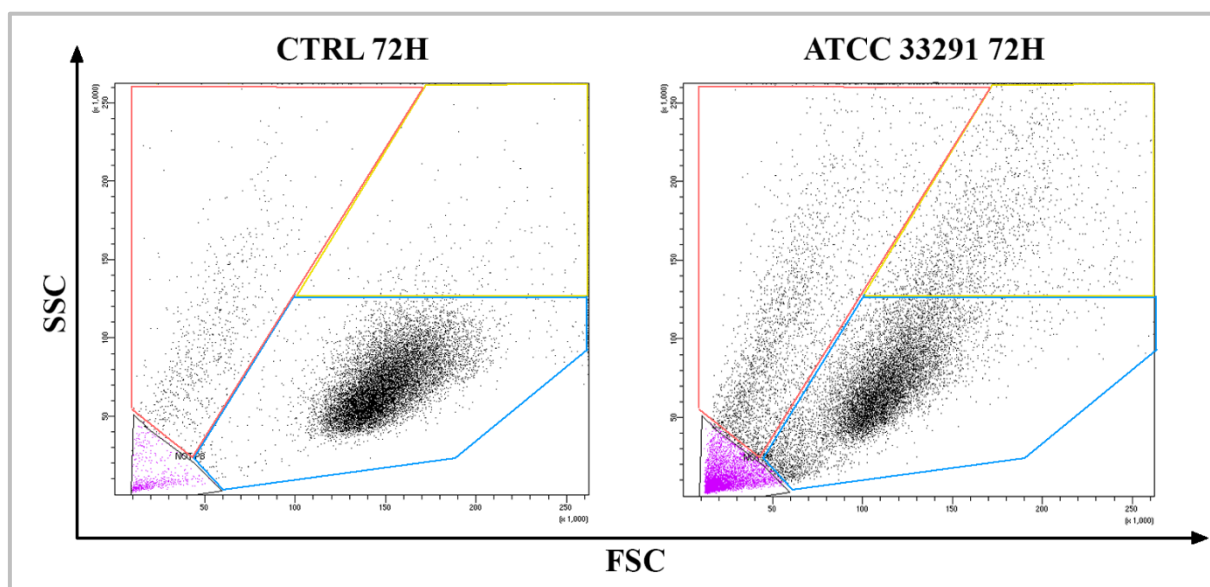


**Fig. 6.1** U937 sub-populations were established depending on the morphological parameters: red gate shows dead cells, yellow gate shows distended cells, blue gate shows viable cells. It was established that total cells were the summary of red, yellow and blue gates. In pink are debris excluded by the analysis. Dot plots in the picture show CTRL untreated cells and cells treated with the *C. jejuni* ATCC 33291 lysate for 72 hours.

## Morphological features, cell death and absolute count

As previously observed in monocytes, morphologic appearance was studied by microscopic and cytometric investigations. Also in U937 cells, *C. jejuni* wild type lysates caused the typical CDT dependent-cellular distension compared to untreated control cells and cells treated with the mutant strain lysate. Trypan blue viability test and absolute counting beads were used for cell counting (see 3.13 and 3.12), revealing that lysates from the wild type strains caused reduction in cell number in U937 cells (data not shown). In addition, AnxV-PI double staining revealed that AnxV-PI positive cells, that represent the apoptotic cells, were particularly present in U937 cells preincubated with the *C. jejuni* ATCC 33291 lysate (**Fig. 6.2 and 6.3**).

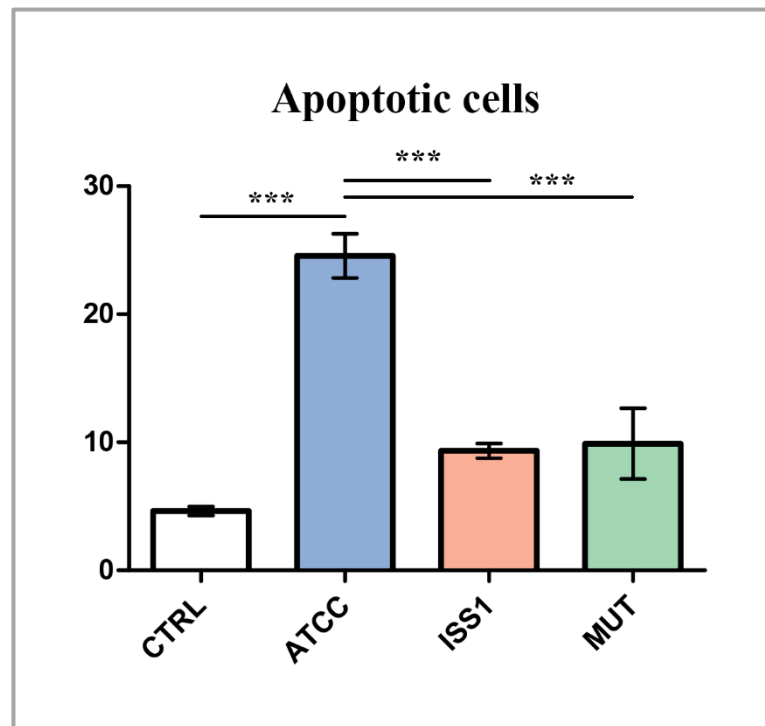


**Fig. 6.2** Histograms of percentage of AnxV-PI positive cells calculated after 72 hours from lysate administration in total cells. Each value is expressed as a mean  $\pm$  SD (Results from  $n \geq 3$  independent experiments). One-way ANOVA with Bonferroni's multiple comparison test revealed: \*\*\* $P < 0.001$  CTRL vs ATCC 33291, \*\*\* $P < 0.001$  ATCC 33291 vs ISS 1, \*\*\* $P < 0.001$  ATCC 33291 vs MUT.

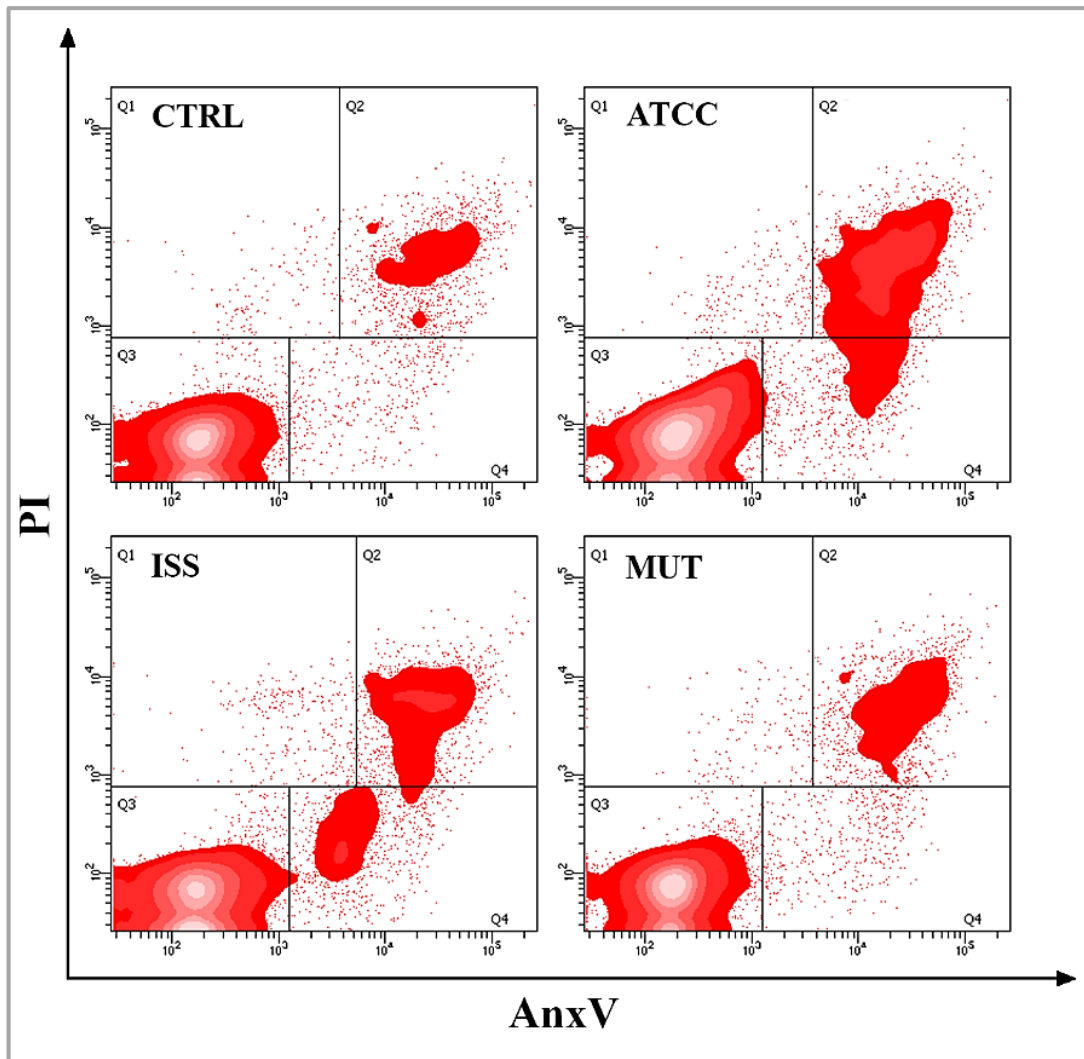


**Fig. 6.3** Density plots of PI vs AnxV MFI of all experimental conditions. Q1 shows PI positive cells, Q4 shows AnxV positive cells, Q2 shows AnxV-PI positive cells, Q3 shows AnxV-PI negative cells and debris.

## Evaluation of cellular division

Efficiency of CDT in G2-M blocking was investigated by means of CFSE labelling. Results at 48 hours showed that *C. jejuni* ATCC 33291 lysate exerted maximally this blocking-effect, whereas lysate from the *C. jejuni* ISS 1 strain was less active, showing percentages of undivided cells slightly higher than cells treated with the lysate from the mutant strain. In fact, as shown in **Fig 6.4**, a big amount of ATCC 33291 infected cells do not enter in mitosis at 48 hours. Of note, this approach not only confirmed data from literature, but also suggested that lysates from different wild type strains can show different effects in U937 cells.

Efficiency of CDT in G2-M blocking was calculated at 72 hours (**Fig. 6.5**). Histograms regarding 1°, 2° and 3° divisions indicated that CDT effects on DNA, not only persist after 72 hours from lysate administration, but also became more evident, particularly for the *C. jejuni* ATCC 33291 lysate.

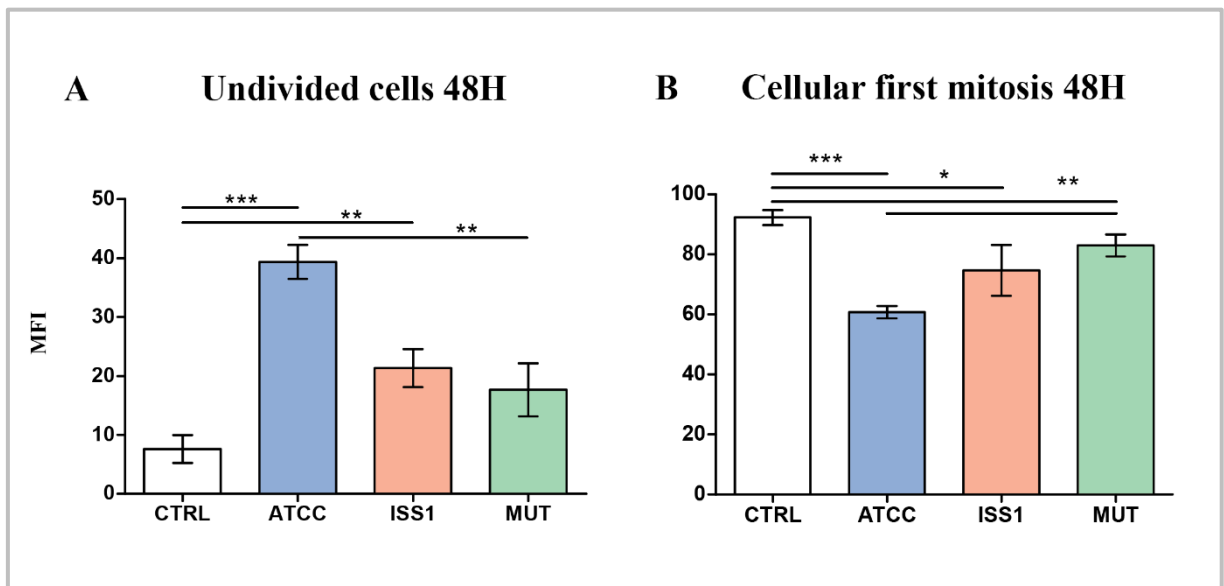


**Fig. 6.4** (A) Histogram of undivided cells calculated in cytometry via CFSE staining at 48 hours. Paired *t* test (two-tailed P value) revealed: \*\*\*P<0.0001 CTRL vs ATCC 33291, \*\*P<0.001 CTRL vs ISS 1, \*\*P<0.001 ATCC 33291 vs MUT. (B) Histogram of divided cells calculated in cytometry via CFSE staining at 48 hours. Paired *t* test (two-tailed P value) revealed: \*\*\*P<0.0001 CTRL vs ATCC 33291, \*P<0.05 CTRL vs ISS 1, \*\*P<0.001 CTRL vs MUT, \*\*P<0.001 ATCC 33291 vs MUT

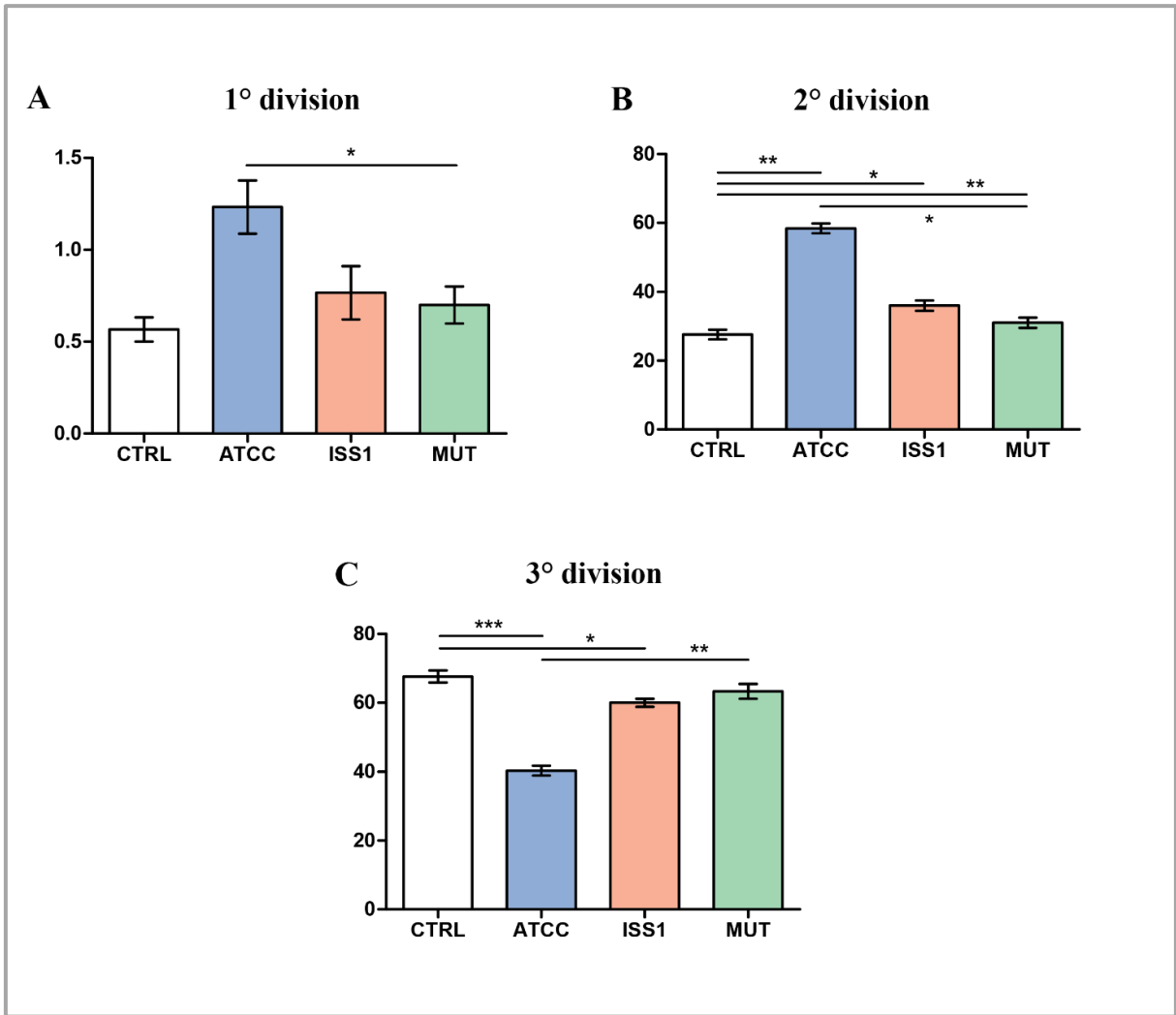


**Fig. 6.5** Histograms of cells in 1°, 2° and 3° division calculated in cytometry via CFSE staining at 72 hours (A) Paired *t* test (two-tailed P value) revealed: \* $P < 0.05$  MUT vs ATCC 33291; (B) \*\* $P < 0.001$  CTRL vs ATCC 33291, \*\* $P < 0.001$  CTRL vs MUT, \* $P < 0.05$  CTRL vs ISS 1, \* $P < 0.05$  MUT vs ATCC 33291; (C) \*\*\* $P < 0.0001$  CTRL vs ATCC 33291, \*\* $P < 0.001$  MUT vs ATCC 33291, \* $P < 0.05$  CTRL vs ISS 1.

### Mitochondrial alterations

Microscopy and cytometric TMRE results reported interesting mitochondrial membrane potential perturbations after treatments (**Fig. 6.6 and 6.7**). Significant changes in TMRE MFI occurred after 72 hours in cells preincubated with the wild type strains; in particular, the *C. jejuni* ATCC 33291 lysate caused a major increase in TMRE MFI in both total and distended U937 cells. Lysates altered mitochondria both functionally and structurally: indeed, confocal pictures highlighted the presence of ‘fragmented’ mitochondria in infected cells, compared to uninfected control cells, where mitochondrial morphology remained unaltered (**Fig. 6.6**).

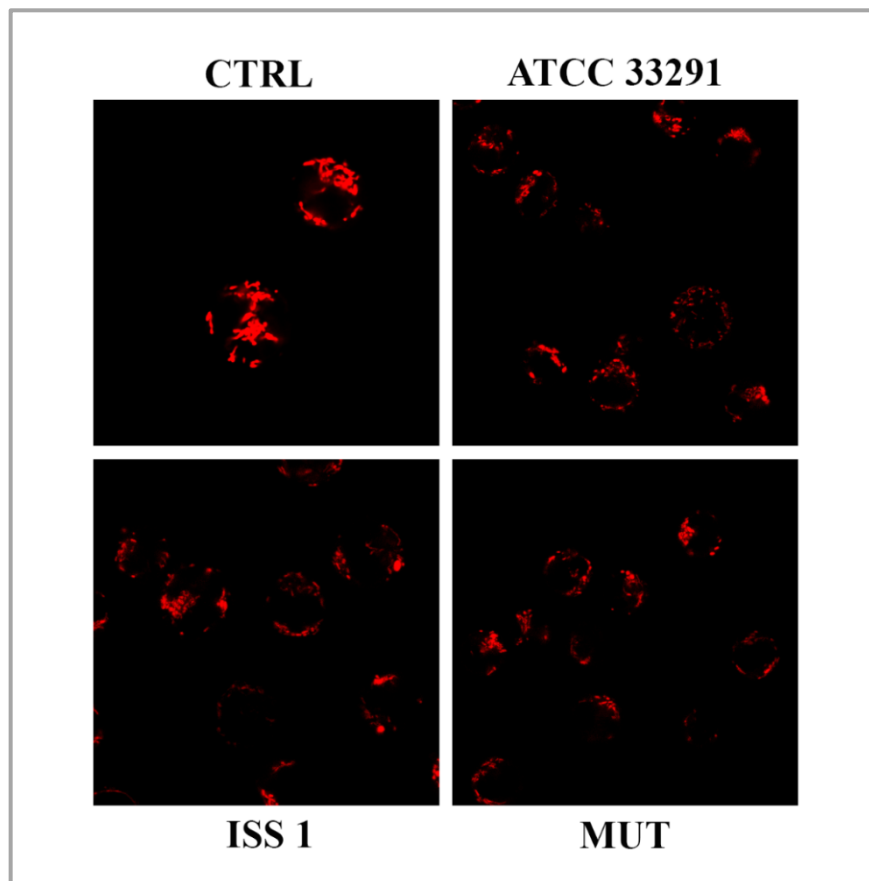


**Fig. 6.6** Single confocal optical sections of TMRE MFI of uninfected cells and infected U937 cells at 72 hours.

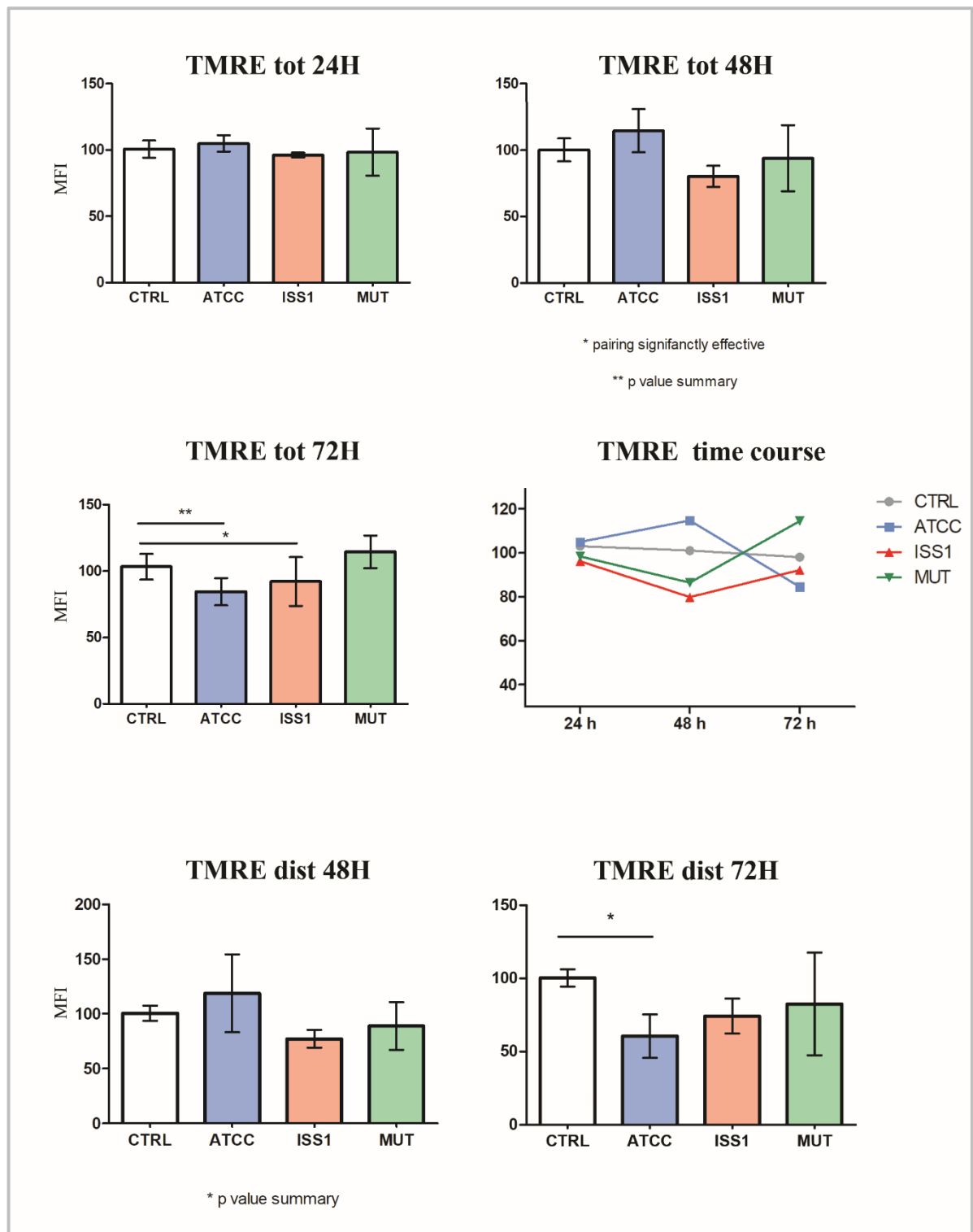


**Fig. 6.7** Histograms of percentage of TMRE positive cells calculated after 24, 48 and 72 hours from lysate administration in total cells (tot) and distended cells (dist). Each value was converted to A.U. setting control as 100. Each value is expressed as a mean  $\pm$  SD (Results from  $n \geq 3$  independent experiments). One-way ANOVA with Bonferroni's multiple comparison test revealed:  $**P < 0.01$  CTRL vs ATCC 33291 at 72 hours (total cells),  $*P < 0.05$  CTRL vs ISS 1 at 72 hours (total cells),  $*P < 0.05$  CTRL vs ATCC 33291 at 72 hours (distended cells).



## Lysosomal alterations

Lysosomal involvement in both apoptotic and survival pathways was monitored by staining U937 cells with LysoTracker Deep Red (LTDR). As shown in **Fig. 6.8**, *C. jejuni* lysates from the wild type strains (in particular ATCC 33291) induced a decrease in amount of LTDR-accumulating lysosomes in U937 cells after 6 hours, followed by a significant increase in amount of LTDR-accumulating lysosomes after 72 hours.

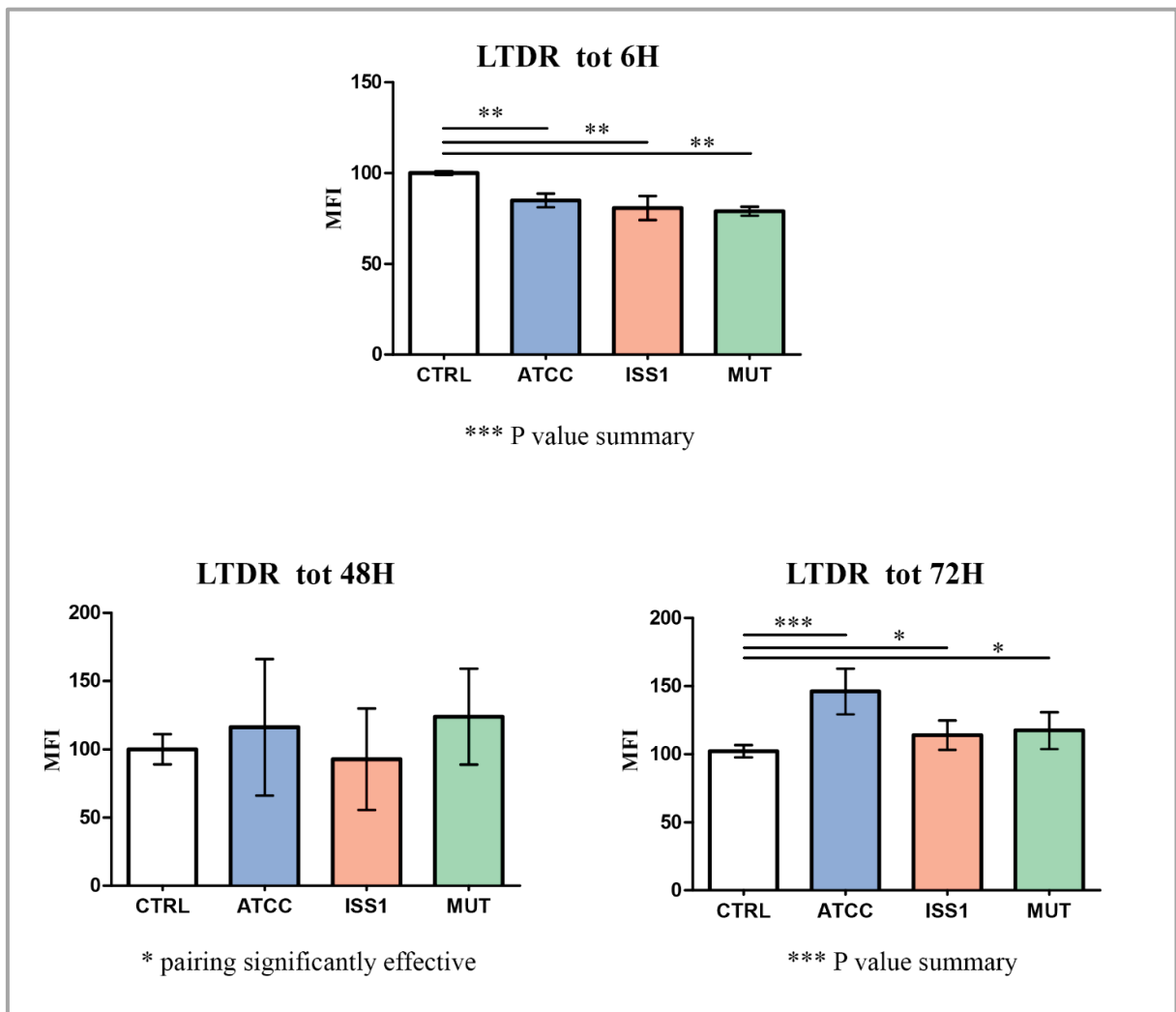


**Fig. 6.8** Histograms of percentage of LTDR positive cells calculated after 6, 48 and 72 hours from lysate administration in total cells. Each value was converted to A.U. setting control as 100. Each value was expressed as a mean  $\pm$  SD (Results from  $n \geq 3$  independent experiments). One-way ANOVA with Bonferroni's multiple comparison test revealed: \*\* $P < 0.01$  CTRL vs ATCC 33291, ISS1 and MUT at 6 hours; \*\*\* $P < 0.001$  CTRL vs ATCC 33291 at 72 hours, \* $P < 0.05$  CTRL vs ATCC 33291 at 72 hours, \* $P < 0.05$  CTRL vs ISS 1 at 72 hours.

### Autophagic vacuole detection

Monodansylcadaverine (MDC) staining, a specific autophagolysosome marker, was used to investigate the involvement of the autophagic machinery in infected U937 cells.

Specially after 72 hours of treatment, MDC MFI increased in U937 cells infected with the *C. jejuni* ATCC 33291 lysate (Fig. 6.9 and 6.10). These results are consistent with LTDR data at 72 hours that show a significant lysosomal destabilization in cells preincubated with this same lysate.

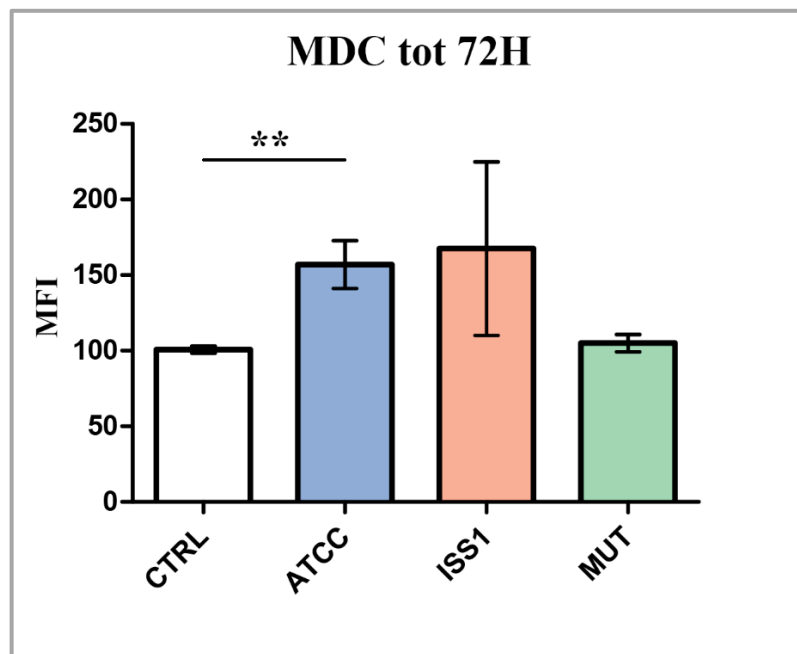


**Fig. 6.9** Histogram of percentage of MDC positive cells calculated after 72 hours from lysate administration in total cells. Each value was converted to A.U. setting control as 100. Each value is expressed as a mean  $\pm$  SD (Results from  $n \geq 3$  independent experiments). Paired *t* test (two-tailed P value) revealed: \*\* $P < 0.01$  CTRL vs ATCC 33291 at 72 hours.

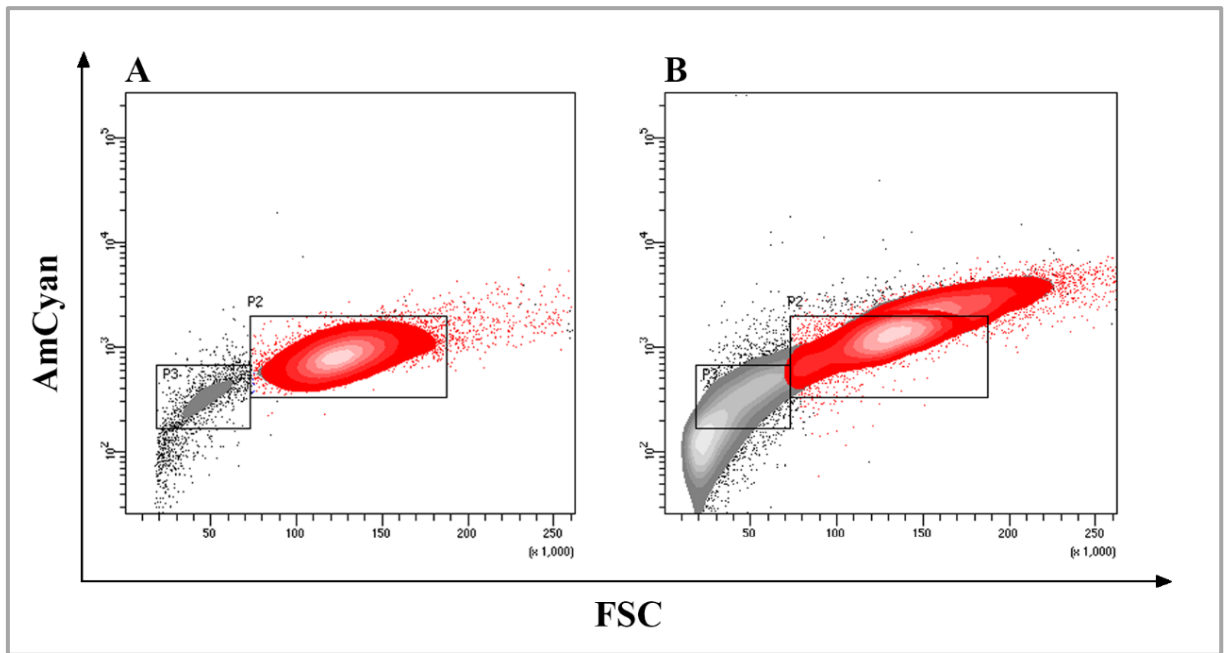


**Fig. 6.10** Density plot of MDC (Am Cyan) vs FSC values of CTRL (A) cells and cells preincubated with the *C. jejuni* ATCC 33291 lysate (B). In red are shown MDC positive cells, in grey are shown MDC negative cells and debris that were not included in the analysis.

### ER stress evaluation

At first, in order to investigate ER stress induced by lysates, U937 cells were stained with ER-Tracker and analysed in both cytometry and confocal microscopy. Results reported in **Fig 6.11** showed that ER stress occurred in U937 cells after 24 hours; afterwards, at 48 and 72 hours, ER modifications were so much intricate that we were not able to define a specific trend. In addition, having observed significant variations in ER MFI at 24 hours in cells preincubated with the *C. jejuni* ATCC 33291 lysate, CHOP protein was quantified by Western blotting at 24 hours. As shown in **Fig. 6.12**, Western blotting of CHOP protein confirmed that *C. jejuni* lysates induced ER stress after 24 hours in U937 cells.

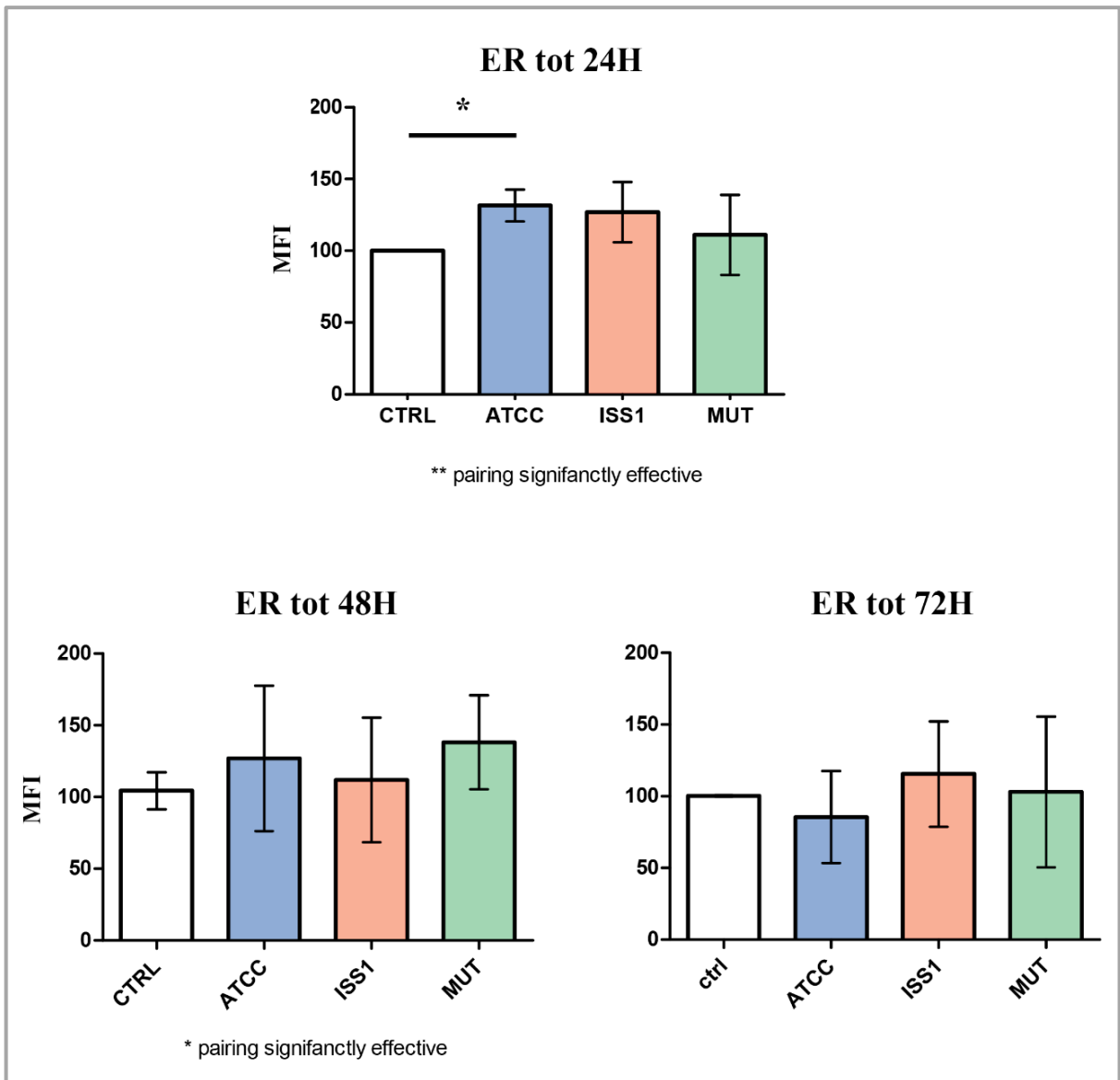


**Fig. 6.11** Histograms of ER Tracker MFI estimated in cells at 24, 48 and 72 hours. Each value was converted to A.U. setting control as 100. Each value is expressed as a mean  $\pm$  SD (Results from  $n \geq 3$  independent experiments). Paired  $t$  test (two-tailed P value) revealed: \* $P < 0.05$  CTRL vs ATCC 33291 at 24 hours.

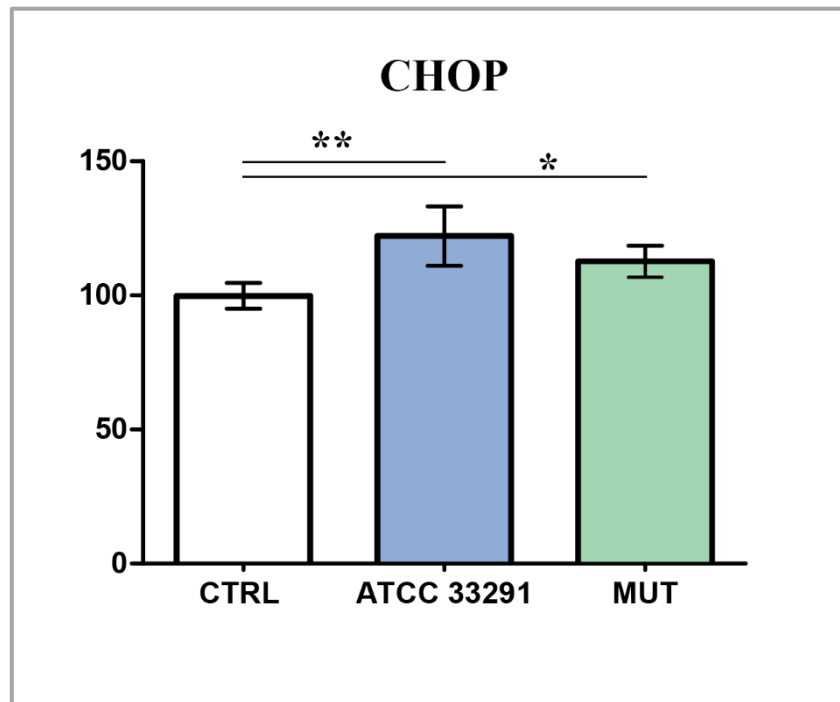


**Fig. 6.12** Quantification of CHOP protein in U937 cells after 24 hours from lysate administration. Welch's unpaired *t* test revealed: \*\* $P=0.004$  CTRL vs ATCC 33291, \* $P=0.043$  CTRL vs MUT.

## Content of intracellular Ca<sup>2+</sup>

Fura 2-AM was used to study variations in content of intracellular Ca<sup>2+</sup>. Both in viable and total cells it was observed a significative increase in intracellular Ca<sup>2+</sup> content after the treatment with the *C. jejuni* ATCC 33291 lysate for 48 hours (**Fig. 6.13**). According to the literature, since Ca<sup>2+</sup> content alterations characterize mostly the earliest phases of the cell death process, they are particularly evident in viable cells, unlike in distended or dead cells.

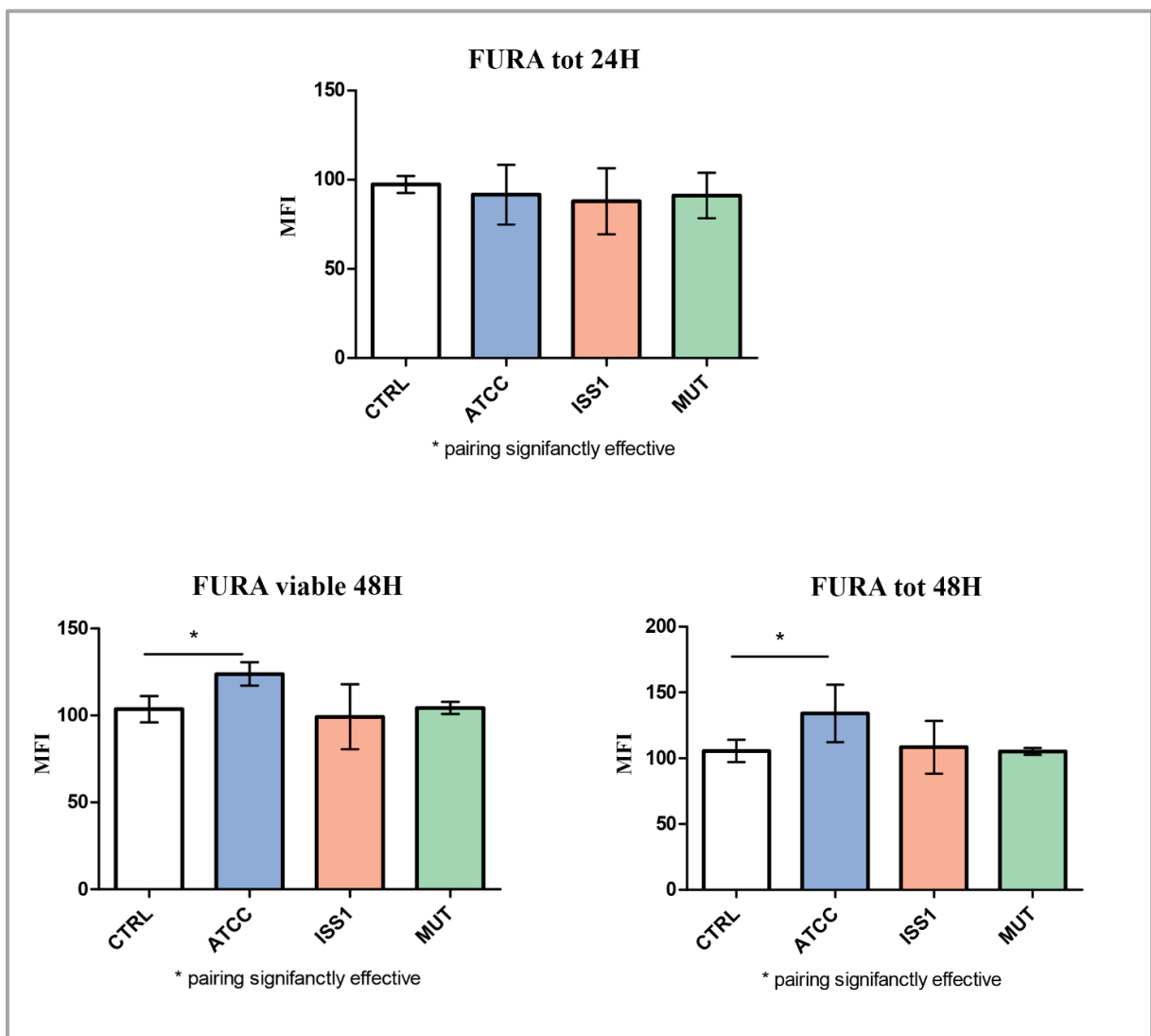


**Fig. 6.13** Histograms of FURA 2-AM MFI estimated in total (tot) and viable U937 cells at 24 and 48 hours. Each value was converted to A.U. setting control as 100. Each value was expressed as a mean  $\pm$  SD (Results from  $n \geq 3$  independent experiments). One-way ANOVA with Bonferroni's multiple comparison test revealed: \* $P < 0.05$  CTRL vs ATCC 33291 at 48 hours in total and viable cells.

## Bcl-2 and pRb detection

Being U937 cells *p53* mutant, to investigate the apoptotic pathway Bcl-2 and pRb proteins were investigated. Preliminary data showed an overexpression of Bcl-2 and pRb in cells preincubated with the wild type lysates, in particular the *C. jejuni* ATCC 33291 lysate, compared to the control. Changes in Bcl-2 (**Fig. 6.14**) and pRb (**Fig. 6.15** and **6.16**) expression were particularly evident in distended cells; as shown in the histograms below, expression of these two proteins was compared in total and distended cells.

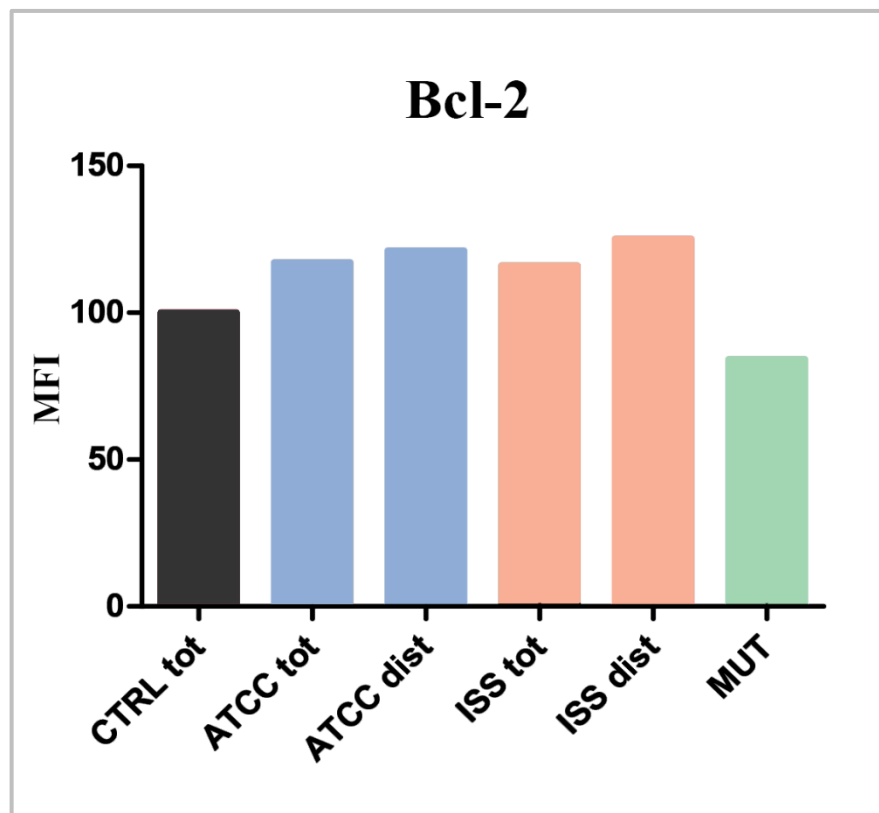


**Fig. 6.14** Histogram of Bcl-2 intracellular content in total (tot) and distended (dist) U937 cells at 72 hours. Each value was converted to A.U. setting control as 100.

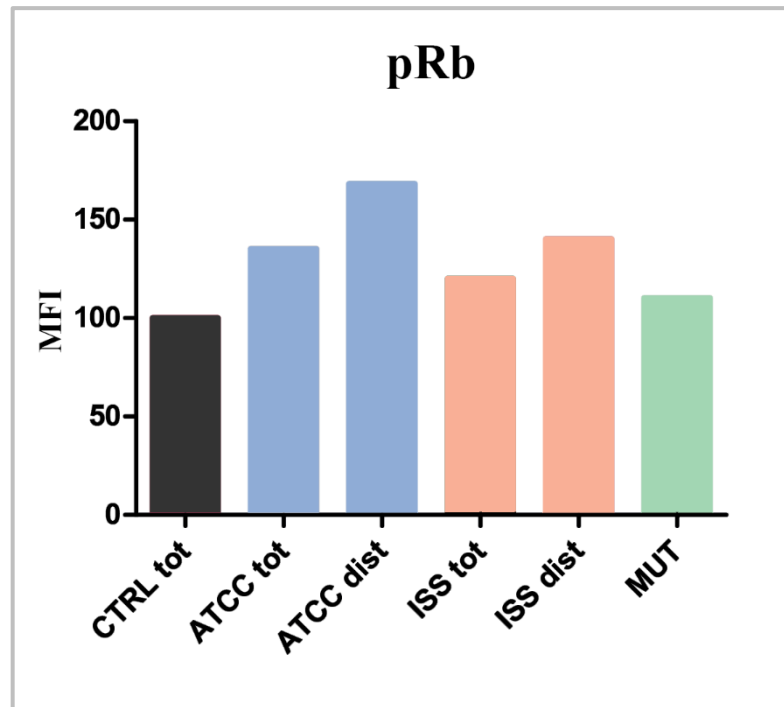


**Fig. 6.15** Histogram of pRb intracellular content in U937 cells at 72 hours. Each value was converted to A.U. setting control as 100.

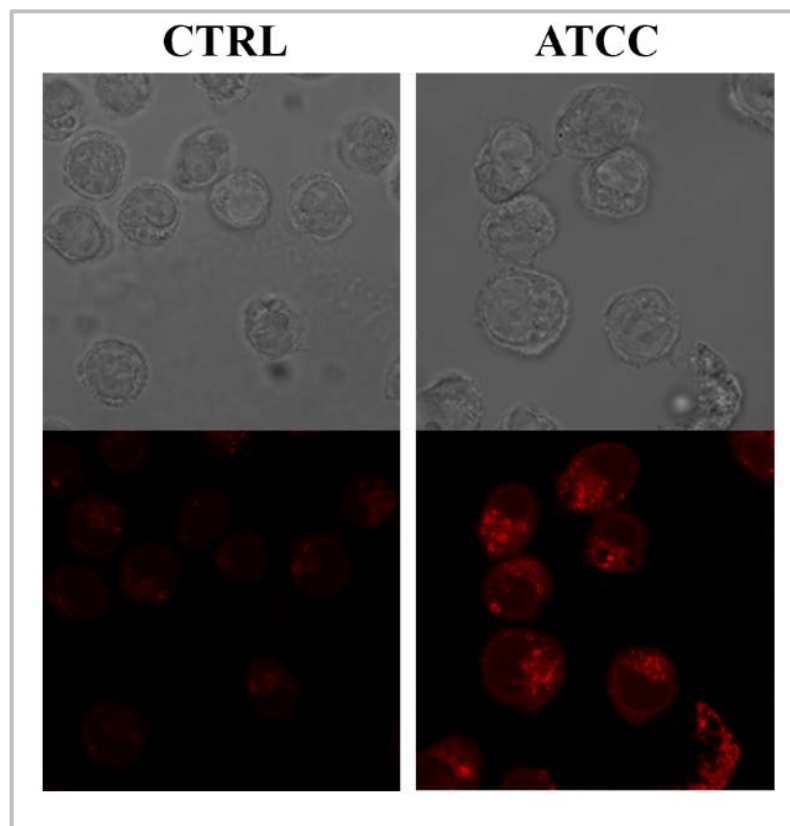


**Fig. 6.16** Single confocal optical sections pRb MFI of untreated cells and U937 cells preincubated with the *C. jejuni* ATCC 33291 lysate for 72 hours.



## Evaluation of intracellular lipid content

To investigate intracellular lipid modifications in U937 cells, LipidTOX and Bodipy fluorescent dyes were used. In **Fig. 6.17**, cytometric results show peculiar staining of both treated and untreated cells after 24, 48 and 72 hours of preincubation with lysates. Notably after 72 hours, important changes in intracellular content of neutral lipids occurred in cells preincubated with the *C. jejuni* ISS 1 lysate. On the contrary, a greater accumulation of peroxidised lipids resulted in U937 cells preincubated for 72 hours with the *C. jejuni* ATCC 33291 lysate (**Fig. 6.18**).

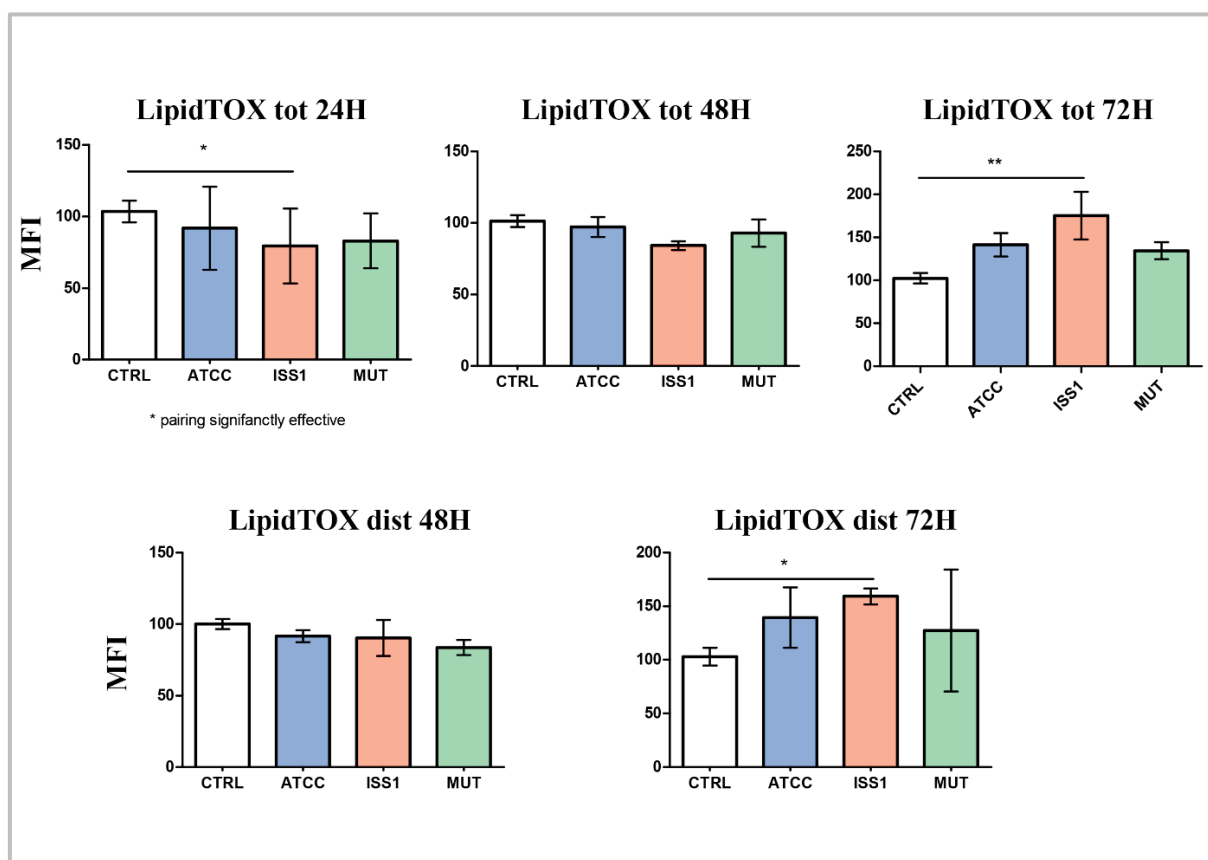


**Fig. 6.17** Histograms of percentage of LipidTOX positive cells was calculated after 24, 48 and 72 hours from lysate administration in total cells (tot) and distended cells (dist). Each value was converted to A.U. setting control as 100. Each value is expressed as a mean  $\pm$  SD (Results from  $n \geq 3$  independent experiments). One-way ANOVA with Bonferroni's multiple comparison test revealed: \* $P < 0.05$  CTRL vs ISS 1 at 24 hours (total cells), \*\* $P < 0.01$  CTRL vs ISS 1 at 72 hours (total cells), \* $P < 0.05$  CTRL vs ISS 1 at 72 hours (distended cells).

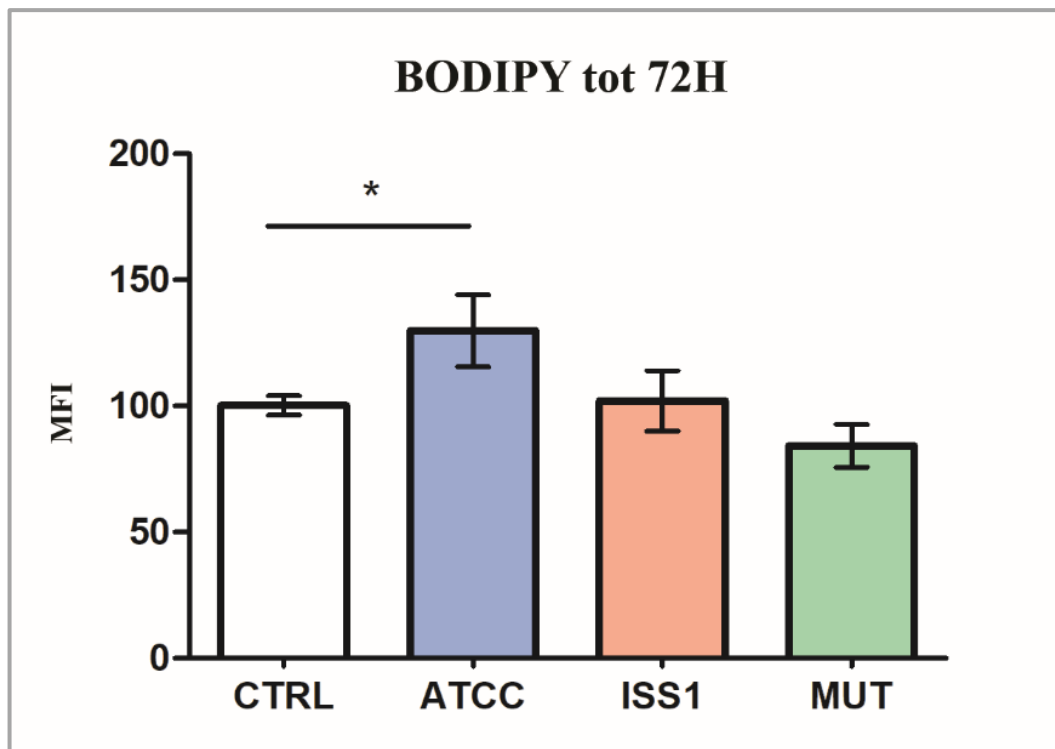


**Fig. 6.18** Histogram of percentage of Bodipy positive cells calculated after 72 hours from lysate administration in total cells. Each value was converted to A.U. setting control as 100. Each value is expressed as a mean  $\pm$  SD (Results from  $n \geq 3$  independent experiments). One-way ANOVA with Bonferroni's multiple comparison test revealed: \* $P < 0.05$  CTRL vs ATCC 33291 at 24 hours.

### **Autophagy associated to mTOR signaling activation**

Activation of autophagy correlated to mTOR signaling involvement, was studied by investigating the effects of RM in U937 cells uninfected or infected with the respective lysates. For the investigated parameters, data from cells preincubated with lysates and RM together were compared to data from cells preincubated only with lysates: basically a ratio between these values was done (RM/without RM).

mTOR blockade caused by RM resulted in a different response of U937 cells to the lysates. As shown in **Fig. 6.19**, important differences were reported between uninfected and infected cells (with lysates) and untreated and treated cells (with RM).

In detail, ratios about ER tracker values reduced in infected cells compared with uninfected cells, demonstrating that the effect of the lysates on host ER was stronger than the effect of the RM. As already affirmed in other chapters, no differences were observed between wild type and mutant strains confirming that CDT might not have a critical role in structural ER modifications and ER stress.

In addition, by using LTDR staining, we observed that in U937 cells preincubated with the wild type lysates, lysosomes responded in the same manner, compared with CTRL and cells MUT, which in turn have a similar trend as well (**Fig. 6.19** and **6.20**).

U937 cells were also stained with MDC, a specific autophagolysosome marker. Whereas control cells and cells preincubated with the lysate from the mutant strain showed the same trend, cells preincubated with the wild type strains showed two different opposite behaviours: the ratio is low in ATCC 33291-infected cells and particularly high in ISS 1-infected cells.

Preliminary data, not shown here, demonstrated the involvement of lipids, stained with LipidTOX and Bodipy, in mTOR mediated autophagy triggered by *C. jejuni* wild type lysates.

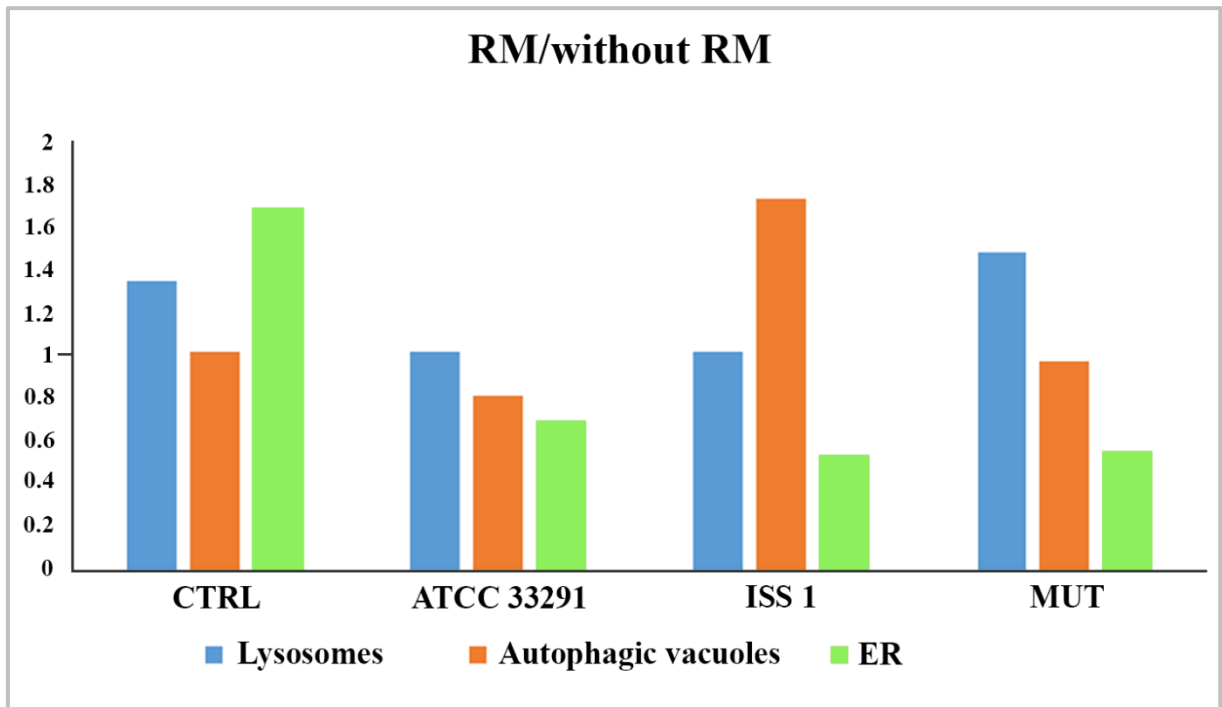


**Fig. 6.19** For investigated parameters, ER (by ER Tracker staining, in green), autophagic vacuoles (by MDC staining, in orange) and lysosomes (by LTDR staining, in blue), a ratio between RM/without RM was carried out for each experimental condition at 72 hours. Each value was converted to A.U. setting untreated cells, that were not treated with RM, as 1; therefore, values higher or lower than 1 have to be interpreted as modulated or not modulated by RM. Basically, where the effect of the lysate was stronger than the effect of RM the ratio resulted lower than 1, on the contrary, where the effect of the lysate was weaker than the effect of RM the ratio resulted higher than 1.

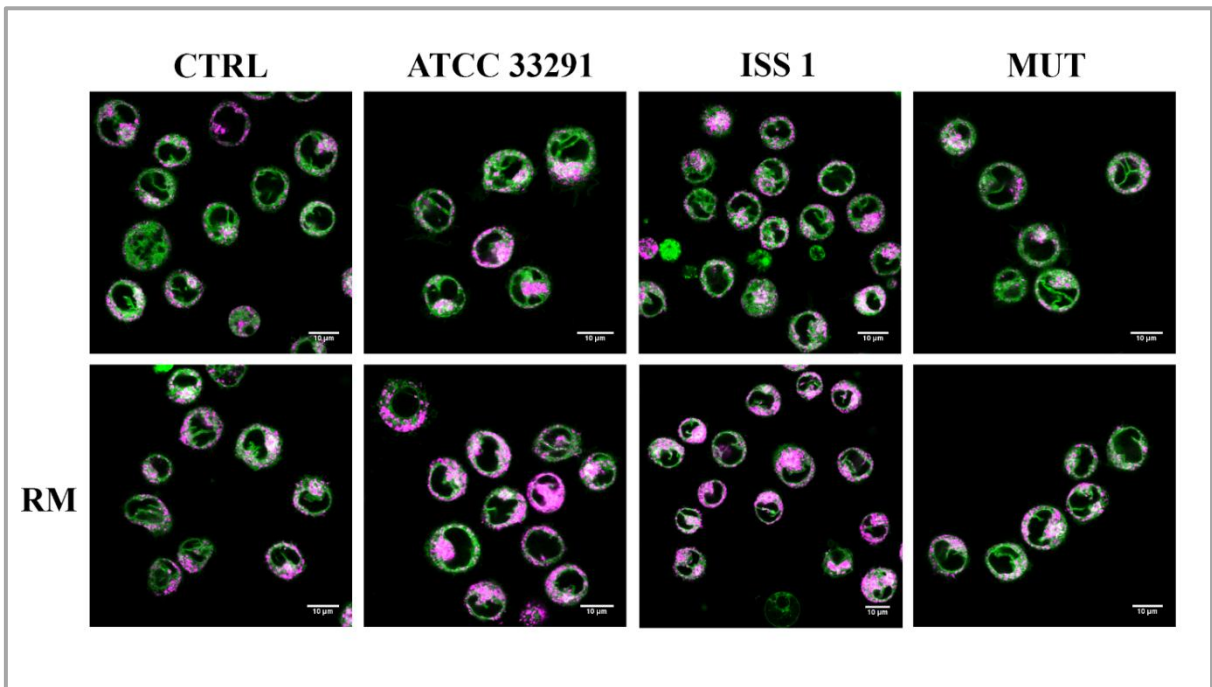


**Fig. 6.20** Single confocal optical sections of ER Tracker MFI (in green) and LTDR MFI (in pink) of untreated U937 cells (CTRL) and U937 cells preincubated with lysates after 72 hours of treatment with and without RM. Where present, co-localization is shown in white. Lower pictures show U937 cells pre-treated with RM for 2 hours before lysate administration. Bars: 10 μm.

### CD14 and ICAM-1 (CD54) variations

CD14 variations during the time course were detected in U937 cells preincubated with lysates (data not shown), although they were not statistically significant. On the contrary, as shown in **Fig 6.21** ICAM-1 expression was upregulated particularly after 72 hours preincubation with the *C. jejuni* ATCC 33291 lysate.

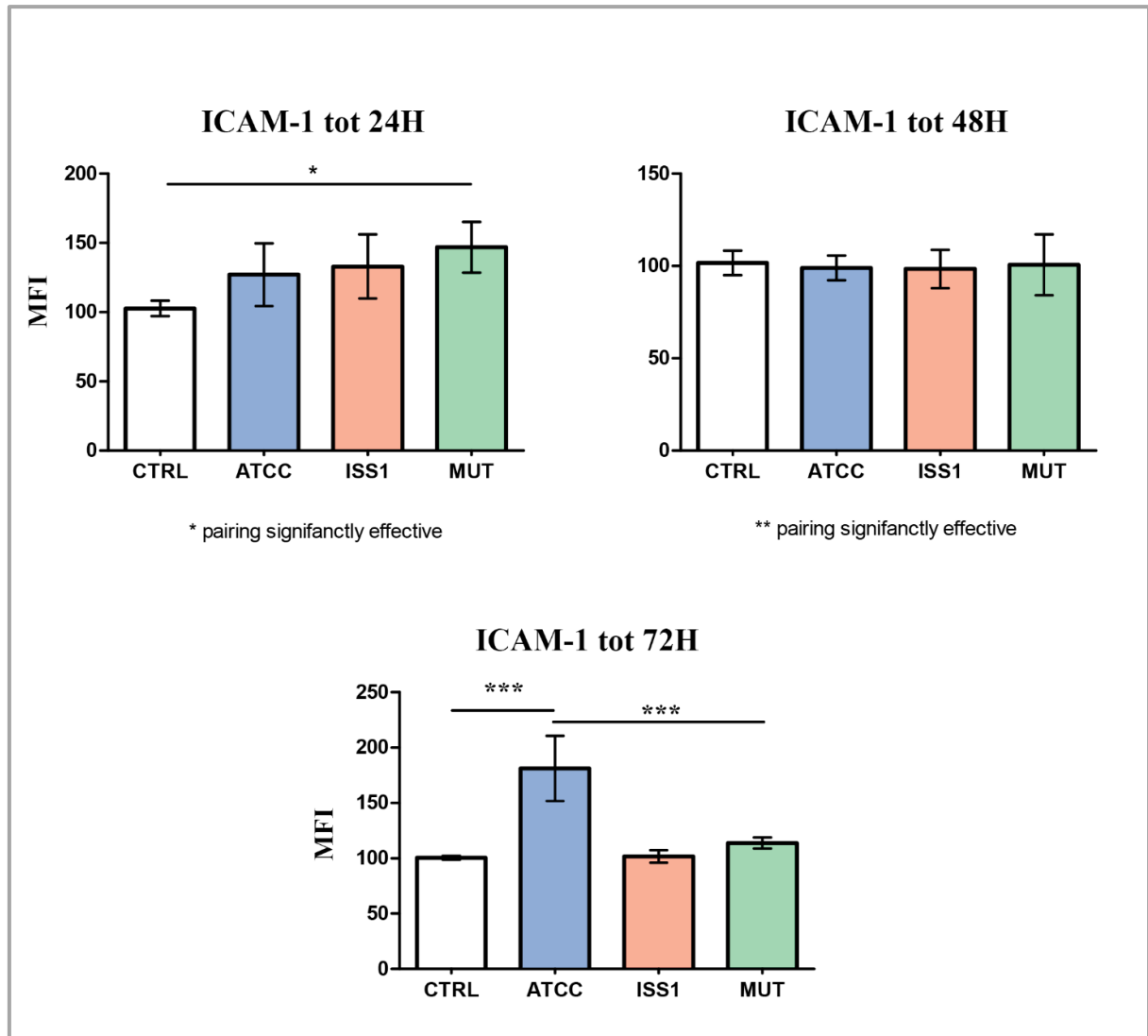


**Fig. 6.21** Histograms of percentage of ICAM-1 positive cells calculated after 24, 48 and 72 hours from lysate administration in total cells (tot) and distended cells (dist). Each value was converted to A.U. setting CTRL as 100. Each value is expressed as a mean  $\pm$  SD (Results from  $n \geq 3$  independent experiments). One-way ANOVA with Bonferroni's multiple comparison test revealed: \* $P < 0.05$  CTRL vs MUT at 24 hours, \*\*\* $P < 0.001$  CTRL vs ATCC 33291 at 72 hours, \*\*\* $P < 0.001$  ATCC 33291 vs MUT at 72 hours.

## Discussion

Although in U937 cells infected with respective lysates the same investigations that were described in the previous chapters were carried out, in this part of the work it was focused the attention not only on total cells, but also on different sub-populations.

Modifications induced by lysates were present mostly in total and distended cells. Distended cells represented the most interesting sub-population because in these cells the CDT certainly acted: they represent the intermediate state between infected and dead cells. In these cells the CDT can act and persist, enhancing the infection spreading. Results about viable/non-apoptotic cells and dead cells were reported only when significant variations were observed. As it was already demonstrated, *C. jejuni* lysates were able to induce morphologic changes, cell cycle arrest, therefore reduction in cell number, and apoptosis in U937 cells in a CDT dependent manner.

Moreover, as demonstrated by **CHOP** and **ER** Tracker results, after 24 hours' infection, ER stress occurred in U937 cells through a CDT-independent manner. The CDT might not have a critical role in ER stress induction, because the mutant strain showed to induce an increase in CHOP protein. This protein is generally activated in different cellular stress conditions and it is shown to modulate the apoptotic pathway.

At the same time point, alterations in adhesion molecules (ICAM-1) resulted in U937 cell surface, leading to inter-cellular adhesion perturbation; this phenomenon *in vivo* is essential for rolling, activation, adhesion, and transmigration of immune cells.

As predicted, ER stress was followed by an increase in  $\text{Ca}^{2+}$  intracellular content at 48 hours' post-infection, that lead to the apoptotic cascade activation by the cell.

Although **pRb** and **Bcl-2** data are preliminary, it is possible to affirm that lysates from the wild type strains were also able to induce an anti-apoptotic (pro-survival) response in U937 cells (at 72 hours), unlike it was observed in monocytes (at 12 hours): it might be probably due to the different response of the changed cell line or the different time point of analysis.

pRb results are consistent with CFSE results confirming an occurred cell cycle arrest. pRb has been reported to cause growth arrest and inhibit apoptosis (Haupt et al, 1995). Upregulation of pRb by *C. jejuni* wild type strains might represent a helpful expedient that this bacterium activates to persist in host cells and to contrast the programmed cell death.

**TMRE** was used to monitor mitochondrial transmembrane potential and mitochondrial function. As previously mentioned, depending on the specific apoptotic stage in which cells are, TMRE MFI can increase or decrease. The *C. jejuni* strain that induced the most relevant

mitochondrial alterations was the ATCC 33291, confirming that this strain favours an intrinsic apoptotic pathway.

In addition, we observed that in both monocytes and U937 cells, lysosomes respond to the lysates by following the same trend: if in monocytes a decrease in **LysoTracker** MFI at 12 hours was followed by an increase at 24-48 hours, in U937 we observed a decrease in LysoTracker MFI at 6 hours that was followed by an important increase at 72 hours. This behaviour is evident in cells preincubated with the *C. jejuni* ATCC 332921 lysate. These findings might suggest that *C. jejuni* triggers in myeloid cells a first pro-survival response, followed by a pro-apoptotic or pro-autophagic response. **LTDR** results are consistent with **MDC** results, confirming that, after 72 hours of treatment, U937 cells respond to stimuli by activating the autophagic machinery, in which lysosomes are largely involved. Activation of autophagy was also proven by investigations carried out in U937 cells pre-treated with RM.

It is known that RM is an efficient inhibitor of mTOR that can induce autophagy in mammal cells. mTOR blockade caused by RM resulted in a different response of U937 cells to the lysates, inducing us to suppose that *C. jejuni* induces some modifications in U937 cells involving mTOR activation.

RM is able to trigger the autophagic flux, trying to re-establish the main stages of autophagolysosomes formation and fusion, when they are altered. Our findings showed that in uninfected cells, RM structurally and functionally alter ER membranes (tubules and sheets) and cause an increase in acidic compartments/ lysosomes. Nevertheless, many differences were found between uninfected and infected cells.

RM results showed that, as predicted, ER is involved in autophagic processes induced by *C. jejuni*, in a CDT independent manner. On the contrary, LTDR data showed that lysosomes are differently recruited by wild type and mutant strains: that means that *C. jejuni* recruits lysosomes in the autophagic pathway in a CDT dependent manner, in particular for the ATCC 33291 strain.

Interesting findings were found for the *C. jejuni* ISS 1 strain. This strain showed an interesting behaviour because it is not particularly able to cause cell death and/or autophagy in U937 cells, as demonstrated by AnxV-PI, CFSE and MDC results. In addition, an increment of autophagolysosomes occurred only after RM treatment, demonstrating that the lysate is not particularly able to induce these mechanisms. Nevertheless, lysosomes are recruited and ER modifications resulted in these cells. It is very likely that this behaviour is due to an alternative route that this specific strain utilizes. It was already reported that the CDT (Medina-Kauwe, 2007) as well as whole *C. jejuni* cells (Watson & Galan, 2008), can deviate



the classical endocytic pathway to evade the intracellular barriers that cells utilize against pathogens. It is very likely that the *C. jejuni* ISS 1 wild type strain utilize this same expedient to avoid host defences and persist undisturbed within host cells. On the contrary, the *C. jejuni* ATCC 33291 strain does not have this ability since U937 cells respond to this strain by strongly activating both apoptotic and autophagic pathways.

Moreover, at 72 hours' post-infection, Bodipy-LipidTOX findings demonstrated that also lipid peroxidation and alterations in intracellular lipid content are caused by *C. jejuni* in a CDT-dependent manner. It is very likely that modifications in peroxidised lipids, that occur in ATCC 33291 infected cells, are a consequence of the activation of the autophagic pathway, whereas modifications in neutral lipid content, that occur in ISS 1 infected cells, are due to the formation of endosomes that allow CDT entrance and persistence.

## 7. U937 cell model: U937 cells preincubated with *C. jejuni* OMVs

### NTA and cytometric evaluations of OMVs

Integrity and size of the OMVs were investigated by using cytometric and NanoSight analyses (**Fig.7.1**). Cytometric analyses were carried out by using Nile Red and SYBR Green stainings; membrane integrity and the potential presence of nucleic acids within OMVs were evaluated. Performed investigations confirmed that OMVs used in subsequent assays were intact and with an average size of 100-120 nm. Nile Red analyses also confirmed that OMVs produced by the wild type strain and its mutant were different in size and membrane content (**Fig. 7.2** and **7.3**). Moreover, SYBR Green analyses revealed an important presence of nucleic acids in OMVs isolated from the *C. jejuni cdtA* mutant, as recently mentioned by O'Donoghue and Krachler (O'Donoghue & Krachler, 2016). The meaning of this finding will be investigated in the future.

### Morphological features, cell death and Ca<sup>2+</sup> intracellular content

Morphologic appearance of uninfected and infected cells was investigated in both cytometry and confocal microscopy; FSC and SSC cytometric parameters were used as indicators of cell size and complexity. Morphological features are appreciable in all confocal pictures below. FSC values of untreated control cells were compared with FSC values of cells treated with OMVs previously isolated. All treatments induced a moderate increase in FSC values and cell enlargement already at 24 hours. Confocal microscopy also showed that U937 cells preincubated with the wild type OMVs (WT) showed the typical apoptotic shrinkage. These findings were confirmed by cytometric AnxV-PI results that revealed the presence of a high percentage of AnxV-PI positive cells (apoptotic cells) in these last (**Fig. 7.4**). Moreover, FURA-2 AM analyses revealed an important increase in intracellular Ca<sup>2+</sup> content in cells preincubated with the OMVs from the wild type strain, compared with the mutant (MUT) and untreated control cells (CTRL) (**Fig. 7.4**).

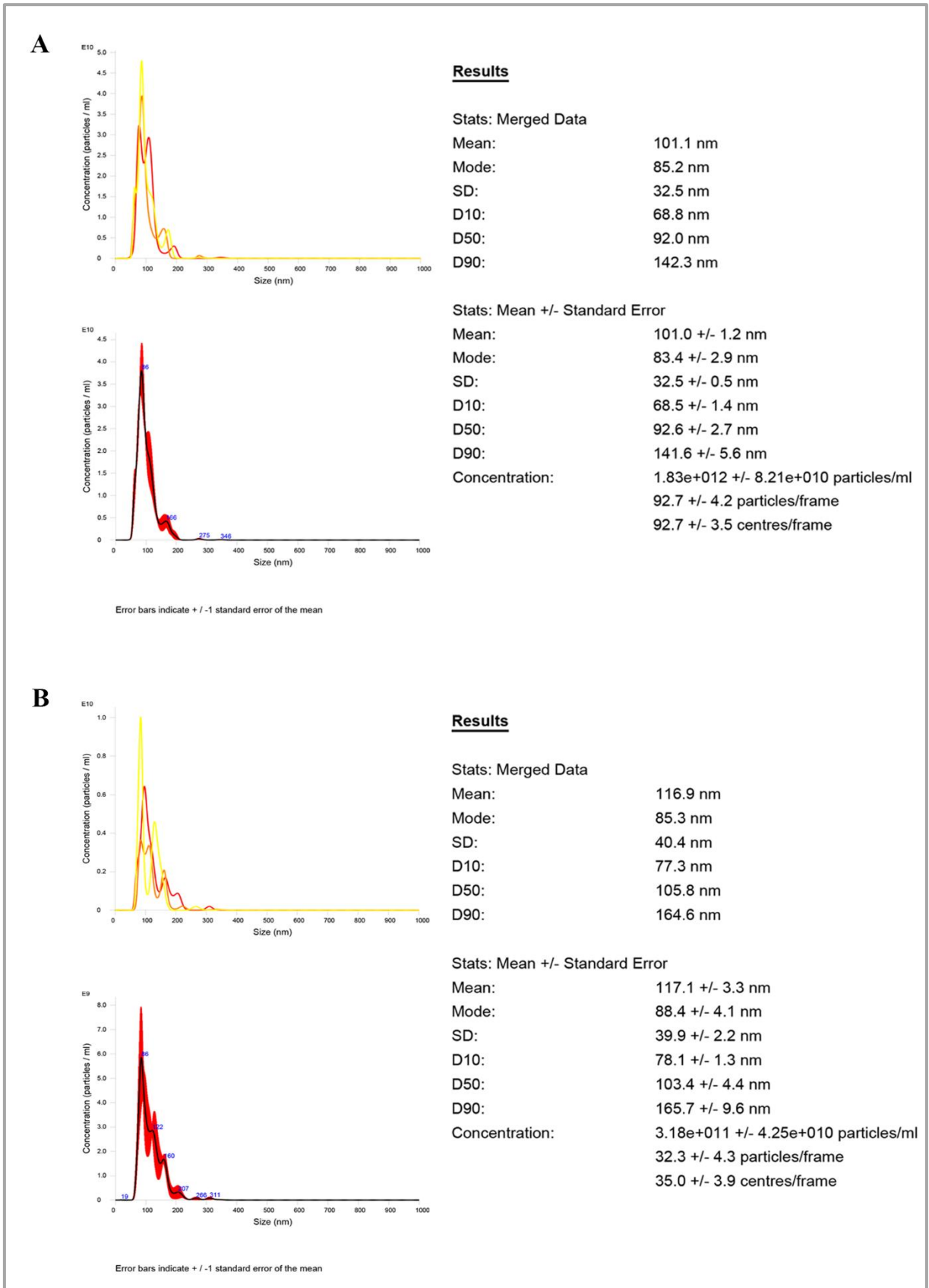


**Fig. 7.1** To verify integrity and size of vesicles from *C. jejuni* 11168H wild type (**A**) and *C. jejuni* 11168H *cdtA* mutant strains (**B**), NTA measurements were performed by using a NanoSight LM20 (NanoSight, U.K).

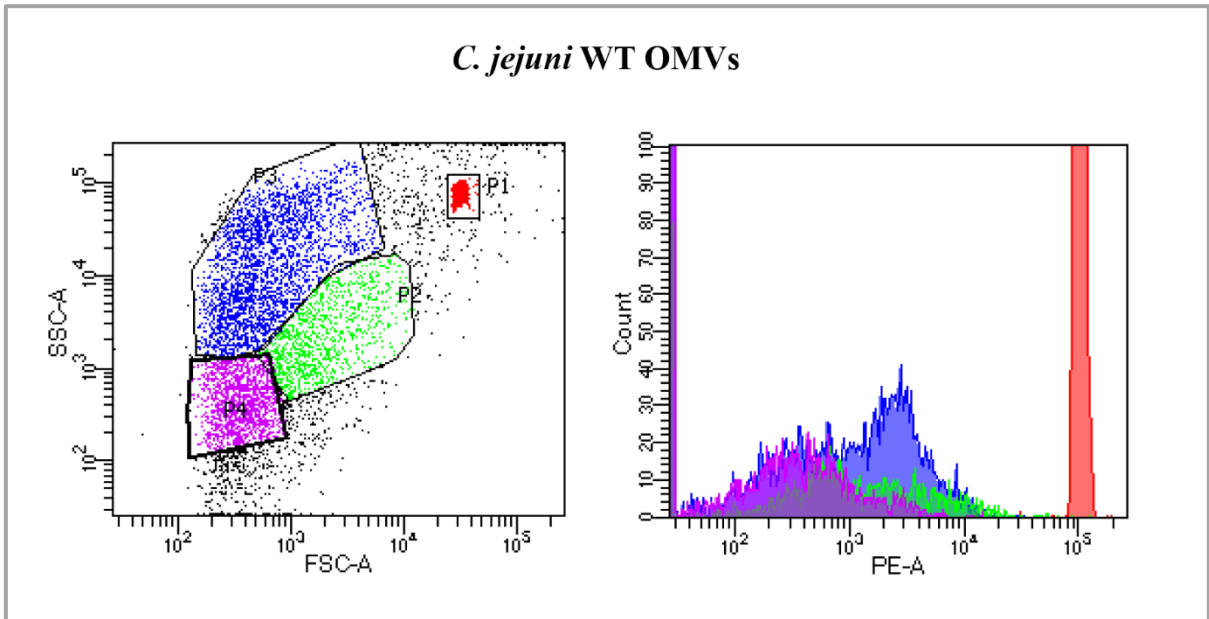


**Fig. 7.2** Cytometric analyses of OMVs previously isolated from the *C. jejuni* 11168H wild type strain and stained with Nile Red (FL2/PE). P1 shows beads used for the absolute count; P2, P3, and P4 are gates drawn around different sized OMVs: P2 are the biggest ones, whereas P3 are the aggregated vesicles: adhesion and aggregation can develop in these kind of samples.

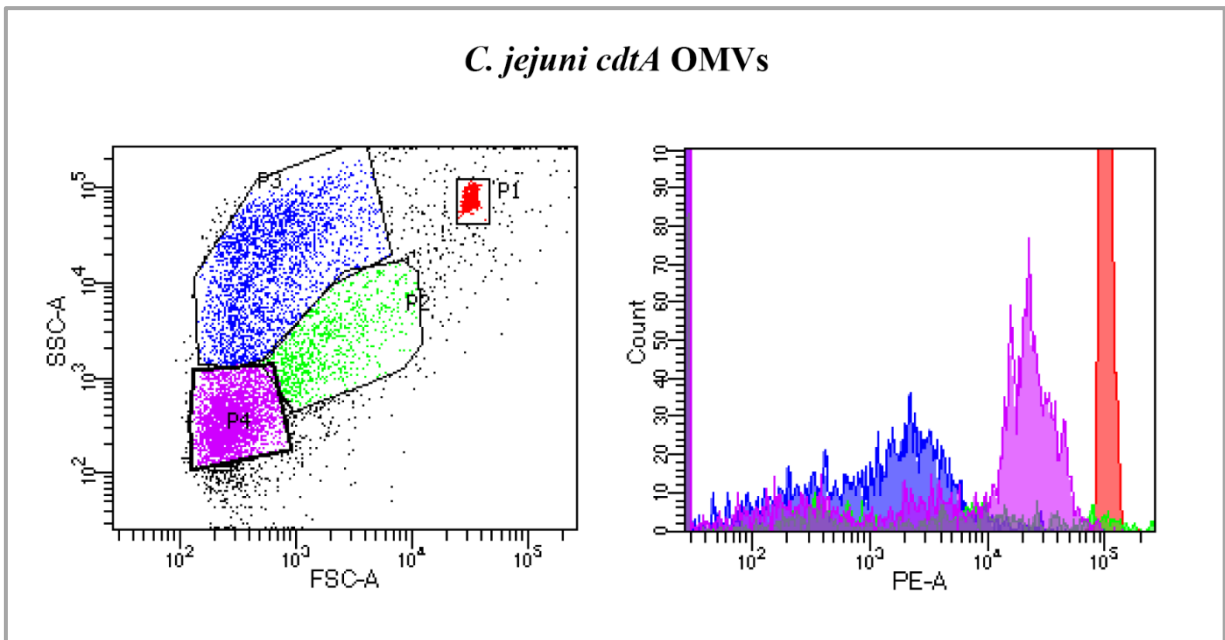


**Fig. 7.3** Cytometric analyses of OMVs previously isolated from the *C. jejuni* 11168H *cdtA* mutant strain and stained with Nile Red. Violet, blue and green histograms are related to P4, P3 and P2 gates, respectively.

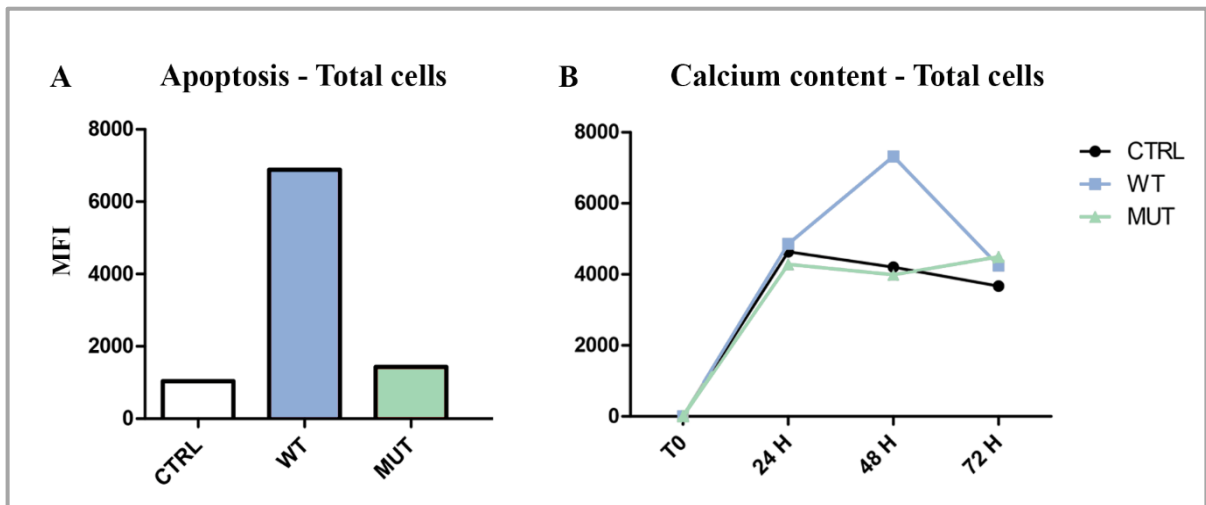


**Fig. 7.4** (A) Histogram of AnxV-PI positive event percentage in U937 total cells after 72 hours of treatment with OMVs isolated from the wild type and mutant strains. (B) Trends of FURA2-AM MFI in total cells for each experimental condition during the time course.

### CD14 and ICAM-1 variations

Specifically, after 72 hours of treatment, U937 cells preincubated with OMVs from the wild type strain, compared with untreated control cells and the counterpart preincubated with OMVs from the mutant strain, showed an important increase in CD14 and ICAM-1 expression. As shown in **Fig. 7.5** and **7.6**, these findings were confirmed by both cytometric and microscopy analyses.

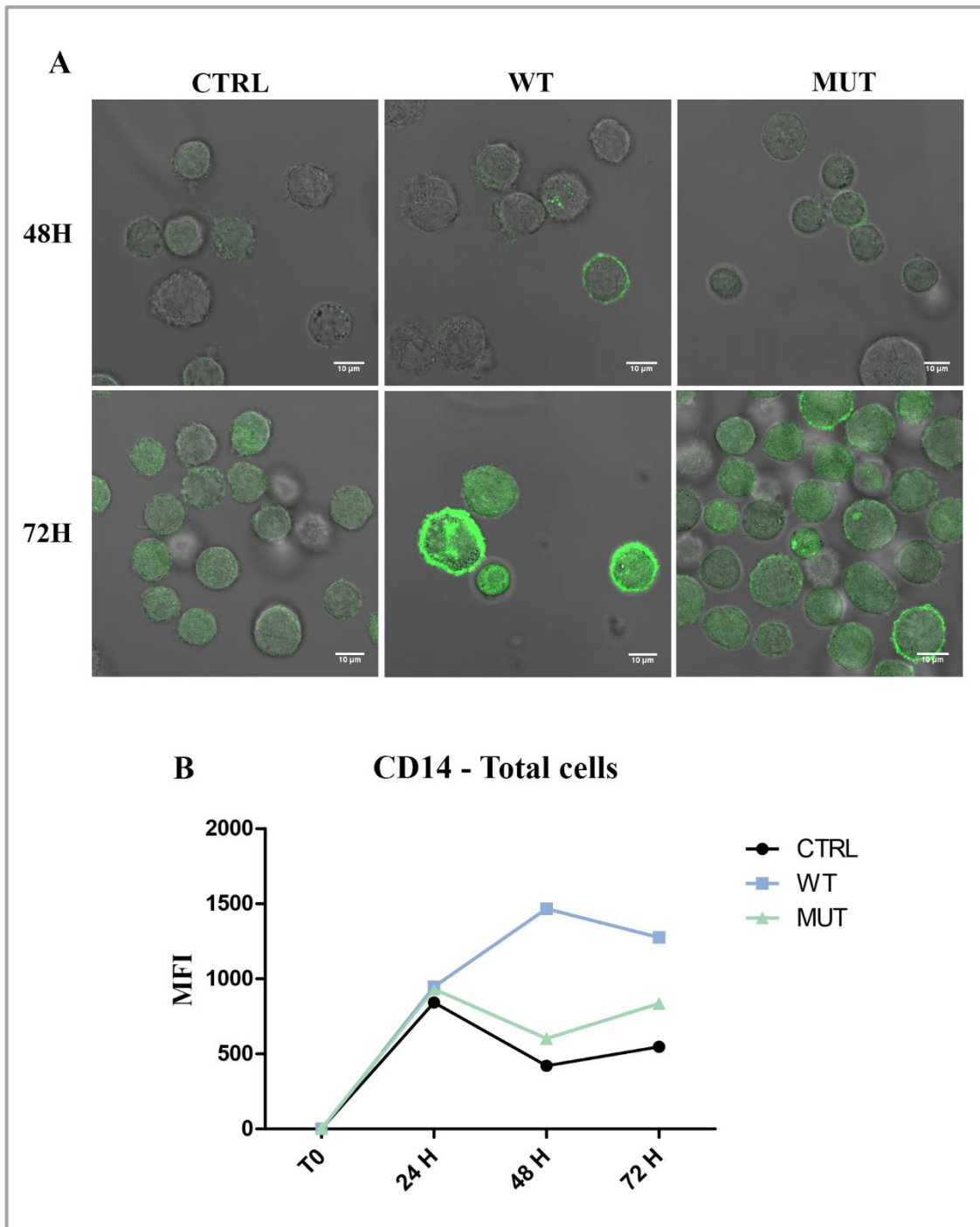


**Fig. 7.5** (A) Single confocal optical sections of CD14-FITC MFI of control and U937 cells preincubated for 48 and 72 hours with *C. jejuni* OMVs. Bars: 10 $\mu$ m. (B) Trends and CD14-FITC MFI in total cells for each experimental condition during the time course.

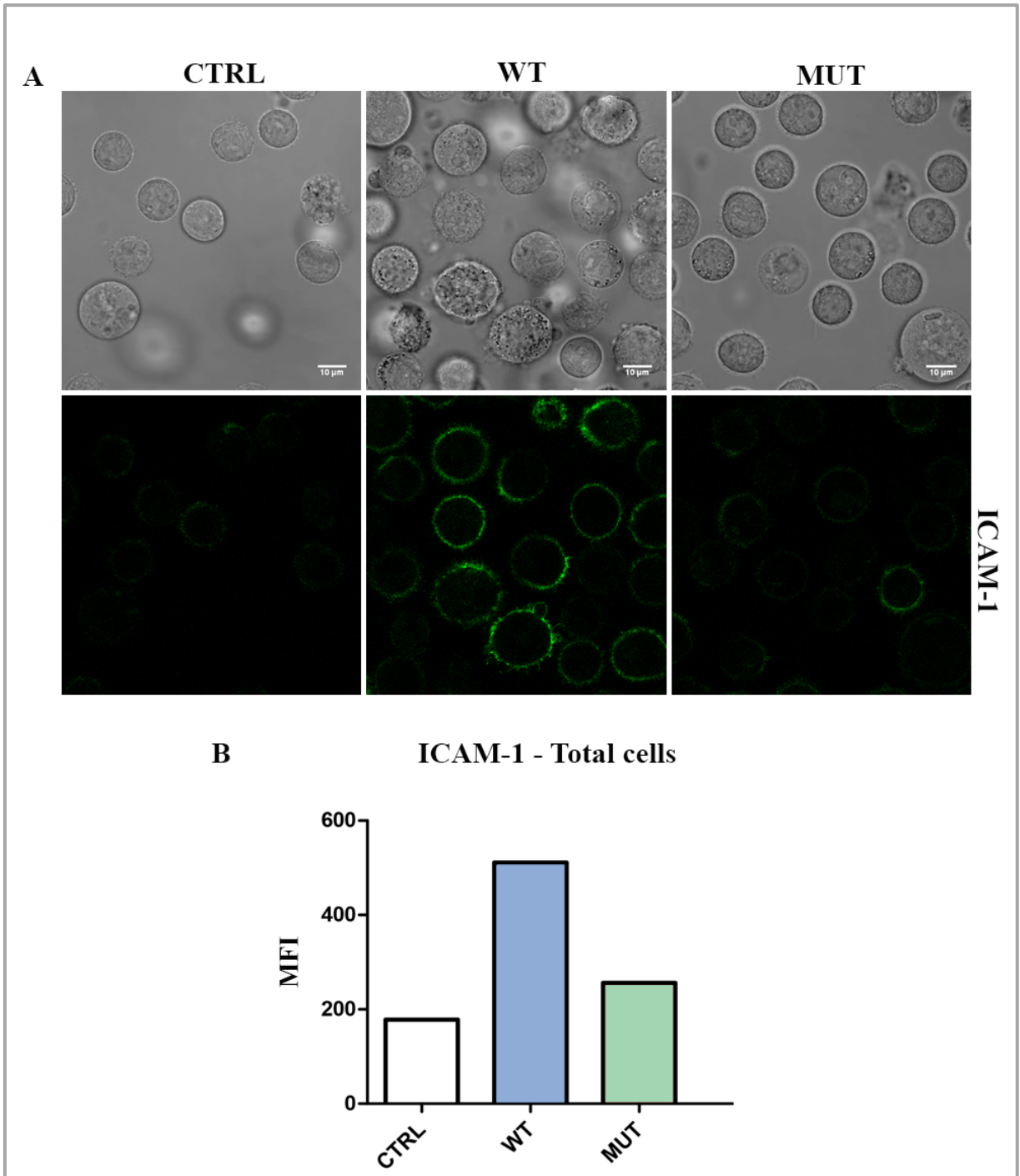


**Fig. 7.6** Single confocal optical sections of ICAM-1 MFI of control and U937 cells preincubated for 72 hours with OMVs. **(B)** Statistical histogram of ICAM-1 MFI in total cells after 72 hours of treatment. Bars: 10 $\mu$ m.

### **Mitochondrial, ER and lipid raft alterations**

Although mitochondrial alterations were appreciable principally in cytometry, ER and lipid raft alterations were evident both in cytometry and confocal microscopy after 48 and 72 hours of treatment (**Fig. 7.7, 7.8, 7.9, 7.10**).

Mitochondrial transmembrane potential, which is considered an important parameter of mitochondrial function, and it is frequently used as an indicator of cell death, was measured by TMRE staining. A TMRE MFI increase was observed in U937 cells after 48 hours of preincubation with OMVs, confirming that mitochondrial transmembrane alterations occurred, that inevitably might have led to the activation of the apoptotic process (**Fig. 7.10A**).

Moreover, an overall increase in CD317 MFI, which was used as lipid rafts marker, was observed after 48 and 72 hours of preincubation with OMVs in all experimental conditions in both cytometry (**Fig. 7.10B**) and confocal microscopy (**Fig. 7.7** and **7.8**).

ER-Tracker Green data also showed ER alterations after 24-48 hours of treatment with both OMVs from the wild type and mutant strains. Therefore, it was possible to affirm that CDT might not be the only player involved in these modifications (**Fig. 7.9**).

### **Lysosomal alterations**

Lysosomal compartments were detected in cytometry and confocal microscopy by LysoTracker Deep Red (LTDR) staining; in this way lysosomal involvement in both apoptotic and survival pathways was monitored. As shown in **Fig. 7.11**, wild type OMVs induced a significant increase in amount of LTDR-accumulating lysosomes in U937 cells after 48 and 72 hours of treatment compared to untreated control cells.



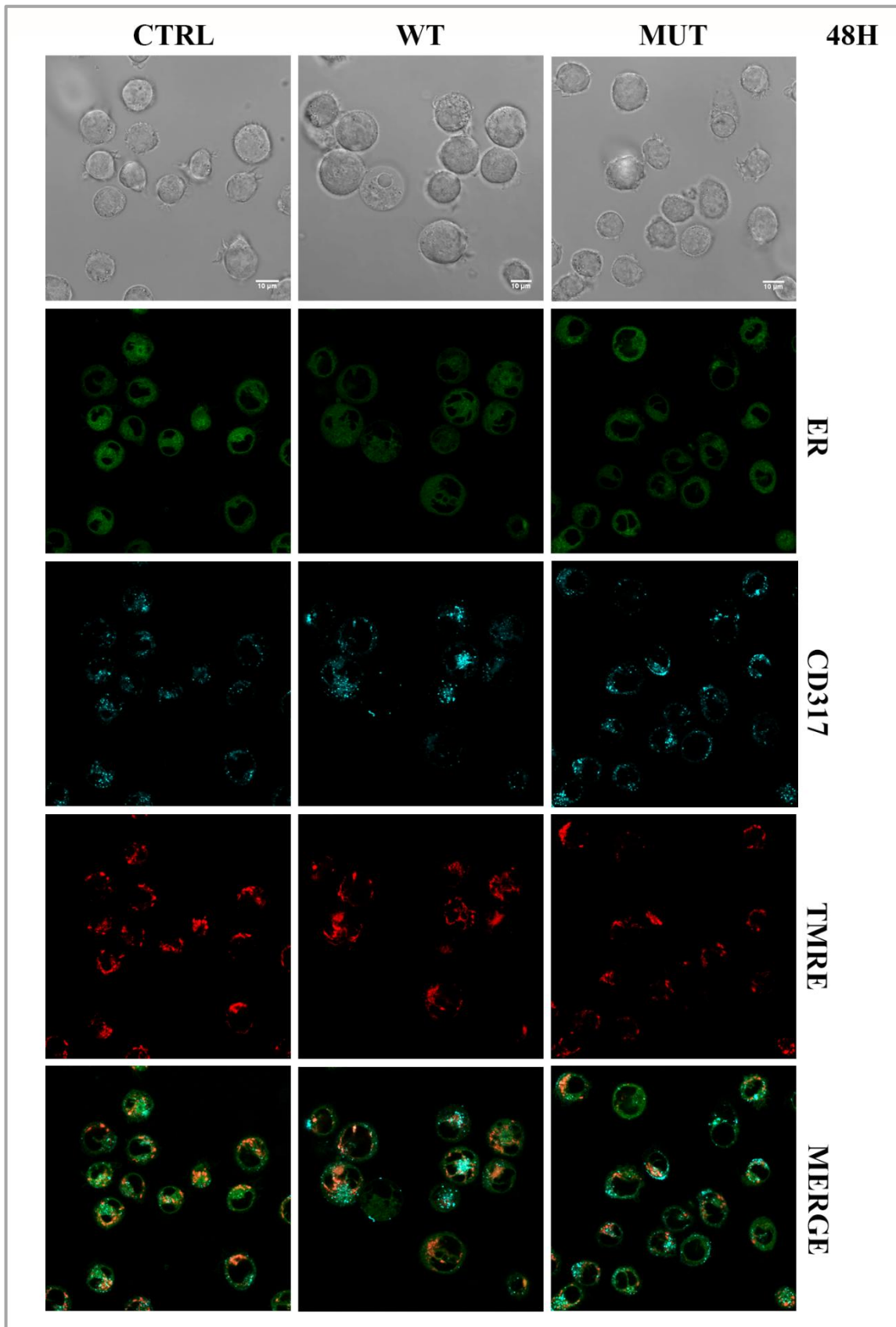


**Fig.7.7** Single confocal optical sections of TMRE, CD317 and ER Tracker of untreated and treated U937 cells after 48 hours of preincubation with OMVs from wild type and mutant strains. Bars: 10 $\mu$ m.

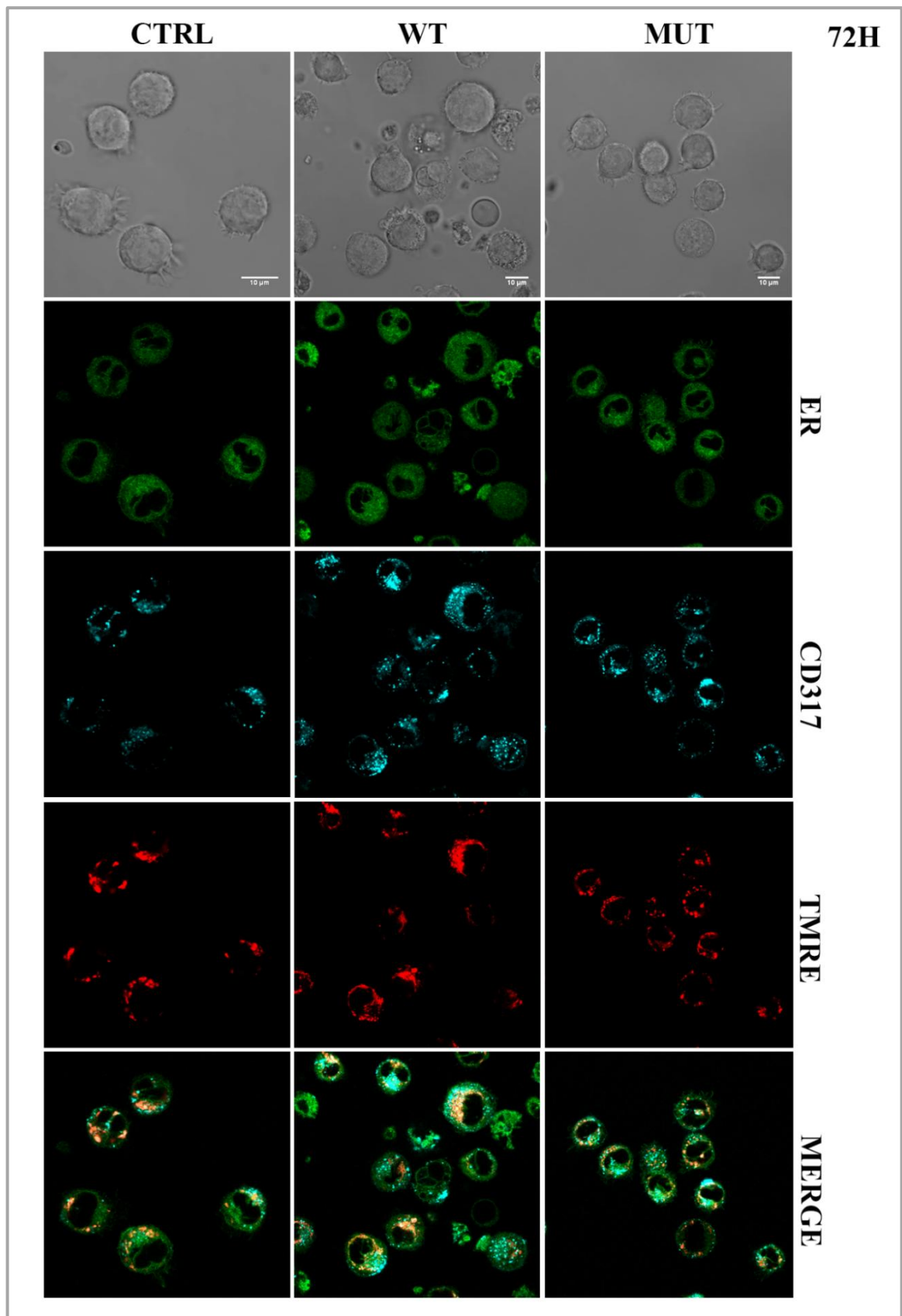


**Fig. 7.8** Single confocal optical sections of TMRE, CD317 and ER Tracker of untreated and treated U937 cells after 72 hours of preincubation with OMVs from wild type and mutant strains. Bars:10 $\mu$ m.

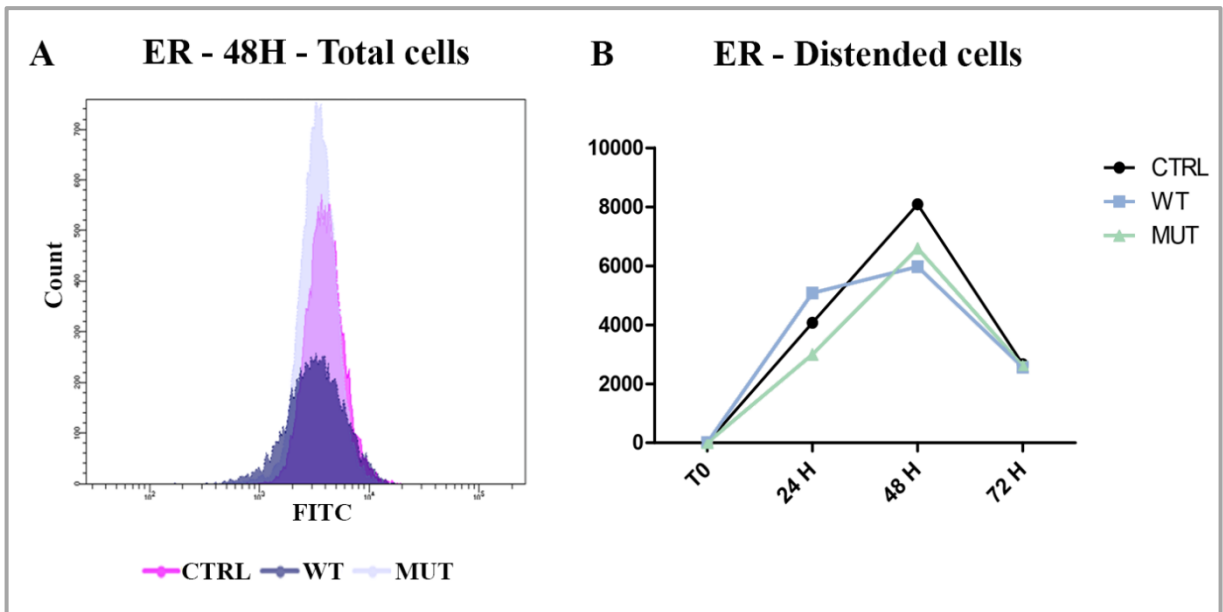


**Fig. 7.9** (A) Cytometric histograms showing ER Tracker MFI in untreated control cells (CTRL), and cells preincubated with OMVs from wild type (WT) and mutant (MUT) strains for 48 hours. (B) Trends of ER Tracker MFI in distended cells for each experimental condition during the time course.

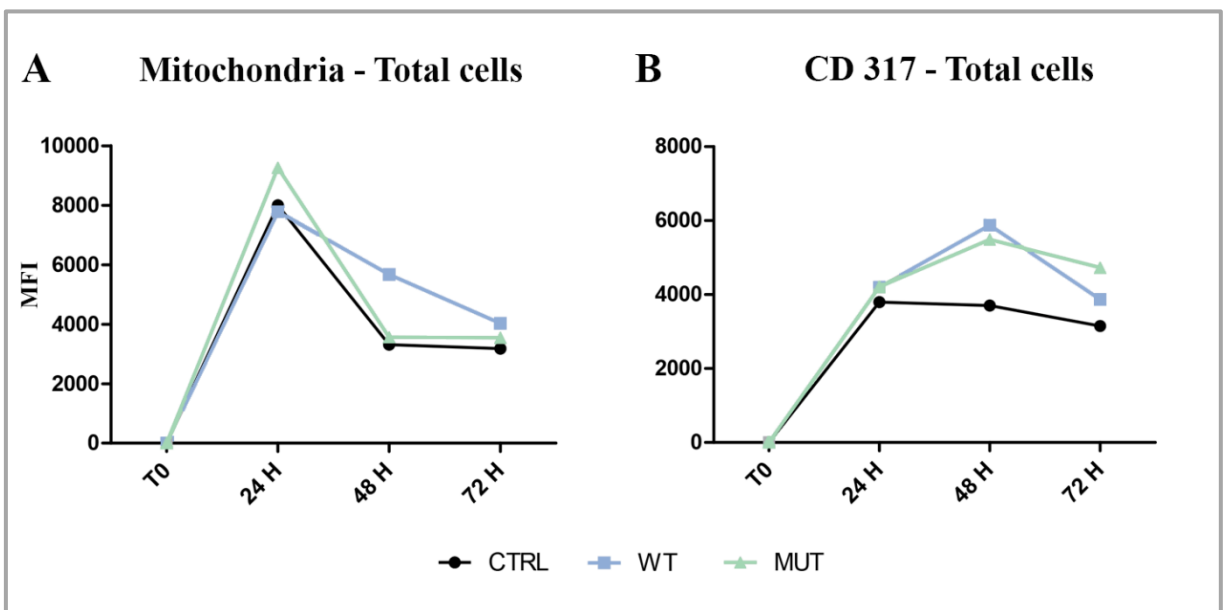


**Fig. 7.10** (A) Trends of TMRE MFI in total cells for each experimental condition during the time course. (B) Trends of CD317 MFI in total cells for each experimental condition during the time course.

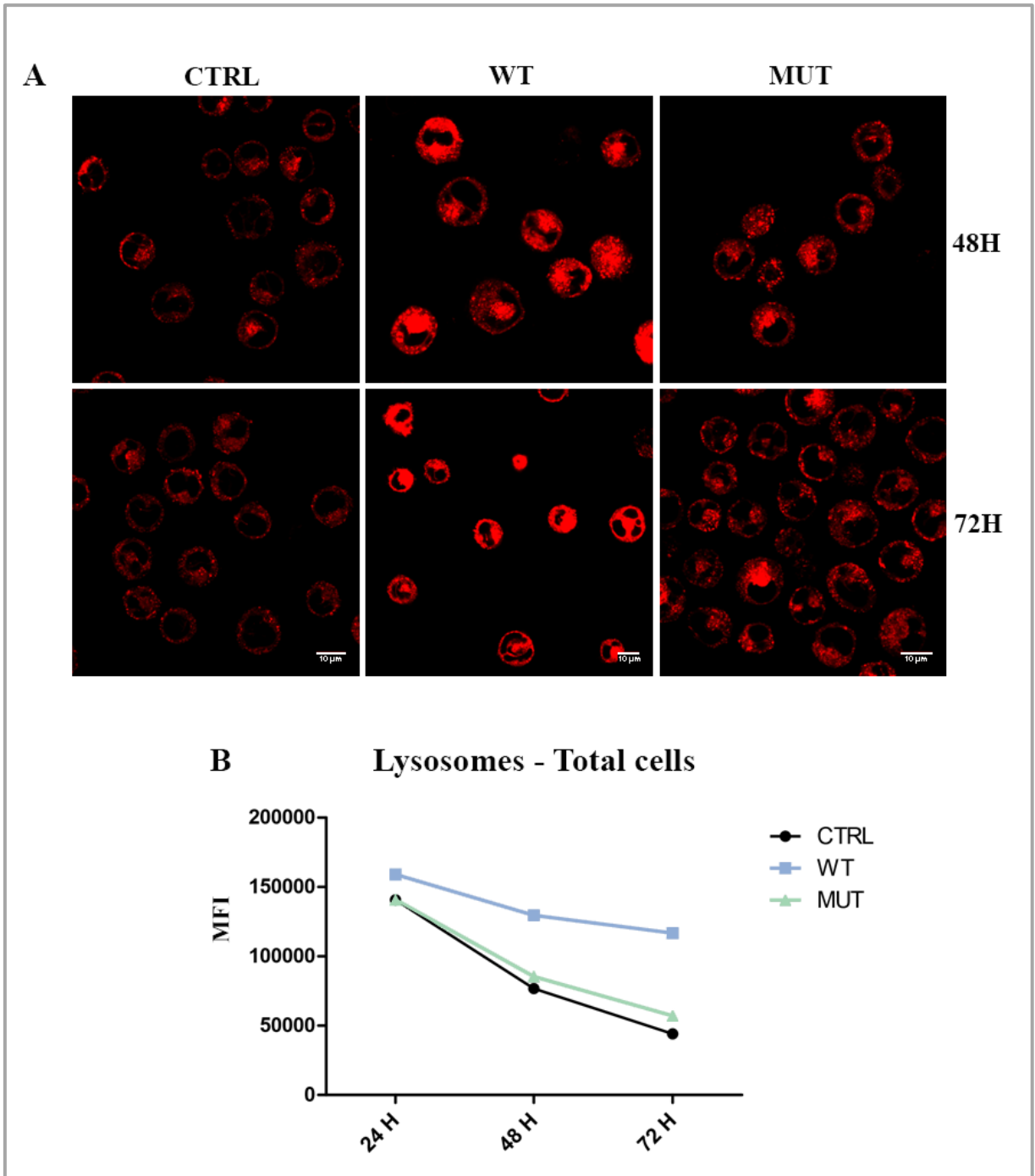


**Fig. 7.11** (A) Single confocal optical sections of LTDR MFI of control and treated U937 cells after 72 hours . (B) Trends of LTDR MFI in total cells for each experimental condition during the time course. Bars: 10 $\mu$ m.

### Evaluation of the intracellular lipid content

To characterize lipid accumulation in U937 cells, fluorescent dyes LipidTOX and Bodipy were used. In Fig.7.12 and 7.13, cytometric and microscopy results show respectively the peculiar staining of both treated and untreated cells. Of note, after 72 hours preincubation with OMVs from the wild type strain, U937 cells showed a great accumulation of peroxidised lipids, although minimal variations in neutral lipid content occurred. More investigations will be necessary to better elucidate the role of *C. jejuni cdtA* mutant OMVs, therefore the role of the CDT in these processes.

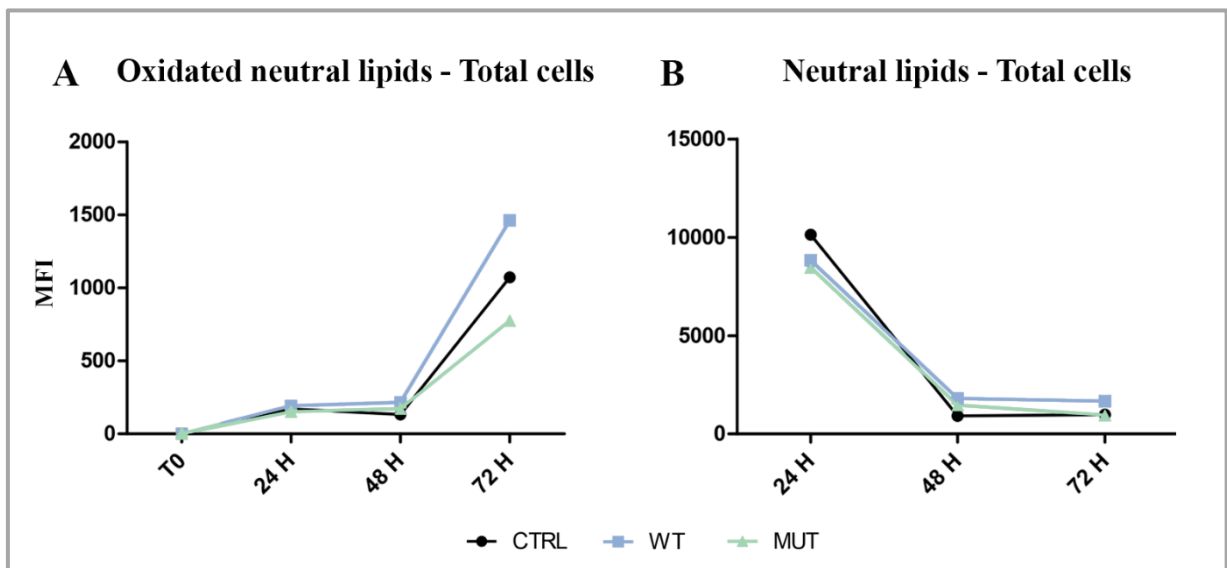


**Fig. 7.12** Trends of Bodipy (A) and LipidTOX (B) MFI in total cells for each experimental condition during the time course.

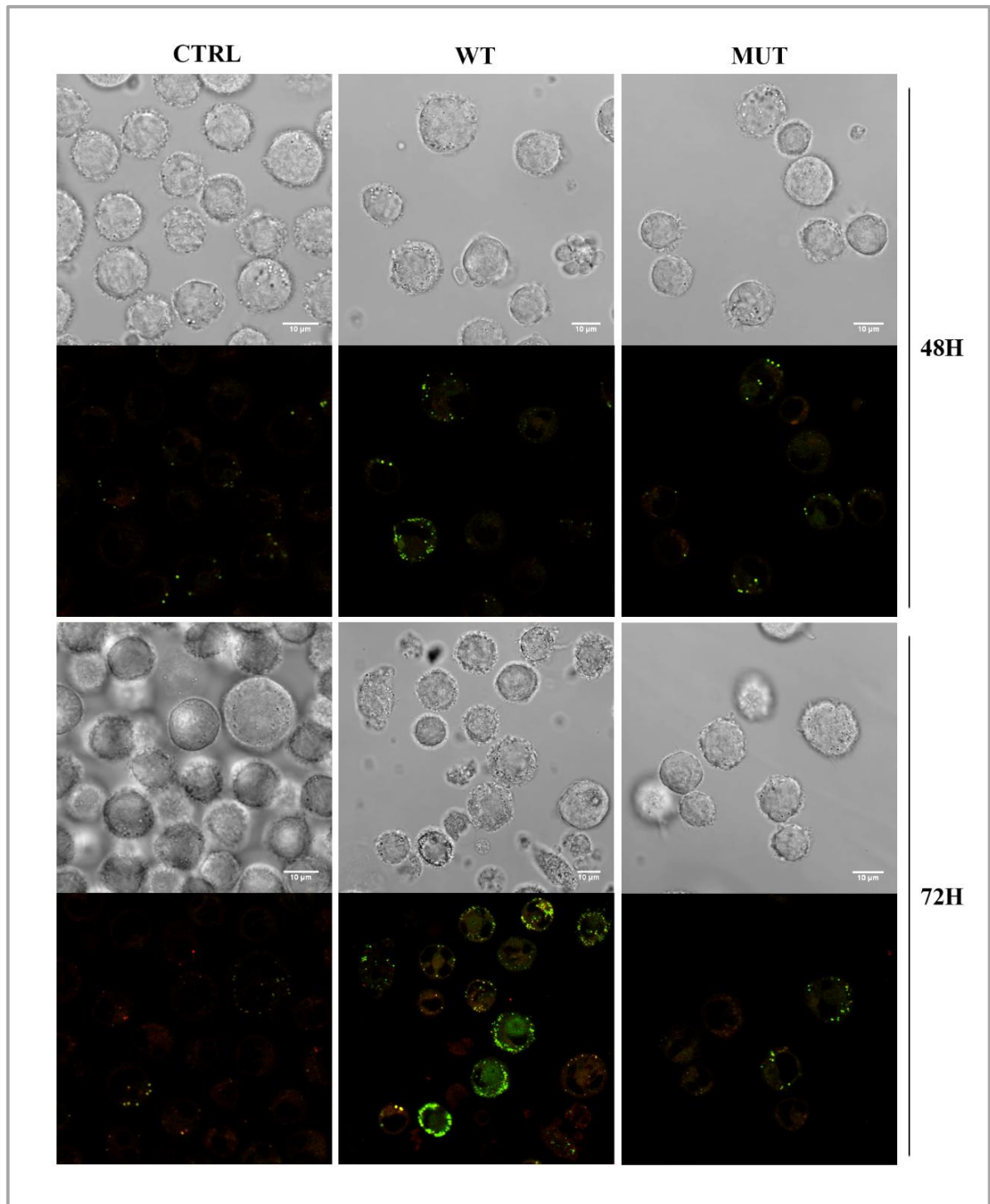


**Fig. 7.13** Single confocal optical sections of LipidTOX (in green) and Bodipy (in red) MFI (merged) of control and treated U937 cells after 48 and 72 hours of treatment. Bars: 10  $\mu$ m.

### Autophagic vacuole detection

MDC staining was used to investigate autophagolysosome formation in U937 cells infected with *C. jejuni* OMVs. As shown in **Fig. 7.14**, cytometric results revealed an important presence of autophagolysosomes in U937 cells infected with OMVs from the wild type strain, already at 48 hours .

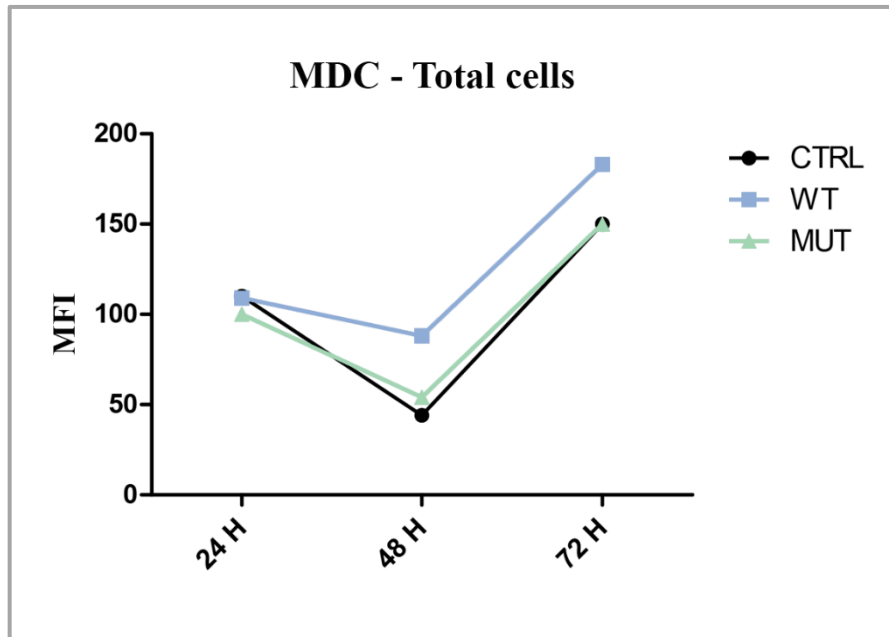


**Fig. 7.14** Trend of MDC MFI in total cells for each experimental condition during the time course.

## Discussion

Although more replicates are needed, preliminary data obtained from U937 cells preincubated with OMVs isolated from *C. jejuni* 11168H wild type and *cdtA* mutant strains confirm results previously obtained with lysates.

AnxV-PI and MDC stainings were used as indicators of cell death and autophagy respectively. In this part of the work, wild type OMVs, compared with OMVs from the mutant strain, induced apoptosis and autophagy in U937 cells via a CDT dependent mechanism, likely much more strongly than lysates (see previous chapter). Moreover, having the treatment induced perturbations in both mitochondrial and lysosomal functions, it is very likely that the apoptotic response involves both intrinsic and extrinsic apoptotic pathways.

Infected cells also showed significant alterations in lipid rafts and intracellular lipid content; this confirm the strong relationship between *C. jejuni* infection and lipids in human cells, already demonstrated in literature. Of note, whereas CD317 data demonstrated the evident involvement of lipid rafts in OMV-mediated *C. jejuni* infection, Bodipy-LipidTOX findings proved the lipid peroxidation caused by *C. jejuni* via CDT. The critical role of the CDT in this process is demonstrated by data from cells infected with OMVs from the mutant strain.

It is well known that  $\text{Ca}^{2+}$  metabolism and ER are strongly interconnected. The elevated levels of intracellular  $\text{Ca}^{2+}$  in cells preincubated with OMVs from the wild type strain demonstrated that a significant release of  $\text{Ca}^{2+}$  from ER stores occurred in these cells. ER and  $\text{Ca}^{2+}$  results, taken together, demonstrate that *C. jejuni* OMVs, from both wild type and mutant strains, are able to induce ER stress, although  $\text{Ca}^{2+}$  modifications are mostly induced by the wild type strain. These findings reveal that, while ER can be targeted by different *C. jejuni* virulence factors, ER  $\text{Ca}^{2+}$  storage can be altered only by a stronger player as the CDT.

It was already established that in human monocytes, CD14 is upregulated by bacterial LPS and contribute to CD14-mediated phagocytosis of Gram-negative bacteria (Grunwald et al, 1996). In this work, wild type OMVs induced CD14 upregulation on U937 surface.

In addition, as predicted, ICAM-1 modifications occurred in U937 cells after the treatment, suggesting that *C. jejuni* OMVs use ICAM-1 as a binding target through which cellular infection is initiated; from this same molecule host response against the pathogen is triggered.



## 8. Human intestinal cell model

### *C. jejuni* induces ER stress response in T84 cells

ER stress response in T84 cells preincubated with *C. jejuni* whole cells was investigated by monitoring the splicing of XBP1 mRNA by RT-PCR, and CHOP protein by Western blotting at 6, 12 and 24 hours' post-infection. In this chapter not only the *C. jejuni cdtA* mutant strain was used but also the *C. jejuni cdtB* mutant strain, as preliminary study concerning the role of the B subunit. Specifically, after 24 hours of infection, a significant increase in the spliced form of XBP1 was revealed in cells preincubated with the wild type 11168H strain (**Fig. 8.1**). After 6 (not shown) and 12 hours, differences were less significant (**Fig. 8.2**). Investigations of the effect of *C. jejuni* CDT mutants (*cdtA* and *cdtB*) resulted in less induction of XBP1 mRNA splicing at 24 hours (**Fig. 8.3**).

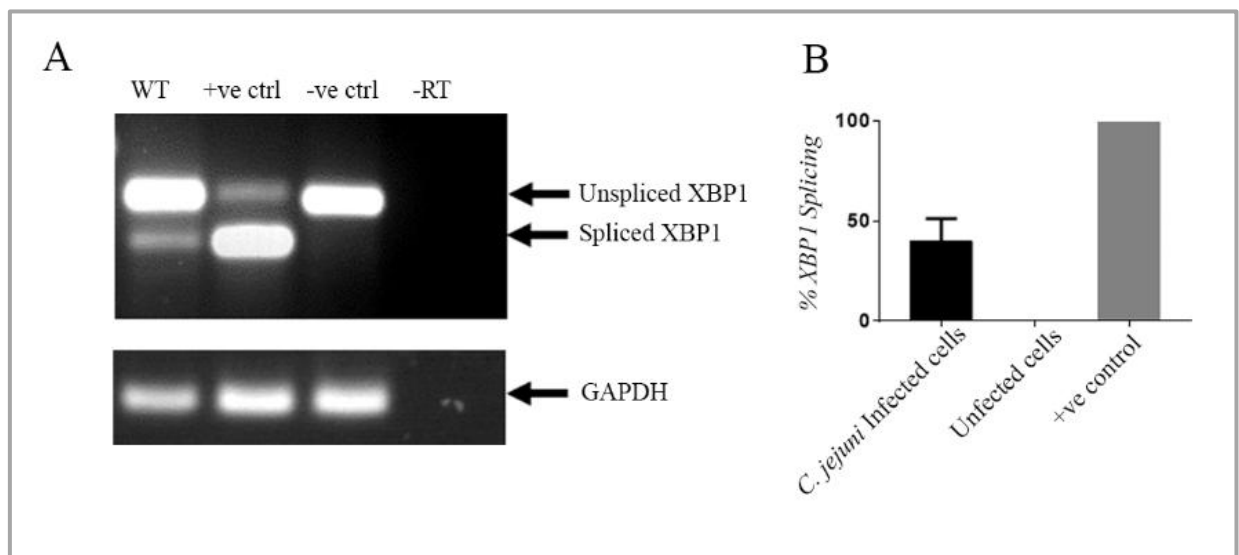


**Fig. 8.1** (A) T84 cells were either uninfected or infected with MOI 100:1 *C. jejuni* wild type 11168H strain. The level of spliced XBP1 mRNA was determined after 24 hours by RT-PCR with normalisation to GAPDH. XBP1 spliced and unspliced mRNA species were resolved by high-density agarose gel. (B) Quantification of XBP1 spliced band intensities from independent results was determined by densitometric analysis. Percentage of Splicing= $\text{spliced}/\text{total} \times 100$ . Bars are combined mean. Positive control was Thapsigargin.

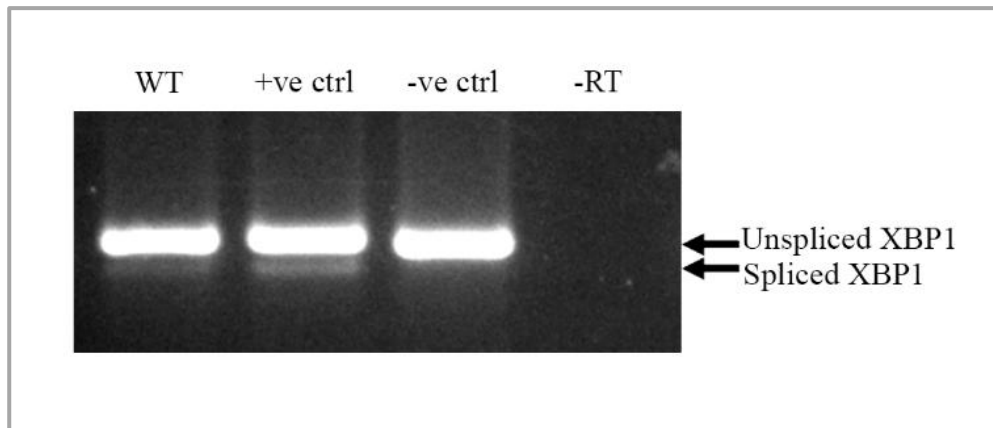


**Fig. 8.2** T84 cells were either uninfected or infected with MOI 100:1 *C. jejuni* wild type 11168H strain. The level of spliced XBP1 mRNA was determined after 12 hours by RT-PCR with normalisation to GAPDH. XBP1 spliced and unspliced mRNA species were resolved by high-density agarose gel. Positive control was Thapsigargin.

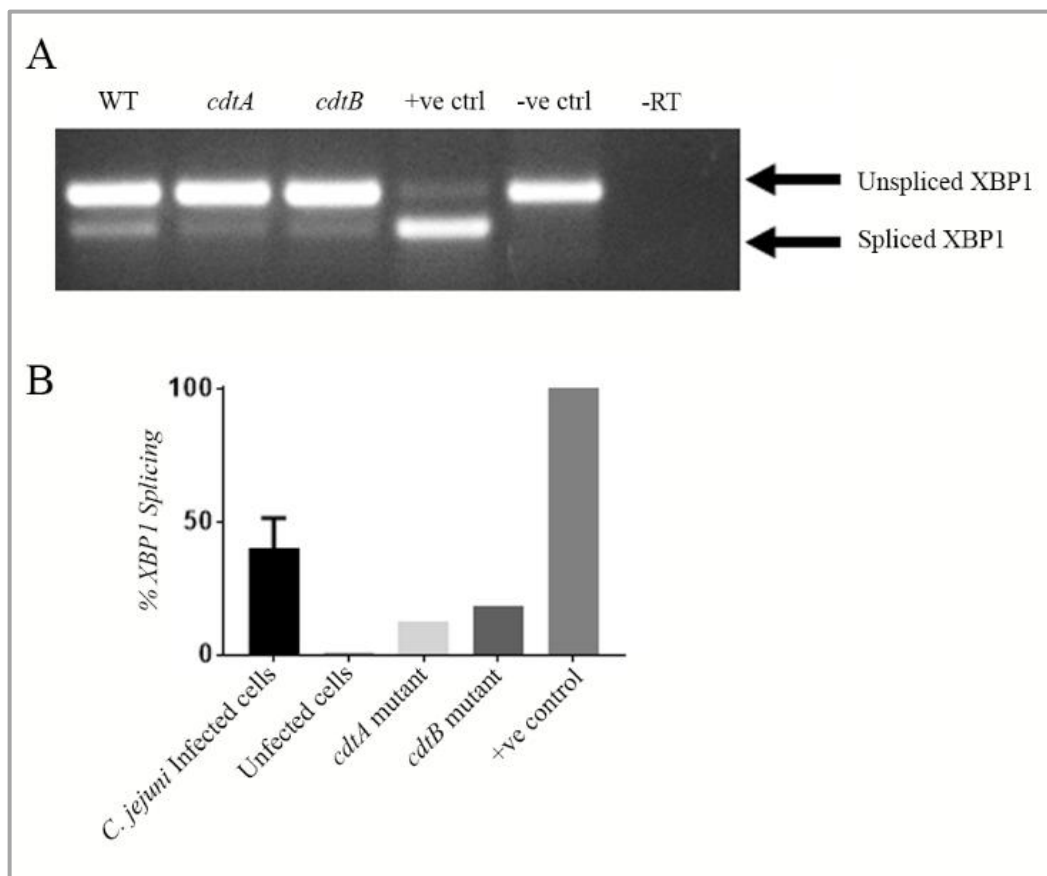


**Fig. 8.3 (A)** T84 cells were either uninfected or infected with *C. jejuni* wild type 11168H strain, *cdtA* and *cdtB* mutants at an MOI 100:1. The level of XBP1s mRNA was determined after 24 hours by RT-PCR with normalisation to GAPDH. XBP1 spliced and unspliced mRNA species were resolved by high-density agarose gel. **(B)** Quantification of XBP1 spliced band intensities from independent results was determined by densitometric analysis. Percentage of Splicing =  $\frac{\text{spliced}}{\text{total}} \times 100$ . Bars are combined mean. Positive control was Thapsigargin.

Preliminary data gained by Western blotting showed a mild increase in CHOP protein (data not shown) in infected cells compared with uninfected cells after 24 hours. According to these data, *C. jejuni* seemed to induce the UPR by inducing XBP1 mRNA splicing in T84 cells *in vitro*. *C. jejuni* CDT mutant results suggested a putative role of the CDT in these processes.

### ***C. jejuni* OMVs induce ER stress response in T84 cells**

ER stress response in T84 cells preincubated with OMVs from *C. jejuni* was investigated by monitoring the splicing of XBP1 mRNA by RT-PCR, and CHOP protein by Western blotting at 6, 12 and 24 hours' post-infection. As previously observed in T84 preincubated with whole *C. jejuni* cells, after 24 hours of infection, a significant increase in the spliced form of XBP1 was revealed in infected cells (**Fig. 8.4**) compared with uninfected cells. Surprisingly, investigations of the effect of *C. jejuni* CDT mutants (*cdtA* and *cdtB*) resulted in more induction of XBP1 mRNA splicing at 24 hours compared with the wild type strain. After 6 and 12 hours, differences were less significant (not shown). Data gained by Western blotting showed an important increase in CHOP protein in cells infected with OMVs compared with uninfected cells after 6 hours (**Fig. 8.5**). According to these data, *C. jejuni* OMVs seemed to induce the UPR by inducing XBP1 mRNA splicing in T84 cells *in vitro* as well as CHOP protein upregulation. According to *C. jejuni* CDT mutant results, more studies are needed to better investigate the putative role of the CDT in OMV-mediated infection.

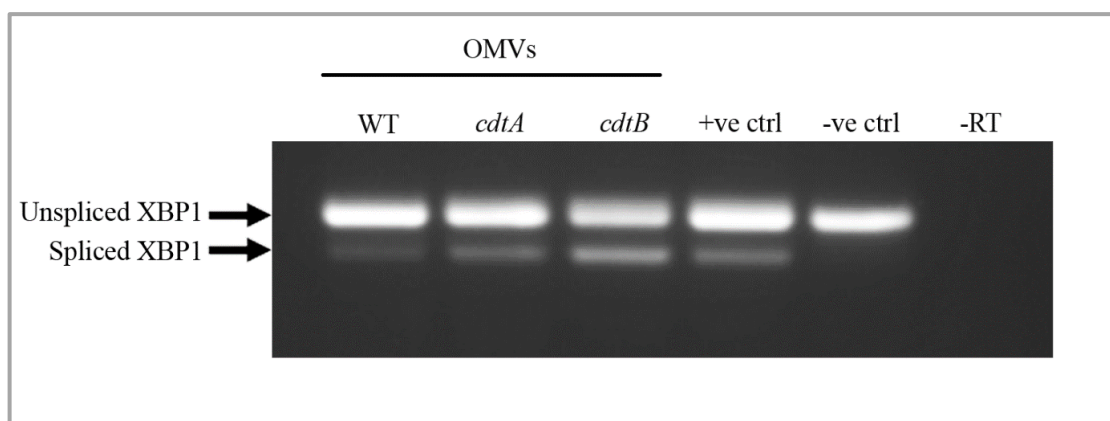


**Fig. 8.4** T84 cells were co-cultured with OMVs isolated from *C. jejuni* 11168H wild-type strain, *cdtA* or *cdtB* mutants. The level of spliced XBP1 mRNA was determined after 24 hours by RT-PCR with normalisation to GAPDH. XBP1 spliced and unspliced mRNA species were resolved by high-density agarose gel. Positive control was Thapsigargin.

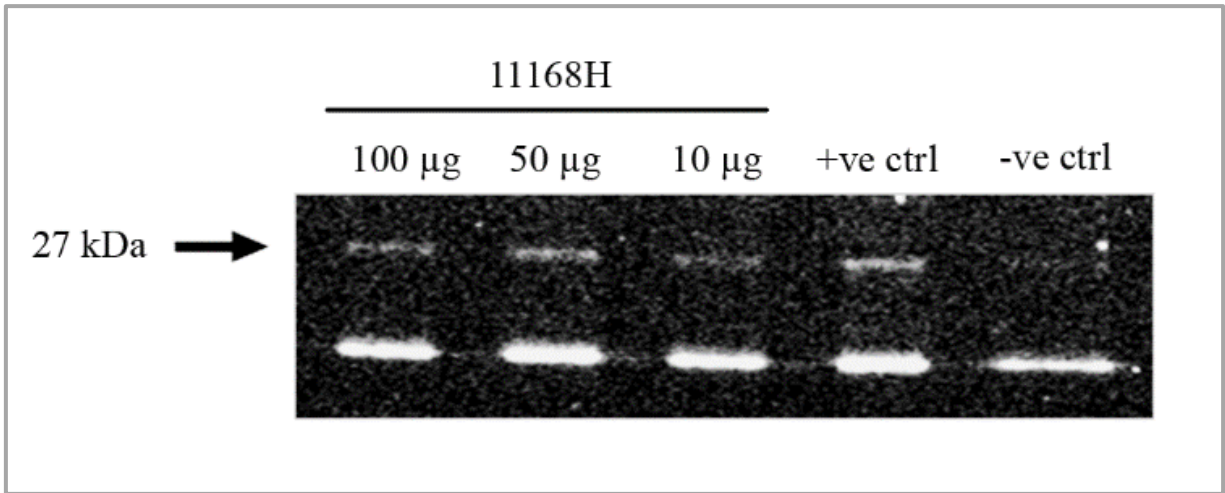


**Fig. 8.5** Infrared fluorescent Western blot for detection of CHOP protein. T84 cells were pre-incubated for 6 hours with OMVs from *C. jejuni* 11168H wild-type strain at different concentrations. Positive control was Thapsigargin.

## Discussion

Findings reported in this chapter are important in understanding the relationship among *C. jejuni*, ER and UPR. IECs showed to detect *C. jejuni* infection as a form of ER stress and subsequently they attempt to activate UPR presumably to support protein folding and eventually induce apoptosis. Splicing of XBP1 and induction of CHOP are key hallmarks of the UPR, and both OMVs and whole *C. jejuni* cells showed to induce the UPR. On the contrary, CDT might not have an important role in ER stress induction and UPR activation (as already affirmed in the previous chapters).

A. Kaser et al. (Kaser et al, 2008) reported that XBP1 is a key element of IBD (inflammatory bowel disease) pathogenesis. XBP1 deletion in IECs resulted in spontaneous enteritis and overactive responses of the IECs to the IBD inducers; this suggested that intestinal inflammation can originate from XBP1 abnormalities in IECs, thus linking cell-specific ER stress to the induction of organ specific inflammation. As described previously (see Introduction), IBD is a post infectious disease strictly associated to *C. jejuni*. Taken together these data show that XBP1 may represent the joining link between *C. jejuni* and IBD. Better investigating the relationship among IBD, *C. jejuni* and XBP1/UPR might be an interesting future intention.

Recent papers have shown that UPR can be activated by two complementary processes: the first one involves the binding of BiP to the luminal domains of the three sensors IRE1, ATF6 and PERK, the other one involves the direct binding of unfolded proteins to the stress-sensing luminal domain (Volmer et al, 2013). Perturbation of lipid composition also activates the UPR. In mammals altered lipid composition leads to ER  $\text{Ca}^{2+}$  depletion (Fu et al, 2011; Li et al, 2004) , that promote ER stress and UPR activation. A recent study reported that the luminal stress-domain of yeast IRE1 was able to be induced by lipid perturbation (Promlek et al, 2011).

Considering the importance of lipid rafts in *C. jejuni* infection and lipid modifications caused by *C. jejuni* (as observed in the previous chapters) future studies may better elucidate if UPR activation in IECs by *C. jejuni* is BiP or lipid dependent.

## 9. Construction of *C. jejuni* 11168H GFP mutant strain

As previously described (Methods 4.17), the CDS/CDS fragment was amplified using designed primers, purified and propagated into the pGEM-T Easy vector. Ligation and transformation into *E. coli* XL-2 cells followed, and transformants were checked by PCR (**Fig. 9.1**).

In the second stage the Km<sup>R</sup> cassette was incorporated into the CDS of interest: ligation and transformation into XL-2 cells were performed and the resultant colonies were checked for the insertion of a Km<sup>R</sup> cassette by carrying out an orientation specific primer PCR and an ISPCR to test positive transformants (**Fig. 9.2**). To check the orientation of the Km<sup>R</sup> cassette, bacteria single colonies were boiled/lysed and subjected to VPPCR using vector specific primers and orientation specific primer PCR (**Fig. 9.3**). The putative construct was finally confirmed using sequencing (**Fig. 9.4**).

Once obtained the putative construct, *C. jejuni* cells were grown to mid-log phase and mixed with the DNA to be transformed by electroporation. Resultant colonies grew up and the effective green fluorescence emitted by bacteria was verified by confocal microscopy (**Fig. 9.5**).

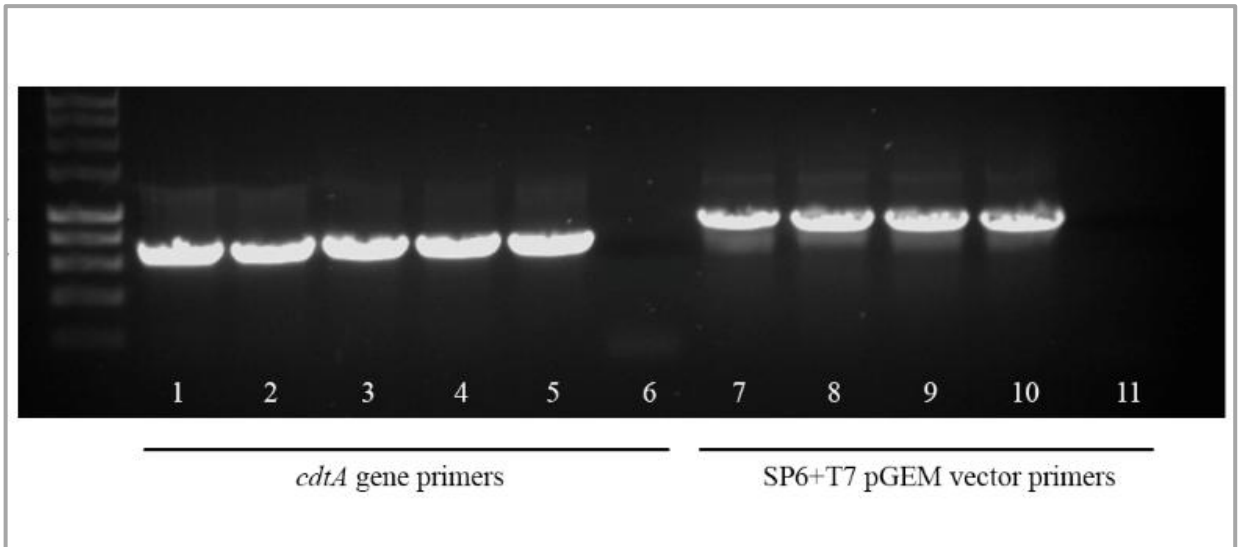


**Fig. 9.1** Electrophoresis from plasmid DNA using *cdtA* gene (lanes 2-5) and SP6 + T7 pGEM vector primers (lanes 8-10). Colony PCR was performed (Methods 4.10) and positive clones were selected. Lanes 1 and 7 represent positive controls; lanes 6 and 11 represent negative controls.

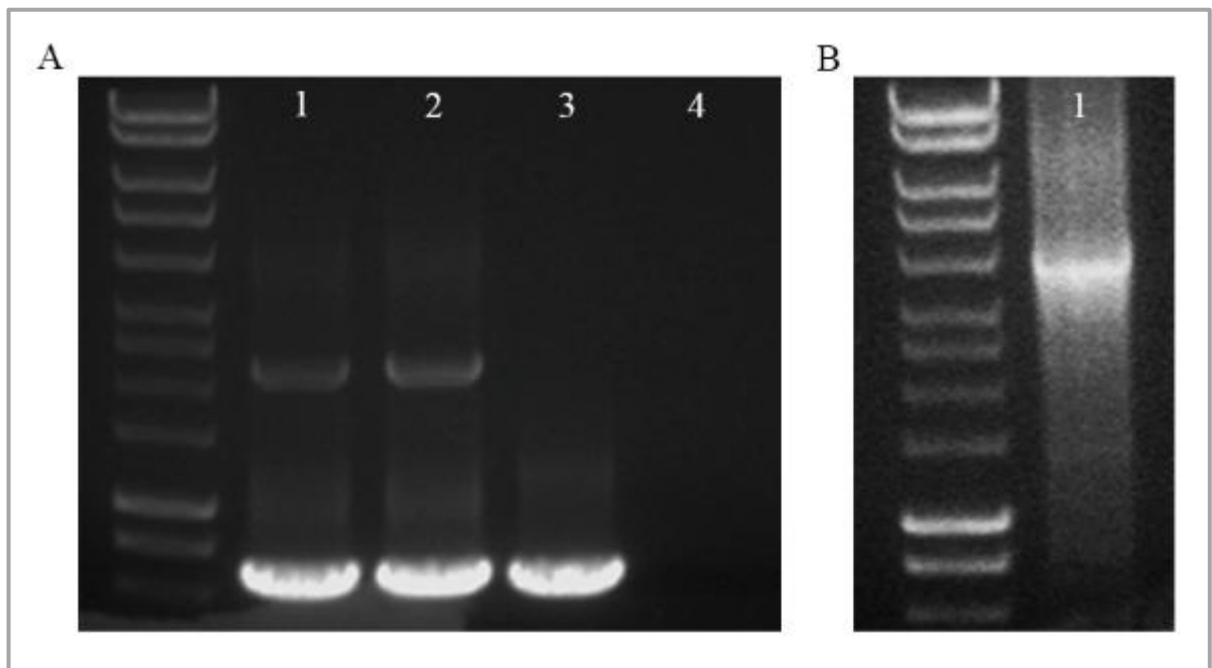


**Fig. 9.2** (A) Electrophoresis from purified plasmid DNA (lanes 1 and 2) (B) Electrophoresis from purified plasmid DNA (lane 1) using IMPCR primers. Colony PCR was performed (Methods 4.10) and positive clones were selected. Lanes 3 and 4 represent positive and negative controls respectively.

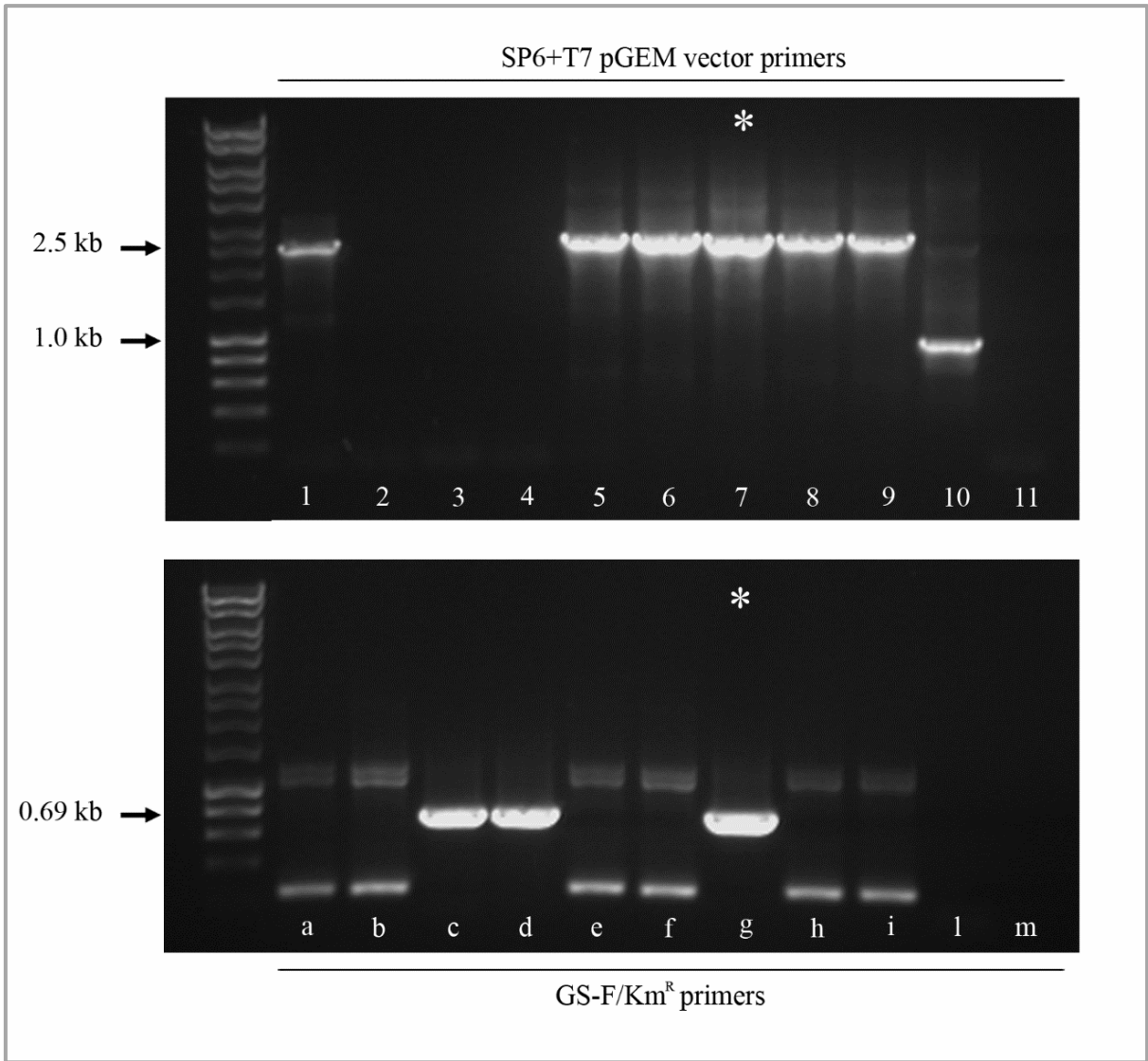


**Fig. 9.3** Electrophoresis from purified plasmid DNA using SP6+T7 pGEM vector primers (lanes **1-9** represent clones) and GS-F/Km<sup>R</sup> orientation specific primers (lanes **a-l** represent clones). Colony PCR was performed (Methods 4.10) and positive clones were selected. Lane **10** represents the positive control; lanes **11** and **m** represent negative controls.



### **Km<sup>R</sup> cassette**

```
CNNTCTATAGATATATTGATAAGCGCGCTGCCTATGCCTTGCCCCCTGAAATCCTTACATA
CGGCGATATCTTCTTATAAGCGTACCGGTTCCAATTTTTTCGCAGTTTAACTTTTCCGACG
CATTTATCGTCTTGGTAGTAAAGATATATTATATATTATCTTATCAGTATTGTCAATATAT
TCAAGGCAATCTGCCTCCTCATCCTCTTCATCCTCTTCGTCTTGGTAGCTTTTTAAATATG
GCGCTTCATAGAGTAATTCTGTAAAGGTCCAATTCTCGTTTTTCATACCTCGGTATAATCTT
ACCTATCACCTCAAATGGTTCGCTGGGTTTATCGATGATAAGCTGTCAAACATGAGAATTC
GAGCTCGGTACCCGGGGATCTAATCCAATTTCTTGTGCTAAAGCCCAAACCGTTAAAGCT
GCTCCGCTAGGGCCTAGAAATGGTTAAAAAATCAGAAACCGCAGGGCGATTTTCAAAAATTA
AAACATCATTTAAAGCTTCGTCTTTAAAGCGAGGATTGATCCCATTTGCTGCATTATTGTT
GGCACTATTGCTTGTCTAGTTAAAGGTGGGGTAATAGGAGTAATAGGTACTAAATCAGCA
CCGCTAATTTAACTTGGAAATTTCTTGATTGGTAGGAAAAGTAGGTTCAAGTCTAGTTTTA
AAGGATCAGTATCTTCAAATTTCTCAAATCACTAGTGAATTCGCGGCCGCCTGCAGGTCGA
CCATATGGGAGAGCTCCCAACGCGTTGGATGCATAGCTTGAGTATTCTATAGTGTCACCTA
AATAGCTTGGCGTAATCATGGTCATAGCTGTTTCCTGTGTGAAATTGTTATCCGCTCACAA
TTCCACACAACATACGAGCCGGAAGCATAAAGTGTAAGCCTGGGGTGCCTAATGAGTGAG
CTAACTCACATTTNATTTGCGTTGCGCTCACTGCCCGCTTTCCAGTCGGGAAANCTGTCNNG
CCAGCTGCATTANNANCNGCNANGNNNNNGGGANAGGNGNTTGCGNATTTGGGNCGCTCNTC
NNTTCNCGCNTCACTGANTCNNNNNNCTNNGNCNNNNGNNTGNNNNNNNNGNNTCANNTCN
NTNANGGNGNNNNNNNGTNTNANNANNGNNNNNNNCNGAANAANNTGNNNNANCAANNN
```

### ***cdtA* gene**

```
NNNNACTTTTCTTACCNATCAAGAAATTCCAAGTTTAATTAGCGGTGCTGATTTAGTACCT
ATTACTCCTATTACCCACCTTTAACTAGAACAGCAATAGTGCCAACAATAATGCAGCAA
ATGGGATCAATCCTCGCTTTAAAGACGAAGCTTTTAATGATGTTTTAATTTTTGAAAATCG
CCCTGCGGTTTCTGATTTTTTAACCATTCTAGGCCCTAGCGGAGCAGCTTTAACGGTTTGG
GCTTTAGCACAAAGGAAATTGGATTAGATCCCCGGGTACCGAGCTCGAATTCTCATGTTTGA
CAGCTTATCATCGATAAACCCAGCGAACCATTTGAGGTGATAGGTAAGATTATACCGAGGT
ATGAAAACGAGAATTGGACCTTTACAGAATTACTCTATGAAGCGCCATATTTAAAAAGCTA
CCAAGACGAAGAGGATGAAGAGGATGAGGAGGCAGATTGCCTTGAATATATTGACAATACT
GATAAGATAATATATAATATATCTTTACTACCAAGACGATAAATGCGTCGGAAAAGTTAAA
CTGCGAAAAAATTGGAACCGGTACGCTTATATAGAAGATATCGCCGTATGTAAGGATTTCA
GGGGCAAGGCATANGCAGCGCGCTTATCAATATATCTATTTAAAANGGGCAAAGCATAAAA
ACTTGCATGGANNANTGCTTTGAAACCCAGGANATAAACCTTATAGCTTGAAAATTCTATC
NTAANNTGTGGATTCAAATCCGGCTCCCN
```

**Fig. 9.4** Sequencing verification of Km<sup>R</sup> cassette and *cdtA* gene.

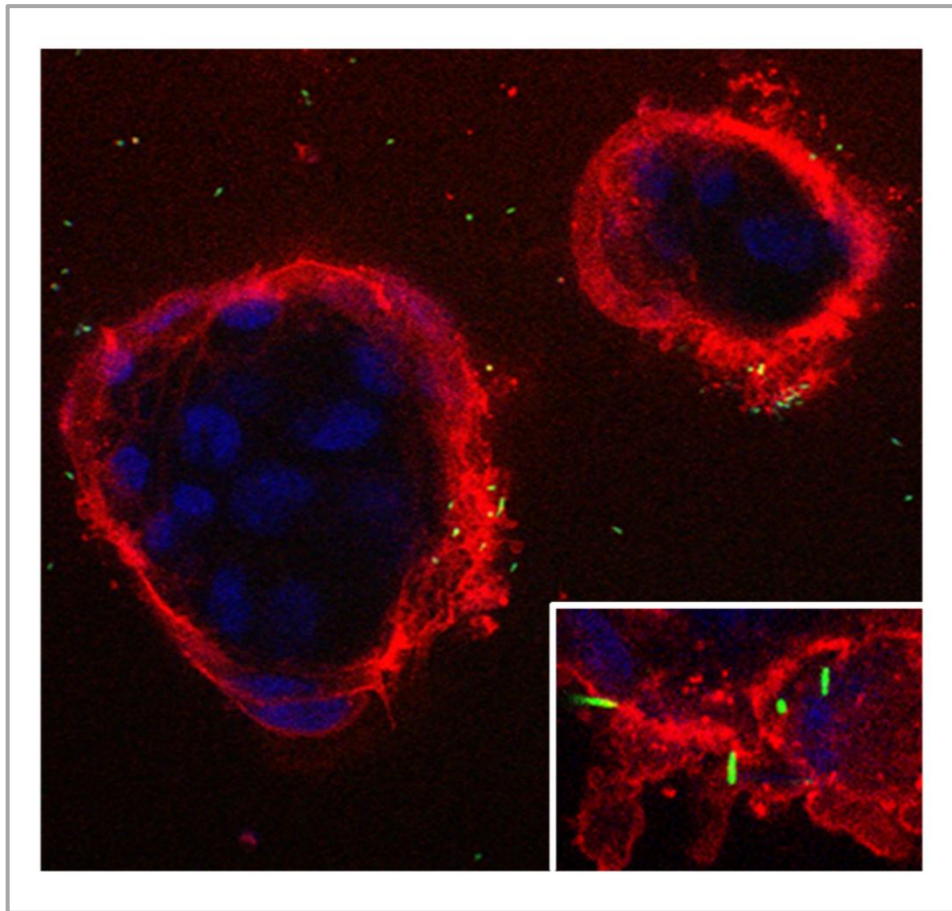


**Fig. 9.5** Visualisation of *C. jejuni* *cdtA* mutant with fluorescence confocal microscopy at 2 hours. T84 cells were grown on round coverslips in 24 well plates overnight. Live bacteria (OD600 0.1) were added and co-incubated for 2 hours. Cells were fixed with paraformaldehyde, washed with PBS, stained and mounted. Cells were immunostained with anti-WGA (Red) to indicate membranes with DAPI (Blue) to indicate nuclei, with *C. jejuni* *cdtA* mutants GFP (Green).

## Discussion

The *C. jejuni* *cdtA* GFP mutant strain realized in this part of the work could be extensively used in future investigations finalized to study the intimate relationship of *C. jejuni* with intracellular compartments contained in human cells, in particular the ER, and the role of the CDT. Only the mutant for the *cdtA* gene was made because of the complexity of the construction process; in the future, realization of *C. jejuni* *cdtB* and *cdtC* mutant strains might be conducted.

## Conclusions

### Role of the CDT in *C. jejuni* infection

The usage of *C. jejuni* *cdt* mutant strains allowed us to investigate the role of the CDT in *C. jejuni* infection mechanisms. Although some modifications seem to be CDT independent, such as ER stress, CD14 and CD59 surface expression; many of the investigated mechanisms are certainly CDT dependent. Of note, cell response to CDT seems time dependent: if in monocytes we observed important modifications at 24-48 hours, in U937 cells important modifications are evident at 48-72 hours. The fact that CDT provokes some modifications in host cells after long time lapses (from 24 to 72 hours) might be essential for the onset of post infectious sequelae such as the GBS. To better study the role of the CDT and the single *cdt* subunits, in the future it could be interesting to investigate the effects of all *C. jejuni* *cdt* mutant strains (*cdtA*, *cdtB* and *cdtC*) in all above-mentioned cell lines, as well as the complements of the respective *cdtA*, *cdtB* and *cdtC* mutants could be made to understand the structural and functional properties of these proteins.

### *Myeloid cells can respond to C. jejuni infection by activating programmed cell death*

Human cells can respond to the CDT by activating apoptosis in order to kill the pathogen, and avoid a possible bacterial spreading. If in normal cells pro-apoptotic and anti-apoptotic signals are constantly on balance, in infected cells an imbalance between these signals arises, as demonstrated by Bcl-2, p53 and pRb findings. In this work, from 6 to 72 hours, we gradually observed which mechanisms are activated by the human cell to die or survive to the *C. jejuni* infection.

**Mitochondria** and **lysosomes** are differently targeted by different *C. jejuni* strains, demonstrating that cells activate different programmed cell death pathways, classical intrinsic or mitochondria-lysosome crosstalk, depending on the specific strain. Although mitochondrial modifications caused by *C. jejuni* CDT are certainly associated to an activation of an intrinsic apoptotic pathway, recruitment of lysosomes can be associated to the activation of both the extrinsic apoptotic pathway and the autophagic pathway, two different pathways that meanwhile are strictly interconnected.

*C. jejuni* can activate the endocytic pathway, the autophagic pathway and the secretory pathway

Particularly interesting is the relationship between *C. jejuni* and lysosomes; we provided evidences about how much these organelles are important for *C. jejuni* infection. **LAMP-1** upregulation, **lysosomal destabilization**, **mTOR** involvement and **autophagy** activation occurred in our cell models suggesting that *C. jejuni* is particularly able to activate the endocytic pathway, the secretory pathway and the autophagic pathway.

The primary functions of the endocytic pathway are degrading and recycling internalized materials and redundant cellular component by using a specialized arsenal of hydrolases and proteases enclosed in membrane bound organelles. Lysosomal proteases can initiate apoptotic signaling by amplifying the apoptotic pathways initiated in/by other cellular components. At the same time, the endocytic system assists the autophagic system in counteracting apoptotic stimuli (Repnik et al, 2013) (Hafner Česen et al, 2012).

Endocytosis has a central role in the uptake of nutrients from extracellular environment and recycling of the plasma membrane and its components, allowing the degradation of potentially harmful molecules, by connecting the transport of degradation-destined cargo from the early recycling circuit to the degradative system (Huotari & Helenius, 2011).

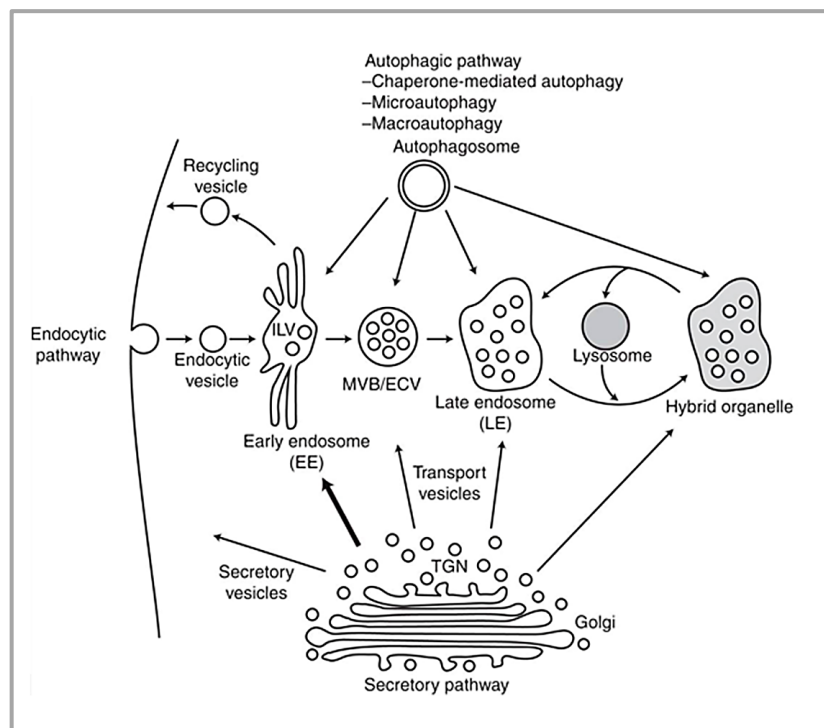


**Fig. 10** Schematic representation of endocytic, autophagic and secretory pathways. *C. jejuni* showed to activate all these routes. (Repnik et al, 2013)

Components that should be degraded are transported to the late endosome (LE), that represents the ‘stomach’ of the cell, through multivesicular bodies (MVB) or endosome carrier vesicles (ECVs) (**Fig. 10**). Enzymes used by LE for degradation process come from the *trans*-Golgi network (TGN). Lysosomes bud off the LE in a process known as lysosome re-formation (Bright et al. 1997). It has recently been shown that lysosome re-formation depends on **mTOR** activation, which in turn depends on monomeric metabolites, which are produced during lysosomal degradation (Yu et al, 2010).

**LAMP** molecules are integral membrane lysosomal proteins that are found in both LEs and lysosomes. They seem to be involved in vesicle trafficking along microtubules and serve as receptors for **chaperone-mediated autophagy** (Patel & Cuervo, 2015). Indeed, there are three different forms of autophagy: Macro-autophagy, chaperone-mediated autophagy and micro-autophagy (Boya et al, 2013). Although additional investigations are needed, our findings demonstrate that *C. jejuni* might activate more than one type of autophagy.

Although lysosomal exocytosis/secretory pathway was studied only in monocytes cells, interesting data were collected. *C. jejuni* virulence factors demonstrated to induce lysosomal exocytosis in monocytes.

The **ER** is a continuous membrane organelle that consists of a nuclear envelope and a peripheral network of tubules and sheets. It also serves as a principal site for protein synthesis and folding, protein glycosylation,  $\text{Ca}^{2+}$  storage and signaling, sterol biosynthesis, and drug metabolism. Thus, the ER is sensitive to alterations in  $\text{Ca}^{2+}$  homeostasis and accumulation of misfolded proteins. Depletion of  $\text{Ca}^{2+}$ , inhibition of glycosylation, exposure to toxins or reactive oxygen species, and/or the accumulation of misfolded proteins in the ER lead to ER stress, and sustained ER stress eventually results in cell death (Rao et al, 2004). In a branch of the UPR, the ER transmembrane kinase/endonuclease IRE1 $\alpha$  and  $\beta$  initiate a novel UPR-mediated mRNA splicing mechanism that leads to the formation of the spliced XBP1 formation. Spliced XBP1 plays an important role in phospholipid synthesis in the ER membranes. These phospholipids allow ER biogenesis and expansion of ER membranes under stress conditions (Sriburi et al, 2004) (Sriburi et al, 2007). ER expansion, through the UPR-mediated activation of lipid biosynthesis, has been reported to alleviate stress.

Different techniques and very different approaches were used in this work to investigate ER stress (Conn, 2011). Experiments with the *C. jejuni* *cdtA* and *cdtB* mutant strains showed ER modifications are CDT independent. Both results from myeloid cells and intestinal cells confirm this hypothesis; as well as both ER Tracker results and molecular investigations showed that *C. jejuni* is able to induce ER expansion and ER stress, but not statistically

significant differences were observed between mutant and wild type strains used in this project. Of note, this work also provides the first evidence that *C. jejuni* induces UPR in human intestinal cells and U937 cells. Although we proved that *C. jejuni* cause ER stress and CHOP activation, more investigations are needed to elucidate the relationship among *C. jejuni*, UPR and monocytes in humans. ER findings are consistent with  $\text{Ca}^{2+}$  data: in cells preincubated with OMVs, we observed that  $\text{Ca}^{2+}$  depletion is mostly induced by the wild type strain, suggesting that ER  $\text{Ca}^{2+}$  storage can be altered only by a stronger player as the CDT. This is only one of the numerous proves that CDT represent a complex and astute system that *C. jejuni* explicate to infect host cells.

ER stress and UPR activation can also lead to autophagy activation, such as alterations in **lipid metabolism**, as demonstrated by Bodipy and LipidTOX findings. ER stress, caused by various stimuli, affects lipid metabolism through modulating the expression levels of key enzymes involved in lipid synthesis or modification (Han & Kaufman, 2016)

Our results showed alterations in lipid content and an increase in peroxidised lipids in U937 preincubated with *C. jejuni* lysates and OMVs. It is likely that lipid content modification after 48-72 hours is a consequence of spliced **XBPI** and UPR activation (Gardner & Walter, 2011).

As demonstrated by MDC results and pre-treatment with RM, *C. jejuni* induce the autophagic processes in myeloid cells, with an important involvement of mTOR, ER and lysosomes. mTOR signaling modulates autophagic responses involved in bacterial killing and clearance (Gutierrez et al, 2004) and it is shown to be involved in host response to *C. jejuni* infection. Sun et al. demonstrated that intestinal inflammation induced by *C. jejuni* is correlated with PI3K/mTOR signaling activation, which can regulate the innate immune host response (Sun et al, 2012). Factors involved in mTOR signaling might be therapeutic targets for campylobacteriosis.

### **Myeloid cells and GBS onset**

**ICAM-1** is a ligand for  $\beta 2$  integrin particularly expressed on monocytes which participate in leucocyte-leucocyte, leucocyte-endothelial and leucocyte-epithelial cell interactions by mediating leucocyte rolling, firm adhesion and subsequent extravasation (Springer, 1994) (Hubbard & Rothlein, 2000). ICAM-1 upregulation enhances antigen presentation and inflammatory response activation, allowing the generation and maintenance of the host response. It was also shown that ICAM-1 mobility can be altered by OMVs produced by

Gram negative bacteria such as *E. coli* (Kim et al, 2013). Moreover, a recent paper reported a significant association between polymorphisms of ICAM-1 and the GBS (Kharwar et al, 2017), suggesting that ICAM-1 could have a possible role in GBS development, also representing a possible genetic marker to GBS susceptibility. In this study we demonstrated that *C. jejuni* activate the inflammatory response by upregulating ICAM-1 expression in a CDT- independent manner, this means that other virulence factors produced by the *C. jejuni* are involved in this process.

The GPI-protein **CD59** is expressed on the surface of several blood cells in order to protect them from the complement-mediated cell lysis. Nevertheless, the complement is an important component of innate immunity as well as a modulator of the adaptive immunity, with a central role in contrasting bacterial infections and removing debris. The critical role of MAC in immune defence is to kill a subset of Gram-negative bacteria, in particular cocci of the phyla *Neisseria*, *Moraxella* and *Haemophilus*, that are inefficiently eliminated by opsonophagocytosis (Morgan et al, 2017). In this thesis there is evidence that *C. jejuni* virulence factors induce CD59 expression, suggesting that *C. jejuni* might interact with CD59 in order to inhibit cell lysis and persist in host cells. This might allow the infection spreading that could lead to the onset of post-infectious sequelae such as the GBS. At present, there are no evidences that *C. jejuni* interact with CD59 in order to infect host cells and lead to GBS. More studies are certainly necessary to better elucidate this topic.

All those modifications, such as **autophagy** activation and/or **pRb** upregulation, that are caused by the bacterium and are finalized to host cell survival and bacterium persistence, have to be considered potentially important for GBS onset. Upregulation of pRb by *C. jejuni* might represent a helpful expedient that this bacterium could activate in order to contrast the programmed cell death that cells activate in response to bacterial infection.

### **CDT internalization**

Although more investigations about lipid rafts are necessary, interesting data were reported about CDT internalization in this work. As demonstrated in U937 cells preincubated with the *C. jejuni* ISS 1 wild type lysate, it is very likely that the CDT produced by this wild type strain is internalized by an alternative route that deviates the classical endocytic pathway, unlike the *C. jejuni* ATCC 33291 strain. Some pathogens utilize alternative routes to enter host cells that may evade the intracellular barriers encountered by the typical clathrin-

mediated endocytic pathway. In the last 15 years, different authors hypothesized a novel model system through which all CDTs are trafficked in a retrograde manner from the cell membrane to the Golgi, and from the Golgi to the ER, in reverse of classical secretion, to translocate to cytosolic targets and nucleus. This mechanism facilitates the entry of pathogens and potential delivery agents (Medina-Kauwe, 2007). The actuation of this expedient is essential for *C. jejuni* persistence within host cells.

### **Importance of OMVs in *C. jejuni* infection**

In this work, it was also studied the importance of OMVs in *C. jejuni* infection. In U937 cells, we compared the effect of *C. jejuni* lysates with OMVs and it was found that in all investigated parameters the effect of the OMVs were more pronounced than lysates, in particular the effects induced by the wild type strain. These findings suggest that, if on the one hand virulence factors contained in *C. jejuni* lysates can cause many modifications and cell death in monocytes/myeloid cells, without the involvement of the viable bacterium and OMVs, on the other hand some modifications such as alteration of Ca<sup>2+</sup> content, intracellular lipid content, ICAM-1 expression and CD14 expression are enhanced by the action of the OMVs.

In conclusion, this work represents a novel approach to investigate the mechanisms that *C. jejuni* uses to cause disease. So far, cytometry, here successfully applied, has been a technique poorly applied in microbiological investigations as well as in *C. jejuni* studies. Moreover, we tried to better understand the relationship among monocytes, *C. jejuni* and Guillain-Barré syndrome; unfortunately, only a few papers focused the attention on this topic in the last decade. The ability of *C. jejuni* to survive within intestinal cells and monocytes, unlike what happens within macrophages, might have a critical role in GBS outset.



## Appendices

### Appendix 1-Primer design

Oligonucleotide primers were designed manually by selecting 15-25 nucleotides, with consideration of melting temperature and GC content. Sequences were checked for the presence of self-dimers and hairpins using the web program IDT SciTools-OligoAnalyzer 3.0 (<https://www.idtdna.com/calc/analyzer>).

*cdtA* sequence:

```
ATGCAAAAATTATAGTTTTTATTTTATGTTGTTTTATGACTTTTTTCTTTATGCATGT
TCTTCTAAATTTGAAAATGTAAATCCTTTGGGGCGTTCATTTGGAGAATTTGAAGATACT
GATCCTTTAAAACTAGGACTTGAACCTACTTTTCCTACCAATCAAGAAATCCAAGTTTA
ATTAGCGGTGCTGATTTAGTACCTATTACTCCTATTACCCACCTTTAACTAGAACAAGC
AATAGTGCCAACAATAATGCAGCAAATGGGATCAATCCTCGCTTTAAAGACGAAGCTTTT
AATGATGTTTTAATTTTTTAAAAATCGCCCTGCGGTTTCTGATTTTTTAACCATTTTAGGC
CCTAGCGGAGCAGCTTTAACGGTTTGGGCTTTAGCACAAGGAAATTGGATTTGGGGCTAT
ACTTTAATCGATAGCAAAGGATTTGGCGATGCTAGAGTTTGGCAACTTTTGCTTTATCCT
AATGATTTTGCAATGATTAATAAATGCCAAAACCAATACTTGTCTTAATGCTTATGGTAAT
GGAATTGTCCATTATCCTTGTGATGCAAGCAATCACGCACAAATGTGGAACTTATCCCT
ATGAGCAATACAGCGGTTCAAATTAATAAATTTAGGAAATGGAAAATGCATACAAGCACCT
ATTACAAATCTTTATGGTGATTTTCACAAGGTTTTTAAAAATTTTACCGTAGAGTGTGCA
AAAAAAGATAATTTTGATCAACAATGGTTTTTAACTACTCCGCCTTTTACCGCAAACCT
TTATATCGCCAAGGAGAGGTACGATGA
```

*cdtA*-F= 5' TGGAGAATTTGAAGATACTG 3'

*cdtA*-R= 5' TCTCCTTGGCGATATAAAG 3'

*cdtB* sequence:

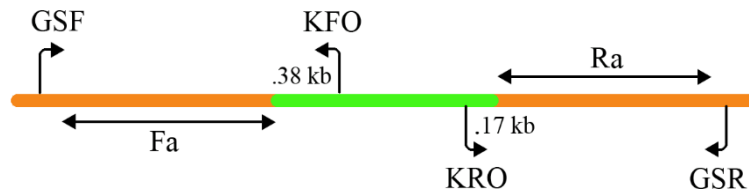
```
ATGAAAAAAAAATTATATGTTTATTTTTATCTTTTAACCTTGCTTTTGCAAATTTAGAAAAT
TTTAATGTTGGCACTTGGAATTTGCAAGGCTCATCCGCAGCCACAGAAAGCAAATGGAGT
GTTAGTGTAAGACAACCTTGTAAGTGGAGCAAACCCCTTAGATATCTTAATGATACAAGAA
GCAGGAACCTTACCAAGAACAGCCACTCCAACAGGACGCCATGTGCAACAAGGTGGAACA
CCTATTGATGAATATGAGTGGAAATTTAGGAACTCTTTCAAGGCCTGATAGGGTTTTTTATT
TATTATTCTCGCGTTGATGTAGGAGCTAATCGTGTAATTTAGCTATAGTTTCAAGAATG
CAAGCTGAAGAAGTGATTGTTTTACCTCCACCTACTACAGTTTCAAGACCCATTATAGGA
ATTCGCAATGGAAATGATGCTTTTTTCAATATCCATGCTTTAGCTAATGGAGGAACAGAT
GTAGGAGCAATTATCACAGCTGTAGATGCACATTTTGCAAATATGCCTCAAGTTAACTGG
ATGATAGCAGGGGATTTTAACCGTGATCCTTCTACTATAACAAGTACAGTGGATAGAGAA
TTAGCAAATAGAATTAGAGTGGTTTTTCCAACTAGCGCAACTCAAGCAAGCGGAGGGACT
CTTGATTATGCAATTACAGGAAATTCAAATAGACAACAAACCTATACTCCACCGCTTTTA
GCTGCGATTTTAATGCTTGCAAGTTTAAGATCTCATATAGTTTCAGATCATTTTCCAGTA
AATTTTAGAAAATTTTAG
```

*cdtB*-F= 5' TAATGTTGGCACTTGG 3'

*cdtB*-R= 5' AAGCGGTGGAGTATAGG 3'

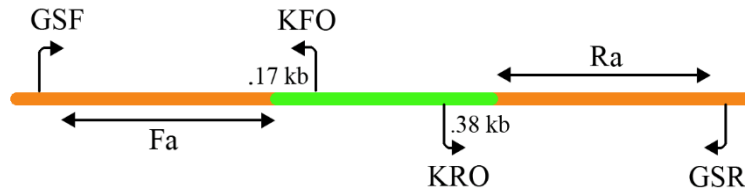
## Appendix 2- Different orientations of the Km<sup>R</sup> cassette

Correct orientation:






$$\text{GSF} + \text{KFO} = \text{Fa} + .38 \text{ kb}$$

Reverse orientation:



$$\text{GSF} + \text{KRO} = \text{Fa} + .17 \text{ kb}$$

$$\text{GSR} + \text{KFO} = \text{Ra} + .38 \text{ kb}$$

-  Oligonucleotide Primer
-  Gene Insert
-  Km<sup>R</sup> cassette

GSF = Gene Specific Forward

GSR = Gene Specific Reverse

KFO = Km<sup>R</sup> forward-out

KRO = Km<sup>R</sup> reverse-out

FA = Forward gene size

## References

- Alexander C, Rietschel ET (2001) Bacterial lipopolysaccharides and innate immunity. *Journal of endotoxin research* **7**: 167-202
- Amano A, Takeuchi H, Furuta N (2010) Outer membrane vesicles function as offensive weapons in host-parasite interactions. *Microbes and infection* **12**: 791-798
- Amaral JD, Xavier JM, Steer CJ, Rodrigues CM (2010) The role of p53 in apoptosis. *Discovery medicine* **9**: 145-152
- Andrews NW (2017) Detection of Lysosomal Exocytosis by Surface Exposure of Lamp1 Luminal Epitopes. In *Lysosomes: Methods and Protocols*, Öllinger K, Appelqvist H (eds), pp 205-211. New York, NY: Springer New York
- Ang CW, Jacobs BC, Laman JD (2004) The Guillain-Barre syndrome: a true case of molecular mimicry. *Trends in immunology* **25**: 61-66
- Arur S, Uche UE, Rezaul K, Fong M, Scranton V, Cowan AE, Mohler W, Han DK (2003) Annexin I is an endogenous ligand that mediates apoptotic cell engulfment. *Developmental cell* **4**: 587-598
- Ashe PC, Berry MD (2003) Apoptotic signaling cascades. *Progress in neuro-psychopharmacology & biological psychiatry* **27**: 199-214
- Avrain L, Vernozy-Rozand C, Kempf I (2004) Evidence for natural horizontal transfer of tetO gene between *Campylobacter jejuni* strains in chickens. *Journal of applied microbiology* **97**: 134-140
- Bacon DJ, Szymanski CM, Burr DH, Silver RP, Alm RA, Guerry P (2001) A phase-variable capsule is involved in virulence of *Campylobacter jejuni* 81-176. *Molecular microbiology* **40**: 769-777
- Bae JS, Yuki N, Kuwabara S, Kim JK, Vucic S, Lin CS, Kiernan MC (2014) Guillain–Barré syndrome in Asia. *Journal of Neurology, Neurosurgery & Psychiatry* **85**: 907-913
- Baichwal RR, Bigbee JW, DeVries GH (1988) Macrophage-mediated myelin-related mitogenic factor for cultured Schwann cells. *Proceedings of the National Academy of Sciences of the United States of America* **85**: 1701-1705
- Balsalobre C, Silvan JM, Berglund S, Mizunoe Y, Uhlin BE, Wai SN (2006) Release of the type I secreted alpha-haemolysin via outer membrane vesicles from *Escherichia coli*. *Molecular microbiology* **59**: 99-112
- Bergman MA, Cummings LA, Barrett SL, Smith KD, Lara JC, Aderem A, Cookson BT (2005) CD4+ T cells and toll-like receptors recognize *Salmonella* antigens expressed in bacterial surface organelles. *Infection and immunity* **73**: 1350-1356
- Bettigole SE, Glimcher LH (2015) Endoplasmic reticulum stress in immunity. *Annual review of immunology* **33**: 107-138

Bischof LJ, Kao CY, Los FC, Gonzalez MR, Shen Z, Briggs SP, van der Goot FG, Aroian RV (2008) Activation of the unfolded protein response is required for defenses against bacterial pore-forming toxin in vivo. *PLoS pathogens* **4**: e1000176

Blaser MJ (1997) Epidemiologic and clinical features of *Campylobacter jejuni* infections. *The Journal of infectious diseases* **176 Suppl 2**: S103-105

Blott EJ, Griffiths GM (2002) Secretory lysosomes. *Nature reviews Molecular cell biology* **3**: 122-131

Bolton F, Coates D, Hinchliffe P, Robertson L (1983) Comparison of selective media for isolation of *Campylobacter jejuni/coli*. *J Clin Pathol* **36**: 78-83

Bomberger JM, Maceachran DP, Coutermarsh BA, Ye S, O'Toole GA, Stanton BA (2009) Long-distance delivery of bacterial virulence factors by *Pseudomonas aeruginosa* outer membrane vesicles. *PLoS pathogens* **5**: e1000382

Bonnington KE, Kuehn MJ (2014) Protein selection and export via outer membrane vesicles. *Biochimica et biophysica acta* **1843**: 1612-1619

Boya P, Reggiori F, Codogno P (2013) Emerging regulation and functions of autophagy. *Nature cell biology* **15**: 713-720

Brando B, Barnett D, Janossy G, Mandy F, Autran B, Rothe G, Scarpati B, D'Avanzo G, D'Hautcourt JL, Lenkei R, Schmitz G, Kunkl A, Chianese R, Papa S, Gratama JW (2000) Cytofluorometric methods for assessing absolute numbers of cell subsets in blood. European Working Group on Clinical Cell Analysis. *Cytometry* **42**: 327-346

Bratton DL, Fadok VA, Richter DA, Kailey JM, Guthrie LA, Henson PM (1997) Appearance of phosphatidylserine on apoptotic cells requires calcium-mediated nonspecific flip-flop and is enhanced by loss of the aminophospholipid translocase. *The Journal of biological chemistry* **272**: 26159-26165

Butler RE, Brodin P, Jang J, Jang MS, Robertson BD, Gicquel B, Stewart GR (2012) The balance of apoptotic and necrotic cell death in *Mycobacterium tuberculosis* infected macrophages is not dependent on bacterial virulence. *PLoS one* **7**: e47573

Calfon M, Zeng H, Urano F, Till JH, Hubbard SR, Harding HP, Clark SG, Ron D (2002) IRE1 couples endoplasmic reticulum load to secretory capacity by processing the XBP-1 mRNA. *Nature* **415**: 92-96

Canonico B, Campana R, Luchetti F, Arcangeletti M, Betti M, Cesarini E, Ciacci C, Vittoria E, Galli L, Papa S, Baffone W (2014) *Campylobacter jejuni* cell lysates differently target mitochondria and lysosomes on HeLa cells. *Apoptosis : an international journal on programmed cell death* **19**: 1225-1242

Canonico B, Cesarini E, Salucci S, Luchetti F, Falcieri E, Di Sario G, Palma F, Papa S (2016) Defective Autophagy, Mitochondrial Clearance and Lipophagy in Niemann-Pick Type B Lymphocytes. *PLoS one* **11**: e0165780

Celli J, Tsolis RM (2015) Bacteria, the endoplasmic reticulum and the unfolded protein response: friends or foes? *Nature reviews Microbiology* **13**: 71-82

Champion OL, Gaunt MW, Gundogdu O, Elmi A, Witney AA, Hinds J, Dorrell N, Wren BW (2005) Comparative phylogenomics of the food-borne pathogen *Campylobacter jejuni* reveals genetic markers predictive of infection source. *Proceedings of the National Academy of Sciences of the United States of America* **102**: 16043-16048

Chattopadhyay MK, Jaganandham MV (2015) Vesicles-mediated resistance to antibiotics in bacteria. *Frontiers in microbiology* **6**: 758

Chazotte B (2011) Labeling lysosomes in live cells with LysoTracker. *Cold Spring Harbor protocols* **2011**: pdb.prot5571

Chipuk JE, Green DR (2005) Do inducers of apoptosis trigger caspase-independent cell death? *Nature reviews Molecular cell biology* **6**: 268-275

Cho JA, Lee AH, Platzer B, Cross BC, Gardner BM, De Luca H, Luong P, Harding HP, Glimcher LH, Walter P, Fiebigger E, Ron D, Kagan JC, Lencer WI (2013) The unfolded protein response element IRE1alpha senses bacterial proteins invading the ER to activate RIG-I and innate immune signaling. *Cell host & microbe* **13**: 558-569

Comrie WA, Li S, Boyle S, Burkhardt JK (2015) The dendritic cell cytoskeleton promotes T cell adhesion and activation by constraining ICAM-1 mobility. *The Journal of cell biology* **208**: 457-473

Conn PM (2011) The unfolded protein response and cellular stress, Part C. Preface. *Methods in enzymology* **491**: xix

Conner SD, Schmid SL (2003) Regulated portals of entry into the cell. *Nature* **422**: 37-44

Cossart P, Sansonetti PJ (2004) Bacterial invasion: the paradigms of enteroinvasive pathogens. *Science (New York, NY)* **304**: 242-248

Cuda CM, Pope RM, Perlman H (2016) The inflammatory role of phagocyte apoptotic pathways in rheumatic diseases. *Nature reviews Rheumatology* **12**: 543-558

Degterev A, Huang Z, Boyce M, Li Y, Jagtap P, Mizushima N, Cuny GD, Mitchison TJ, Moskowitz MA, Yuan J (2005) Chemical inhibitor of nonapoptotic cell death with therapeutic potential for ischemic brain injury. *Nature chemical biology* **1**: 112-119

Diaz G, Melis M, Batetta B, Angius F, Falchi AM (2008) Hydrophobic characterization of intracellular lipids in situ by Nile Red red/yellow emission ratio. *Micron (Oxford, England : 1993)* **39**: 819-824

DiRienzo JM (2014) Uptake and processing of the cytolethal distending toxin by mammalian cells. *Toxins* **6**: 3098-3116

Dixon SD, Huynh MM, Tamilselvam B, Spiegelman LM, Son SB, Eshraghi A, Blanke SR, Bradley KA (2015) Distinct Roles for CdtA and CdtC during Intoxication by Cytolethal Distending Toxins. *PLoS one* **10**: e0143977

Dlakic M (2001) Is CdtB a nuclease or a phosphatase? *Science (New York, NY)* **291**: 547

Dong H, Xiang Q, Gu Y, Wang Z, Paterson NG, Stansfeld PJ, He C, Zhang Y, Wang W, Dong C (2014) Structural basis for outer membrane lipopolysaccharide insertion. *Nature* **511**: 52-56

Ellis TN, Kuehn MJ (2010) Virulence and immunomodulatory roles of bacterial outer membrane vesicles. *Microbiology and molecular biology reviews* : *MMBR* **74**: 81-94

Elmi A, Nasher F, Jagatia H, Gundogdu O, Bajaj-Elliott M, Wren B, Dorrell N (2016) Campylobacter jejuni outer membrane vesicle-associated proteolytic activity promotes bacterial invasion by mediating cleavage of intestinal epithelial cell E-cadherin and occludin. *Cellular microbiology* **18**: 561-572

Elmi A, Watson E, Sandu P, Gundogdu O, Mills DC, Inglis NF, Manson E, Imrie L, Bajaj-Elliott M, Wren BW, Smith DG, Dorrell N (2012) Campylobacter jejuni outer membrane vesicles play an important role in bacterial interactions with human intestinal epithelial cells. *Infection and immunity* **80**: 4089-4098

Elwell CA, Dreyfus LA (2000) DNase I homologous residues in CdtB are critical for cytolethal distending toxin-mediated cell cycle arrest. *Molecular microbiology* **37**: 952-963

Eskelinen EL (2006) Roles of LAMP-1 and LAMP-2 in lysosome biogenesis and autophagy. *Molecular aspects of medicine* **27**: 495-502

Farre JC, Subramani S (2016) Mechanistic insights into selective autophagy pathways: lessons from yeast. *Nature reviews Molecular cell biology* **17**: 537-552

Fernandez-Moreira E, Helbig JH, Swanson MS (2006) Membrane vesicles shed by Legionella pneumophila inhibit fusion of phagosomes with lysosomes. *Infection and immunity* **74**: 3285-3295

Friedman CR, Hoekstra RM, Samuel M, Marcus R, Bender J, Shiferaw B, Reddy S, Ahuja SD, Helfrick DL, Hardnett F, Carter M, Anderson B, Tauxe RV (2004) Risk Factors for Sporadic Campylobacter Infection in the United States: A Case-Control Study in FoodNet Sites. *Clinical Infectious Diseases* **38**: S285-S296

Fu S, Yang L, Li P, Hofmann O, Dicker L, Hide W, Lin X, Watkins SM, Ivanov AR, Hotamisligil GS (2011) Aberrant lipid metabolism disrupts calcium homeostasis causing liver endoplasmic reticulum stress in obesity. *Nature* **473**: 528-531

Fuchs Y, Steller H (2015) Live to die another way: modes of programmed cell death and the signals emanating from dying cells. *Nature reviews Molecular cell biology* **16**: 329-344

Galdiero M, D'Isanto M, Vitiello M, Finamore E, Peluso L, Galdiero M (2001) Porins from Salmonella enterica serovar Typhimurium induce TNF-alpha, IL-6 and IL-8 release by CD14-independent and CD11a/CD18-dependent mechanisms. *Microbiology* **147**: 2697-2704

Galluzzi L, Kepp O, Krautwald S, Kroemer G, Linkermann A (2014) Molecular mechanisms of regulated necrosis. *Seminars in cell & developmental biology* **35**: 24-32

Gardner BM, Walter P (2011) Unfolded proteins are Ire1-activating ligands that directly induce the unfolded protein response. *Science (New York, NY)* **333**: 1891-1894

Gargi A, Tamilselvam B, Powers B, Prouty MG, Lincecum T, Eshraghi A, Maldonado-Arocho FJ, Wilson BA, Bradley KA, Blanke SR (2013) Cellular interactions of the cytolethal distending toxins from *Escherichia coli* and *Haemophilus ducreyi*. *The Journal of biological chemistry* **288**: 7492-7505

Ge Z, Schauer DB, Fox JG (2008) In vivo virulence properties of bacterial cytolethal-distending toxin. *Cellular microbiology* **10**: 1599-1607

Ghasemi M, Khodaei N, Salari S, Eliassi A, Saghiri R (2014) Gating behavior of endoplasmic reticulum potassium channels of rat hepatocytes in diabetes. *Iranian biomedical journal* **18**: 165-172

Gilbert M, Parker CT, Moran AP (2008) *Campylobacter jejuni* Lipooligosaccharides: Structures and Biosynthesis. In *Campylobacter*, Third Edition. American Society of Microbiology

Godschalk PCR, Heikema AP, Gilbert M, Komagamine T, Ang CW, Glerum J, Brochu D, Li J, Yuki N, Jacobs BC, van Belkum A, Endtz HP (2004) The crucial role of *Campylobacter jejuni* genes in anti-ganglioside antibody induction in Guillain-Barré syndrome. *The Journal of clinical investigation* **114**: 1659-1665

Goodfellow JA, Willison HJ (2016) Guillain-Barre syndrome: a century of progress. *Nature reviews Neurology* **12**: 723-731

Grant CC, Konkel ME, Cieplak W, Jr., Tompkins LS (1993) Role of flagella in adherence, internalization, and translocation of *Campylobacter jejuni* in nonpolarized and polarized epithelial cell cultures. *Infection and immunity* **61**: 1764-1771

Griffin JW, Li CY, Ho TW, Tian M, Gao CY, Xue P, Mishu B, Cornblath DR, Macko C, McKhann GM, Asbury AK (1996) Pathology of the motor-sensory axonal Guillain-Barre syndrome. *Annals of neurology* **39**: 17-28

Grunwald U, Fan X, Jack RS, Workalemahu G, Kallies A, Stelter F, Schutt C (1996) Monocytes can phagocytose Gram-negative bacteria by a CD14-dependent mechanism. *Journal of immunology (Baltimore, Md : 1950)* **157**: 4119-4125

Guerra L, Teter K, Lilley BN, Stenerlow B, Holmes RK, Ploegh HL, Sandvig K, Thelestam M, Frisan T (2005) Cellular internalization of cytolethal distending toxin: a new end to a known pathway. *Cellular microbiology* **7**: 921-934

Guerry P (2007) *Campylobacter* flagella: not just for motility. *Trends in microbiology* **15**: 456-461

Guerry P, Ewing CP, Schirm M, Lorenzo M, Kelly J, Pattarini D, Majam G, Thibault P, Logan S (2006) Changes in flagellin glycosylation affect *Campylobacter* autoagglutination and virulence. *Molecular microbiology* **60**: 299-311

Guerry P, Poly F, Riddle M, Maue AC, Chen YH, Monteiro MA (2012) *Campylobacter* polysaccharide capsules: virulence and vaccines. *Frontiers in cellular and infection microbiology* **2**: 7

Guerry P, Szymanski CM (2008) *Campylobacter* sugars sticking out. *Trends in microbiology* **16**: 428-435



Guerry P, Szymanski CM, Prendergast MM, Hickey TE, Ewing CP, Pattarini DL, Moran AP (2002) Phase variation of *Campylobacter jejuni* 81-176 lipooligosaccharide affects ganglioside mimicry and invasiveness in vitro. *Infection and immunity* **70**: 787-793

Gundogdu O, Bentley SD, Holden MT, Parkhill J, Dorrell N, Wren BW (2007) Re-annotation and re-analysis of the *Campylobacter jejuni* NCTC11168 genome sequence. *BMC Genomics* **8**: 162

Gutierrez MG, Master SS, Singh SB, Taylor GA, Colombo MI, Deretic V (2004) Autophagy is a defense mechanism inhibiting BCG and *Mycobacterium tuberculosis* survival in infected macrophages. *Cell* **119**: 753-766

Hafner Česen M, Pegan K, Špes A, Turk B (2012) Lysosomal pathways to cell death and their therapeutic applications. *Experimental Cell Research* **318**: 1245-1251

Haghjoo E, Galan JE (2004) *Salmonella typhi* encodes a functional cytolethal distending toxin that is delivered into host cells by a bacterial-internalization pathway. *Proceedings of the National Academy of Sciences of the United States of America* **101**: 4614-4619

Hamasaki M, Yoshimori T (2010) Where do they come from? Insights into autophagosome formation. *FEBS letters* **584**: 1296-1301

Han J, Kaufman RJ (2016) The role of ER stress in lipid metabolism and lipotoxicity. *Journal of lipid research* **57**: 1329-1338

Harding HP, Zhang Y, Bertolotti A, Zeng H, Ron D (2000) Perk is essential for translational regulation and cell survival during the unfolded protein response. *Molecular cell* **5**: 897-904

Harding HP, Zhang Y, Ron D (1999) Protein translation and folding are coupled by an endoplasmic-reticulum-resident kinase. *Nature* **397**: 271-274

Hartung HP, Toyka KV (1990) T-cell and macrophage activation in experimental autoimmune neuritis and Guillain-Barre syndrome. *Annals of neurology* **27 Suppl**: S57-63

Haupt Y, Rowan S, Oren M (1995) p53-mediated apoptosis in HeLa cells can be overcome by excess pRB. *Oncogene* **10**: 1563-1571

Havelaar AH, van Pelt W, Ang CW, Wagenaar JA, van Putten JPM, Gross U, Newell DG (2009) Immunity to *Campylobacter*: its role in risk assessment and epidemiology. *Critical reviews in microbiology* **35**: 1-22

Heinzelmann M, Bosshart H (2005) Heparin binds to lipopolysaccharide (LPS)-binding protein, facilitates the transfer of LPS to CD14, and enhances LPS-induced activation of peripheral blood monocytes. *Journal of immunology (Baltimore, Md : 1950)* **174**: 2280-2287

Helms JB, Zurzolo C (2004) Lipids as targeting signals: lipid rafts and intracellular trafficking. *Traffic (Copenhagen, Denmark)* **5**: 247-254

Hendrixson DR, DiRita VJ (2004) Identification of *Campylobacter jejuni* genes involved in commensal colonization of the chick gastrointestinal tract. *Molecular microbiology* **52**: 471-484

Hickey TE, Majam G, Guerry P (2005) Intracellular survival of *Campylobacter jejuni* in human monocytic cells and induction of apoptotic death by cytolethal distending toxin. *Infection and immunity* **73**: 5194-5197

Hofmann K, Tomiuk S, Wolff G, Stoffel W (2000) Cloning and characterization of the mammalian brain-specific, Mg<sup>2+</sup>-dependent neutral sphingomyelinase. *Proceedings of the National Academy of Sciences of the United States of America* **97**: 5895-5900

Hofreuter D (2014) Defining the metabolic requirements for the growth and colonization capacity of *Campylobacter jejuni*. *Frontiers in cellular and infection microbiology* **4**

Hogg RC, Adams DJ (2001) An ATP-sensitive K(+) conductance in dissociated neurones from adult rat intracardiac ganglia. *The Journal of physiology* **534**: 713-720

Horvitz HR (1999) Genetic control of programmed cell death in the nematode *Caenorhabditis elegans*. *Cancer research* **59**: 1701s-1706s

Hu L, Tall BD, Curtis SK, Kopecko DJ (2008) Enhanced microscopic definition of *Campylobacter jejuni* 81-176 adherence to, invasion of, translocation across, and exocytosis from polarized human intestinal Caco-2 cells. *Infection and immunity* **76**: 5294-5304

Huang J, Brumell JH (2009) Autophagy in immunity against intracellular bacteria. *Current topics in microbiology and immunology* **335**: 189-215

Hubbard AK, Rothlein R (2000) Intercellular adhesion molecule-1 (ICAM-1) expression and cell signaling cascades. *Free radical biology & medicine* **28**: 1379-1386

Hughes RA, Swan AV, van Doorn PA (2014) Intravenous immunoglobulin for Guillain-Barre syndrome. *The Cochrane database of systematic reviews*: Cd002063

Huotari J, Helenius A (2011) Endosome maturation. *The EMBO journal* **30**: 3481-3500

Hüttemann M, Helling S, Sanderson TH, Sinkler C, Samavati L, Mahapatra G, Varughese A, Lu G, Liu J, Ramzan R, Vogt S, Grossman LI, Doan JW, Marcus K, Lee I (2012) Regulation of mitochondrial respiration and apoptosis through cell signaling: Cytochrome c oxidase and cytochrome c in ischemia/reperfusion injury and inflammation. *Biochimica et Biophysica Acta (BBA) - Bioenergetics* **1817**: 598-609

Inoki K, Li Y, Zhu T, Wu J, Guan KL (2002) TSC2 is phosphorylated and inhibited by Akt and suppresses mTOR signalling. *Nature cell biology* **4**: 648-657

Ismail S, Hampton MB, Keenan JI (2003) *Helicobacter pylori* outer membrane vesicles modulate proliferation and interleukin-8 production by gastric epithelial cells. *Infection and immunity* **71**: 5670-5675

Ivanov AI, Nusrat A, Parkos CA (2004) Endocytosis of epithelial apical junctional proteins by a clathrin-mediated pathway into a unique storage compartment. *Molecular biology of the cell* **15**: 176-188

Jervis AJ, Butler JA, Wren BW, Linton D (2015) Chromosomal integration vectors allowing flexible expression of foreign genes in *Campylobacter jejuni*. *BMC microbiology* **15**

Jones MA, Marston KL, Woodall CA, Maskell DJ, Linton D, Karlyshev AV, Dorrell N, Wren BW, Barrow PA (2004) Adaptation of *Campylobacter jejuni* NCTC11168 to high-level colonization of the avian gastrointestinal tract. *Infect Immun* **72**: 3769-3776

Jones MA, Totemeyer S, Maskell DJ, Bryant CE, Barrow PA (2003) Induction of proinflammatory responses in the human monocytic cell line THP-1 by *Campylobacter jejuni*. *Infection and immunity* **71**: 2626-2633

Kaakoush NO, Castano-Rodriguez N, Mitchell HM, Man SM (2015) Global Epidemiology of *Campylobacter* Infection. **28**: 687-720

Kakuda T, DiRita VJ (2006) Cj1496c encodes a *Campylobacter jejuni* glycoprotein that influences invasion of human epithelial cells and colonization of the chick gastrointestinal tract. *Infection and immunity* **74**: 4715-4723

Kaparakis-Liaskos M, Ferrero RL (2015) Immune modulation by bacterial outer membrane vesicles. *Nature reviews Immunology* **15**: 375-387

Kaparakis M, Turnbull L, Carneiro L, Firth S, Coleman HA, Parkington HC, Le Bourhis L, Karrar A, Viala J, Mak J, Hutton ML, Davies JK, Crack PJ, Hertzog PJ, Philpott DJ, Girardin SE, Whitchurch CB, Ferrero RL (2010) Bacterial membrane vesicles deliver peptidoglycan to NOD1 in epithelial cells. *Cellular microbiology* **12**: 372-385

Kapperud G, Skjerve E, Bean NH, Ostroff SM, Lassen J (1992) Risk factors for sporadic *Campylobacter* infections: results of a case-control study in southeastern Norway. *Journal of clinical microbiology* **30**: 3117-3121

Karlyshev AV, Everest P, Linton D, Cawthraw S, Newell DG, Wren BW (2004) The *Campylobacter jejuni* general glycosylation system is important for attachment to human epithelial cells and in the colonization of chicks. *Microbiology* **150**: 1957-1964

Karlyshev AV, Henderson J, Ketley JM, Wren BW (1999) Procedure for the investigation of bacterial genomes: random shot-gun cloning, sample sequencing and mutagenesis of *Campylobacter jejuni*. *BioTechniques* **26**: 50-52, 54, 56

Karlyshev AV, Ketley JM, Wren BW (2005) The *Campylobacter jejuni* glycome. *FEMS microbiology reviews* **29**: 377-390

Karlyshev AV, Linton D, Gregson NA, Wren BW (2002) A novel paralogous gene family involved in phase-variable flagella-mediated motility in *Campylobacter jejuni*. *Microbiology* **148**: 473-480

Kaser A, Lee AH, Franke A, Glickman JN, Zeissig S, Tilg H, Nieuwenhuis EE, Higgins DE, Schreiber S, Glimcher LH, Blumberg RS (2008) XBP1 links ER stress to intestinal inflammation and confers genetic risk for human inflammatory bowel disease. *Cell* **134**: 743-756

Kesty NC, Mason KM, Reedy M, Miller SE, Kuehn MJ (2004) Enterotoxigenic *Escherichia coli* vesicles target toxin delivery into mammalian cells. *The EMBO journal* **23**: 4538-4549

Ketley JM (1997) Pathogenesis of enteric infection by *Campylobacter*. *Microbiology* **143** ( Pt 1): 5-21

- Kharwar NK, Prasad KN, Singh K, Paliwal VK, Modi DR (2017) Polymorphisms of IL-17 and ICAM-1 and their expression in Guillain-Barre syndrome. *The International journal of neuroscience* **127**: 680-687
- Kiehlbauch JA, Albach RA, Baum LL, Chang KP (1985) Phagocytosis of *Campylobacter jejuni* and its intracellular survival in mononuclear phagocytes. *Infection and immunity* **48**: 446-451
- Kim JH, Yoon YJ, Lee J, Choi E-J, Yi N, Park K-S, Park J, Lötvall J, Kim Y-K, Gho YS (2013) Outer Membrane Vesicles Derived from *Escherichia coli* Up-Regulate Expression of Endothelial Cell Adhesion Molecules In Vitro and In Vivo. *PLoS one* **8**: e59276
- Knauer R, Lehle L (1999) The oligosaccharyltransferase complex from yeast. *Biochimica et biophysica acta* **1426**: 259-273
- Konkel ME, Klena JD, Rivera-Amill V, Monteville MR, Biswas D, Raphael B, Mickelson J (2004) Secretion of virulence proteins from *Campylobacter jejuni* is dependent on a functional flagellar export apparatus. *Journal of bacteriology* **186**: 3296-3303
- Kouokam JC, Wai SN, Fallman M, Dobrindt U, Hacker J, Uhlin BE (2006) Active cytotoxic necrotizing factor 1 associated with outer membrane vesicles from uropathogenic *Escherichia coli*. *Infection and immunity* **74**: 2022-2030
- Kulp A, Kuehn MJ (2010) Biological functions and biogenesis of secreted bacterial outer membrane vesicles. *Annual review of microbiology* **64**: 163-184
- Kurosaka K, Takahashi M, Watanabe N, Kobayashi Y (2003) Silent cleanup of very early apoptotic cells by macrophages. *Journal of immunology (Baltimore, Md : 1950)* **171**: 4672-4679
- Kuwabara S, Yuki N (2013) Axonal Guillain-Barré syndrome: concepts and controversies. *The Lancet Neurology* **12**: 1180-1188
- Landmann R, Knopf HP, Link S, Sansano S, Schumann R, Zimmerli W (1996) Human monocyte CD14 is upregulated by lipopolysaccharide. *Infection and immunity* **64**: 1762-1769
- Lara-Tejero M, Galan JE (2000) A bacterial toxin that controls cell cycle progression as a deoxyribonuclease I-like protein. *Science (New York, NY)* **290**: 354-357
- Lara-Tejero M, Galan JE (2001) CdtA, CdtB, and CdtC form a tripartite complex that is required for cytolethal distending toxin activity. *Infection and immunity* **69**: 4358-4365
- Larsen JC, Szymanski C, Guerry P (2004) N-linked protein glycosylation is required for full competence in *Campylobacter jejuni* 81-176. *Journal of bacteriology* **186**: 6508-6514
- Lee AH, Iwakoshi NN, Glimcher LH (2003) XBP-1 regulates a subset of endoplasmic reticulum resident chaperone genes in the unfolded protein response. *Molecular and cellular biology* **23**: 7448-7459
- Ley K, Laudanna C, Cybulsky MI, Nourshargh S (2007) Getting to the site of inflammation: the leukocyte adhesion cascade updated. *Nature reviews Immunology* **7**: 678-689

Li H, Mao G, Carlson J, Leng SX (2015a) A novel flow cytometry-based tool for determining the efficiency of human cytomegalovirus infection in THP-1 derived macrophages. *Journal of virological methods* **221**: 127-130

Li Y, Ge M, Ciani L, Kuriakose G, Westover EJ, Dura M, Covey DF, Freed JH, Maxfield FR, Lytton J, Tabas I (2004) Enrichment of endoplasmic reticulum with cholesterol inhibits sarcoplasmic-endoplasmic reticulum calcium ATPase-2b activity in parallel with increased order of membrane lipids: implications for depletion of endoplasmic reticulum calcium stores and apoptosis in cholesterol-loaded macrophages. *The Journal of biological chemistry* **279**: 37030-37039

Li ZT, Zhang RL, Bi XG, Xu L, Fan M, Xie D, Xian Y, Wang Y, Li XJ, Wu ZD, Zhang KX (2015b) Outer membrane vesicles isolated from two clinical *Acinetobacter baumannii* strains exhibit different toxicity and proteome characteristics. *Microbial pathogenesis* **81**: 46-52

Lin JH, Li H, Yasumura D, Cohen HR, Zhang C, Panning B, Shokat KM, Lavail MM, Walter P (2007) IRE1 signaling affects cell fate during the unfolded protein response. *Science (New York, NY)* **318**: 944-949

Lindmark B, Rompikuntal PK, Vaitkevicius K, Song T, Mizunoe Y, Uhlin BE, Guerry P, Wai SN (2009) Outer membrane vesicle-mediated release of cytolethal distending toxin (CDT) from *Campylobacter jejuni*. *BMC microbiology* **9**: 220

Llobet E, Tomas JM, Bengoechea JA (2008) Capsule polysaccharide is a bacterial decoy for antimicrobial peptides. *Microbiology* **154**: 3877-3886

Luchetti F, Canonico B, Arcangeletti M, Guescini M, Cesarini E, Stocchi V, Degli Esposti M, Papa S (2012) Fas signalling promotes intercellular communication in T cells. *PLoS one* **7**: e35766

Luchetti F, Crinelli R, Cesarini E, Canonico B, Guidi L, Zerbinati C, Di Sario G, Zamai L, Magnani M, Papa S, Iuliano L (2017) Endothelial cells, endoplasmic reticulum stress and oxysterols. *Redox biology* **13**: 581-587

Lum JJ, Bauer DE, Kong M, Harris MH, Li C, Lindsten T, Thompson CB (2005) Growth factor regulation of autophagy and cell survival in the absence of apoptosis. *Cell* **120**: 237-248

Ma Y, Brewer JW, Diehl JA, Hendershot LM (2002) Two distinct stress signaling pathways converge upon the CHOP promoter during the mammalian unfolded protein response. *Journal of molecular biology* **318**: 1351-1365

Magira EE, Papaioakim M, Nachamkin I, Asbury AK, Li CY, Ho TW, Griffin JW, McKhann GM, Monos DS (2003) Differential Distribution of HLA-DQ $\beta$ /DR $\beta$  Epitopes in the Two Forms of Guillain-Barré Syndrome, Acute Motor Axonal Neuropathy and Acute Inflammatory Demyelinating Polyneuropathy (AIDP): Identification of DQ $\beta$  Epitopes Associated with Susceptibility to and Protection from AIDP. *The Journal of Immunology* **170**: 3074-3080

Maiuri MC, Zalckvar E, Kimchi A, Kroemer G (2007) Self-eating and self-killing: crosstalk between autophagy and apoptosis. *Nature reviews Molecular cell biology* **8**: 741-752

Marino G, Niso-Santano M, Baehrecke EH, Kroemer G (2014) Self-consumption: the interplay of autophagy and apoptosis. *Nature reviews Molecular cell biology* **15**: 81-94

Mashburn-Warren L, McLean RJ, Whiteley M (2008) Gram-negative outer membrane vesicles: beyond the cell surface. *Geobiology* **6**: 214-219

Mashburn LM, Whiteley M (2005) Membrane vesicles traffic signals and facilitate group activities in a prokaryote. *Nature* **437**: 422-425

McNeil PL (2002) Repairing a torn cell surface: make way, lysosomes to the rescue. *Journal of cell science* **115**: 873-879

Medina-Kauwe LK (2007) "Alternative" endocytic mechanisms exploited by pathogens: new avenues for therapeutic delivery? *Advanced drug delivery reviews* **59**: 798-809

Menck K, Behme D, Pantke M, Reiling N, Binder C, Pukrop T, Klemm F (2014) Isolation of human monocytes by double gradient centrifugation and their differentiation to macrophages in teflon-coated cell culture bags. *Journal of visualized experiments : JoVE*: e51554

Menendez D, Inga A, Resnick MA (2009) The expanding universe of p53 targets. *Nature reviews Cancer* **9**: 724-737

Mevorach D, Karbian N, Tabib A. (2016) The Natural History of Homozygous Cys89Tyr CD59 Deficiency in Infancy: Differences and Similarities to PNH. *Am Soc Hematology*.

Michel V, Bakovic M (2007) Lipid rafts in health and disease. *Biology of the cell* **99**: 129-140

Mishu B, Blaser MJ (1993) Role of infection due to *Campylobacter jejuni* in the initiation of Guillain-Barre syndrome. *Clinical infectious diseases : an official publication of the Infectious Diseases Society of America* **17**: 104-108

Mizushima N, Komatsu M (2011) Autophagy: renovation of cells and tissues. *Cell* **147**: 728-741

Mondal A, Tapader R, Chatterjee NS, Ghosh A, Sinha R, Koley H, Saha DR, Chakrabarti MK, Wai SN, Pal A (2016) Cytotoxic and Inflammatory Responses Induced by Outer Membrane Vesicle-Associated Biologically Active Proteases from *Vibrio cholerae*. *Infection and immunity* **84**: 1478-1490

Morgan BP, Boyd C, Bubeck D (2017) Molecular cell biology of complement membrane attack. *Seminars in cell & developmental biology*

Morooka T, Umeda A, Amako K (1985) Motility as an intestinal colonization factor for *Campylobacter jejuni*. *Journal of general microbiology* **131**: 1973-1980

Munafo DB, Colombo MI (2001) A novel assay to study autophagy: regulation of autophagosome vacuole size by amino acid deprivation. *Journal of cell science* **114**: 3619-3629

Nalca A, Rangnekar VM (1998) The G1-phase growth-arresting action of interleukin-1 is independent of p53 and p21/WAF1 function. *The Journal of biological chemistry* **273**: 30517-30523

- Neimann J, Engberg J, Molbak K, Wegener HC (2003) A case-control study of risk factors for sporadic campylobacter infections in Denmark. *Epidemiology and infection* **130**: 353-366
- Neu C, Sedlag A, Bayer C, Förster S, Crauwels P, Niess JH, van Zandbergen G, Frascaroli G, Riedel CU (2013) CD14-Dependent Monocyte Isolation Enhances Phagocytosis of *Listeria monocytogenes* by Proinflammatory, GM-CSF-Derived Macrophages. *PloS one* **8**
- Norbury CJ, Hickson ID (2001) Cellular responses to DNA damage. *Annual review of pharmacology and toxicology* **41**: 367-401
- Nuijten PJ, van Asten FJ, Gaastra W, van der Zeijst BA (1990) Structural and functional analysis of two *Campylobacter jejuni* flagellin genes. *The Journal of biological chemistry* **265**: 17798-17804
- O'Donoghue EJ, Krachler AM (2016) Mechanisms of outer membrane vesicle entry into host cells. *Cellular microbiology* **18**: 1508-1517
- Ogata M, Hino S, Saito A, Morikawa K, Kondo S, Kanemoto S, Murakami T, Taniguchi M, Tanii I, Yoshinaga K, Shiosaka S, Hammarback JA, Urano F, Imaizumi K (2006) Autophagy is activated for cell survival after endoplasmic reticulum stress. *Molecular and cellular biology* **26**: 9220-9231
- Ogawara K, Kuwabara S, Mori M, Hattori T, Koga M, Yuki N (2000) Axonal Guillain-Barre syndrome: relation to anti-ganglioside antibodies and *Campylobacter jejuni* infection in Japan. *Annals of neurology* **48**: 624-631
- Park SH, Blackstone C (2010) Further assembly required: construction and dynamics of the endoplasmic reticulum network. *EMBO reports* **11**: 515-521
- Parkhill J, Wren BW, Mungall K, Ketley JM, Churcher C, Basham D, Chillingworth T, Davies RM, Feltwell T, Holroyd S, Jagels K, Karlyshev AV, Moule S, Pallen MJ, Penn CW, Quail MA, Rajandream MA, Rutherford KM, van Vliet AH, Whitehead S, Barrell BG (2000) The genome sequence of the food-borne pathogen *Campylobacter jejuni* reveals hypervariable sequences. *Nature* **403**: 665-668
- Patel B, Cuervo AM (2015) Methods to study chaperone-mediated autophagy. *Methods (San Diego, Calif)* **75**: 133-140
- Pathirana RD, Kaparakis-Liaskos M (2016) Bacterial membrane vesicles: Biogenesis, immune regulation and pathogenesis. *Cellular microbiology* **18**: 1518-1524
- Pattingre S, Tassa A, Qu X, Garuti R, Liang XH, Mizushima N, Packer M, Schneider MD, Levine B (2005) Bcl-2 antiapoptotic proteins inhibit Beclin 1-dependent autophagy. *Cell* **122**: 927-939
- Promlek T, Ishiwata-Kimata Y, Shido M, Sakuramoto M, Kohno K, Kimata Y (2011) Membrane aberrancy and unfolded proteins activate the endoplasmic reticulum stress sensor Ire1 in different ways. *Molecular biology of the cell* **22**: 3520-3532
- Qu X, Zou Z, Sun Q, Luby-Phelps K, Cheng P, Hogan RN, Gilpin C, Levine B (2007) Autophagy gene-dependent clearance of apoptotic cells during embryonic development. *Cell* **128**: 931-946

- Rao MR, Naficy AB, Savarino SJ, Abu-Elyazeed R, Wierzba TF, Peruski LF, Abdel-Messih I, Frenck R, Clemens JD (2001) Pathogenicity and Convalescent Excretion of Campylobacter in Rural Egyptian Children. *American Journal of Epidemiology* **154**: 166-173
- Rao RV, Ellerby HM, Bredesen DE (2004) Coupling endoplasmic reticulum stress to the cell death program. *Cell death and differentiation* **11**: 372-380
- Raudsepp P, Brüggemann DA, Andersen ML (2014) Detection of radicals in single droplets of oil-in-water emulsions with the lipophilic fluorescent probe BODIPY665/676 and confocal laser scanning microscopy. *Free Radical Biology and Medicine* **70**: 233-240
- Reed JC (2002) Apoptosis-based therapies. *Nature reviews Drug discovery* **1**: 111-121
- Rees JH, Soudain SE, Gregson NA, Hughes RA (1995) Campylobacter jejuni infection and Guillain-Barre syndrome. *The New England journal of medicine* **333**: 1374-1379
- Repnik U, Cesen MH, Turk B (2013) The endolysosomal system in cell death and survival. *Cold Spring Harbor perspectives in biology* **5**: a008755
- Rhodes KM, Tattersfield AE (1982) Guillain-Barre syndrome associated with Campylobacter infection. *British medical journal (Clinical research ed)* **285**: 173-174
- Rodriguez J, Lazebnik Y (1999) Caspase-9 and APAF-1 form an active holoenzyme. *Genes & development* **13**: 3179-3184
- Roy D, Liston DR, Idone VJ, Di A, Nelson DJ, Pujol C, Bliska JB, Chakrabarti S, Andrews NW (2004) A process for controlling intracellular bacterial infections induced by membrane injury. *Science (New York, NY)* **304**: 1515-1518
- Rutkowski DT, Kaufman RJ (2004) A trip to the ER: coping with stress. *Trends in cell biology* **14**: 20-28
- Salucci S, Burattini S, Baldassarri V, Battistelli M, Canonico B, Valmori A, Papa S, Falcieri E (2013) The peculiar apoptotic behavior of skeletal muscle cells. *Histology and histopathology* **28**: 1073-1087
- Sampaziotis F, Kokotas S, Gorgoulis VG (2002) P53 possibly upregulates the expression of CD58 (LFA-3) and CD59 (MIRL). *Medical hypotheses* **58**: 136-140
- Savill J, Fadok V (2000) Corpse clearance defines the meaning of cell death. *Nature* **407**: 784-788
- Schendel SL, Montal M, Reed JC (1998) Bcl-2 family proteins as ion-channels. *Cell death and differentiation* **5**: 372-380
- Schmitt CA, Fridman JS, Yang M, Baranov E, Hoffman RM, Lowe SW (2002) Dissecting p53 tumor suppressor functions in vivo. *Cancer cell* **1**: 289-298
- Schroder M, Kaufman RJ (2005) ER stress and the unfolded protein response. *Mutation research* **569**: 29-63



- Schwartz AL, Brandt RA, Geuze H, Ciechanover A (1992) Stress-induced alterations in autophagic pathway: relationship to ubiquitin system. *The American journal of physiology* **262**: C1031-1038
- Scorrano L, Oakes SA, Opferman JT, Cheng EH, Sorcinelli MD, Pozzan T, Korsmeyer SJ (2003) BAX and BAK regulation of endoplasmic reticulum Ca<sup>2+</sup>: a control point for apoptosis. *Science (New York, NY)* **300**: 135-139
- Sehgal SN (2003) Sirolimus: its discovery, biological properties, and mechanism of action. *Transplantation proceedings* **35**: 7s-14s
- Shenker BJ, Hoffmaster RH, Zekavat A, Yamaguchi N, Lally ET, Demuth DR (2001) Induction of apoptosis in human T cells by *Actinobacillus actinomycetemcomitans* cytolethal distending toxin is a consequence of G2 arrest of the cell cycle. *Journal of immunology (Baltimore, Md : 1950)* **167**: 435-441
- Shimizu S, Kanaseki T, Mizushima N, Mizuta T, Arakawa-Kobayashi S, Thompson CB, Tsujimoto Y (2004) Role of Bcl-2 family proteins in a non-apoptotic programmed cell death dependent on autophagy genes. *Nature cell biology* **6**: 1221-1228
- Siegl C, Rudel T (2015) Modulation of p53 during bacterial infections. *Nat Rev Micro* **13**: 741-748
- Simons K, Toomre D (2000) Lipid rafts and signal transduction. *Nature reviews Molecular cell biology* **1**: 31-39
- Sinha S, Prasad KN, Pradhan S, Jain D, Jha S (2004) Detection of preceding *Campylobacter jejuni* infection by polymerase chain reaction in patients with Guillain-Barre syndrome. *Transactions of the Royal Society of Tropical Medicine and Hygiene* **98**: 342-346
- Smith JL, Bayles DO (2006) The contribution of cytolethal distending toxin to bacterial pathogenesis. *Critical reviews in microbiology* **32**: 227-248
- Smith PK, Krohn RI, Hermanson GT, Mallia AK, Gartner FH, Provenzano MD, Fujimoto EK, Goeke NM, Olson BJ, Klenk DC (1985) Measurement of protein using bicinchoninic acid. *Analytical biochemistry* **150**: 76-85
- Song S, Tan J, Miao Y, Li M, Zhang Q (2017) Crosstalk of autophagy and apoptosis: Involvement of the dual role of autophagy under ER stress. **232**: 2977-2984
- Springer TA (1994) Traffic signals for lymphocyte recirculation and leukocyte emigration: the multistep paradigm. *Cell* **76**: 301-314
- Sriburi R, Bommasamy H, Buldak GL, Robbins GR, Frank M, Jackowski S, Brewer JW (2007) Coordinate regulation of phospholipid biosynthesis and secretory pathway gene expression in XBP-1(S)-induced endoplasmic reticulum biogenesis. *The Journal of biological chemistry* **282**: 7024-7034
- Sriburi R, Jackowski S, Mori K, Brewer JW (2004) XBP1. *a link between the unfolded protein response, lipid biosynthesis, and biogenesis of the endoplasmic reticulum* **167**: 35-41
- Strober W (2001) Trypan blue exclusion test of cell viability. *Current protocols in immunology / edited by John E Coligan [et al]* **Appendix 3**: Appendix 3B

Sun L, Wang X (2014) A new kind of cell suicide: mechanisms and functions of programmed necrosis. *Trends in biochemical sciences* **39**: 587-593

Sun X, Threadgill D, Jobin C (2012) *Campylobacter jejuni* Induces Colitis Through Activation of Mammalian Target of Rapamycin Signaling. *Gastroenterology* **142**: 86-95.e85

Svensson LA, Tarkowski A, Thelestam M, Lagergard T (2001) The impact of *Haemophilus ducreyi* cytolethal distending toxin on cells involved in immune response. *Microbial pathogenesis* **30**: 157-166

Szymanski CM, Burr DH, Guerry P (2002) *Campylobacter* protein glycosylation affects host cell interactions. *Infection and immunity* **70**: 2242-2244

Szymanski CM, Yao R, Ewing CP, Trust TJ, Guerry P (1999) Evidence for a system of general protein glycosylation in *Campylobacter jejuni*. *Molecular microbiology* **32**: 1022-1030

Tamai R, Asai Y, Ogawa T (2005) Requirement for intercellular adhesion molecule 1 and caveolae in invasion of human oral epithelial cells by *Porphyromonas gingivalis*. *Infection and immunity* **73**: 6290-6298

Thibault P, Logan SM, Kelly JF, Brisson JR, Ewing CP, Trust TJ, Guerry P (2001) Identification of the carbohydrate moieties and glycosylation motifs in *Campylobacter jejuni* flagellin. *The Journal of biological chemistry* **276**: 34862-34870

Thomas S, Preda-Pais A, Casares S, Brumeanu TD (2004) Analysis of lipid rafts in T cells. *Molecular immunology* **41**: 399-409

Treacy-Abarca S, Mukherjee S (2015) *Legionella* suppresses the host unfolded protein response via multiple mechanisms. *Nature communications* **6**: 7887

Trieu-Cuot P, Gerbaud G, Lambert T, Courvalin P (1985) In vivo transfer of genetic information between gram-positive and gram-negative bacteria. *The EMBO journal* **4**: 3583-3587

van den Berg B, Walgaard C, Drenthen J, Fokke C, Jacobs BC, van Doorn PA (2014) Guillain-Barre syndrome: pathogenesis, diagnosis, treatment and prognosis. *Nature reviews Neurology* **10**: 469-482

van Doorn PA, Kuitwaard K, Walgaard C, van Koningsveld R, Ruts L, Jacobs BC (2010) IVIG treatment and prognosis in Guillain-Barre syndrome. *Journal of clinical immunology* **30 Suppl 1**: S74-78

van Doorn PA, Ruts L, Jacobs BC (2008) Clinical features, pathogenesis, and treatment of Guillain-Barre syndrome. *The Lancet Neurology* **7**: 939-950

Van Rhijn I, Bleumink-Pluym NM, Van Putten JP, Van den Berg LH (2002) *Campylobacter* DNA is present in circulating myelomonocytic cells of healthy persons and in persons with Guillain-Barre syndrome. *The Journal of infectious diseases* **185**: 262-265

van Schadewijk A, van't Wout EF, Stolk J, Hiemstra PS (2012) A quantitative method for detection of spliced X-box binding protein-1 (XBP1) mRNA as a measure of endoplasmic reticulum (ER) stress. *Cell stress & chaperones* **17**: 275-279

van Sluijters DA, Dubbelhuis PF, Blommaart EF, Meijer AJ (2000) Amino-acid-dependent signal transduction. *The Biochemical journal* **351 Pt 3**: 545-550

van Vliet AH, Wooldridge KG, Ketley JM (1998) Iron-responsive gene regulation in a campylobacter jejuni fur mutant. *Journal of bacteriology* **180**: 5291-5298

Vandamme P, Dewhirst FE, Paster BJ, On SLW (2015) Campylobacter. In *Bergey's Manual of Systematics of Archaea and Bacteria*. John Wiley & Sons, Ltd

Vanden Berghe T, Linkermann A, Jouan-Lanhouet S, Walczak H, Vandenabeele P (2014) Regulated necrosis: the expanding network of non-apoptotic cell death pathways. *Nature reviews Molecular cell biology* **15**: 135-147

Vattem KM, Wek RC (2004) Reinitiation involving upstream ORFs regulates ATF4 mRNA translation in mammalian cells. *Proceedings of the National Academy of Sciences of the United States of America* **101**: 11269-11274

Vazquez CL, Colombo MI (2009) Assays to assess autophagy induction and fusion of autophagic vacuoles with a degradative compartment, using monodansylcadaverine (MDC) and DQ-BSA. *Methods in enzymology* **452**: 85-95

Verbeke P, Welter-Stahl L, Ying S, Hansen J, Häcker G, Darville T, Ojcius DM (2006) Recruitment of BAD by the <named-content xmlns:xlink="http://www.w3.org/1999/xlink" content-type="genus-species" xlink:type="simple">Chlamydia trachomatis</named-content> Vacuole Correlates with Host-Cell Survival. *PLoS pathogens* **2**: e45

Volmer R, van der Ploeg K, Ron D (2013) Membrane lipid saturation activates endoplasmic reticulum unfolded protein response transducers through their transmembrane domains. *Proceedings of the National Academy of Sciences of the United States of America* **110**: 4628-4633

Vousden KH, Lane DP (2007) p53 in health and disease. *Nature reviews Molecular cell biology* **8**: 275-283

Wassenaar TM, Engelskirchen M, Park S, Lastovica A (1997) Differential uptake and killing potential of Campylobacter jejuni by human peripheral monocytes/macrophages. *Medical microbiology and immunology* **186**: 139-144

Wassenaar TM, van der Zeijst BA, Ayling R, Newell DG (1993) Colonization of chicks by motility mutants of Campylobacter jejuni demonstrates the importance of flagellin A expression. *Journal of general microbiology* **139 Pt 6**: 1171-1175

Watson RO, Galan JE (2008) Campylobacter jejuni survives within epithelial cells by avoiding delivery to lysosomes. *PLoS pathogens* **4**: e14

Wei MC, Zong WX, Cheng EH, Lindsten T, Panoutsakopoulou V, Ross AJ, Roth KA, MacGregor GR, Thompson CB, Korsmeyer SJ (2001) Proapoptotic BAX and BAK: a requisite gateway to mitochondrial dysfunction and death. *Science (New York, NY)* **292**: 727-730

- Wilson DL, Bell JA, Young VB, Wilder SR, Mansfield LS, Linz JE (2003) Variation of the natural transformation frequency of *Campylobacter jejuni* in liquid shake culture. *Microbiology* **149**: 3603-3615
- Wolfson JJ, May KL, Thorpe CM, Jandhyala DM, Paton JC, Paton AW (2008) Subtilase cytotoxin activates PERK, IRE1 and ATF6 endoplasmic reticulum stress-signalling pathways. *Cellular microbiology* **10**: 1775-1786
- Wullschleger S, Loewith R, Hall MN (2006) TOR signaling in growth and metabolism. *Cell* **124**: 471-484
- Yin XM, Luo Y, Cao G, Bai L, Pei W, Kuharsky DK, Chen J (2002) Bid-mediated mitochondrial pathway is critical to ischemic neuronal apoptosis and focal cerebral ischemia. *The Journal of biological chemistry* **277**: 42074-42081
- Yoshida H, Okada T, Haze K, Yanagi H, Yura T, Negishi M, Mori K (2000) ATF6 activated by proteolysis binds in the presence of NF-Y (CBF) directly to the cis-acting element responsible for the mammalian unfolded protein response. *Molecular and cellular biology* **20**: 6755-6767
- Yoshida H, Okada T, Haze K, Yanagi H, Yura T, Negishi M, Mori K (2001) Endoplasmic reticulum stress-induced formation of transcription factor complex ERSF including NF-Y (CBF) and activating transcription factors 6alpha and 6beta that activates the mammalian unfolded protein response. *Molecular and cellular biology* **21**: 1239-1248
- Young KT, Davis LM, Dirita VJ (2007) *Campylobacter jejuni*: molecular biology and pathogenesis. *Nature reviews Microbiology* **5**: 665-679
- Yu L, McPhee CK, Zheng L, Mardones GA, Rong Y, Peng J, Mi N, Zhao Y, Liu Z, Wan F, Hailey DW, Oorschot V, Klumperman J, Baehrecke EH, Lenardo MJ (2010) Termination of autophagy and reformation of lysosomes regulated by mTOR. *Nature* **465**: 942-946
- Yuki N, Taki T, Inagaki F, Kasama T, Takahashi M, Saito K, Handa S, Miyatake T (1993) A bacterium lipopolysaccharide that elicits Guillain-Barre syndrome has a GM1 ganglioside-like structure. *The Journal of experimental medicine* **178**: 1771-1775
- Zaas DW, Duncan M, Rae Wright J, Abraham SN (2005) The role of lipid rafts in the pathogenesis of bacterial infections. *Biochimica et biophysica acta* **1746**: 305-313
- Zaika AI, Wei J, Noto JM, Peek RM (2015) Microbial Regulation of p53 Tumor Suppressor. *PLoS pathogens* **11**: e1005099
- Zilbauer M, Dorrell N, Boughan PK, Harris A, Wren BW, Klein NJ, Bajaj-Elliott M (2005) Intestinal innate immunity to *Campylobacter jejuni* results in induction of bactericidal human beta-defensins 2 and 3. *Infection and immunity* **73**: 7281-7289